Thermal and Strength Characteristics of Soil-Biochar-Biopolymer Composite Backfill

A Thesis

Submitted in Partial Fulfilment of the Requirements

for the Degree of

Doctor of Philosophy

By

Deepak Patwa

(Roll No. 186104013)

Department of Civil Engineering

Indian Institute of Technology Guwahati

Guwahati-781039, India

May 2023

Thermal and Strength Characteristics of Soil-Biochar-Biopolymer Composite Backfill

A Thesis

Submitted in Partial Fulfilment of the Requirements

for the Degree of

Doctor of Philosophy

By

Deepak Patwa

(Roll No. 186104013)

Department of Civil Engineering

Indian Institute of Technology Guwahati

Guwahati-781039, India

May 2023

Candidate's Declaration

The work reported in this thesis is original and was carried out by me during my tenure as a Ph.D. student at the Department of Civil Engineering, Indian Institute of Technology Guwahati (IITG), Guwahati, Assam, India. This thesis has not formed the basis for the award of any degree, diploma, associateship, membership, or similar title of any university or institution.

Date: 29-05-2023

Deepak Patwa

Ph.D. Student
Registration No. 186104013
Department of Civil Engineering
Indian Institute of Technology Guwahati

CERTIFICATE

This is to certify that the thesis titled **"Thermal and Strength Characteristics of Soil-Biochar-Biopolymer Composite Backfill"** submitted by Deepak Patwa (Registration No. 186104013) for the award of the degree of Doctor of Philosophy is an authentic record of the results obtained from research work carried out under our supervision and guidance at the Department of Civil Engineering, Indian Institute of Technology Guwahati. The thesis work, in my opinion, has reached the requisite standards fulfilling the requirement for an award of the degree of Doctor of Philosophy. To the best of our knowledge, this work is not submitted elsewhere for the award of any other degree or diploma.

Date: 29/05/2023
IIT Guwahati

Dr. Ravi K.
Associate Professor
Department of Civil Engineering,
Indian Institute of Technology Guwahati

Date: 29-5-2023
IIT Guwahati

Prof. Sreedeep S.
Professor
Department of Civil Engineering,
Indian Institute of Technology Guwahati

Acknowledgments

I am grateful to many people who have supported me during the realization of my doctoral research. First and foremost, I would like to cordially express my deep sense of gratitude and heartfelt thanks to my supervisor, **Dr. Ravi K.** (Associate professor, IIT Guwahati), and **Prof. Sreedeep S.** (Professor, IIT Guwahati). I particularly thank them for introducing me to geo-environmental engineering and training me to assess the existing real-life geotechnical challenges around us. I am grateful to them for always being available for discussions and for the motivation that I required most for my research, especially during tough times. I will be forever indebted to their excellent guidance, encouragement, and affection. My supervisors contributed greatly to my understanding of the research area through valuable discussions, ideas, and useful comments.

I express my sincere thanks to the members of my Doctoral Committee, **Dr. Arindam Dey, Dr. Anjan Kumar S.**, and **Dr. Pankaj Kalita,** for their constructive comments, valuable suggestions, and continuous encouragement at various stages of the research work. My sincere thanks to all the faculty of Geotechnical Engineering Division, Department of Civil Engineering of institutes for the course works done in masters in which they introduced various concepts and provided critical insight into the Geotechnical engineering subjects. I am thankful to Central Instruments Facility (CIF) of IIT Guwahati for providing research facility which helped in my research work. I would also like to thank **Prof. T.V. Bharat** and **Prof. Ankit Garg** for their excellent classes on unsaturated soil mechanics and geo-environmental engineering.

Special thanks need to be mentioned to my senior research colleague, Dr. Chandrabhanu Gupt and Dr. Anant Aishwarya Dubey, for giving their precious motivations and remarks related to my research work. Further, I would also like to thank my seniors Dr. Rohini C Kale, Dr. Atma Prakash, Dr. Sanandam Bordoloi, Dr. Vinay Gadi, Dr. Abhishek

Saha, Dr. Partha Das, and Dr. Chandi Patra their continuous support and guidance towards my research work. I am really thankful to Mr. Hariram Upadhay, Mr. Samarjyoti Kalita, and Mrs. Syeda Reshima Begum for their help in carrying out laboratory experiments.

I sincerely acknowledge the affectionate forbearance and continuous motivations received from my research colleagues and friends Mr. Ankti Srivastava, Mr. Himanshu Yadav, Mr. Surender Singh, Mr. Alok Chandra, Mr. Jhilam Sinha, Mr. Manas Jyoti Bora, Mr. Niranjan Borah, Mr. Safik Khan, Ms. Urbashi Bordoloi, Dr. Harrison Hihu Muigai, Mr. Ajit Kumar, Ms. Dhritilekha Deka, Ms. Deepali Anand, Mr. Utla Chandra Sekhar, and Mr. Sandeep Kumar Mondal.

I highly appreciate the Ministry of Human Resource Development (MHRD), India, for providing me the financial assistance at IIT Guwahati for all the necessary facilities to successfully complete this research work.

Most importantly, I would also like to extend my gratitude towards my parents, Mr. Ram Lal Patwa and Late. Mrs. Shimla Devi for their prayers, unconditional love, and support. I am forever indebted to my beloved, Ms. Priyanka Patwa, for her sacrifices and support.

Above all, I owe it all to almighty God for granting me the wisdom, health, and strength to undertake this research task and enabling me to its completion.

Deepak Patwa

Abstract

Thermal backfill is essential for underground crude oil pipelines, crude oil storage tanks, and geo-energy storage units. The major function of such backfills is to prohibit heat migration from the source as well as sub-structural stability. Often the thermal characteristics of locally available soils are not adequate for thermal backfill applications. Hence, it is required to modify the native soil by amending it with appropriate materials that possess suitable thermal characteristics and provide enhanced sub-structural stability. Biochar is a low thermal conductive, highly chemically stable, and eco-friendly material and has the potential to mitigate heat loss and may increase soil strength. However, the thermal characteristics of soil-biochar composite (SBC) in the compacted condition in view of applying it as thermal backfill material have largely been unaddressed in literature. Therefore, this study aims to explore the possibility of biochar-based soil composite as thermal backfill material.

In the current study, two types of locally available soil (highly plastic silt and clayey sand) and three types of biochar (hardwood biochar, water hyacinth biochar, and sugarcane bagasse biochar) are used to investigate the applicability of SBC as thermal backfills. The thesis is comprised of five different scopes of study. First, the applicability of SBC was tested under dry states, wet states, and near-saturation states by varying dry density (1.1 to 1.3 Mg m^{-3}) and the molding water content from 10 to 30%. The experimental results revealed that the SBC has lower thermal conductivity (*K*) and volumetric heat capacity (*C*) compared to bare soil under dry, wet, and near-saturation conditions. Second, the thermal and strength characteristics of SBC were tested at the density recommended for thermal backfill (i.e., at optimum moisture content, OMC, and maximum dry density, MDD) considering different soil types, biochar types, and biochar particles size fraction at varying biochar content. It was observed from the results that the SBC has lower *K* and *C* values than bare soil, and it depends upon the soil types, biochar types, and biochar particle size fractions amended to the soil. A maximum of 37 and 27% reduction in *K* and *C* values of soils was observed. However, the UCS of soil also reduces with biochar amendment, which depends upon soil type and particle size fractions.

The third part of the study was designed to develop the thermal backfill in such a way that it would provide the same thermal insulation as SBC and also have high strength. The biopolymer-based soil stabilization requires a considerably low quantity of biopolymer for soil strength improvement. Therefore, incorporating biopolymer in the SBC can help in developing a high-strength sustainable composite capable of providing efficient thermal insulation. The clay loam soil is amended with 2.5% to 7.5% (w/w) biochar and 0.5% to 1.5% (w/w) of

biopolymer and their various combinations. Out of nine SBPC devised in the current study, five composites exhibited superior strength and lowered thermal conductivity than the bare soil in both conditions, i.e., OMC state and upon drying. The findings of this study establish the synergistic attributes of biopolymer and biochar amendment for developing a high-strength and low thermal-conductive soil composite.

Fourth, a bench-scale study on the thermal insulation efficiency of SBC and SBPC in terms of heat transfer was conducted to facilitate field-scale applications. A soil column was fabricated, and the radial distribution of heat transfer was investigated using a heater rod and temperature sensors installed in the radial direction in the soil column. The SBC and SBPC exhibit lower temperatures than bare soil at all radial distances. Fifth, an investigation of the changes in thermal characteristics of biochar produced at various pyrolysis temperatures was performed to optimize energy consumption and minimize the material cost for the desired applications. It was observed that the thermal conductivity of produced biochars was found to be in a narrow range of 0.102 to 0.132 $Wm^{-1}K^{-1}$ for all the produced biochars. A pyrolysis temperature of 400ºC is determined to be a suitable temperature regardless of the feedstock type because of the least energy consumption, considerable yield, required thermal characteristics, and carbon stability for the design period. The finding from the current study unravels the potential of biochar-based thermal backfill to restrict heat transfer from energy storage facilities. Therefore, the proposed SBC and SBPC can be utilized effectively as thermal backfill material for underground crude oil pipelines, crude oil storage tanks, subsurface cold storage, and geothermal energy storage systems to improve their performance.

Keywords: Thermal backfill; Biochar; Biopolymer; Thermal and strength characteristics; Heat transfer; Energy optimization; Pyrolysis temperature

CONTENTS

CHAPTER 3 MATERIALS AND THEIR CHARACTERIZATION

CHAPTER 4 INFLUENCE OF INITIAL MOLDING PARAMETERS AND MOISTURE MIGRATION ON THERMAL CHARACTERISTICS OF SOIL-BIOCHAR COMPOSITE

CHAPTER 5 INFLUENCE OF BIOCHAR TYPES AND BIOCHAR FRACTIONS ON THERMAL AND STRENGTH CHARACTERISTICS OF SBC

List of figures

List of tables

List of symbols/abbreviations

Symbol/ Abbreviation	Description
TAS	Thermally active structures
K	Thermal conductivity ($Wm^{-1}\ K^{-1}$)
C	Volumetric heat capacity ($MJ\ m^{-3}\ K^{-1}$)
$Wm^{-1}\ K^{-1}$	Watt per meter per Kelvin
$MJ\ m^{-3}\ K^{-1}$	Megajoule per meter per Kelvin
OMC	Optimum moisture content
MDD	Maximum dry density
SBC	Soil-biochar composite
SBPC	Soil-biochar-biopolymer composite
cP	Centipoise
UCS	Unconfined compressive strength (MPa)
Temp	Temperature
$Mg\ m^{-3}$	Megagram per meter cube
$Mg\ ha^{-1}$	Megagram per hectare
$tonnes\ ha^{-1}yr^{-1}$	Tonnes per hectare per year
g/cc	Gram per centimetre cube
BpS	Biopolymer-stabilized soil
RS	Residual soil
HWBC	Hardwood biochar
WHBC	Water hyacinth biochar
SBBC	Sugarcane bagasse biochar
ρ_d	Dry density
w	Water content
BC	Biochar content
MLR	Multiple linear regression
S_d	Sensitivity index
MH	Highly plastic silty soil
SC	Clayey sand
g/l	Gram per liter

WH	Water hyacinth
SB	Sugarcane bagasse
FESEM	Field emission scanning electron microscopy
XRD	X-Ray diffraction
TGA	Thermogravimetric analysis
FTIR	Fourier-transform infrared spectroscopy

CHAPTER 1

INTRODUCTION

1.1 Overview

Thermally active structures (TAS) are defined as substructures that need to either dissipate or store heat for their efficient operation. Underground TAS such as nuclear waste repositories, high power voltage cables, and geothermal heat exchangers are desired to have high thermal conductivity for quick dissipation of heat (Sah and Sreedeep, 2014; Wang et al., 2016; Ocłoń, 2021), whereas TAS such as crude oil pipelines, crude oil storage tank, subsurface cold-storage, and geo-energy storage units are desired to have maximum thermal insulation for long-term heat storage (Başer et al., 2018; Danielewicz et al., 2016; Otomi et al., 2020). Most of the TAS are generally installed in surrounding locally available soils as backfills. The major function of such backfills is either to dissipate the heat from the source efficiently (e.g., underground high-power voltage cables) or prohibit the heat from the source (underground crude oil pipelines and storage tanks), as well as sub-structural stability. Often the thermal characteristics of locally available soils are not adequate for thermal backfill applications. Hence, it is required to modify the native soil by amending it with some appropriate materials. Soil thermal characteristics such as thermal conductivity (K) and volumetric heat capacity (C) are among the important soil physical properties and dominate the conduction and distribution of heat in the soil. The values of soil thermal characteristics depend on the soil type and its composition, gradation, soil density, porosity, water content, and organic content (Abu-Hamdeh and Reeder, 2000; Abu-Hamdeh, 2003; Dec et al., 2009; Tong et al., 2020). Therefore, these backfills could be engineered further by modifying the abovementioned attributes to develop a dual-functioning material that possesses suitable thermal characteristics and provide enhanced sub-structural stability.

While previous and contemporary researchers have attempted extensively to develop quick heat-dissipating backfills with high thermal conductivity (Tang et al., 2008; Sah and Sreedeep, 2014; Wang et al., 2016; Ocłoń, 2021), the studies on the development of heat-insulating thermal backfills are scarce (Başer et al., 2018; Xiao et al., 2019). Besides, the modern age demands eco-friendly ways of developing sustainable infrastructure, and therefore, low-carbon footprint construction materials that can contribute to the circular economy are being explored globally.

Previous studies suggest that the amendment of biochar in soil decreases its thermal characteristics, which is influenced by the changes in soil material composition and total porosity (Usowicz et al., 2016; Zhao et al., 2016; Liu et al., 2018). Primarily, biochar is a by-product of the biofuel extraction process through the thermochemical conversion of waste biomass (Lehmann and Joseph, 2015; Muigai et al., 2021). Thus, the application of biochar in large-scale engineering projects not only has the potential to develop an efficient thermal backfill for heat mitigation but also leads to waste management required for a circular economy strategy. Biochar is a highly porous, highly chemically stable, and eco-friendly material with a very low thermal conductivity compared to soils (Gupta and Kua, 2017; Pariyar et al., 2020). The pictorial description of underground crude oil pipelines and the schematic diagram of the proposed thermal backfill are presented in Fig. 1.1.

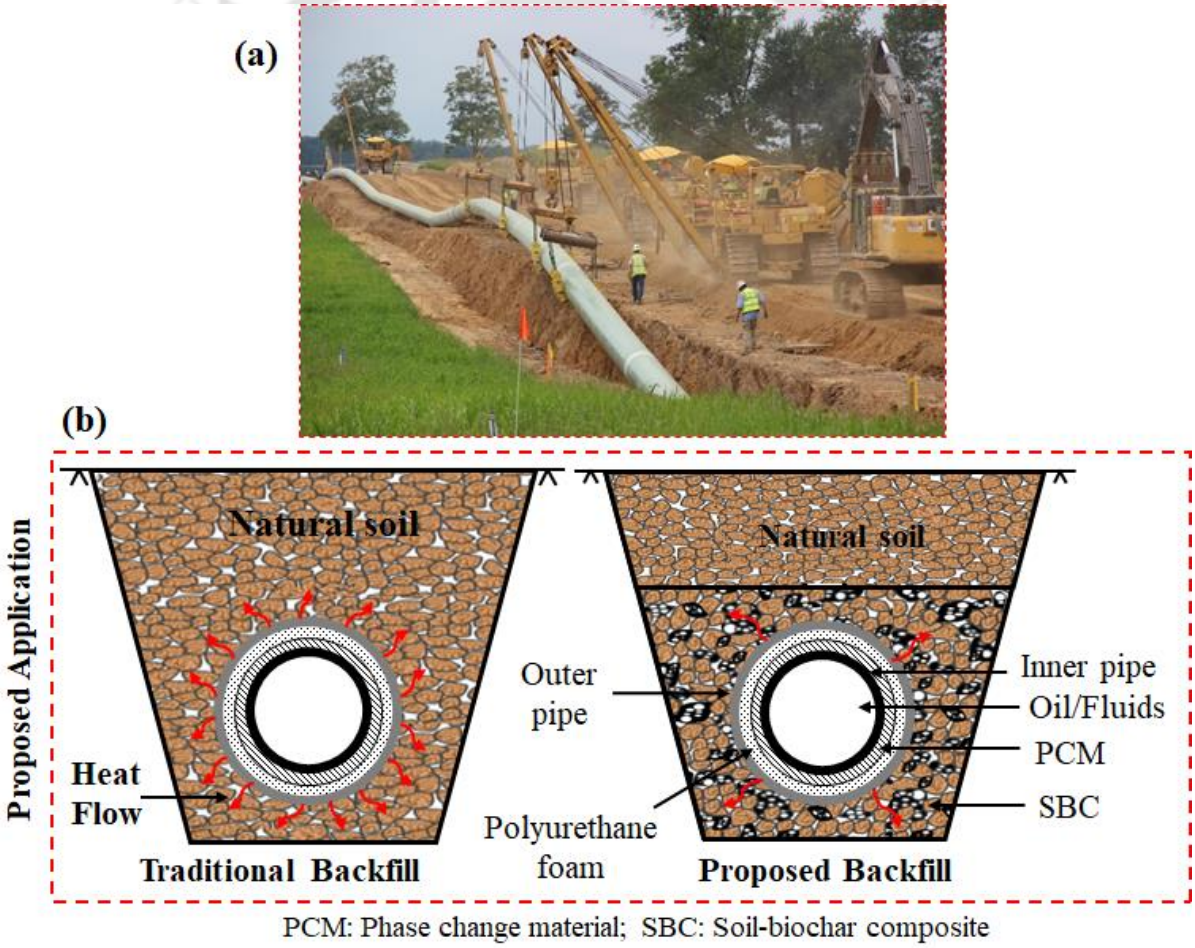

Figure 1.1 (a) Pictorial description of underground crude oil pipelines (extended from www.michiganradio.org); (b) Schematics diagram of traditional and proposed thermal backfill

Photograph of (a) is taken from https://www.michiganradio.org/environment-science/2013-08-23/285-miles-of-new-oil-pipeline-being-installed-across-michigan-neighbors-in-the-path

The abovementioned studies were conducted in the context of its application in agriculture to control heat fluctuation to optimize crop production. However, these studies do not propose the application of biochar as thermal backfill material. The backfill should be compacted to a minimum of 95% of the maximum dry density (MDD) to ensure structural stability, as recommended by Howard (1996), which is not discussed in the literature. Moreover, the underground thermal backfill material might often interact with moisture due to groundwater movement and rainfall, which increases the soil's thermal characteristics resulting in more heat loss from the thermal backfill. Therefore, it is critical to investigate the effects of the initial molding state and subsequent moisture interaction on the thermal characteristics of soil-biochar composite (SBC). Interestingly, there is a contradiction in the literature on the influence of biochar amendment on soils. A few studies have reported that biochar addition improves the strength of the soil-biochar matrix (Haque et al., 2014; Reddy et al., 2015; Sadasivam and Reddy, 2015; Sudhakar et al., 2017; Williams et al., 2020), while others have reported a significant deterioration in the strength characteristics (Busscher et al., 2010; Ahmed et al., 2017; Bora et al., 2021; Ng et al., 2022). It should be noted that the strength characteristics of the SBC are dependent upon the soil type, biochar type, and biochar amendment rate. Therefore, there is a need to re-examine the influence of different biochar types and particle size fractions on the thermal and strength characteristics of SBC.

In the case of strength reduction with the amendment of biochar in soil, there is a need for an eco-friendly binder that can control the strength of the SBC while maintaining thermal conductivity. Most of the soil strength improvement techniques, such as cementation, geo-polymerization, and bio-mineralization, result in an increase in thermal conductivity (Balaji et al., 2017; Cheng et al., 2021; Ocłoń, 2021; Xiao et al., 2021). Moreover, previous studies examined the applicability of biopolymers such as xanthan gum, guar gum, and gellan gum in the stabilization of coarse and fine-graded soil (Chang et al., 2016, 2015; Muguda et al., 2017; Qureshi et al., 2017; Vydehi and Moghal, 2022). The biopolymer-based soil stabilization (BpS) requires a considerably low quantity of biopolymer for soil strength improvement (Ramachandran et al., 2021). Therefore, the interest of the current study is shifted toward the thermal and strength characteristics of soil-biochar-biopolymer composite (SBPC).

Heat transfer in the soil mainly depends upon the initial degree of saturation, thermal characteristics of soil, porosity, and pore geometry of the soil matrix (Moradi et al., 2015, 2016). The amendment of biochar in the soil changes its material composition and increases

the total porosity of soil matrix (Usowicz et al., 2016; Zhao et al., 2016; Liu et al., 2018), which can affect the heat transfer in the soil-biochar composite. However, there is limited study on heat transfer in soil amended with biochar (Zhang et al., 2015). Therefore, there a bench-scale study on the thermal insulation efficiency through SBC and SBPC in terms of heat transfer is required to facilitate field-scale applications. Moreover, the preparation of biochar from biomass involves an energy-intensive pyrolysis process. The thermal characteristics of any material depend upon its mineralogical composition, surface structural characteristics, and physicochemical properties, which might be controlled by the pyrolysis temperature (Klett et al., 2004; Hassan et al., 2020; Pariyar et al., 2020; Zhang et al., 2020; Nzediegwu et al., 2021). The manufacturing process of biochar should meet the minimum energy consumption requirements to minimize the material cost. Therefore, it is required to investigate the changes in thermal characteristics of biochar produced at various pyrolysis temperatures to optimize the energy consumption for the desired applications.

1.2 Need of the study

The demand for energy worldwide will continue to increase, and oil and natural gas are two of the most important energy sources. The world demand for crude oil has increased from 60 million barrels per day to 84 million barrels per day in the period of 1990 to 2010 (Hasan et al., 2010). This increased heavy crude oil production requires an adequate means of transportation for storage or to the refinery. In view of this, pipelines remain the most convenient means for continuous and economical transportation of crude oils and their products (Hart, 2014). Transporting heavy crude oil via pipeline is usually challenging due to their high density and viscosity (>1,000 cP) and very low mobility at reservoir temperature. Heating is one of the means of enhancing the flow properties of heavy crude oil, which reduces the viscosity by several orders of magnitude with increasing temperature. The major challenge associated with heating and transporting heavy crude oil via pipeline is the heat losses to the surrounding soil. Usually, the initial temperature of the crude oil pipelines reaches as high as 100 °C (Park and Seo, 2018). The surrounding soil temperature is significantly lower than the initial temperature of the crude pipelines, which often leads to the deposition of hydrates and wax if the temperature descends below 50 °C (Park and Seo, 2018; Olajire, 2021). The necessity to efficiently mitigate the heat loss from TAS, such as crude oil pipelines, crude oil storage tanks, and geo-energy storage units, has motivated this study. It is established from the literature that biochar is a low thermal characteristics material, and SBC have lower thermal characteristics than bare soil. Therefore, an insulation

layer of SBC as a thermal backfill material can be used to mitigate heat transfer. However, a thorough investigation is required to evaluate the thermal characteristics of SBC in the compacted condition in view of applying it as thermal backfill material.

1.3 Broad objectives of the study

The biochar amendment in soil decreases the thermal characteristics of soil, and the addition of biopolymer increases soil strength. However, the thermal characteristics of SBC and SBPC in the compacted condition in view of applying it as thermal backfill material have largely been unaddressed in literature. Based on the gap in existing literature, the broad objective of this study is to investigate the thermal and strength characteristics of SBC and SBPC as thermal backfill material. The proposed assessment is expected to provide a better understanding of the SBC as a thermal backfill material to mitigate thermal migration.

1.4 Organization of thesis

The thesis is organized into nine chapters as follows,

Chapter 1 gives a general overview of the thesis, motivation behind this research work, and its importance.

After the introductory chapter, the details of the previous works have been reported in **Chapter 2** in the form of a literature review. The literature review chapter has been further subdivided to specifically discuss the studies relevant to the defined objectives. After performing a critical appraisal of the literature, the main objective and scope of the work have been described.

Chapter 3 provides details about the used materials and characterization of used materials in this study to meet the research objectives.

Chapter 4 presents an investigation of the influence of initial molding parameters (dry density and molding water content) on the thermal characteristics of soil-biochar composites (SBC). From the measured data, a linear regression was performed along with the sensitivity analysis to quantify the relationship between thermal characteristics and the initial molding state (dry density, initial water content, and biochar content) for SBC. The findings have been supported by morphological analysis.

Chapter 5 presents the influence of the amendment of different biochar types, such as hardwood biochar, water hyacinth biochar, and sugarcane bagasse biochar, on the thermal characteristics of soil. Furthermore, investigation on amendment of different biochar particle size fractions on the thermal and strength characteristics of soil. Three different factions,

namely coarse (4.75-2 mm), medium (2-0.425 mm), and fine (0.425-0.075mm), were used in this chapter. The strength characteristics of SBC are evaluated using the unconfined compression strength (UCS) test. The findings have been supported by microstructural and mineralogical analysis.

Chapter 6 presents an investigation of the thermal and strength characteristics of a thermal backfill inspired by the synergistic biochar-biopolymer amendment in soil. The clay-rich soil, best performing medium fraction biochar, and xanthan gum biopolymer blended in different content that can be tailored for its strength and thermal characteristics. Moreover, while the backfill is prepared at the OMC for maximum density, moisture loss is inevitable while insulating TAS. Therefore, all the specimens were examined at OMC and MDD state and after drying to investigate the influence of moisture loss on the strength and thermal conductivity of the proposed thermal backfill. The findings are supported by the microstructural analysis.

Chapter 7 presents an investigation of the thermal insulation performance of proposed SBC and SBPC for mitigating heat transfer through a bench-scale study. The thermal insulation efficiency of the proposed SBC and SBPC is investigated by fabricating an SBC and SBPC column of an internal diameter of 300 mm and a height of 200 mm. For heat transfer investigation, a heater rod was installed at the center of the soil column, and temperature sensors were installed at different radial distances from the heater rod to monitor the temperature distribution profile.

Chapter 8 presents an investigation of the changes in physicochemical and thermal characteristics of biochar produced at various pyrolysis temperatures to optimize the energy consumption for the desired applications. Two locally available waste biomass, i.e., water hyacinth and sugarcane bagasse, are pyrolyzed at temperature ranges from 300 ℃-700 ℃. The optimum pyrolysis temperature is defined based on the least energy consumption, high yield, low thermal characteristics, and carbon stability.

Chapter 9 summarises the conclusions, major contributions, and future scope of the study.

CHAPTER 2

LITERATURE REVIEW

2.1 Introduction

A detailed understanding of the physical, chemical, thermal, and strength characteristics of soil-biochar composite is essential to evaluate its feasibility as thermal backfill material for thermally activated structures. This chapter presents a basic understanding of thermal characteristics, mechanism of heat flow in soil, and factors influencing the thermal characteristics of soil. Thereafter, a comprehensive review of the published literature on thermal and strength characteristics of soil-biochar composite is presented in this chapter. Subsequent sections in this chapter give an overview of the stabilization of soil using biopolymer and the influence of pyrolysis temperature on the physical, chemical, and surface characteristics of biochar produced from water hyacinth and sugarcane bagasse biomass. In the last section, a critical appraisal was made based on the reviewed literature highlighting the research gaps, followed by the objective and scopes of the present work.

2.2 Thermal characteristics of soil

Thermal characteristics of soil are of great importance in several engineering projects where heat transfer occurs through the soil. These projects include crude oil pipelines, crude oil storage tank, subsurface cold storage, and geo-energy storage units where maximum thermal insulation are desired for long-term heat storage (Danielewicz et al., 2016; Başer et al., 2018; Otomi et al., 2020). However, projects such as nuclear waste repositories, high power voltage cables, and geothermal heat exchangers are desired to have high soil thermal conductivity for quick heat dissipation (Sah and Sreedeep, 2014; Wang et al., 2016; Ocłoń, 2021). The thermal characteristics of soil include thermal conductivity (K), thermal diffusivity (D), and volumetric heat capacity (C). Thermal conductivity is the amount of heat passing through the unit cross-section of the geomaterial under a unit temperature gradient applied in the direction of heat flow (Hillel, 2013). Thermal diffusivity (D) is the ratio of thermal conductivity to specific heat. It indicates how materials or soil adjust their temperature with respect to the surroundings. A high thermal diffusivity value implies the capability for rapid and considerable changes in temperature. Volumetric heat capacity is defined as the quantity of heat required to change the temperature of a unit volume of a

geomaterial by 1°C. It is the product of the mass-specific heat c (cal/g °C) and the density (g/cc).

2.3 Mechanism of heat flow through soils

While the flow of heat by conduction is the predominating mechanism, all possible mechanism is employed for the flow of heat from warmer to cooler regions. The temperature levels, in particular, as well as the soil composition and structure, affect the contribution of each possible mechanism to heat transfer. Heat dissipation through moist soil occurs in a number of complex forms, the predominant one being by conduction through the solid-liquid matrix. Convection and radiation generally have relatively small or negligible effects, but they may have a noticeable influence in certain situations. To account for conduction, convection, and radiation in soil pores, one effective parameter may be used. Water phase changes from liquid to vapors significantly affect the heat transfer process. In unsaturated soils, moisture may migrate by the process of evaporation followed by vapor diffusion and subsequent condensation at another place, thus leading to heat transfer. The theoretical studies of heat transfer in soils generally consider the soil to be homogeneous and assume that all processes of heat transfer take place uniformly throughout the porous medium (De Vries, 1963). In reality, vapor transfer or air convection occurs only in the air-filled pore space and fluid movement only in the water-filled pore space, while evaporation or condensation is associated with the water/air interfaces.

Heat conduction occurs in all the soil constituents, i.e., in the soil solids, the water (liquid, vapor, or ice), and the pore air. Conduction operates in air or water vapor by the process of a collision between the molecules and a consequent increase in their mean kinetic energy as heat passes from warmer to cooler regions. A similar mechanism is partly responsible for heat conduction in liquid water; however, energy transfer by breaking hydrogen bonds in water also appears to contribute to conduction. Heat is conducted through the soil will take all available paths. Paths through contacting solid grains nearly provide the major part of conductive heat transfer, but contact resistance may exist. Other paths consist of portions of solid grains and fluid-filled pore spaces in the soil mass.

Convection is a mass transport phenomenon resulting from temperature gradients. It is caused in fluids by changes in density with temperature. At higher temperatures, the density of the fluid is lower, resulting in an upward displacement. Heat transfer by convection increases rapidly with an increase in soil pore diameter above a few millimeters,

with an increase in ground temperature above 30°C. The influence of convection is generally very small for particles less than 1 to 2 mm in size (De Vries, 1963).

Radiation occurs across air spaces by heat energy propagation as electromagnetic waves. The temperature of the radiating body is the most important factor, the flow of heat being proportional to the fourth power of the absolute temperature. In soils, radiation usually makes a negligible contribution to heat transfer. The effect is particularly noticeable for nearly dry gravel-size material. Radiation can play a significant part in heat transfer in dry coarse crushed-stone materials (Farouki, 1981).

2.4 Factors influencing thermal characteristics of soil

Thermal characteristics of soils are determined by many factors such as mineralogical composition, particle size, gradation, packing geometry, dry density, porosity, water content, temperature, pore size, pore shape, pore orientation, and spatial arrangement of pores, etc. (Brandon and Mitchell, 1989). The above factors are explained below in detail.

2.4.1 Soil type and composition

The influence of soil types and mineral composition has been studied by many researchers (Farouki, 1981; Abu-Hamdeh and Reeder, 2000; Singh and Devid, 2000; Tarnawski et al., 2015; Li et al., 2021). The literature reveals that fine-grained or cohesive soil and peaty soil exhibit lower thermal characteristics than granular soil. Since heat flowing through soil must flow through the solid mineral's grain and the medium in which they are embedded, the thermal conductivity of soil depends on the thermal characteristics of its component materials and interparticle contact (Yun and Santamarina, 2008). Sand with quartz as the principal constituent has higher thermal conductivity. Thermal characteristics for some of the soil constituents are represented in Table 2.1 (Bejan and Kraus, 2003). Brandon and Mitchell (1989) stated that the higher the percentage of quartz content in sand, higher the thermal conductivity value, provided all other factors remain the same. Fine-grained soils, clay-rich soil, and peaty soil have lower thermal conductivity in comparison to coarse-grained soils (Côté and Konrad, 2005a; Barry-Macaulay et al., 2013). The type of clay minerals present in the soil also influences thermal conductivity (Tang et al., 2008).

Table 2.1. Thermal characteristics of a common constituent in soil

Material	Thermal conductivity ($Wm^{-1}K^{-1}$)	Thermal diffusivity (m^2/s) $\times 10^{-7}$	Heat capacity ($kJ\ kg^{-1}K^{-1}$)
Quartz	8.4	43.08	0.73
Granite	1.70-4.00	-12	0.89
Gypsum	0.51	4.7	1.09
Mica	0.75	2.95	0.88
Clay	1.28	10	0.88
Limestone	1.26-1.33	-5	0.90
Marble	2.80	13	0.81
Sandstone	1.60-2.10	10-13	0.71
Air (25 ˚C)	0.025	0.21	1.00
Water (25 ˚C)	0.59	1.43	4.20

2.4.2 Particle size gradation

Well-graded soils conduct heat better than poorly-graded soils because the smaller grains can fit in the interstitial positions between the larger grains, thus increasing the density and the mineral-to-mineral contact (Brandon and Mitchell, 1989; Singh and Devid, 2000). The shape of soil particles determines the surface contact area between particles, which affects the ability of the soil to conduct heat. The thermal conductivity reduces with decreasing particle size due to reduced surface contact between adjacent particles.

2.4.3 Dry density

The density of soil has an important influence on thermal characteristics. The presence of air with its low thermal characteristics decreases the overall thermal characteristics of the soil as compared to that of its solid components. Therefore, well-compacted soil will have high thermal characteristics by reducing the total void volume and improving contact between the solid grains (Abu-Hamdeh and Reeder, 2000; Singh and Devid, 2000; Sah and Sreedeep, 2014; Tong et al., 2020).

2.4.4 Moisture content

The moisture content is an important factor affecting thermal characteristics of soil (Tong et al., 2020). When water is added to the soil, it tends to distribute itself in a thin film around a solid grain of the soil. This water film provides a path for the heat and bridges the air gaps between the solid particles. Additional water, over and above that required for film formation, serves to fill voids that were occupied with air. Since the thermal characteristics of air are much lower than water (Table 2.1), the inclusion of water in the soil would

considerably increase the thermal characteristics of soil. It has been reported that the greatest increase in thermal characteristics is found from dryness to about 10% of the voids saturated with water, and there is very little change above 30% of the voids saturated (Sah and Sreedeep, 2014; Zhang et al., 2017). The moisture content also indirectly influences thermal characteristics since higher density can be achieved by adding water to the soil.

2.4.5 Additives

Additives are used with soil materials in various ways and, for several purposes, cause an increase or decrease in soil thermal conductivity. The treatment of soil by the addition of cement, lime, bio-cementation, or other binders for strength improvement or another purpose may increase thermal conductivity (Balaji et al., 2017; Cheng et al., 2021; Xiao et al., 2021). Increasing the percentage of soil organic matter decreased thermal conductivity (Abu-Hamdeh and Reeder, 2000). Similarly, clay sample mixed with sawdust reduces thermal conductivity (Folaranmi, 2009).

2.5 Influence of biochar amendment on density and moisture content of SBC

Soil bulk density and change in moisture content are the most studied properties after the application of biochar. Omondi et al. (2016) performed a meta-analysis of literature data published by October 2015 and quantified the influence of biochar on selected soil physical properties. Their study reported that, on average, soil bulk density was remarkably reduced by 7.6%, whereas soil porosity and available water holding capacity significantly increased by 8.4% and 15.1%. Similarly, Blanco-Canqui (2017) collected data from 22 published literature in the year of 2016 and reported that the amendment of biochar in soil reduces the bulk density by 3% to 31% in 19 out of 22 soils, which demonstrates that bulk density commonly decreases with biochar amendment. On average, bulk density decreased by 12%, which depends upon the biochar type and type of soil. As explained above in section 2.4.3 and section 2.4.4, the thermal characteristics of the material are majorly influenced by the dry density and moisture content of the material. In this context, the influence of biochar amendment on the compaction characteristics (i.e., optimum moisture content and maximum dry density) of soil from the published literature is presented in Table 2.2. The reviewed literature indicates that the amendment of biochar increases the OMC of soil while the MDD of soil is noted to decrease depending upon the soil type, biochar types, biochar particles size fractions, and biochar amendment rate (Ni et al., 2018; Garg et al., 2019; Williams et al., 2020; Puspanathan et al., 2022).

Table 2.2 Influence of biochar amendment on compaction characteristics of soil

References	Soil type	Biochar			Parameter measured	
		Feedstock	Pyrolysis Temp (˚C)	Mix proportion	OMC	MDD
Sudhakar et al. (2017)	Clayey silt (97%) +Highly plastic clay (3%)	Sugarcane bagasse	500	15%, 20%, and 25% (w/w)	Increased by 8%	Decreased by 8.4%
Ni et al. (2018)	Silty sand	Peanut shell	500	10% (w/w)	Increased	Decreased
Garg et al. (2019)	Clayey sand	Water hyacinth	350-400	5% and 10% (w/w)	Increased by 12%	Decreased by 13%
Williams et al. (2020)	Highly plastic clay	Residual pine	Not Available	5, 10, 20, and 30% (w/w)	Marginally Increased (less than 1%)	Decreased by 34%
Bora et al. (2021)	Silty sand	Water hyacinth (WH), poultry litter (PL), saw dust (SD), and peanut shell (PS)	WH (390), PL (450), SD (530), and PS (510)	5% and 10% (w/w)	Increased	Decreased
Ng. et al. (2022)	Silty sand	Peanut shell and wood	500	5% (w/w)	Increased by 42% and 40% for Peanut shell and wood biochar	Decreased by 8% and 12% for Peanut shell and wood biochar
Puspanathan et al. (2022)	Clayey sand	Palm	500	1%, 2%, and 4% (w/w)	Increased	Decreased

2.6 Influence of biochar amendment on thermal characteristics of SBC

Thermal conductivity, thermal diffusivity, and volumetric heat capacity have immense importance in understanding the heat migration process through geomaterials. Extensive research on the thermal characteristics of soil has been conducted by several researchers (Farouki, 1981; Gangadhara Rao and Singh, 1999; Abu-Hamdeh and Reeder,

2000; Abu-Hamdeh, 2003; Dec et al., 2009; Usowicz et al., 2013; Zhang et al., 2017; Tong et al., 2020). However, there is limited literature available on the thermal characteristics of soil-biochar composite. The amendment of biochar, which is highly porous (Lehmann and Joseph, 2015) and water absorptive (Blanco-Canqui, 2017), in soil may alter its thermal characteristics mainly by changing the pore size network of the soil (Zhang et al., 2013; Usowicz et al., 2016; Zhao et al., 2016). The influence of biochar on soil thermal characteristics has been reviewed and discussed in detail below.

Zhang et al. (2013) conducted a long-term field experiment on sandy loam soil to investigate the effects of biochar amendment on soil thermal characteristics in Huantai County, China, and reported that soil thermal conductivity was decreased by biochar addition. They found that after five years, soil thermal conductivity decreased significantly by 3.48% and 7.49% for biochar application rates of 4.5 and 9.0 tonnes ha^{-1} compared to non-amended control soil. They observed that biochar amendment reduced the seasonal and diurnal soil temperature fluctuations: the daily mean temperature and diurnal amplitude changes were reduced by ±0.4 and ±0.8°C, respectively.

Usowicz et al. (2016) quantify the effect of biochar from wood off cuts on the thermal characteristics of loess soil under grassland (G) and fallow (F) in the temperate climate of Poland. The biochar at an amount of 0, 10, 20, and 30 Mg ha^{-1} was incorporated to a depth of 0-15 cm under F and remained on the surface under G. They reported that the type of land use influenced the effect of biochar addition on the soil thermal characteristics, i.e., grassland and fallow, and the form and rate of biochar application. They found the addition of biochar at application rates of 10, 20, and 30 Mg ha^{-1} reduced soil thermal conductivity and diffusivity compared to control soil. This can be attributed to the increasing soil porosity and air content, which displays considerably lower thermal conductivity and diffusivity than other soil components. They also studied the particle size (<0.5, 0.5–1, 1–2, 2–5, and >5 mm) effect of biochar and observed that there was no sizeable effect of the biochar on the thermal characteristics under grassland, where biochar was applied on the soil surface. They noticed that the thermal conductivity and diffusivity of the five different textured of pure biochar were substantially lower than the mix of all the fractions. The highest thermal conductivity was marked in a mixture of all sizes, possibly because the smaller particles partially fill the spaces between the larger particles.

Zhao et al. (2016) conducted a 340 days study to investigate the effects of a seven-year consecutive application of biochar on thermal characteristics. The field experiment was

performed on sandy loam at different growing stages of corn and wheat using heat pulse method. The biochar was amended at two application rates: 4.5 tonnes $ha^{-1}yr^{-1}$ and 9.0 tonnes $ha^{-1}yr^{-1}$. They documented that when compared to non-amended soil, applying corncob biochar to sandy loam soil at two different rates decreased soil thermal conductivity and thermal diffusivity by 0.3 to 32.2% and 0.6 to 21.5%, respectively. These findings appear to be attributed primarily to the relatively lower thermal conductivity and diffusivity of the biochar and variations in soil physical properties (e.g., bulk density and water content) caused by biochar. In contrast, no correlation was found between soil volumetric heat capacity and biochar.

Liu et al. (2018) conducted the experiment on disturbed and undisturbed clayey sand at controlled water content and investigated the effects of biochar application on soil thermal characteristics using heat pulse method. Disturbed clayey red soil was compacted with a bulk density of 1.3 g/cc with wheat straw biochar at application rates (w/w) of 0%, 0.5%, 1.0%, 1.5%, 2.0%, and 2.5%. They documented that for disturbed soil columns, biochar application cannot directly affect soil thermal properties by changing soil solid substances composition at application rates up to 2.5% w/w. However, there was a significant decrease in thermal conductivity, thermal capacity, and diffusivity upon biochar application for undisturbed soil. This is due to the increase of the soil's total porosity, which is mainly attributed to the increase in the meso-and macro-porosity.

The literature review indicates that biochar application can reduce soil thermal characteristics and moderate soil temperature. It also shows that biochar can impact soil thermal characteristics by altering other soil properties (bulk density, porosity, and water content). The extent of changes in soil thermal characteristics might depend on the degree of changes in other soil properties after biochar application.

2.7 Influence of biochar amendment on strength characteristics of SBC

The thermal backfill structure should also have adequate strength to sustain self-weight. Therefore, it is important to understand and quantify the effect of biochar amendment on the strength characteristics of the soil. The influence of biochar amendment on the strength of soil has been reviewed and elaborated in detail below. Table 2.3 highlights the review of some currently available literature on the influence of biochar amendment on the strength characteristics of soil.

2.7.1 Shear strength parameters

Busscher et al. (2010) conducted a surface penetration test and reported that the inclusion of biochar at a rate of 0.5%, 1%, and 2% (w/w) to sand decreased shear strength. Lu et al. (2014) investigated the shear strength of an expansive clayey soil by incorporating rice husk biochar (RHB) at 2%, 4%, and 6% (w/w) for the incubation period of 180 days in a glasshouse. The cohesion of soil decreases with amendment up to 4%, and after that, it increases. However, the internal friction angle of soil increases with all percentages of biochar amendment. The effect of biochar amendment under different types of soil is presented in Fig. 2.1 and Fig. 2.2. In expansive clayey soil, Zong et al. (2014) conducted the direct shear test and found that application of three types of biochar, including wheat straw biochar (SB), woodchips biochar (WCB), and wastewater sludge biochar (WSB) at the amendment rate of 2%, 4%, and 6% (w/w) reduced cohesion (c) significantly but increased internal friction angle (ϕ) (refer to Fig. 2.1). However, in a similar study performed on silt loam soil, Zong et al. (2016) mentioned that biochar reduced the cohesion, but had no significant effect on internal friction angle (ϕ) (refer to Fig. 2.2).

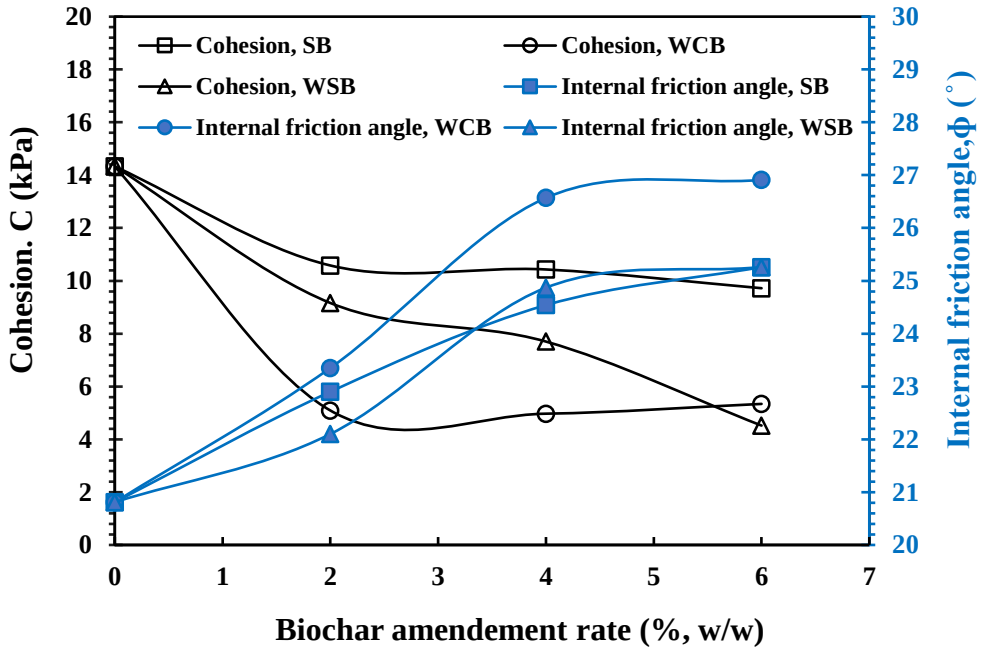

Figure 2.1 Effect of biochar amendment on cohesion and friction angle under clayey soil

Table 2.3 Review of currently available literature on biochar effect on soil strength behavior

References	Soil type	Biochar			Parameter measured		
		Feedstock	Pyrolysis Temp (˚C)	Mix proportion	Cohesion	Friction angle	Unconfined Compressive Strength
Busscher et al. (2009)	Sand	Pecan	700	0.5, 1, 2% (w/w)	Decreased	Decreased	N
Haque et al. (2014)	Clayey soil	Greenwaste	NA	10, 20% (w/w)	N	N	Increased
Lu et al. (2014)	Clayey soil	Rice husk	NA	2, 4, 6% (w/w)	Decreased	Increased	N
Zong et al. (2014)	Clayey soil	Woodchip, Wastewater sludge (WS), Wheat straw,	500	2, 4, 6% (w/w)	Decreased	Increased	N
Sadasivam and Reddy (2015a)	Silty clay	Pine and Fir wood	520	2, 5, 10% (w/w)	Increased	Increased	N
Sadasivam and Reddy (2015b)	Silty clay	Hardwood	500	10% (w/w)	Increased	Increased	N
Reddy et al. (2015)	Silty clay	Wood pellet	520	5, 10, 20% (w/w)	Increased	Increased	N
Zong et al. (2016)	Silt loam	Woodchip, Wheat straw, WS	500	2, 4, 6% (w/w)	Decreased	No effect	N
Ahmed et al. (2017)	Silt loam	Maple wood	500	2, 5, 10% (w/w)	Decreased	Decreased	N
Ajayi and Horn (2017)	Fine sand, sandy loam	Woodchip	500-600	50 or 100 g kg^{-1}	Decreased, Increased	Decreased, Increased	N
Kelly et al. (2017)	Clayey soil	Switchgrass	500-700	25, 50 and 100 g kg^{-1}	Increased	Increased	N
Sudhakar et al. (2017)	Clayey silt (97%) +Highly plastic clay (3%)	Sugarcane bagasse	500	15%, 20%, and 25% (w/w)	N	N	Increased
Williams et al. (2020)	Highly plastic clay	Residual pine	NA	5, 10, 20, and 30% (w/w)	N	N	Increased

References	Soil type	Biochar			Parameter measured		
		Feedstock	Pyrolysis Temp (˚C)	Mix proportion	Cohesion	Friction angle	Unconfined Compressive Strength
Bora et al. (2021)	Silty sand	water hyacinth (WH), poultry litter (PL), saw dust (SD), and peanut shell (PS)	WH (390), PL (450), SD (530), and PS (510)	5 and 10% (w/w)	N	N	Decreased
Ng. et al. (2022)	Silty sand	Peanut shell and wood biochar	500	5% (w/w)	Decreased	Decreased	N

NA: Not available; N: Not measured

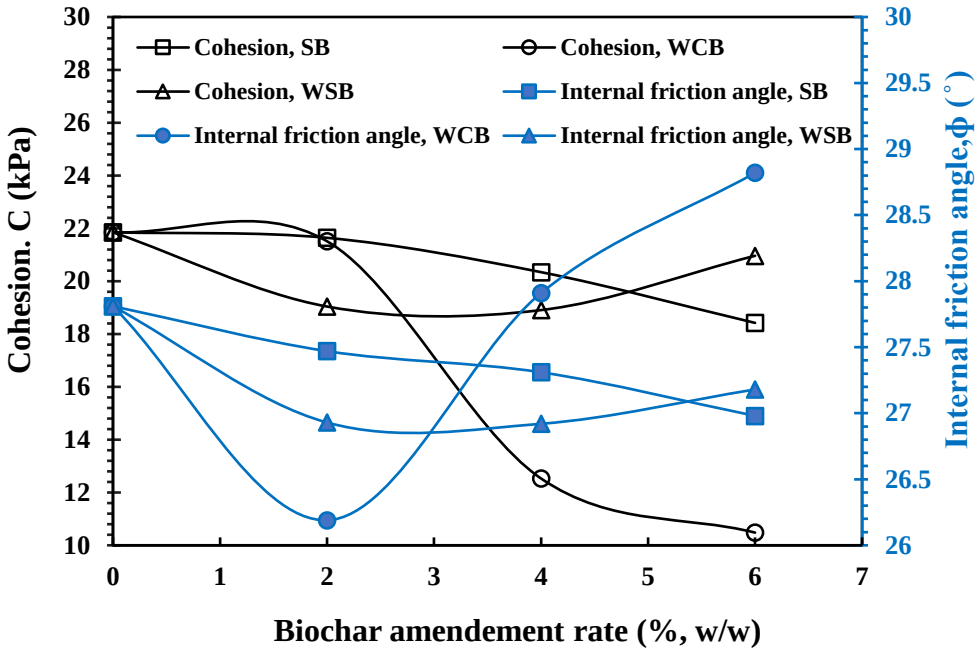

Figure 2.2 Effect of biochar amendment on cohesion and friction angle under silt loam

In a moist (15% water by weight) silty clay soil (obtained from landfill cover), the inclusion of the Pine wood and Fir wood biochar at an amendment rate of 10% (w/w) improved shear strength (parameters c and ϕ) achieved through the direct shear test (Sadasivam and Reddy, 2015). Similarly, Reddy et al. (2015) mentioned that the inclusion of wood pellet biochar having different sizes (< 2mm, < 850 micron, and < 425 micron) at 5%, 10%, and 20% (w/w) amendment rates to a landfill cover soil (silty clay) under wet (20% by weight) condition increased shear strength obtained in a direct shear test. Moreover, the improvement was controlled by the biochar amendment rate and particle size of biochar. Keeping the biochar content (%) held constant, they demonstrate that as biochar particle size increases, the shear strength of the material increases as well. In the abovementioned study, the test was not performed at the maximum possible compaction states (i.e., OMC and MDD) of the SBC, which changes with the amendment of biochar in soil.

Ahmed et al. (2017) conducted a vane shear test at optimum density and moisture (OMC and MDD) condition of a silty loam soil amended with wood biochar of different particle size (PS) ranges 0.5-212 µm (PS1), 212-425 µm (PS2), and 425-850 µm (PS3) at the rate of 2, 5 and 10% (w/w) respectively. The variation of shear strength is presented in Fig. 2.3. The test samples of biochar-amended soil were prepared at higher water content (21.4%) compared to the control soil (16.5%). They reported a lower shear strength of biochar-amended soil with respect to the bare soil (without biochar), which is attributed to the reduced cohesion of silt loam particles amended with the carbonaceous material. Further,

the addition of biochar increases the water and lowers the suction value of biochar-amended soil (858 kPa) as compared to bare soil (221 kPa) also contributes to a decrease in the shear strength of soil.

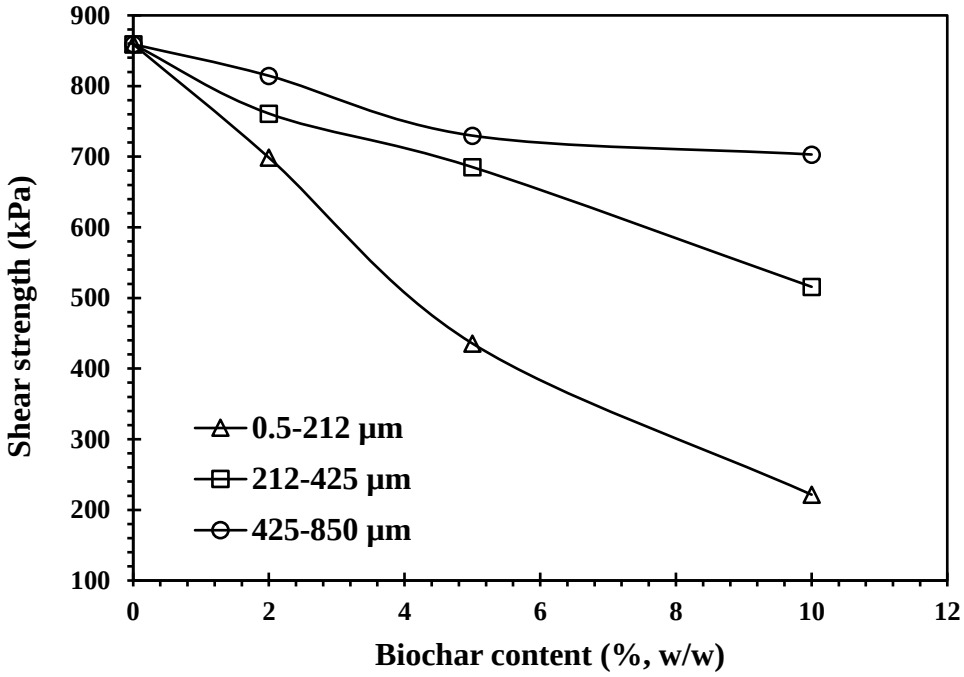

Figure 2.3 Effect of biochar particles size on shear strength of silty loam soil

Ajayi and Horn (2017) investigated the effect of woodchip biochar amendment on micro-structural development, micro-and macro-structural stability, and resilience of two differently textured soils, fine sand (FS) and sandy loam (SL), at the application rate of 50 or 100 g kg^{-1}. They observed that the shear behavior of soil-biochar composites depends on the texture of the amended soil, the rate of biochar amendment, and the water potential. They reported a decrease in shear strength for fine sand and an increase in shear strength for sandy loam. Kelly et al. (2017) conducted a fall cone test to measure the shear strength of two clayey soil amended with biochar derived from switchgrass at three levels 25, 50, and 100 g kg^{-1}. They observed that the limited increase in shear strength which depends on the texture and clay mineralogy of the amended soil, the rate of biochar amendment, and the water potential.

Ng et al. (2022) conducted the direct shear test to assess the shearing behavior of biochar-amended completely decomposed granite (CDG). They prepared the soil sample by mixing CDG with peanut shell biochar and wood biochar at a mass ratio of 5% and compacted it at 95% of the maximum dry density. They reported a 20% reduction in peak shear strength of biochar-amended CDG, which is credited to the lower initial dry density of

the soil and crushing of biochar particles during shearing. However, CDG amended with both types of biochar has negligible effects on the ultimate shear strength, which is governed by friction between soil particles.

2.7.2 Unconfined compressive strength (UCS)

Haque et al. (2014) established that the amendment of 10% to 20% (w/w) of biochar in clayey soil decreased the amount of lime required by the conventional stabilizing method from 10% to 2% (w/w) by enhanced soil strength (unconfined compressive strength, UCS) through creating interface cementation, surface deposition, and pore space filling.

The variation of UCS of SBC with different biochar content is presented in Fig. 2.4. Sudhakar et al. (2017) conducted the UCS test on the sugarcane bagasse biochar amended landfill cover soil, which is a mixture of 97% clayey silt and 3% highly plastic clay. The biochar particle size was less than 300 micron, and the rate of biochar amendments was kept at 15%, 20%, and 25% (w/w). They noticed the increase in unconfined compressive strength (UCS) of the amended soil till the biochar content of 20%. However, with a further increase in biochar content equal to 25%, they have found the declining value of UCS (refer to Fig. 2.4).

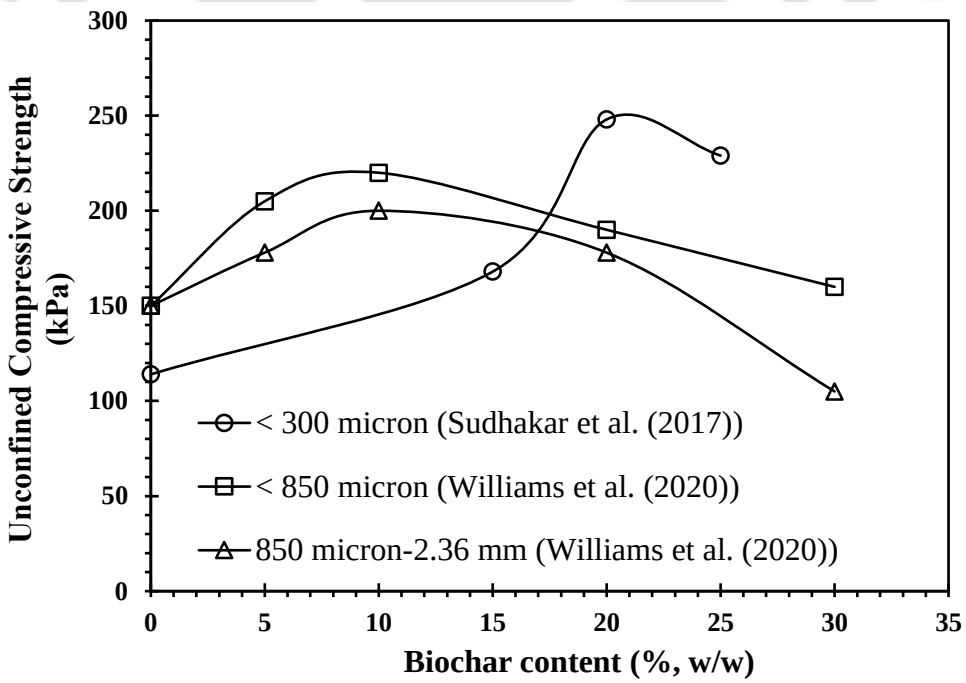

Figure 2.4 Effect of biochar content on UCS value of clayey silt and highly plastic clay

This may be attributed to the decrease in the interlocking capacity of soil due to the presence of fine biochar particles. Similarly, Williams et al. (2020) conducted the unconfined

compressive strength (UCS) test and investigated the effect of biochar amendment at the rate of (5, 10, 20, and 30% w/w) using coarse size (850 micron-2.36 mm) and fine size (less than 850 micron) biochar on Buckshot clay (Highly plastic clay). They reported that increment in the UCS value of soil till the 10% of biochar amendment. However, with the further increment of biochar content, they noticed that the UCS value of soil decreased.

Bora et al. (2021) conducted the UCS test at OMC and MDD states and investigated the influence of different biochar amendments and rates of amendment on the silty sand soil. The in-house produced biochar was made from animal and plant origin such as water hyacinth (WH), poultry litter (PL), saw dust (SD), and peanut shell (PS), and amendment rates were fixed as 5% and 10% (w/w). They observed that the peanut shell biochar gave a comparable UCS value of SBC compared to bare soil for different compaction conditions. However, a reduction in the UCS was found for all the other three soil-biochar composites sourced from water hyacinth, sawdust, and poultry litter.

2.8 Soil stabilization using biopolymer

Biopolymers are naturally occurring polymers produced via biological processes. These biopolymers are polysaccharides composed of a large network of bonded monosaccharide units. These monosaccharide units may be the simplest form of carbohydrates, which have carbon atoms bonded with hydroxyl groups (e.g., glucose, fructose, or galactose). Each monosaccharide unit in the polysaccharide easily interacts with water and form "hydrogels" when mixed with water. In the case of sandy soil, these hydrogels coat the surface of soil particles, form a bridge between soil grains, and bind the soil grains together (Chang et al., 2015), while in clays, in addition to coating, the stabilization is also achieved through either hydrogen and/or ionic bonding with clay particles depending on the intrinsic properties of the biopolymers chosen (Chang et al., 2015; Chen et al., 2013).

Cabalar and Canakci (2011) investigated the influence of xanthan gum on the strength of sandy soil via direct shear tests. They prepare the samples by mixing the loose sand with xanthan gum solution solutions of 1%, 3%, and 5% by mass of soil and create a homogenous paste. The prepared homogenous paste was then compacted at desired density and cured at room temperature for 7, 26, and 50 days. Thereafter, the cured samples were tested in direct shear. They reported that the samples with greater xanthan gum solutions of 3% and 5% had a higher angle of internal friction than those of bare samples, indicating that

the addition of xanthan gum improved soil strength. Further, it was also documented that the strength improvement was achieved within seven days of curing time, and no significant improvement in strength was noticed after seven days.

Chang et al. (2015) investigated the strengthening effect of xanthan gum on different soil types, namely sand (poorly graded sand), natural soil (poorly graded sand with silt), red yellow soil (clay with low plasticity), and kaolinitic clay (clay with high plasticity). Soils were mixed with 0.5%, 1%, and 1.5% of xanthan gum biopolymer (w/w) of soil and tested for compressive strength on 40mm×40mm×40mm cubical samples cured at 20 ℃ for 28 days.

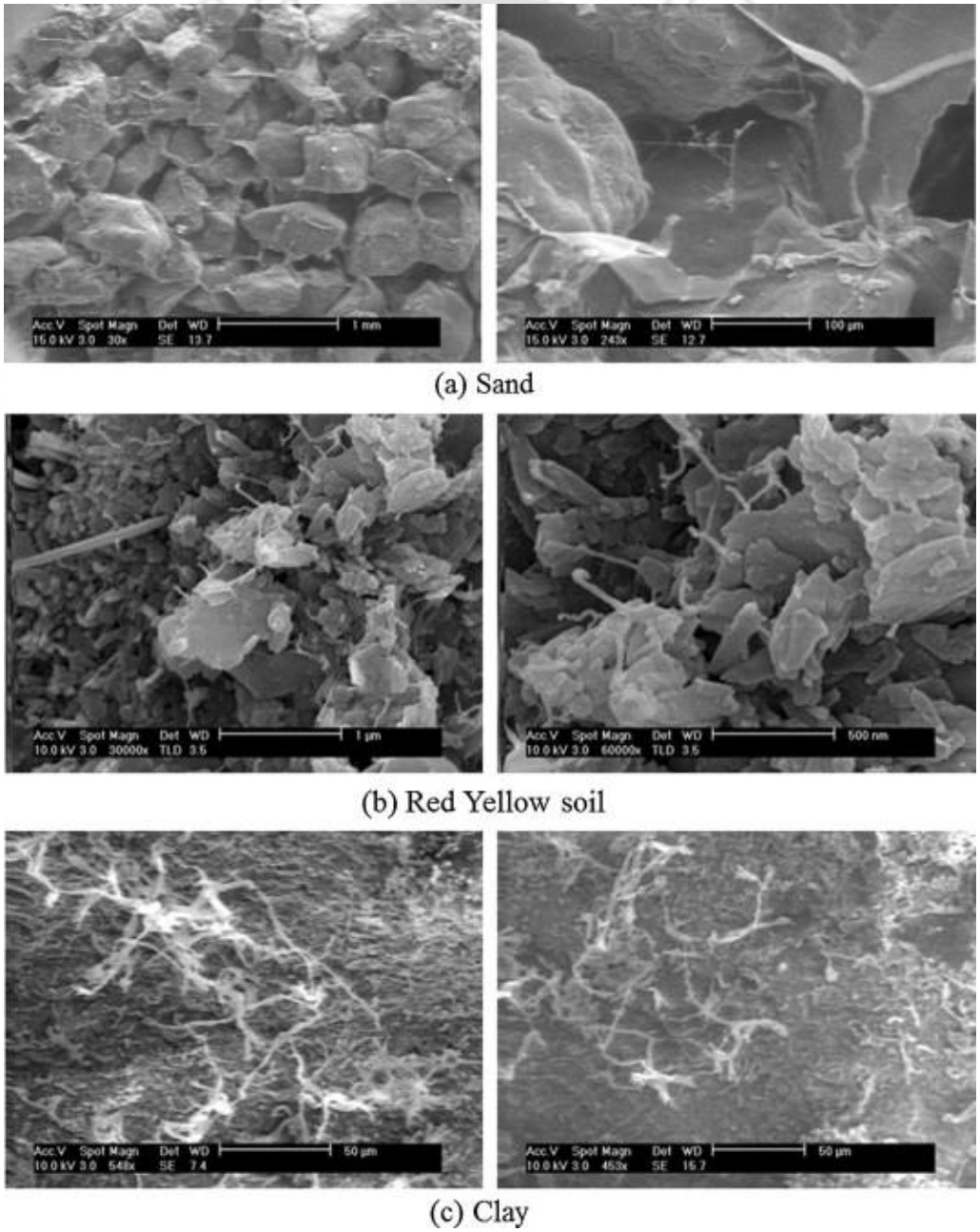

(a) Sand

(b) Red Yellow soil

(c) Clay

Figure 2.5 FESEM micrograph of xanthan gum-treated soil

They reported that the treated soils have more strength than the bare soils. From the micrographical analysis shown in Fig. 2.5, they found that in the case of sand, xanthan gum coated the grain surfaces and increased the interparticle contact area, while in clays, xanthan gum strands directly linked the clay particles, and these links are caused due to hydrogen bonding.

In another study, Chang et al. (2016) investigated the effect of gellan gum on the geotechnical behavior of cohesionless sand using an unconfined compression test and a direct shear test. The gellan gum content was kept at 0.5%, 1%, 2%, and 5% of the sand mass, and tests were performed under different moisture conditions: initial, dried, and re-submerged. In the initial condition, the samples were tested immediately after cooling. In dry condition, the samples were fully dried for 28 days at room temperature (20 °C), while in a re-submerged condition, the dried samples were submerged in water for 24 h before testing. The unconfined compression test was performed on a cubic sample of dimension 50 mm×50 mm×50 mm, and a direct shear test was conducted on a prepared sample of disk-shaped gellan gum-sand samples with a 50 mm diameter and 20 mm height. It was reported from the study that the gellan-gum-treated sand exhibited a higher UCS value compared to untreated sand. In terms of shear strength, a large improvement in cohesion and the friction angle of the sands in initial, dried, and re-submerged conditions.

Latifi et al. (2016) investigated the effect of xanthan gum on two fine-grained clays, viz., bentonite and kaolinite. The two soils were treated with 0.5%, 1%, 1.5%, 2%, and 2.5% of xanthan gum and tested for their unconfined compressive strength at 3, 7, 28, and 90 days. They found the maximum strength at 1.5% xanthan gum treated soil has higher strength as compared to untreated soil. Based on these UCS results, they also conducted the direct shear test at 1.5% content of xanthan gum on both soils. It was reported that there was a substantial increase in cohesion for both soils with curing, while the increase in the angle of internal friction was marginal. Further, it was also documented that significant changes in the treated soil occurred within 28 days of curing.

Qureshi et al. (2017) studied the strengthening effect of xanthan gum on desert sand through an unconfined compression test and slake durability test. Xanthan gum content was selected as 1%, 2%, 3%, and 5.0% of the dry soil mass. For comparison purposes, the sand specimens were also treated with 10 % cement. They documented that the xanthan gum substantially increases the UCS of the treated sand. The UCS increases with xanthan gum content up to 2% and thereafter decreases with an increase in xanthan gum content. The UCS

of sand treated with a cement content of 10% was in the same order as that of the 1% treatment with xanthan gum. It was noted from the slake durability test that the slake durability index of the sand treated with 3% xanthan gum was higher than that of the sand treated with 10% cement, indicating better durability performance of the xanthan-gum-treated sand.

Muguda et al. (2020) investigate the potential of guar and xanthan gum as stabilizers in earthen construction materials by conducting the durability test and hygroscopic test. In their study, different samples configuration such as cylindrical, brick, and tiles of different dimensions were fabricated. Thereafter, they conducted standard durability tests such as contact, suction, dip, and Geelong drip tests. From the results of dip and Geelong drip tests, it was reported that the biopolymer stabilized material performed better than untreated samples, while results from contact and suction tests did not show significant differences in behavior between untreated samples and biopolymer stabilized samples. The results of the hygroscopic test reported a higher moisture buffering value of biopolymer stabilized materials than untreated samples, therefore requiring less operational energy to maintain good indoor air quality within an earthen building.

2.9 Influence of pyrolysis temperatures on properties of biochar

The properties of biochar are highly dependent on biochar feedstock, pyrolysis temperature, and residence time (Zhao et al., 2013; Azargohar et al., 2014; Yuan et al., 2015; Zhang et al., 2017; Pariyar et al., 2020; Zhang et al., 2020; Muigai et al., 2021). The thermal characteristics of any material rely hugely on its mineralogical composition, surface structural characteristics, and physicochemical properties (Klett et al., 2004; Nzediegwu et al., 2021). The mineralogical composition, surface structural characteristics, and physicochemical properties of biochar are majorly influenced by the pyrolysis temperatures (Yuan et al., 2015; Hassan et al., 2020; Pariyar et al., 2020; Zhang et al., 2020; Muigai et al., 2021). Table 2.4 summarizes the most recent literature available on the effect of pyrolysis temperature on the microstructural and physicochemical properties of biochar generated from sugarcane bagasse (SB) and water hyacinth (WH). The pyrolysis temperature influences the essential features of biochar, such as ash content, pH, electrical conductivity, chemical composition, atomic ratio (H/C and O/C ratio), specific surface area (SSA), and total pore volume.

Table 2.4 Influence of pyrolysis temperature on physicochemical and surface characteristics of the produced biochar from SB and WH

References	Feedstock/ Biomass	Pyrolysis Temp (°C)	Ash (%)	pH	EC	H/C ratio	O/C ratio	SSA, TPV	APD
Melo et al. (2013)	SB	400,500, 600,700	Increased	Increased	Increased	Decreased	Decreased	NA	NA
Domingues et al. (2017)	SB	350,450,750	Increased	Increased	Increased	Decreased	Decreased	NA	NA
Kameyama et al. (2017)	SB	400,600,800	Increased till 600 and decreased at 800	Increased	Nearly constant	Decreased	Decreased	NA	NA
Zhang et al. (2017a)	SB	350-900@50 increment	Increased	Increased	Increased	Decreased	Decreased	NA	NA
Sun et al. (2018)	SB	300,400, 500,600	Increased	NA	NA	Decreased	Decreased	Increased	Decreased
Moradi-Choghamarani et al. (2019)	SB	300,400, 500,600	NA	NA	NA	Decreased	Decreased	Increased	Decreased
Chatterjee et al. (2020)	SB	500,600, 700,800	Increased	NA	NA	Inconsistent trend	Inconsistent trend	Increased	Decreased
Li et al. (2016)	WH	300,500,700	Increased	Increased	NA	Decreased	Inconsistent trend	Increased	Increased till 500 and decreased at 700
Huang et al. (2021)	WH	300 and 600	NA	NA	NA	Decreased	Decreased	Increased	Decreased
Muigai et al. (2021)	SB, WH	350 and 550	Increased	Increased	Increased	Decreased	Decreased	Increased	Decreased

SB: Sugarcane bagasse; WH: Water hyacinth; EC: Electrical conductivity; SSA: Specific surface area; TPV: Total pore volume; APD: Average pore diameter; NA: Not available

2.10 Critical appraisal of the literature review and research gap

Thermally active structures (TAS) such as crude oil pipelines, crude oil storage tanks, subsurface cold-storage, and geo-energy storage units are desired to have maximum thermal insulation for long-term heat storage. Heat loss is one of the major problems in TAS. Hence, there is a need for the application of thermal backfill material that can reduce heat loss from these projects. The locally available soil could be amended with low thermal characteristics material to reduce heat loss. A review of the existing literature has demonstrated that amendment of biochar in soil decreases its thermal characteristics, which depends on the type of soil, type of biochar, and amendment rate. The existing studies were conducted in the context of its application in agriculture to control heat fluctuation to optimize crop production. However, the understanding of the effect of dry density and moisture content of soil-biochar composite samples was not focused on in the existing studies, which majorly influences the thermal characteristics of the material.

The critical review highlights that the amendment of different biochar types and biochar particle size fractions in the soil changes soil material composition, change in total porosity, pore size distribution, and physicochemical properties in a different manner. Further, the different biochar types and biochar particle size fractions can also influence the optimum moisture content and dry density differently due to their unique water-holding capacity and porosity, which could subsequently influence thermal characteristics. Additionally, the reviewed literature also indicates that the shear strength parameters and unconfined compressive strength may increase or decrease with biochar inclusion in soil, and it depends on factors such as type of soil, type of biochar, particle size fraction of biochar, and biochar amendment rate. The available literature does not firmly confirm the improved strength characteristics of SBC.

A review of the existing literature has indicated that the SBC can be used as a potential thermal backfill material for the mitigation of heat loss. However, the design criteria of thermal backfill need to be assessed based on the density states, which are not considered in the existing studies. Moreover, the interaction of the SBC with the natural moisture migration due to groundwater movement and rainfall has not been systematically studied in the previous literature. The increase or decrease in the moisture level of thermal backfill could increase or decrease the thermal characteristics of SBC, resulting in more or less heat loss from the thermal backfill. Therefore, it is essential to investigate the effects of the initial molding state (initial dry density and molding water content) and subsequent

moisture interaction on the thermal characteristics of SBC. Moreover, an investigation on the influence of biochar amendment produced from different waste biomass and different biochar particle size fractions on thermal characteristics of soil is remarkably needed in view of applying as thermal backfill.

The thermal backfill structure should also have adequate strength to sustain self-weight. Therefore, there is a need to re-examine the influence of biochar amendment on the strength characteristics of soil in addition to its thermal characteristics considering soils of different textures, different biochar types, amendment rate, and biochar particle size fractions. In the case of strength reduction with the amendment of biochar in soil, a small quantity of biopolymer could be used to improve the strength of SBC. However, there is a lack of literature on the thermal characteristic of biopolymer-stabilized soil (BpS). Therefore, an investigation of the thermal characteristics of BpS and soil-biochar-biopolymer composite (SBPC) is essential in addition to the strength characteristics of BpS and SBPC.

Heat transfer in the soil mainly depends upon the initial degree of saturation, thermal characteristics of the soil, porosity, and pore geometry of the soil matrix. However, there is limited study on the investigation of heat transfer in biochar-amended soil. Therefore, to investigate the thermal insulation efficiency in terms of heat transfer through SBC and SBPC, a bench-scale study is also necessary to move toward field-scale applications. It is well established from the reviewed literature that the properties of biochar are highly dependent on biochar feedstock, pyrolysis temperature, and residence time. The thermal characteristics of any material depend upon its mineralogical composition, surface structural characteristics, and physicochemical properties, which might be controlled by the pyrolysis temperature. Therefore, it is required to investigate the changes in thermal characteristics of biochar produced at various pyrolysis temperatures to optimize the energy consumption requirements to minimize the material cost for the desired applications.

2.11 Objective and scopes of the work

The primary objective of the proposed research work is to explore the utility of soil-biochar composites (SBC) and soil-biochar-biopolymer composites (SBPC) as thermal backfill material. The study aims to transform waste biomass into biochar and evaluate its utilization and impact on the thermal characteristics of soil. Accordingly, the scopes of the study are outlined as follows-

1. In-house production of biochar from waste biomass using pyrolysis followed by physical, chemical, thermal, and microstructural characterization.
2. To study the influence of initial molding parameters, biochar type, and biochar particle size fraction on thermal and strength characteristics of SBC.
3. Investigation of thermal and strength characteristics of soil-biochar-biopolymer composite (SBPC).
4. To investigate the thermal insulation efficiency of the SBC and SBPC for mitigation of heat loss in thermal backfill.
5. Development of energy-efficient biochar for thermal backfill application.

CHAPTER 3

MATERIALS AND THEIR CHARACTERIZATION

In order to achieve the stipulated objective, the materials used in this research work are presented in this chapter. It includes basic geotechnical characterization of soils. This chapter presents the physical, chemical, mineralogical, and microstructural characterization of used soils and biochars.

3.1 Materials

Two natural soils of different textures viz., (i) RS1 (ii) RS2, suitable for thermal backfill, collected from a nearby natural vegetative slope inside the campus of Indian Institute of Technology Guwahati, Assam, India, were used in the present study. Both selected soils were surface soils collected within a depth of 20 cm from the ground surface. Dead roots, stones, and other impurities in the soil were removed, and the soil was sieved through a 4.75 mm sieve. Three types of biochar (based on the different types of waste biomass) were used in the current study. Among the three biochar, one is commercial biochar produced by Greenfield Eco Solutions Pvt. Ltd., Jodhpur, Rajasthan, India, from a hardwood of mesquite (*Prosopis juliflora*). The other two biochar were produced from the locally available biomass of water hyacinth stem (*Eichhornia crassipes*, an aquatic plant) and sugarcane bagasse. Xanthan gum, a commercially available biopolymer manufactured by Sigma Aldrich, was also used in the current study.

3.2 Biochar production

The commercial biochar is produced from a hardwood of mesquite (*Prosopis juliflora*) as feedstock at 500 °C and 45 minutes residence time. The purchased biochar mass was initially in a large particulate form. For the small-scale laboratory test, the obtained biochar was crushed using a mechanical grinder, air-dried, passed through a 4.75 mm sieve, and stored in an airtight container. Biomass of water hyacinth (WH) and sugarcane bagasse (SB) were collected from a lake and local market in Amingaon, North-East, India (latitude 26.1847 °N, longitude 91.6672 °E). All the required WH plants were collected from the same water body in a single day to minimize any genetic variation. Both the feedstocks were first rinsed with running water to remove dirt and eliminate contaminants. The collected waste biomasses were air-dried and cut to a size of nearly 30 mm to ensure the complete pyrolysis

of feedstock in the furnace. Further, they were oven-dried at 60 °C for 72 hours and stored in an airtight container. The thermogravimetric analysis (TGA) was initially done on both raw biomasses to decide the pyrolysis temperature of the feedstock. Previous researchers suggested that the breakdown of hemicellulose, cellulose, and lignin occurs stagewise at temperatures approximately 195–255 °C, 235–345 °C, and 275–500 °C, respectively (Chen et al., 2019; Tomczyk et al., 2020). Derivative thermogravimetric (DTG) curve shows that the maximum degradation of biomass was observed at 312 °C and 332 °C for water hyacinth and sugarcane bagasse, respectively. Hence, as per the TGA and DTG curve of the feedstock (Fig. 3.1), the pyrolysis temperature in the pyrolyzer was selected at 500 °C for both feedstocks. Slow pyrolysis was selected as the pyrolysis method for biochar production as it offers the highest yield of biochar (Manyà, 2012). The biomass was pyrolyzed at 500 °C, at a heating rate of 10 °C min^{-1} and a holding time of 45 min in a fixed batch reactor under an argon atmosphere (Muigai et al., 2021). The produced biochars from pyrolysis were pulverized, passed through a 2 mm sieve, and kept in an airtight container for further testing.

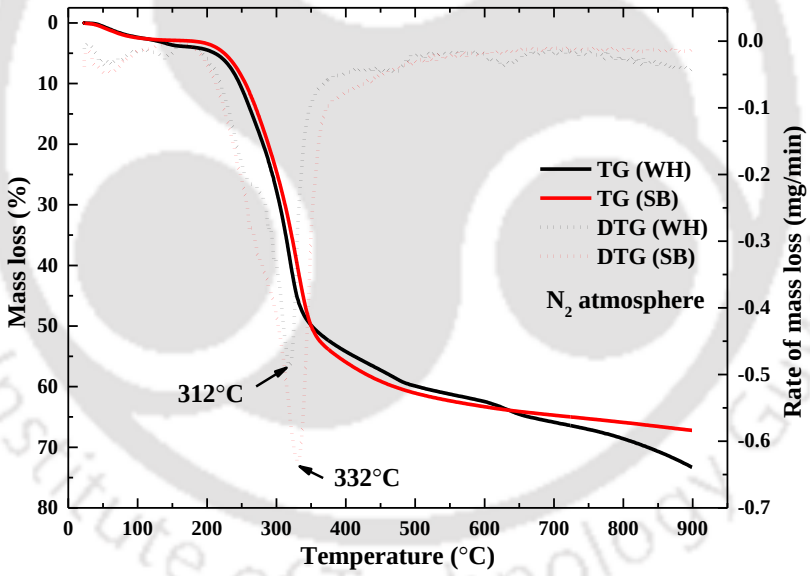

Figure 3.1 TGA and DTG curve of WH and SB biomass

3.3 Basic characterization of soil

The basic physical and geotechnical properties of the soils are performed following the guidelines recommended in the ASTM standard. The soil index properties, such as particle size distribution, specific gravity, consistency limits, and the compaction characteristics of soils, were determined according to ASTM standards (ASTM D422-63, 2007; ASTM D4318-10, 2010; ASTM D698-12, 2012; ASTM D854-14, 2014). Based on these above characterizations, the soil samples were classified according to the unified soil

classification system (USCS) and the United States Department of Agriculture (USDA). The tests were conducted in triplicates, and the average value obtained from these tests is reported in Table 3.1. The standard deviation of the triplicate measurements from the average for specific gravity was ± 0.03. Similarly, the standard deviation of the triplicate measurements from the average for Atterberg limits varied between ±1.02 to ±1.58. The MH (Highly plastic silt) soil exhibited a specific surface area (m^2g^{-1}) of 41.35±1.38, while the SC (Clayey sand) soil displayed a value of 9.95±1.12.

Table 3.1 Basic geotechnical properties of the used soils

Properties	RS1	RS2
Coordinates	26.1965 ˚N; 91.6962 ˚E	26.1889 ˚N; 91.6951 ˚E
Environmental temperature (℃)	29±3 ℃	29±3 ℃
Relative humidity (%)	80-90	80-90
Specific gravity	2.71	2.69
Particle size distribution (%)		
Coarse sand (4.75–2 mm)	0.8	2.7
Medium sand (2–0.425 mm)	12.1	15.1
Fine sand (0.425–0.075 mm)	9.1	35.3
Silt (0.075-0.002mm)	39.74	36.81
Clay (< 0.002 mm)	38.26	10.09
Atterberg limits (%)		
Liquid limit	54.42	37.13
Plastic limit	35.25	26.21
Shrinkage limit	30.12	19.12
Plasticity index	19.17	10.92
USCS soil classification	MH	SC
USDA soil classification	Clay loam	Sandy loam
Taxonomy	Ultisols	Ultisols
Specific surface area ($m^2 g^{-1}$)	41.35	9.95

3.4 Basic characterization of biochar

The proximate analysis of the biomass and biochar produced was carried out following the guidelines of the American Society for Testing and Materials (ASTM). Moisture content, ash content, volatile matter, and fixed carbon content were determined using ASTM standards (ASTM D3173-17, 2017; ASTM D3174-12, 2018; ASTM D3175-20, 2020; ASTM D3172-13, 2021). The CHNS elemental analyzer was used to determine the elemental analysis (percentage of C, H, N, and S) of biomass and biochars (Eurovector, EuroEA3000, Country: Italy). The difference between other elements (ASTM E870-82, 2019) was used to compute the oxygen content (O), [O (%) = 100 - (C+ H +N +Ash)]. The H/C and O/C atomic ratios were computed to measure the carbon stability of biochar in soil.

The pH and EC of soil, biochar, and SBC were determined according to Carter, 1993, and IBI standard 2.1, 2015 using pH and EC electrodes (EUTECH instruments, ECPC 270043S, Singapore). The weight to volume (solid: water) ratio was kept as 1:20, 1:10, and 1:10 for biochar, soil, and soil biochar mixes, respectively. The zeta potential of biochar was measured using Electrophoretic Light Scattering method (Make: Anton Paar, Model: Litesizer™ 500, USA). A solution of 0.1 g biochar in 100 ml deionized water was prepared, and a small amount of the solution was placed into the sample well in the Zeta-Meter System. The water holding capacity (WHC) of biochar was determined by immersing a known weight of oven-dried biochar with deionized water for 48 hours. Thereafter, the wet weight of biochar was measured after gravity drained for 2 hours through a Whatman grade 1 filter paper. The WHC was expressed as the ratio of water retained weight to the initial weight of dry sample. The tests were conducted in triplicates, and the average value obtained from these tests is reported in Table 3.2.

Table 3.2 Physicochemical, surface, and pore characteristics of biochars

Properties	HWBC	WHBC	SBBC
Feedstock	Hard Wood of mesquite	Water hyacinth stem	Sugarcane bagasse
Pyrolysis process	Slow pyrolysis	Slow pyrolysis	Slow pyrolysis
Pyrolysis temperature (°C)	500	500	500
Proximate Analysis (%)			
Moisture content	10.12	5.12	6.09
Volatile matter	12.84	20.04	15.42
Ash content	2.12	24.45	3.82
Fixed carbon[a]	74.92	50.39	74.67
Ultimate Analysis (%)			
Carbon (C)	74.01	48.28	78.93
Hydrogen (H)	3.05	2.14	3.57
Nitrogen (N)	0.18	1.04	0.74
Oxygen (O)	20.64	24.09	12.94
Atomic ratios			
H:C	0.49	0.53	0.54
O:C	0.21	0.37	0.12
C:N	479.69	54.16	124.44
Specific gravity	1.498	1.046	0.605
pH	7.79	9.84	9.16
EC (mS cm^{-1})	0.560	19.44	1.52
Zeta potential (mV)	-27.2	-46.2	-64
Water holding capacity (%)	212.07	616.20	874.08
Specific surface area ($m^2 g^{-1}$)	100.729	30.806	21.787
Average pore diameter (nm)	2.723	6.175	8.423
Total pore volume ($cm^3 g^{-1}$)	0.068	0.047	0.045

[a] By difference; Values are represented as mean value ± standard deviation

The standard deviation of the triplicate measurements from the average for proximate analysis results varied between ±0.12 to ±1.42. The hardwood biochar (HWBC) exhibited a specific gravity of 1.498±0.03, while the water hyacinth biochar (WHBC) and sugarcane bagasse biochar (SBBC) showed a specific gravity of 1.046±0.02 and 0.605±0.02, respectively. The standard deviation of the triplicate measurements from the average for pH, electrical conductivity (EC), and Zeta potential results was ± 0.02, ±0.01 to ±0.12, and ±1.1 to ±1.4. The biochar has high pH due to its base cation concentrations and high electrical conductivity (EC) due to the presence of higher soluble salts in the biochar (Chintala et al., 2014). The WHBC exhibited higher pH and electrical conductivity (EC) as compared to HWBC and SBBC. This is attributed to the presence of a higher amount of ash content in WHBC than in HWBC and SBBC (Sangani et al., 2020; Muigai et al., 2021). Moreover, biochar has a high water-holding capacity, which is primarily credited to the higher surface area, intra-pores, and presence of various functional groups (Zhang and You, 2013). The WHC of SBBC has the highest value (874±18.5%), while the WHBC and the HWBC had the WHC of 606±8.6% and 212±4.0%. This might be due to the high differential pore volume and higher zeta potential value of SBBC than WHBC and HWBC. Microstructural characterization of soil and biochar

3.5 Microstructural characterization of soil and biochar

The surface morphology of the sample was captured using field emission scanning electron microscopy (FESEM) (Make: Zeiss, Model: Gemini 300, Oberkochen, Germany). The same instrument was also used for Energy dispersive X-ray spectroscopy (EDX) analysis. A small amount of oven-dried samples collected post-tests were mounted on an aluminum stub, and the sample was coated with a 20 nm gold coating for SEM analysis. The surface morphology of HWBC, WHBC, and SBBC is presented in Fig. 3.2, respectively. The honeycomb structure of intra-pores in biochar is due to the presence of lignin, cellulose, and hemicellulose biopolymer. During pyrolysis, the cellulose and hemicellulose degrade first, and lignin degrades last. This thermal decomposition led to the porous nature of biochar.

The mineralogical composition of the sample was determined by X-Ray diffraction (XRD) equipped with Cu-kα X-ray source D/tex ultra 250 solid-state detectors (λ = 1.54 A). (Make: Rigaku, Model: SmartLab9KW, Japan). The oven-dried samples were micro-ionized for the XRD analysis. The sample was scanned with a step size of 0.02° for 5°-70° diffraction angles at a scanning speed of 20° 2θ/min. Thereafter, obtained XRD data was analyzed using previously published data and the International Centre for Diffraction Data (ICDD-PDF).

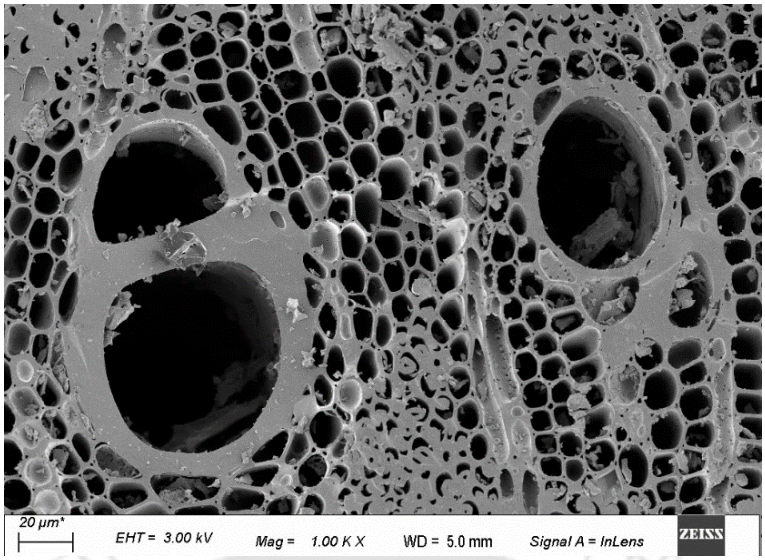

(a)

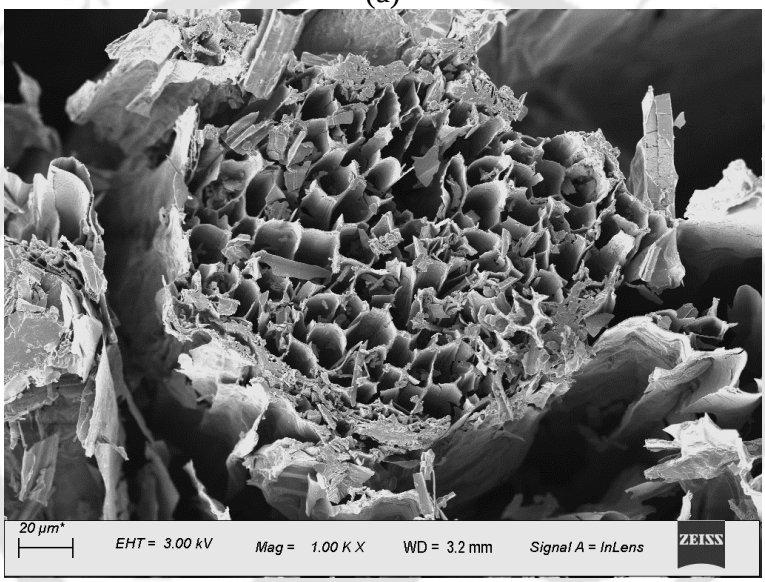

(b)

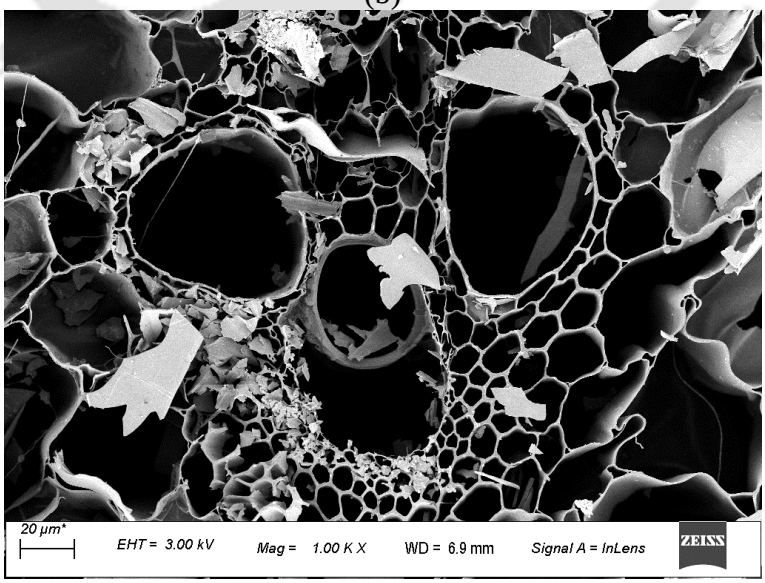

(c)

Figure 3.2 Surface morphology of (a) HWBC, (b)WHBC, and (c) SBBC

The XRD spectra of soils and biochars are presented in Fig. 3.3. The XRD diffractograms reveal that Quartz (Q) is a predominant material, followed by Mica (M), Halite (Ha), Hematite (He), and Kaolinite (K) in both MH and SC soil. For HWBC, the peak corresponds mainly to quartz (Q) (2θ = 26.6°) and calcite (C) (2θ = 29.3°). Comparatively, for the WHBC, the peak mainly corresponds to the quartz (Q) (2θ = 26.6°), sylvite (S) (2θ = 28.3°, 50.2°), and calcite (C) (2θ = 29.3°). The carbon content present in the SBBC is completely amorphous, which is reflected in the amorphous hump between 15° and 30° 2θ Bragg's angle.

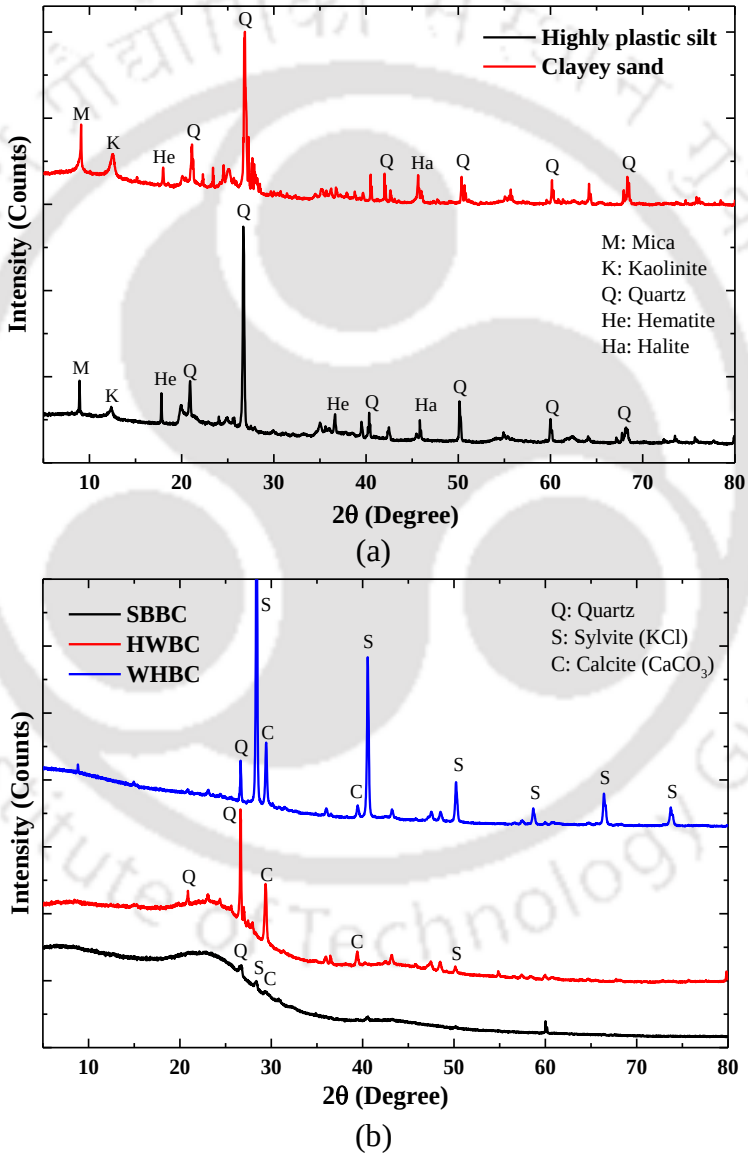

Figure 3.3 X-ray diffraction spectra of (a) soil; and (b) biochar used in this study

The surface functional groups were identified using the Attenuated Total Reflectance (ATR) method on the Fourier-transform infrared spectroscopy (FTIR) spectra of powdered biomass and biochar recorded by an FTIR spectrometer (PerkinElmer, Spectrum Two,

Waltham, MA, USA). The analysis was performed in the range of 400-4000 wavenumbers with 20 consecutive scans at 4.0/cm resolution in transmittance mode. FTIR spectra of used soils and biochar used in the current study are presented in Fig. 3.4 (a and b).

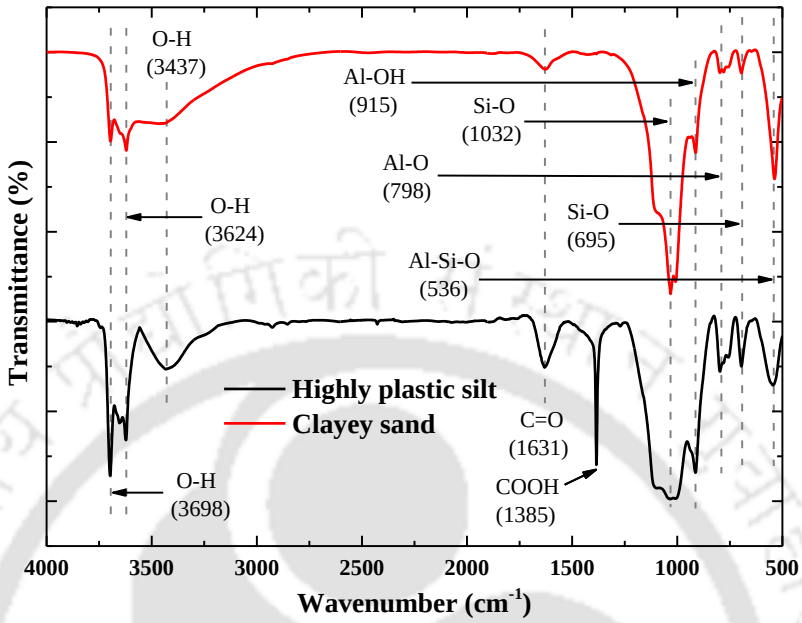

(a)

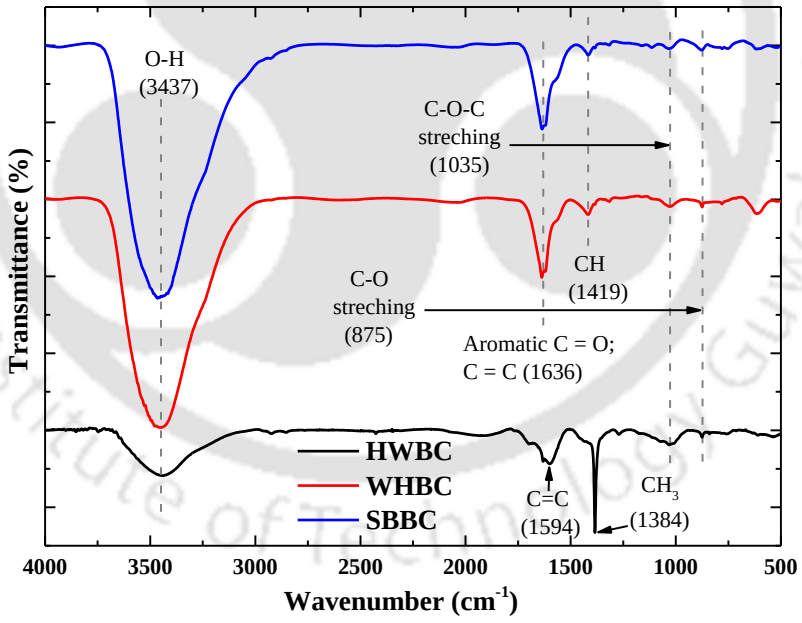

(b)

Figure 3.4 FTIR spectra of (a) soils and (b) biochars

The specific surface area (SSA), intraparticle pore size, pore size distribution, and intra-pore volume were determined on dry samples via N_2 adsorption at 77 K using surface area and pore size analyzer (Make: Quantachrome, Model: Autosorb-IQ MP, USA). The soil and biochar samples were degassed at a temperature of 120 ℃ and 200 ℃ for 3 and 6 hours, respectively, after drying them in an oven at 105 °C overnight.

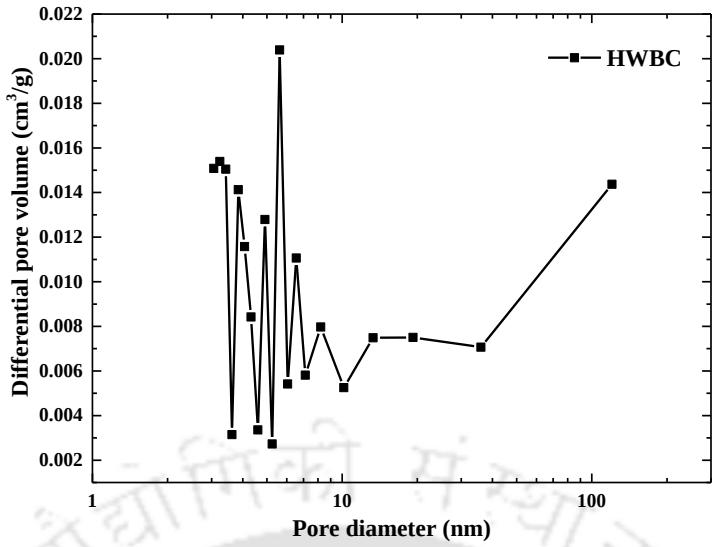

(a)

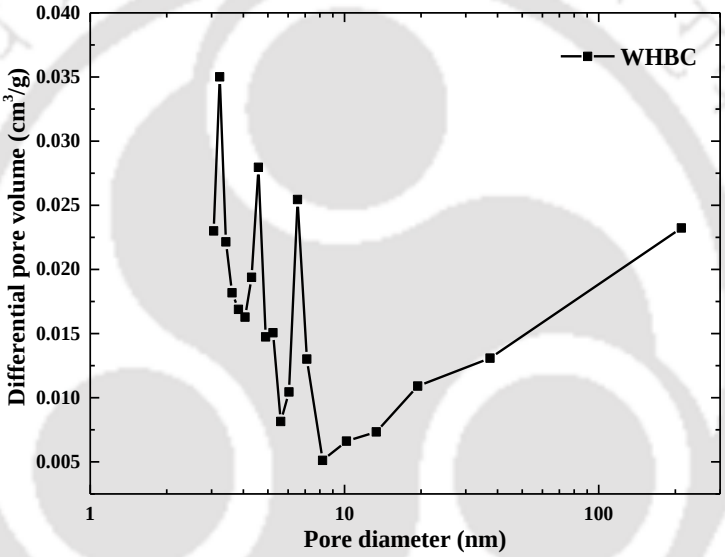

(b)

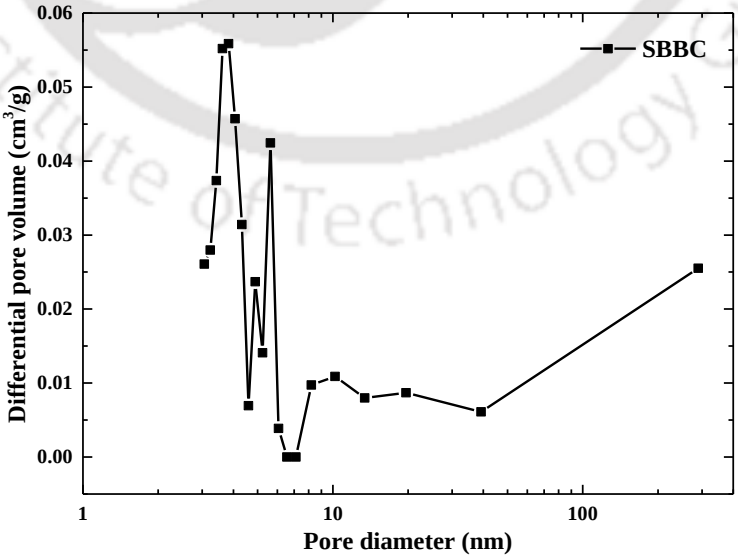

(c)

Figure 3.5 Pore size distribution of (a) HWBC; (b) WHBC; (c) SBBC

The hardwood biochar (HWBC) exhibited a BET surface area of 100.73 $m^2 g^{-1}$, while the WHBC and SBBC showed a specific gravity of 30.81 $m^2 g^{-1}$ and 21.79 $m^2 g^{-1}$, respectively. Fig. 3.5 presents the pore size distribution of different types of biochar. It can be observed from the figure that the maximum number of pores lies within 20 nm for all types of biochar. The HWBC has a maximum pores size of 120.38 nm, while the WHBC and SBBC possess a maximum pores size of 211.37 nm and 289.83 nm, respectively.

A thermogravimetric analyzer was used to investigate the thermal stability of biomass and biochar using differential thermogravimetric (DTG) and thermogravimetric analysis (TGA) (Netzsch, STA449F3A00, Germany). The samples were weighed into an Al_2O_3 crucible (about 7 mg to 8 mg dry weight), and the temperature was raised from 25 °C to 900 °C in a nitrogen environment at a rate of 10 °C/min. Fig. 3.6 presents the thermogravimetric analysis of soils and different types of biochar, reflecting the thermal stability of soils and biochar. The mass loss in the temperature range of 50–200 °C is generally regarded as dehydration due to the loss of free water between the clay layers. The subsequent mass loss in the soil between 400 and 600 °C is due to the removal of structural water from the clay mineral (Priyadharshini et al., 2019). The mass loss in biochar before 110 °C is generally regarded as moisture removal. The subsequent mass loss can be primarily attributed to the decomposition of organic matter in biochar.

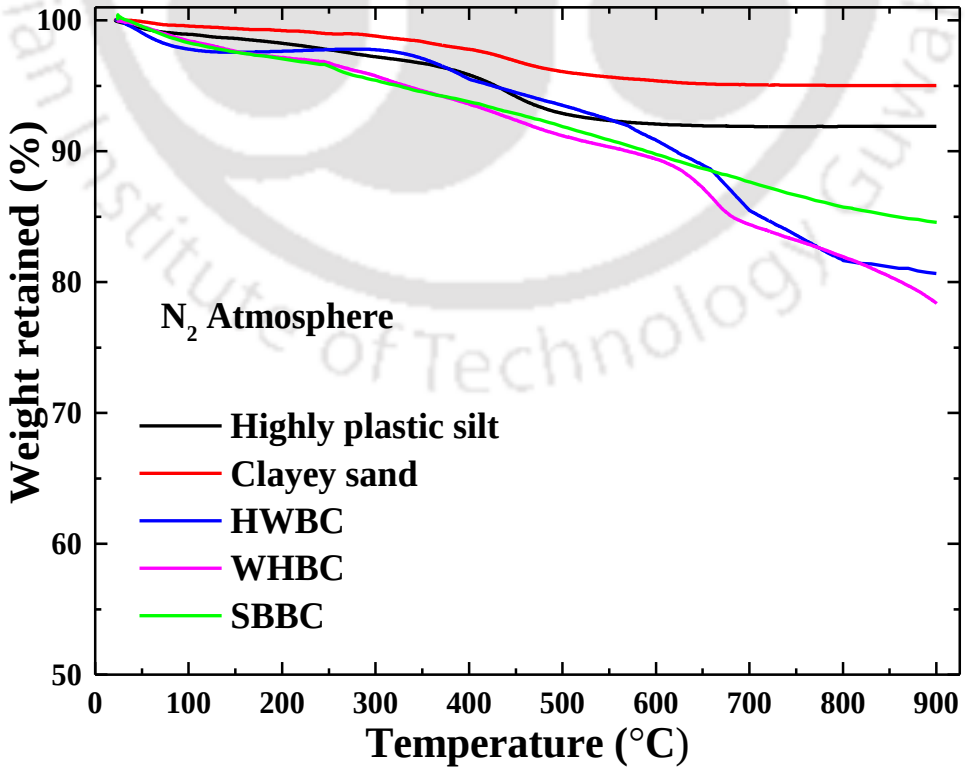

Figure 3.6 TGA of soils and biochars

CHAPTER 4

INFLUENCE OF INITIAL MOLDING PARAMETERS AND MOISTURE MIGRATION ON THERMAL CHARACTERISTICS OF SOIL-BIOCHAR COMPOSITE

4.1 Introduction

It is evident from the literature that biochar amendment in soil decreases its thermal characteristics (Usowicz et al., 2016; Zhao et al., 2016; Liu et al., 2018). However, all the studies were mainly conducted in the context of its application in agriculture to control heat fluctuation to optimize crop production. In the above study, the effect of dry density was not considered. Liu et al. (2018) documented that the biochar application rate of up to 2.5% had no substantial influence on soil thermal characteristics compacted at a particular dry density of 1.3 Mg m^{-3} and distinct soil moisture content. However, the influence of higher biochar amendment (5% to 15%) on soil thermal characteristics corresponding to different initial molding states has not been well explored by Liu et al. (2018).

During field application, it may not always be possible to achieve the desired controlled and fully known initial compaction conditions (Ghosh and Pekkat, 2019). Hence, it is important to appraise the changes in thermal characteristics as a function of the initial molding state. Moreover, the underground granular material might often interact with moisture due to groundwater movement and rainfall. With groundwater movement and rainfall, the water infiltrates into the soil, which increases the soil's thermal characteristics resulting in more heat loss from the thermal backfill (Tong et al., 2020). Therefore, it is imperative to envisage the effects of the initial molding state and subsequent moisture interaction on the thermal characteristics of such SBC. Moreover, determining the relationships between the thermal characteristics of SBC and its compaction characteristics, such as dry density (ρ_d), molding water content (w), and biochar content (BC), is paramount for designing its field-scale application.

Therefore, this chapter explores the influence of the molding parameters (dry density and molding water content) on the thermal characteristics of soil with biochar amendment rates of 5% to 15%. In this chapter, a highly plastic silty soil and hardwood biochar sieved through a 2 mm sieve were used. Considering measured results, soil and biochar-specific multiple linear regression (MLR) equations were established for quantifying thermal

characteristics as a function of ρ_d, w, and BC. The MLR equations were further verified with independent laboratory measurements for SBC, along with a sensitivity analysis. Further, a correlation was explored between the change in K and C with the change in the degree of saturation of soil and SBC. A summary of the work plan can be comprehended by the flow chart in Fig. 4.1.

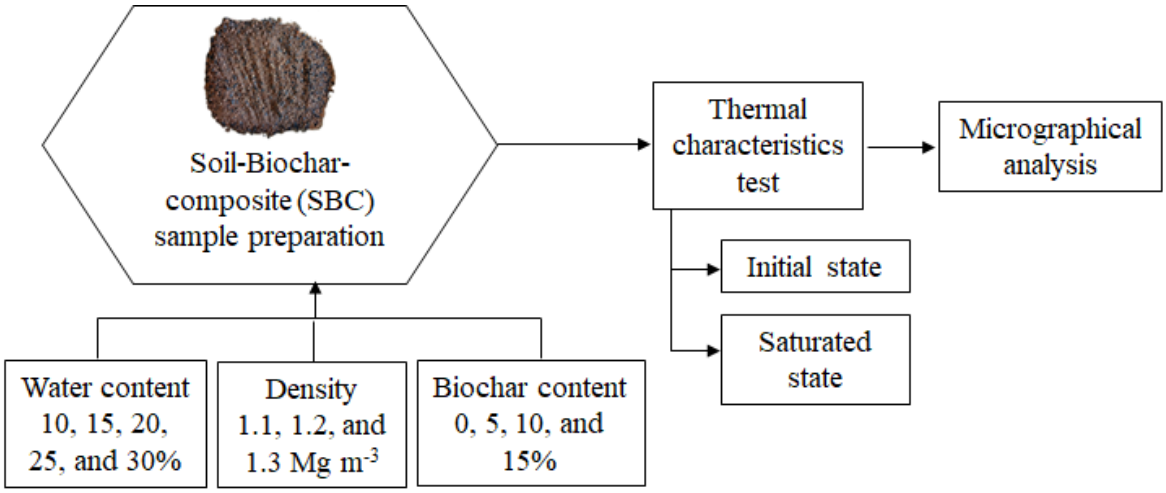

Figure 4.1 Summary of the experimental plan to investigate the influence of molding parameters and moisture migration

4.2 Compaction characteristics

The compaction characteristics (i.e., optimum moisture content (OMC) and maximum dry density (MDD) of the bare soil and SBC were determined using the guidelines recommended in ASTM standard (ASTM D698-12, 2012). Laboratory experiments were performed on the mixtures of soil and biochar at different weight proportions. The dry soil and biochar were mixed manually for 15 minutes, and proper care was taken to achieve a homogeneous mixture. Further, the distilled water was added to the dry sample and mixed thoroughly to minimize any lumps' formation. The moist soil or soil-biochar mixes were kept in closed plastic bags for 24 hours in a desiccator to allow uniform moisture distribution throughout the soil mass.

4.3 Sample preparation and test setup

For the preparation of soil-biochar composite (SBC) samples, a calculated amount of dry soil and biochar were weighed considering the volume of mold and target density. After that, weighed soil mass and biochar were homogenously mixed on a glass plate using a spatula first. Later, the precalculated amount of distilled water equal to the target moisture

content of the samples was mixed thoroughly with soil-biochar mixes. The moist SBC was kept in closed plastic bags for 24 hours in a desiccator to allow uniform distribution of moisture throughout the sample.

The soil and SBC samples were prepared at a dry density (ρ_d) of 1.1, 1.2, and 1.3 Mg m^{-3}. The molding water content was kept at 10%, 15%, 20%, 25%, and 30% by dry weight of soil. The biochar content was selected as 5%, 10%, and 15% dry weight of soil. The molding water content is defined as the initial water content used for sample preparation. It is recommended to compact the thermal backfill at a minimum of 95% of MDD to attain strength and stability (Howard, 1996). Therefore, the maximum density was selected as 1.3 Mg m^{-3} on the basis of obtained MDD for 15% SBC. The thermal characteristics were not determined on a completely dry sample due to difficulty in compacting and probe insertion in the SBC at a higher dry density. To prepare samples, a precalculated quantity of biochar and soil was thoroughly mixed with a predetermined quantity of distilled water to attain the molding water content. Additionally, to ensure that the sample was evenly moist throughout, the moist SBC was stored in sealed polyethylene bags in a desiccator for 24 hours. The moist sample was then compacted in the cylindrical container in three layers using a static loading machine and a plunger to achieve the required dry density.

4.3.1 Thermal characteristics measurement

The thermal characteristics of pure biochar, soils, and SBC specimens were measured using KD2 Pro Dual-needle SH-1 sensors developed by Decagon Devices Inc., Pullman, WA, which works on the transient heat flow method. The sensors have two parallel probes 30 mm long and 1.3 mm diameter with 6 mm spacing and can measure thermal conductivity (*K*), volumetric heat capacity (*C*), and thermal diffusivity (D) by employing the dual needle heat pulse method. The detailed background theory of thermal probe to measure soil thermal properties of soil can be found in Sah and Sreedeep (2014). The thermal characteristics of the biochar, soils, and SBC were measured by compacting in an acrylic mold with an inner diameter of 80 mm and a height of 60 mm. The selected dimension is sufficient to prohibit the boundary effect due to the needle probe's heating (Brandon and Mitchell, 1989; Cai et al., 2015). The distance between the probe and the outer boundary (i.e., acrylic wall) was 5.86 times the probe-to-probe spacing to avoid any boundary effect, which is more than the recommended value (i.e., 2.37 times) provided by Campbell et al. (1991).

The experimental setup for the measurement of thermal characteristics is presented in Fig. 4.2. To evaluate the thermal characteristics of the biochar; it was compacted in a three-layer structure without using static compaction by periodically tamping the side wall of the cylindrical container. To measure the thermal characteristics of SBC, a sharp-edge dummy steel needle with a diameter slightly less than the actual probe was used to create a dummy hole to enable easy penetration of the needle probe in the compacted sample. The thermal probe was allowed to attain equilibrium with soil temperature before measurements as per the recommendation outlined in KD2 Pro (2016). In order to measure the thermal characteristics at the initial and saturated state, the thermal probe was placed into the samples' top surface in the middle.

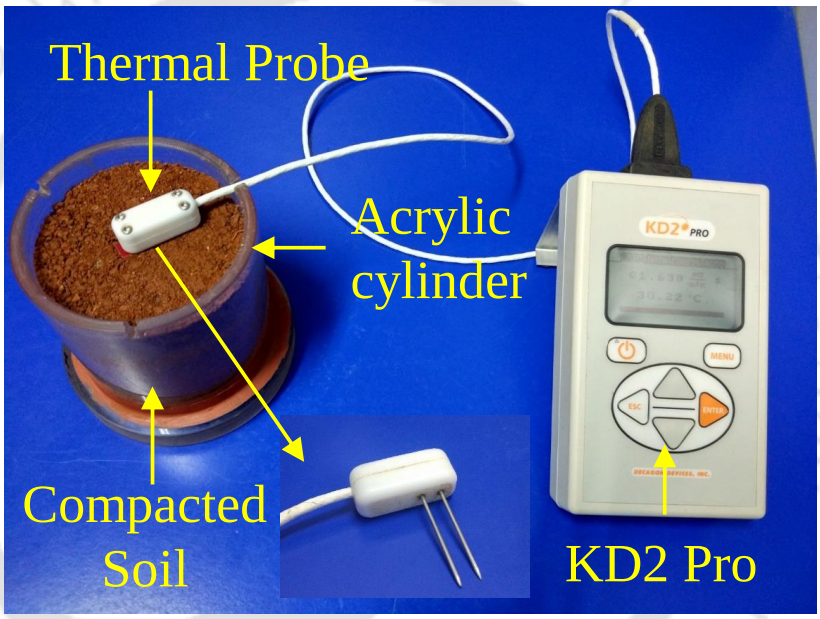

Figure 4.2 Experimental setup for thermal characteristics measurement

To investigate the influence of moisture migration on thermal characteristics, the experimental setup was modified, as shown in Fig. 4.3. To measure the thermal characteristics in a saturated state, a duplicate set of SBC samples was further saturated with distilled water by injecting water from the bottom of the sample under a constant head (50 mm) using Mariotte's bottle. A porous stone and a Whatman 42 filter paper were placed at the base of the cylindrical mold for uniform water circulation. The sample was considered to be saturated when the water overflowed at a constant rate from the upper water outlet of the mold. Overall, 180 sets of measurements of thermal characteristics were conducted for both initial state and saturated states. For each test condition, three replicate samples were examined to ensure the consistency of the thermal data, and their average value was stated.

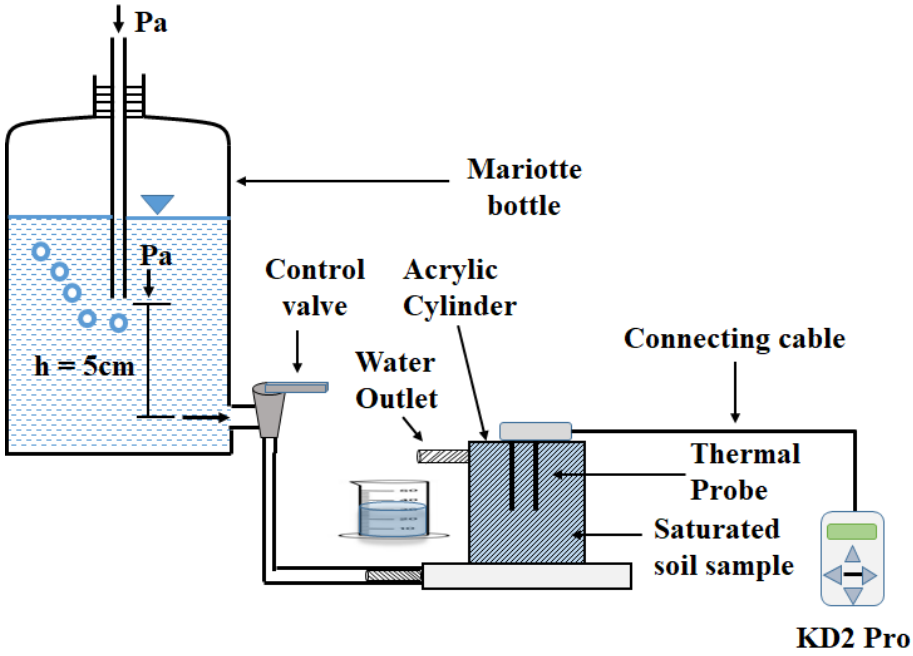

Figure 4.3 Experimental setup for measuring thermal characteristics of SBC in the saturated state

4.4 Multiple linear regression (MLR) and sensitivity analysis

4.4.1 Development of MLR

The impact of initial molding parameters (ρ_d and w) and biochar content (BC) on *K* and *C* for specific soil and their quantitative relationship was examined using multiple linear regression (MLR) analysis. The common structure of the simple MLR is

$$y = \beta_0 + \beta_1 x_1 + \beta_2 x_2 + \cdots + \beta_k x_k + e \quad (4.1)$$

where y is the estimated variable (*K* and *C* in this case). The parameters β_1, β_2,….., β_k are the regression coefficients related with x_1, x_2..., x_k respectively, and e is the random error component (Ghosh and Pekkat, 2019). For MLR analysis, 120 measured values were randomly chosen from the total 180 thermal measured values. The competence of the developed regression equations was accessed by R^2 value. Thereafter, the adequacy of the developed MLR equations was validated using another set of 60 measured thermal characteristics data points for bare soil and SBC.

4.4.2 Sensitivity analysis

The influence of input variables (w, ρ_d, and BC) on the thermal characteristics of soil and SBC was quantified by a sensitivity index evaluated by a one-at-a-time measure (Saraiva et al., 2017). The sensitivity index was calculated by the method of difference, which is

based on the difference between the system response y_{ij} and the base solution β for variations in a particular variable. For y_{ij}, i varies from 1 to m, where m is the total number of variables, and j=1-n, where n is the number of evenly spaced sample points. The sensitivity index S_d (x_i) is computed by

$$S_d(x_i) = \frac{\sum_{j=1}^{n} S_{ij}}{n} \tag{4.2}$$

where x_i is the variable; and S_{ij} = partial sensitivity index for the j_{th} sample point of the curve x_i and expressed by

$$S_{ij} = \frac{|y_{ij} - \beta|}{\sum_{i=1}^{m} |y_{ij} - \beta|} \tag{4.3}$$

Eqs. (4.2) and (4.3) were used to establish a quantitative depiction of the sensitivity index of each variable taken in the current study (γ, *w*, and BC). This technique aids in determining how sensitive the variables are to changes in percentage.

4.4.3 Statistical analysis

Two-way analyses of variance (ANOVA) were carried out in Minitab software (Version 17.3.1) which was used to understand whether the independent factors such as water content (w), density (ρ_d), and biochar content (BC) had an impact on the dependent variable (*K* and *C*). The experimental data were analyzed at a confidence level of 95% to define the statistical significance of independent parameters (molding water content, initial dry density, and biochar content) on the dependent (or response) variable (*K* and *C*). It means that when the observed *P*-value is less than 0.05, the difference is regarded as statistically significant.

4.5 Results and discussion

4.5.1 Effect of biochar amendment on the physicochemical properties of soil

The soil exhibited a specific gravity of 2.71, and it was observed to be reduced by 4%, 8%, and 10% while adding 5%, 10%, and 15% biochar content, respectively. This is primarily explained by the substitution of dense soil particles (higher specific gravity) with lightweight and porous biochar particles, which increase air entrapment (Reddy et al., 2015). The pH of bare soil was 4.77, and it was increased by 12%, 21%, and 32 % while adding 5%, 10%, and 15% biochar content, respectively. Similarly, the electrical conductivity (EC) of bare soil was 45.10 µS cm^{-1}, and it was found to be enhanced by 186%, 305%, and 436%

for the respective addition of 5%, 10%, and 15% biochar content. The increase in soil pH and EC can be accredited to the alkalinity, calcium carbonate, and base cation concentration of the biochar (Chintala et al., 2014). The variation of OMC and MDD of bare soil with different biochar content is presented in Table 4.1. The MDD of bare soil was 1.58 Mg m^{-3}, and it was observed to be reduced by 9%, 14%, and 18% for the respective addition of 5%, 10%, and 15% biochar content. The relatively smaller density and larger porosity of biochar compared to the soil are primarily responsible for the reduction in dry density of soil with biochar incorporation (Blanco-Canqui, 2017). Additionally, air entrapment caused by the amendment of extremely porous biochar lowers the compressibility of the composite sample at provided compaction energy, resulting in a reduced dry density (Reddy et al., 2015). The OMC of the studied soil was 22.72 %, and it was found to be enhanced by 16%, 27%, and 39% with the addition of 5%, 10%, and 15% biochar content, respectively. The increment in the OMC of soil is mainly ascribed to the larger surface area and higher pore volume of biochar particles, which increase the water absorptive capability of soil biochar composite (Blanco-Canqui, 2017).

Table 4.1 Effect of biochar on physicochemical and compaction characteristics of the soil

Content by dry weight: %		Soil-Biochar composite				
Soil	Biochar	Specific gravity, G_S	pH	EC (µS cm^{-1})	OMC (%)	MDD (Mg m^{-3})
100	0	2.71±0.011	4.77±0.026	45.10±0.577	22.72	1.58
95	5	2.61±0.013	5.35±0.010	128.83±0.651	26.25	1.44
90	10	2.48±0.015	5.79±0.021	182.43±4.406	28.75	1.36
85	15	2.43±0.010	6.30±0.031	241.83±3.121	31.52	1.29

4.5.2 *Thermal characteristics of biochar*

The *K* and *C* of the biochar used in this study were measured as 0.134 $Wm^{-1}K^{-1}$ and 0.752 $MJm^{-3}K^{-1}$ at the dry density of 0.478 Mg m^{-3}. Previous researchers also reported a similar value (Usowicz et al., 2016; Zhao et al., 2016; Liu et al., 2018). Compared to the approximate *K* values of sand (1.5-3 $Wm^{-1}K^{-1}$), clay (0.5-1 $Wm^{-1}K^{-1}$), and water (0.595 $Wm^{-1}K^{-1}$, at 20 °C), the observed *K* value of biochar was significantly lower (Lu et al., 2007; Zhang et al., 2017). Similarly, the measured *C* value of biochar was lesser than the approximate *C* value of water (4.184 $MJm^{-3}K^{-1}$), soil organic matter (2.5 $MJm^{-3}K^{-1}$), and soil mineral (1.9 $MJm^{-3}K^{-1}$) (Hanson et al., 2000; Zhao et al., 2016). The presence of intra-pores air in the biochar skeleton is primarily responsible for the lesser *K* and *C* values of biochar,

which is chiefly caused due to the lower *K* and *C* values of air (0.025 $Wm^{-1}K^{-1}$ and 0.00125 $MJm^{-3}K^{-1}$) (Liu et al., 2018). Moreover, biochar also has a lesser *K* value due to the existence of organic content in it (Zhao et al., 2016). Therefore, the amendment of biochar is anticipated to diminution the *K* and *C* of soil.

4.5.3 Thermal characteristics of SBC

Fig. 4.4 and Fig. 4.5 present the variations of *K* and *C* with molding water content at different dry densities for different soil-biochar composites at initial and saturated states. The biochar content is designated by BC in the above figure. It was observed that the SBC has lower *K* and *C* values as compared to bare soil, which is statistically significant ($P < 0.05$). In the case of the initial state (partially saturated state), the soil *K* value was found to be decreased by 16%, 22%, and 26%, and the *C* value by 9%, 15%, and 19% with the respective addition of 5%, 10%, and 15% biochar at a dry density of 1.2 Mg m^{-3} and 20% water content. The observed trend was found to be in the same line with other densities and water content. Similar results were also reported by various researchers for soil biochar composite (Usowicz et al., 2016; Zhao et al., 2016; Liu et al., 2018). This is attributed to the lesser *K* and *C* values of biochar itself, which provide resistance in heat transfer between soil grains, resulting in lower thermal characteristics of SBC. Additionally, the rise in organic fraction with the incorporation of biochar also decreases the soil's thermal characteristics (Dec et al., 2009; Zhao et al., 2016). To prove our hypothesis, a small piece of (approximately 5 mm) SBC sample was extracted from the compacted soil sample to examine the heat transfer mechanism in SBC. A micrographic analysis was undertaken by FESEM analysis, which revealed the underlying heat transfer mechanism in SBC at a microscale. It is clearly visible from Fig. 4.6 that the biochar particles are entrapped between the soil grains providing resistance in heat transfer between soil grains, resulting in reduced thermal characteristics of the SBC.

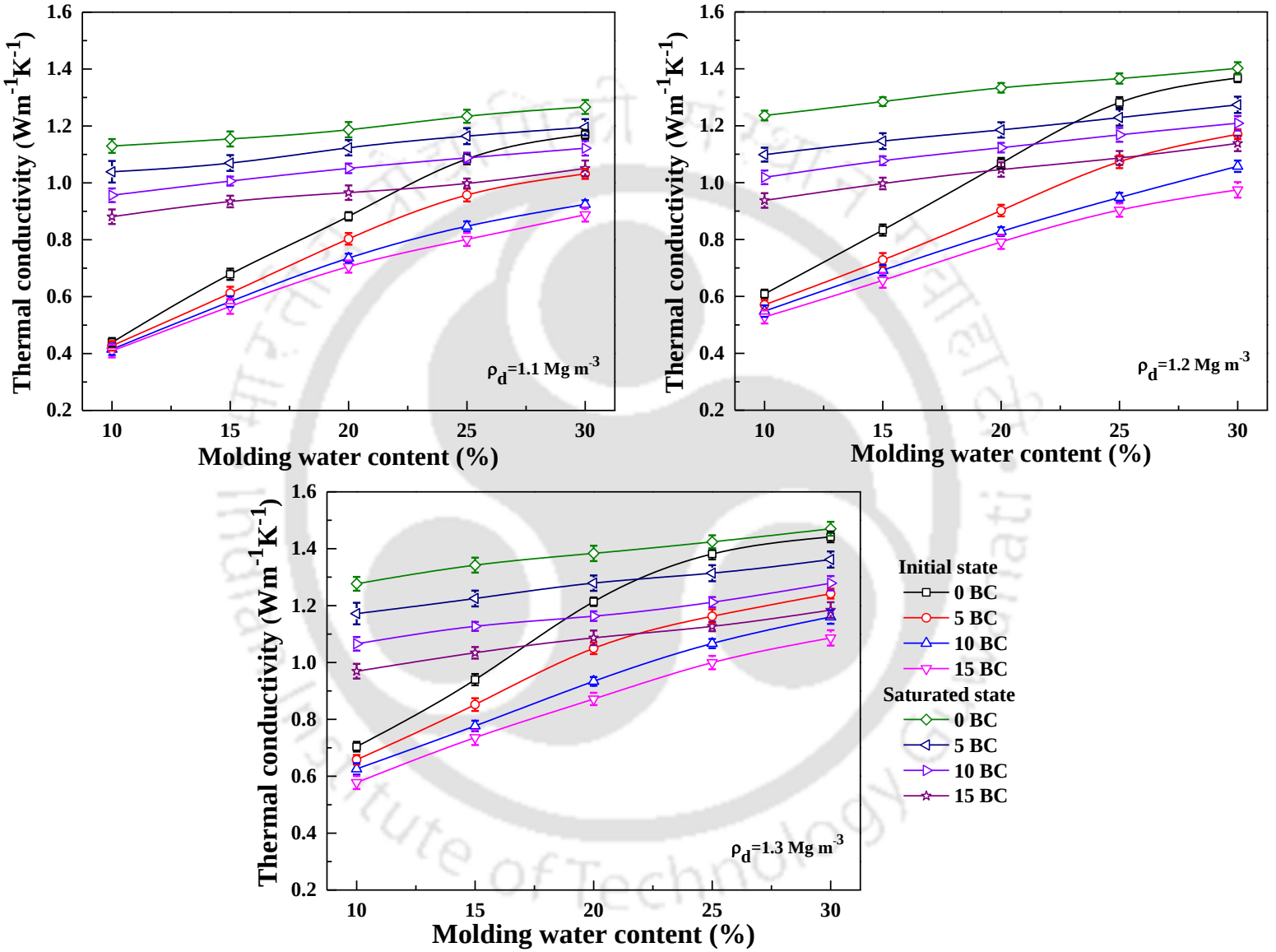

Figure 4.4 Variation of *K* of SBC at different initial molding states and saturated states, BC= Biochar content)

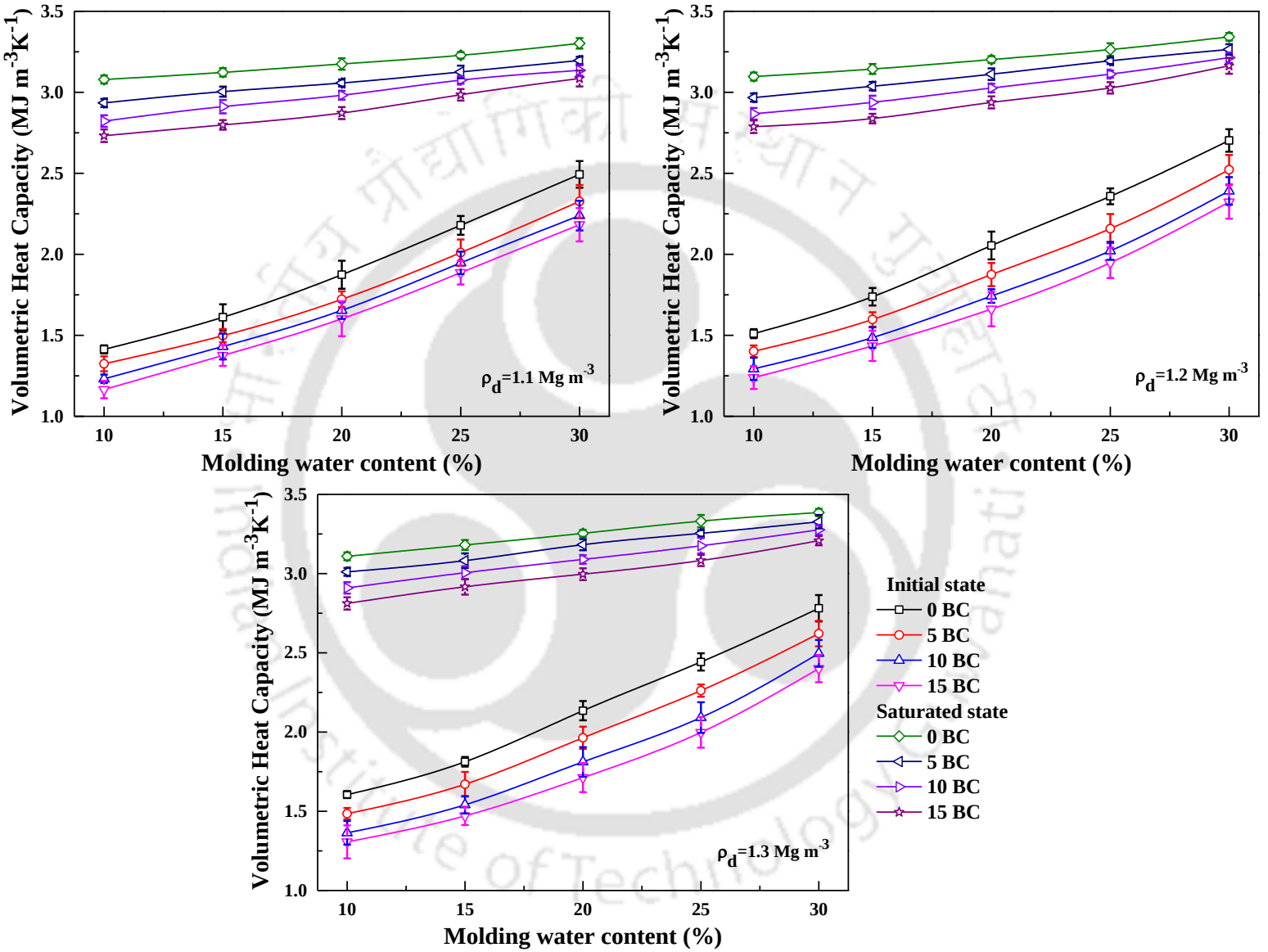

Figure 4.5 Variation of *C* of SBC at different initial molding states and saturated states

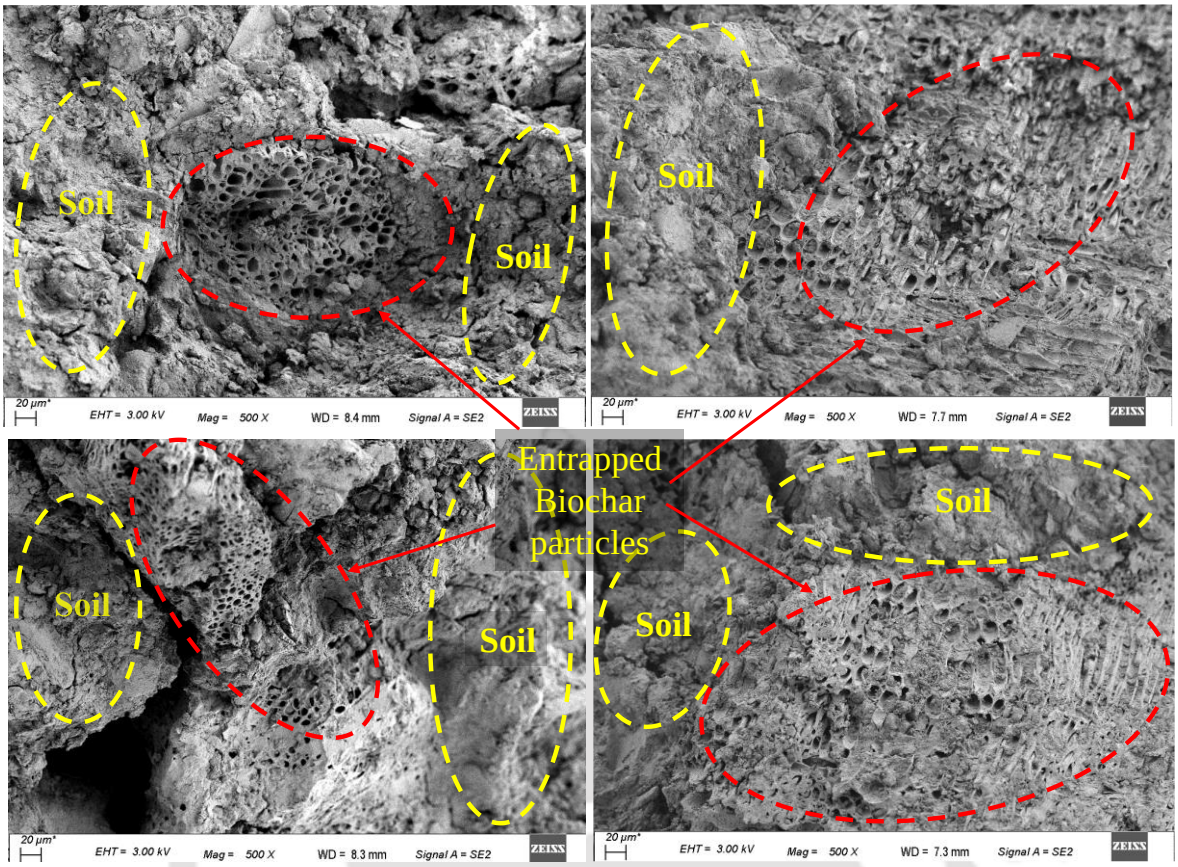

Figure 4.6 FESEM micrograph of SBC

4.5.3.1 Influence of biochar content

It was also noted from Fig. 4.4 and Fig. 4.5 that the margin of decrease in thermal characteristics of SBC was reduced with an increase in biochar percentage above 10% amendment. A probable reason for this can be ascribed to the decrease in total porosity of SBC with a higher biochar content (15% BC). The thermal characteristics of the SBC at a particular dry density are governed by two aspects: (i) thermal characteristics of soil and biochar; (ii) total porosity of SBC. The decrement effect is mainly associated with the lower thermal characteristics of biochar itself, while the increment effect is due to the reduced total porosity of soil-biochar composites. Fig. 4.7 presents the conceptual diagram showing decreased soil porosity with increased biochar content at a particular dry density in dry conditions. Since the mold volume is fixed and at a particular dry density, the weight of the soil sample is also fixed. With the increase in biochar content, the heavy soil particles get replaced with lighter biochar particles. This results in an increase in the total volume of the soil-biochar composite, leading to a reduction in its porosity. Therefore, at a higher amendment rate (15%), the incremental effect in thermal characteristics of the SBC due to its reduced porosity is more prominent than the decremental effect due to biochar itself.

Hence, a marginal decrease in thermal characteristics of the SBC was noted at 15% biochar amendment.

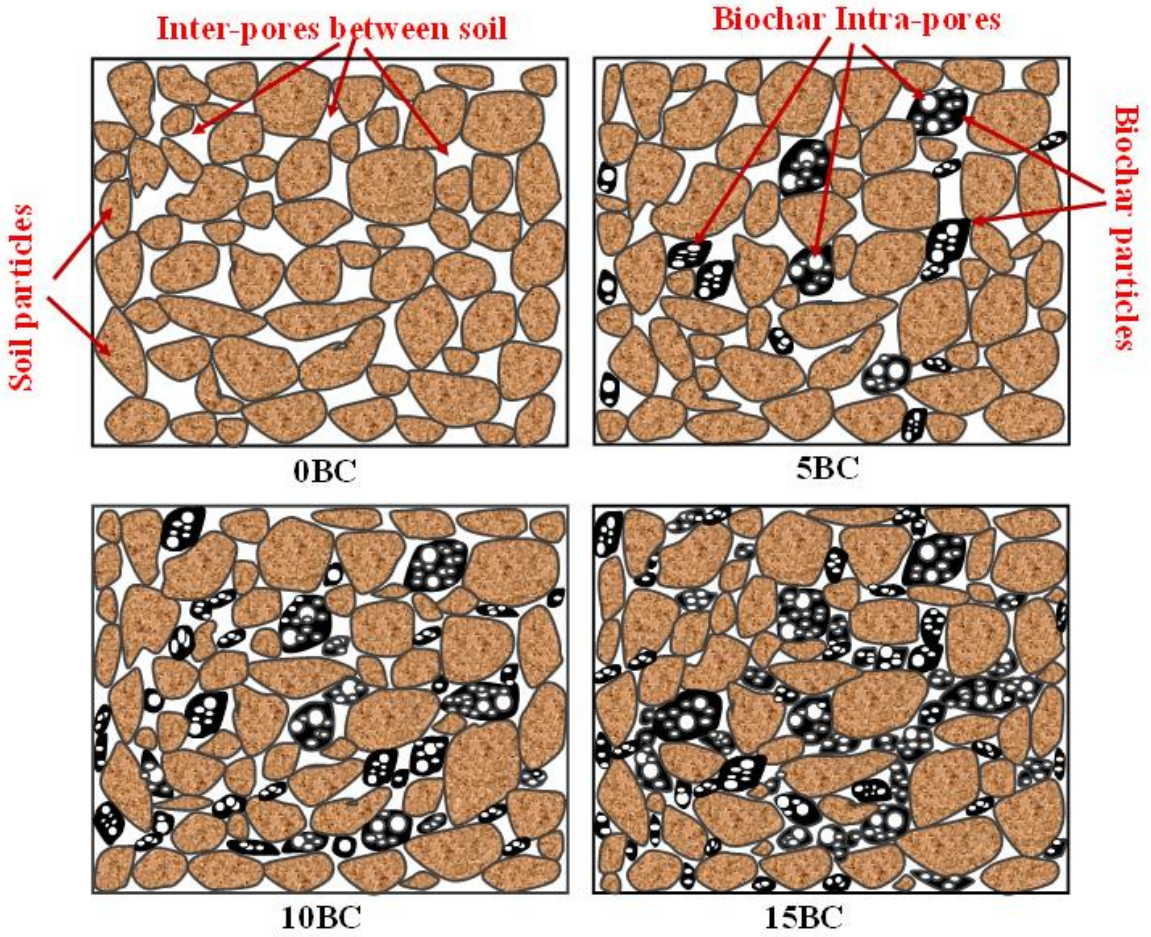

Figure 4.7 Schematic representation of decrease in porosity of SBC with increasing biochar content

4.5.3.2 Influence of water content

In the case of initial state, it can be noted from Fig. 4.4 and Fig. 4.5 that the *K* and *C* of soil and SBC increase with an increase in molding water content. This is primarily attributed to the greater *K* and *C* of water compared to air. A significant increase in *K* value was found up to 25% water content, and the increment rate was slightly reduced thereafter. The variation in *K* was found to increase almost in a linear fashion with an increase in molding water content. A similar linear variation in *K* for sand-clay (70:30) mixture and curvilinear variation of pure sand was also stated by (Zhang et al., 2017). Fig. 4.8 shows the conceptual diagram showing an increase in contact area in SBC with an increase in molding water content at a particular dry density. In dry states (at 10% molding water content), owing to the much lower *K* and *C* of air than the other soil constituent, the heat transmissions mostly

occur via the contact points between the soil particles and soil-biochar particles. With the further increase in molding water content (15% - 20%), more water accumulates around the contact points and forms the water meniscus (water bridges) between the soil particles and soil-biochar particles. This results in the increase in contact area between soil particles resulting in the increase in heat conduction from one soil grain to another (Tarnawski et al., 2002; Hall and Allinson, 2009). With the subsequent increase in molding water content (25% - 30%), the width of contact area will be increased, and more amount of water will also enter into the intra-pores of biochars, which increases thermal characteristics. In addition, it was also found that an increase in dry density increases the *K* and *C* values of both bare soil and SBC. This is mainly because of increased interparticle contact area with increased density, which reduces the thermal resistance among soil particles and improves *K* and *C*. However, the influence of dry density on *K* and *C* is not dominant as compared to moisture content.

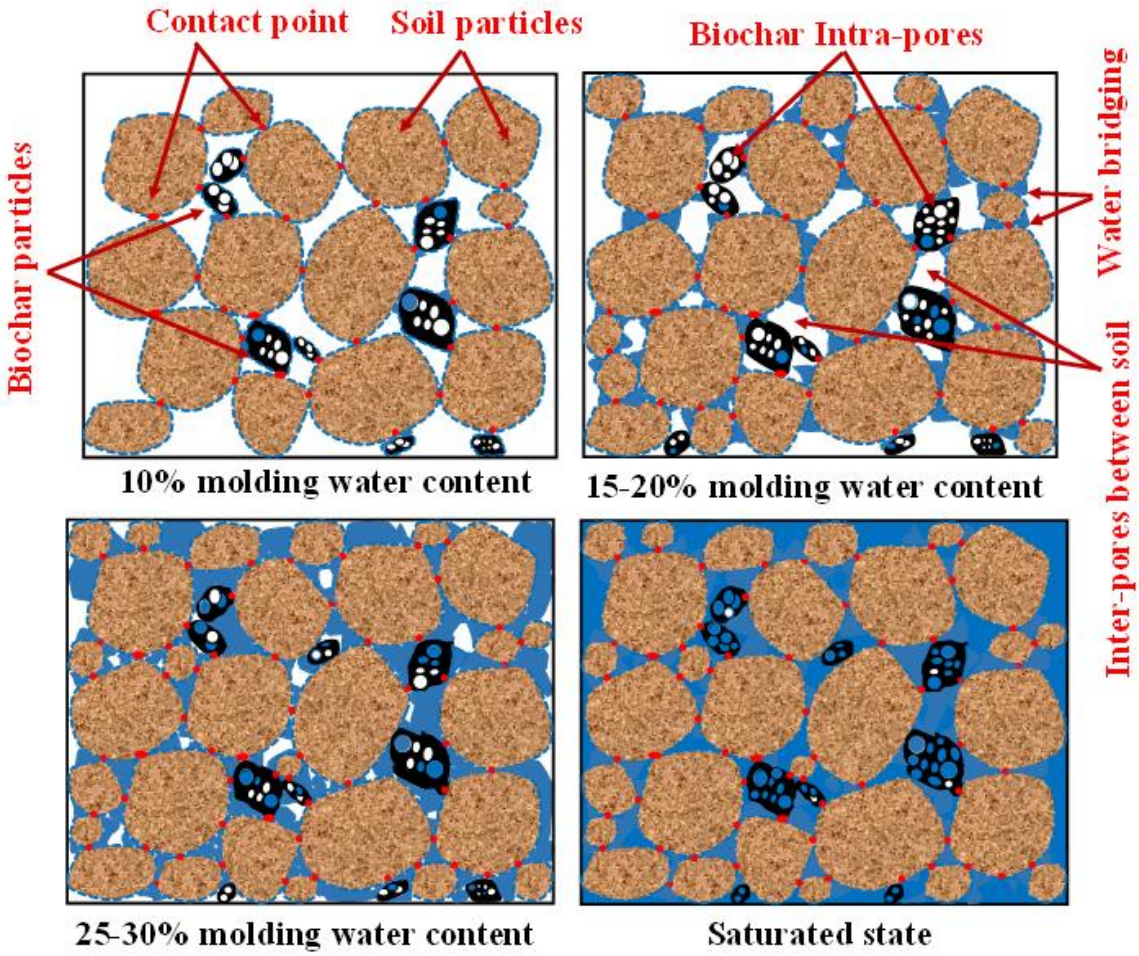

Figure 4.8 Schematic representation of an increase in contact area in SBC with an increase in water content

To measure the thermal characteristics in a saturated state, the duplicate set of SBC samples was saturated, as explained earlier, and then *K* and *C* values were noted. A percentage increment in *K* and *C* values of saturated bare soil and SBC were evaluated with respect to the initial state (partially saturated state). The *K* value was found to be increased by 86%, 56%, 36%, 23%, and 14% at the 10%, 15%, 20%, 25%, and 30% molding water content for the dry density of 1.2 Mg m^{-3} and 10% biochar amendment rate (see Fig. 4.4). Likewise, the *C* was found to be surged by 122%, 98%, 74%, 54%, and 34% at the 10%, 15%, 20%, 25%, and 30% molding water content (see Fig. 4.5). Similar trends were noted for *K* and *C* values at the dry densities of 1.1 Mg m^{-3} and 1.3 Mg m^{-3} for different biochar amendment rates. This is mainly credited to the rise in water content in the samples after saturation. The increase in water content will replace the soil inter-particle pore air and mostly intra-pore air of biochar. This results in an increase in *K* and *C* values due to higher *K* and *C* values of water than that of air. Furthermore, it can also be noted from Fig. 4.4 that the percentage increment in *C* value at saturated state was higher than that of *K* value. It is because the *C* value of water is much higher (3346 times) than the *C* value of air, while the *K* value of water is only 24 times more than the *K* value of air. In addition to this, the percentage increment in the *K* and *C* values of bare and SBC at a saturated state was observed to be less at higher dry densities. This is attributed to the lower volume of voids in the samples at higher density. This means that the increase in volume of water in samples upon saturation is less at a higher density as compared to the samples prepared at a lower density which have a high volume of voids that can absorb more water upon saturation.

Furthermore, it is noteworthy to observe from Fig. 4.4 and Fig. 4.5 that in the case of a saturated state, a marginal increase in saturated *K* and *C* values of SBC were also found with an increase in molding water content. This is mainly credited to the change in clay particle orientation (i.e., flocculated and dispersed structure) and change in pore size distribution with different molding water content (refer to Fig. 4.9). It is strongly established that the clay particles have flocculated structure at water content below optimum moisture content, and it becomes dispersed at water content at higher side of OMC (Holtz et al., 1981). The clay particles oriented in edge-to-face contact in the flocculated structure, resulting in a smaller contact area and lower *K* and *C* values. The dispersed structure has face-to-face contact between clay particles, resulting in a larger contact area and greater *K* and *C* values. The results are also verified with micrographic analysis using FESEM analysis. A cubic soil sample of a dimension of approximately 4 mm was taken out from the compacted soil

samples. Thereafter, a surface morphology study was carried out, which shows the flocculated and dispersed structure of soil particles prepared at different molding water content (see Fig. 4.10).

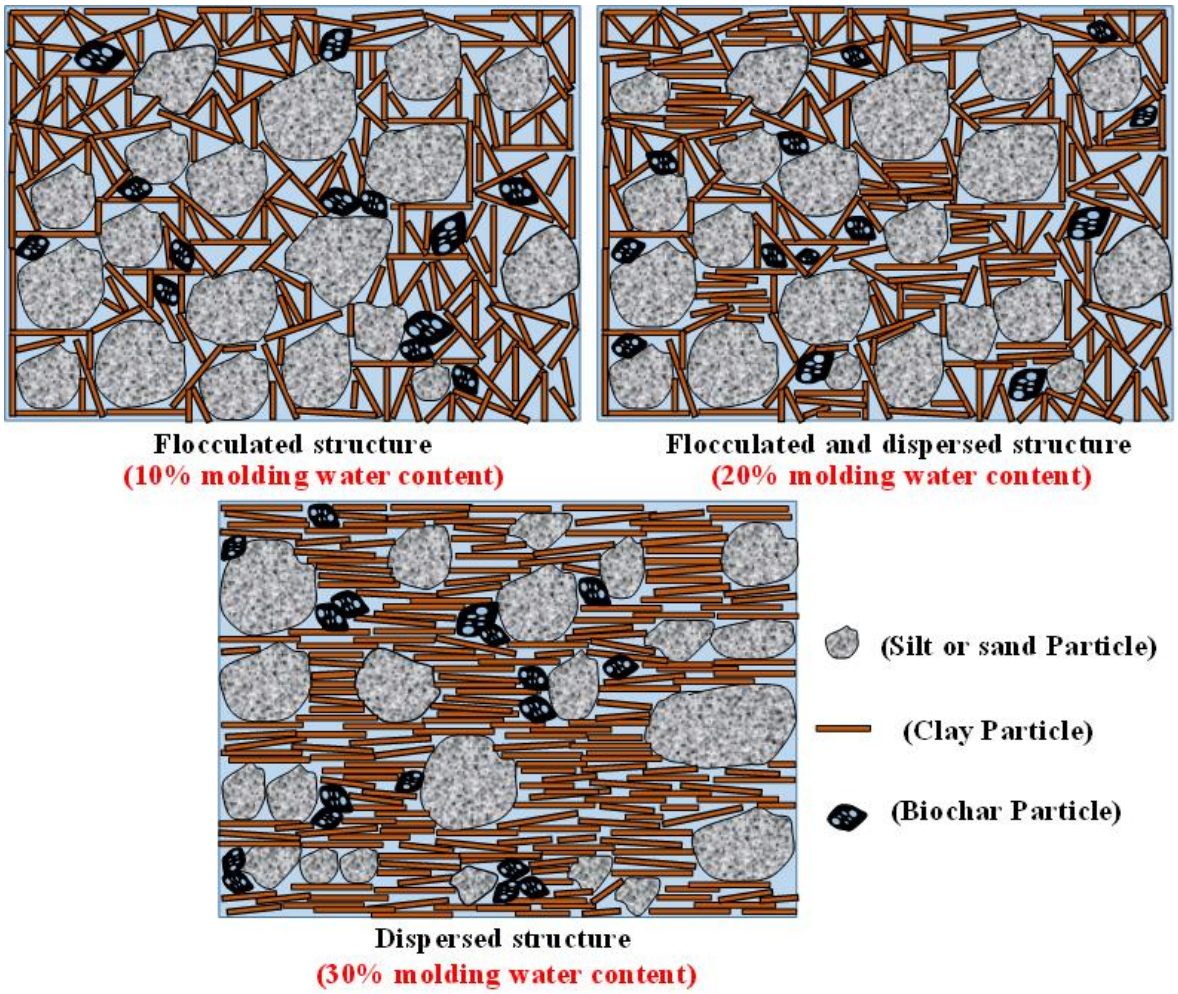

Figure 4.9 Schematic representation of clay particles orientation with molding water content

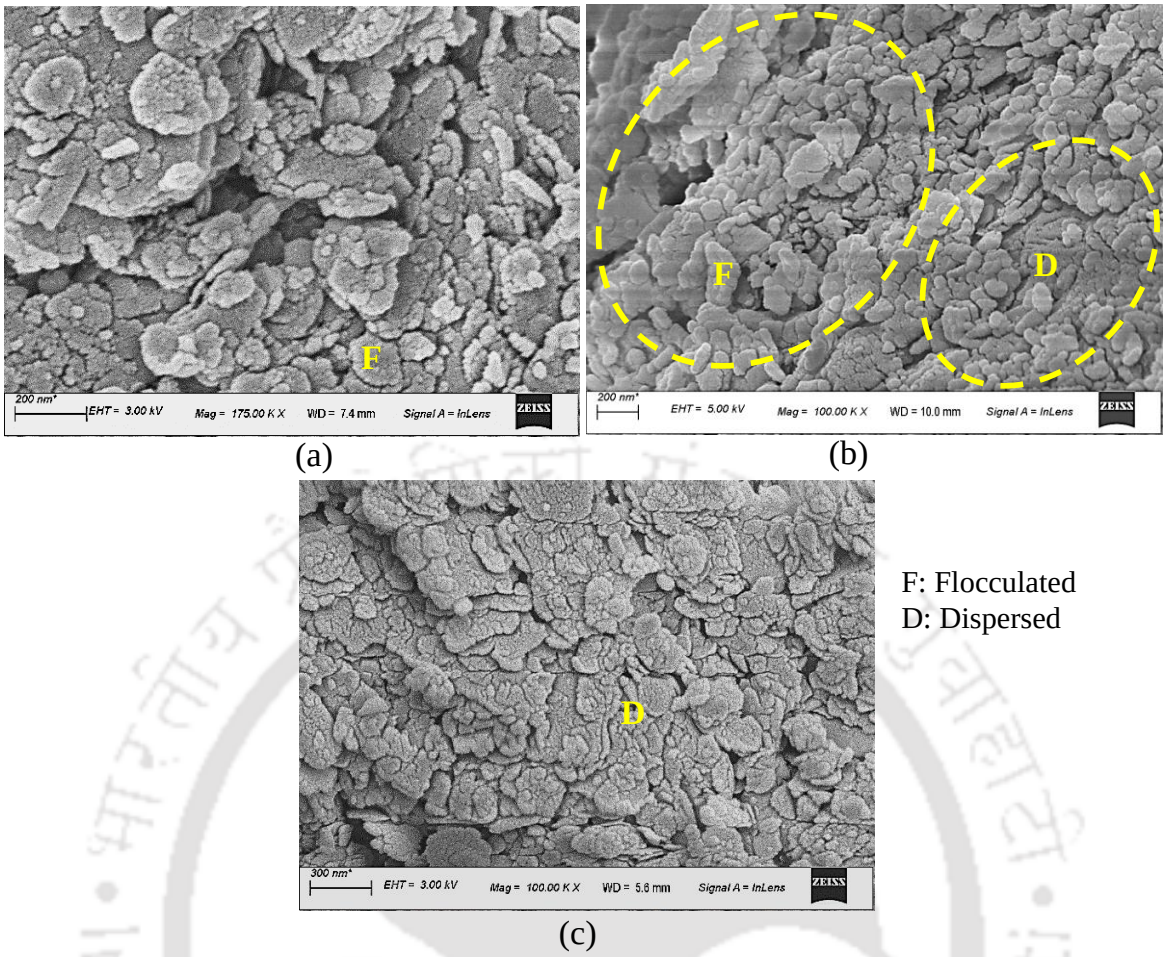

Figure 4.10 SEM micrograph evidence for clay particles orientation in SBC at a dry density of 1.3 Mg m^{-3} and molding water content of (a) 10 %, (b) 20%, and (c) 30%

4.5.4 Multiple linear regression and sensitivity analysis

A simple MLR equation was formulated and is listed in Eqs. (4.4) and (4.5).

$$K = -0.9899 + 1.149\gamma + 0.029908w - 0.016071BC \quad (4.4)$$

$$C = -0.282 + 0.9929\gamma + 0.05547w - 0.02106BC \quad (4.5)$$

Where, ρ_d = initial dry density, w = molding water content, and BC = Biochar content.

The competence of the MLR equations was validated by sixty independent thermal characteristics measurements conducted on soil and SBC for initial state (partially saturated) samples. The fitted R^2 values for *K* and *C* are 0.945 and 0.965, with a *P*-value less than 0.005. Fig. 4.11 compares measured and estimated thermal characteristics of bare and SBC for initial state conditions. All predicted *K* and *C* data were within ±10% of the measured *K* and *C* values. Hence, the developed equation could be considered to estimate *K* and *C* by

taking the initial molding state of the sample, which is comparatively simple. This MLR equation can be a valuable initial estimate for a known *w*, ρ_d, and BC for various field applications where it is difficult to measure thermal measurement. However, the generalization of such regression equations demands standardization through testing various soil amendments with different types of biochar.

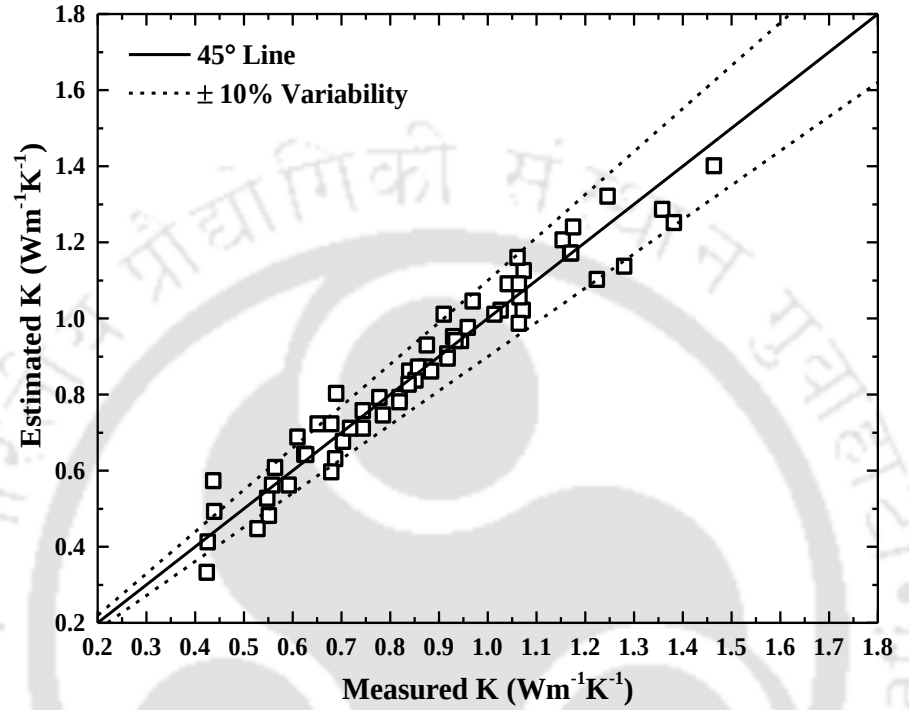

(a)

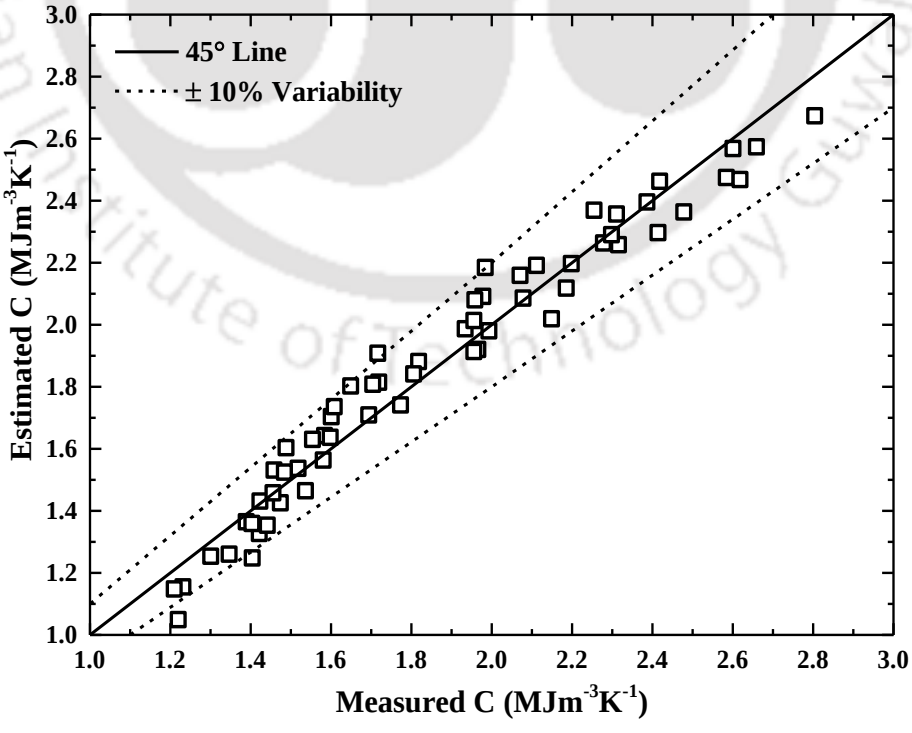

(b)

Figure 4.11 Variation of the measured and estimated *K* and *C* of soil and SBC

Fig. 4.12 shows a spider diagram (Saraiva et al., 2017) which forms the basis of the method of difference for illustrating the sensitivity of variables. A spider diagram representing the output variation in thermal characteristics (*K* and *C*) for a certain percentage change in the input variables considered one at a time (*w*, ρ_d, and BC), illustrating the sensitivity of input variables. The reference *K* and *C* values (measured data) corresponding to a particular density, molding water content, and biochar content (ρ_d =1.2 Mg m^{-3}, *w* =20%, and BC =10%) of input variables are shown in Fig. 4.12. The spider graph presents a consistent representation of variable sensitivity. It was observed from Fig. 4.12 that the *K* and *C* value is highly sensitive to ρ_d, followed by *w* and BC. For the sake of brevity, other spider diagrams that also displayed the same information are not presented here. The results from the spider diagram were used to determine the sensitivity index (S_d) using Eq. (3) for all the multiple linear regression equations. Table 4.2 presents the quantitative sensitivity index (S_d) values, indicating that the initial dry density, ρ_d, significantly influenced *K* and *C* determination, followed by *w* and BC. The findings show the significance of knowing the initial molding state of soil and SBC for determining thermal characteristics. The influence of variables on *K* and *C* and their quantitative relationship illustrated in this study are beneficial for determining thermal behavior in the field. This will have wide application in several projects where there is a heat migration from the source.

Table 4.2 Sensitivity index (S_d) of different input parameters for thermal characteristics

State	Input parameter	Thermal conductivity	Volumetric heat capacity
Initial molding state	*w*	0.280	0.442
	ρ_d	0.645	0.474
	BC	0.075	0.084

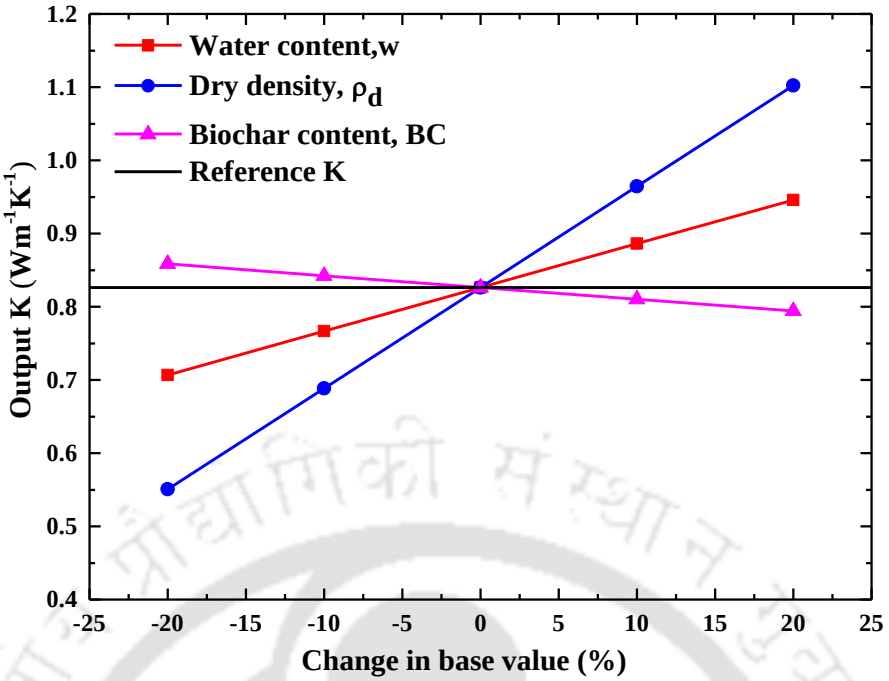

(a)

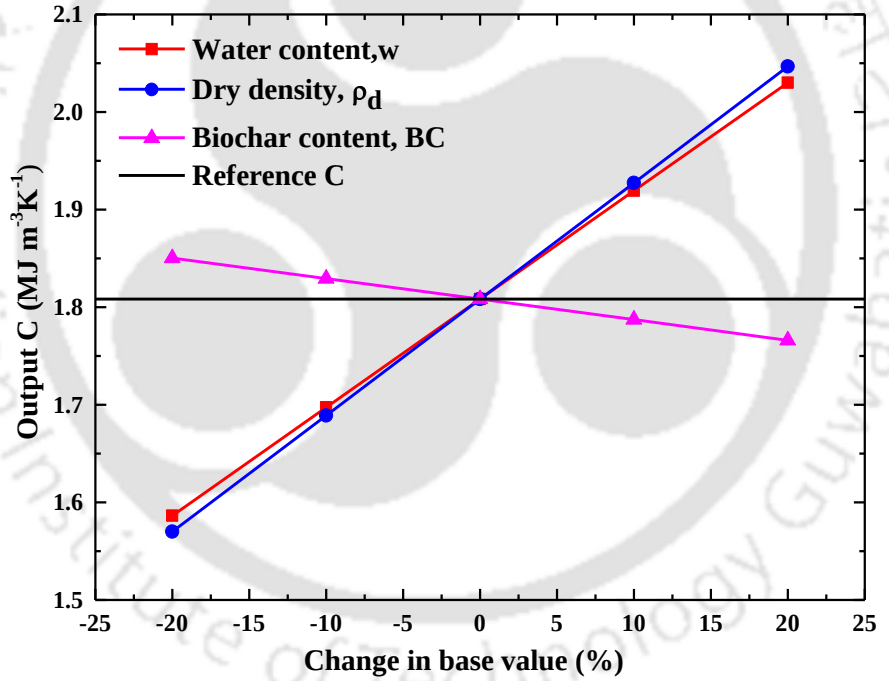

(b)

Figure 4.12 Influence of input parameters on thermal characteristics of soil and SBC

4.5.5 Correlation of thermal characteristics with degree of saturation

Fig. 4.13 presents the relationship between the change in ΔK and ΔC with the change in degree of saturation (ΔS) for soil amended with different biochar content. It can be observed from the figure that both ΔK and ΔC increase with ΔS. The measured values were best fitted, and a power function ($a\Delta S^b$) correlation ($R^2 > 0.94$ for ΔK and $R^2 > 0.84$ for ΔC) between ΔK and ΔC with ΔS was observed for soil and soil-biochar mixes. At lower ΔS, an

increasing trend of ΔK can be noted with an increase in biochar content (BC). Moreover, at ΔS between 60% and 70%, the increase in BC in soil has a negligible effect on the ΔK. On the contrary, at higher ΔS, the increase in BC in the soil tends to decrease the ΔK.

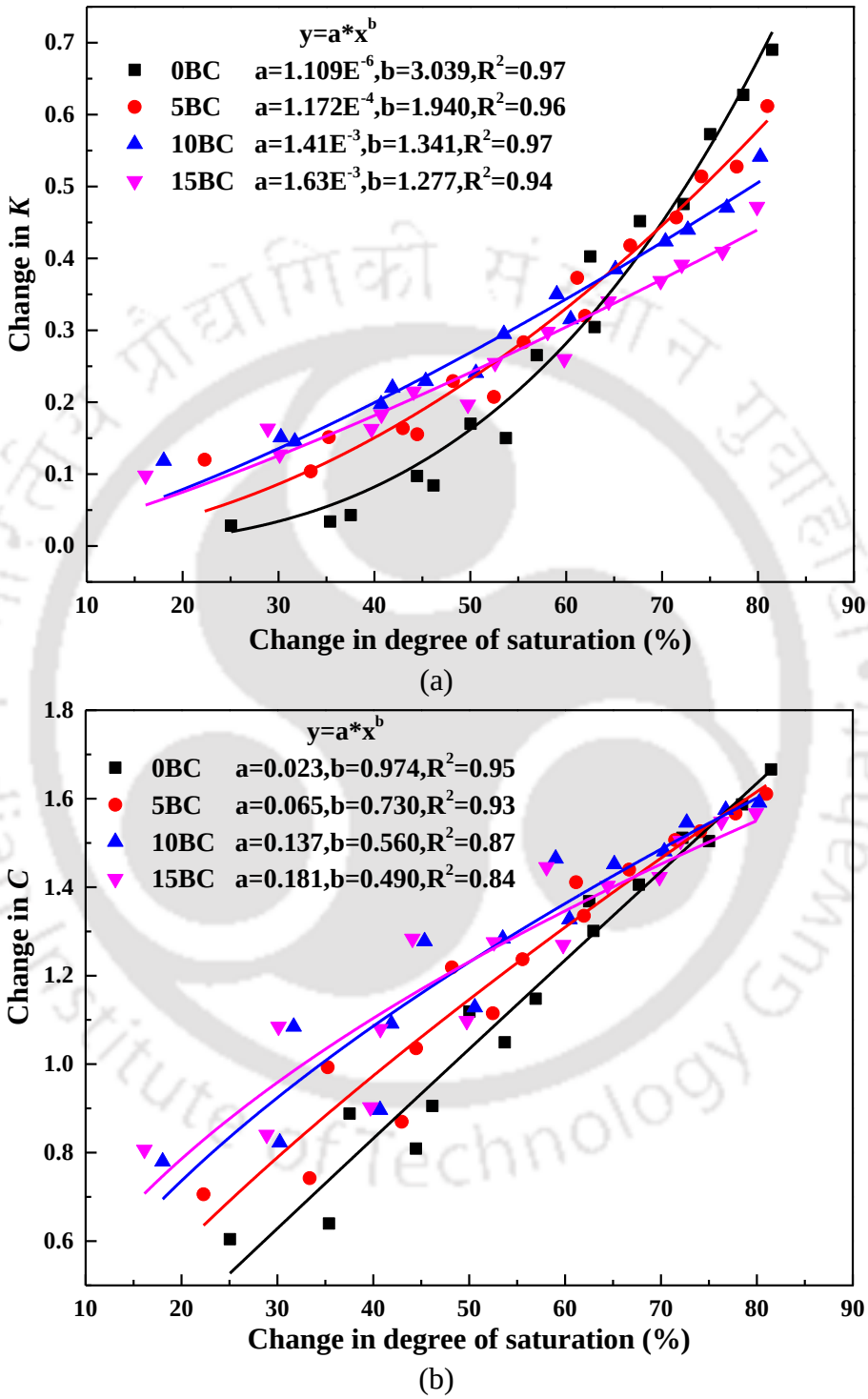

Figure 4.13 Correlations between *K* and *C* with degree of saturation

Similarly, at lower ΔS, an increase in ΔC can be observed with the increase in BC in soil. However, at higher ΔS, the change in ΔC with BC becomes nearly constant. These relationships suggest that higher biochar has lower 'a' and 'b' values indicating higher

stability to the change in degree of saturation. Therefore, higher biochar content indicates relatively stable performance in dry to rainy seasons.

4.6 Summary

This study explores the potential of a sustainable geomaterial that can enhance the performance of essential thermally active structures with minimal environmental impact. For this purpose, this study investigates the influence of the initial molding state on the *K* and *C* of SBC. The *K* and *C* were measured for the initial molding states (molding water content, biochar content, and dry density). Further, the duplicate soil samples were saturated to investigate the influence of moisture interaction with the thermal characteristics, i.e., *K* and *C* values at the saturated state. The main findings from the present study can be highlighted as follows:

- The *K* of the SBC was found to be consistently decreasing with incremental biochar amendment. This is due to the entrapped biochar particles between the soil particles that have an intra-porous structure. Moreover, the margin of decrease in thermal characteristics of SBC was reduced with an increase in biochar percentage above 10% amendment.
- The thermal characteristics of the SBC were greatly influenced by the molding water content. With the increase in molding water content, the liquid-solid contact improves, and the flocculated particles change to dispersed orientation leading to a steady increase in the thermal characteristics.
- Upon saturation, the thermal conductivity of the SBC improved significantly. Interestingly, the *K* and *C* values at saturated state differ marginally for the SBC samples with different molding water content at a particular density, which is credited to the orientation of the clay particles. The results suggest that the molding water content has a more dominant influence in controlling the thermal characteristics of SBC.
- The estimated *K* and *C* values from MLR equations matched well with the measured results, and the difference is well within ±10%. The sensitivity index indicates that the ρ_d significantly influences *K* and *C* values, followed by *w* and BC for all SBC.

It is rational to design the thermal backfill in a dry state due to its minimum thermal conductivity, ensuring the optimized performance of thermally activated structures. However, the interaction of thermal backfill with moisture is very common in the field due to groundwater movement and rainfall. This chapter highlighted that the performance of

SBC is hampered drastically upon saturation due to a 70% to 150% increase in thermal conductivity. Moreover, a relationship between the thermal characteristics of different blends of the proposed SBC with initial molding parameters (dry density, molding water content, and biochar content) has been formulated using MLR. The proposed equations can be useful for practicing civil and environmental engineers designing large-scale biochar applications in thermal backfills. However, it should also be noted that these equations are specific to the soil and biochar used in the present chapter. It is suggested to validate the accuracy of the MLR equation using limited experimental data before field application.

CHAPTER 5
INFLUENCE OF BIOCHAR TYPES AND BIOCHAR FRACTIONS ON THERMAL AND STRENGTH CHARACTERISTICS OF SBC

5.1 Introduction

The design criteria of thermal backfill need to be assessed based on the density states recommended by Howard (1996). The backfill should be compacted to a minimum of 95% of MDD, and moisture content should be in between 2% of dry of OMC and 2% of wet of OMC. The findings from the previous chapter clearly indicate that SBC has lower thermal characteristics than bare soil for a particular dry density in both initial states and saturated states. However, it is necessary to quantify the influence of biochar amendment on thermal characteristics of soil based on the density criteria of thermal backfill. The thermal backfill structure should also have adequate strength to sustain self-weight. In recent years, some researchers documented the increase in the shear strength of soil with biochar amendment (Haque et al., 2014; Reddy et al., 2015; Sadasivam and Reddy, 2015; Sudhakar et al., 2017; Williams et al., 2020), while some others reported the decrease in shear strength of soil with biochar addition (Lu et al., 2014; Zong et al., 2014, 2016; Ahmed et al., 2017; Ajayi and Horn, 2017; Bora et al., 2021). The contradictory result from existing literature confirms that the type of biochar, amendment rate, particle size fraction of biochar, and type of soil influence the shear strength of SBC.

The amendment of different biochar types and biochar particles size fractions in the soil can influence the soil thermal characteristics differently due to the changes in soil material composition, change in total porosity, pore size distribution, and physicochemical properties (Burrell et al., 2016; Głąb et al., 2016; Liu et al., 2018). Further, the different biochar types and biochar particle size fractions can also influence the optimum moisture content and dry density differently due to their unique water-holding capacity and porosity (Williams et al., 2020; Bora et al., 2021). Therefore, investigation on the influence of biochar amendment produced from different waste biomass and different biochar particle size fractions on thermal characteristics of soil is remarkably needed in view of applying as thermal backfill. Moreover, there is a need to reexamine the influence of biochar amendment on strength characteristics of soil in addition to its thermal characteristics.

5.2 Sample preparation and test setup

In the study reported in this chapter, different types of SBC were tested using various biochar types and different biochar particle size fractions. The hardwood biochar (HWBC), water hyacinth (WHBC), and sugarcane bagasse biochar (SBBC) passed through a 2 mm sieve were used to investigate the influence of biochar type on the thermal characteristics of SBC. Two soil types (MH and SC) and three biochar amendment rates were selected in this study. The biochar amendment rates were kept as 2.5%, 5%, and 7.5% by weight of dry soil.

Further, to investigate the influence of different biochar particle size fractions on the thermal and strength characteristics of SBC, the hardwood biochar was sieved into three different particle size fractions, namely, coarse (4.7 mm-2 mm), medium (2 mm-0.425 mm), and fine (0.425 mm-0.075 mm) as displayed in Fig. 5.1. Here also, two soil types (MH and SC) and three biochar amendment rates were selected, and the amendment rates were kept as 5%, 10%, and 15% by weight of dry soil.

The compaction characteristics of the bare soil and SBC were determined using the guidelines recommended in ASTM D-698-12, 2012.

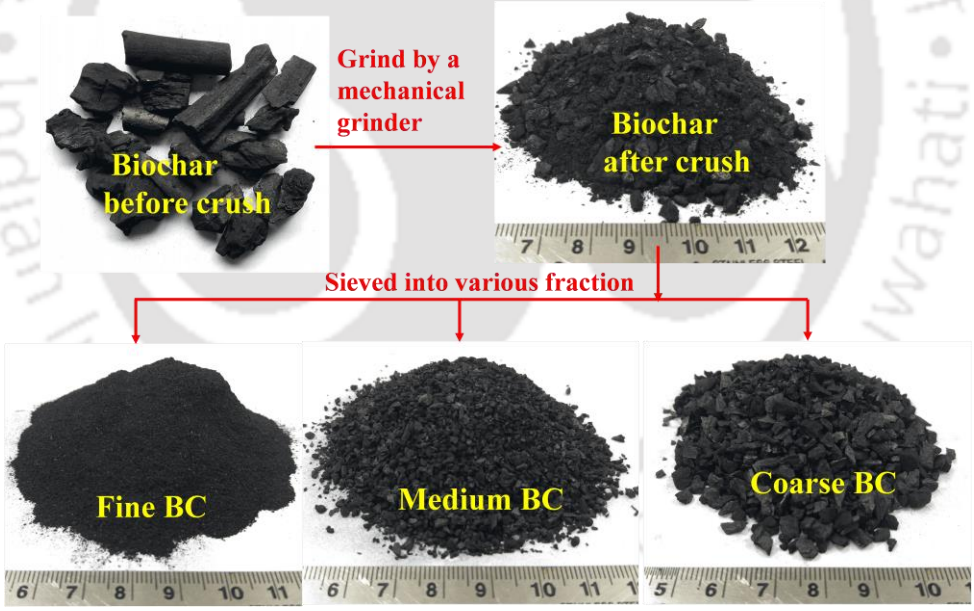

Figure 5.1 Preparation of different biochar particles size fractions

5.2.1 Thermal characteristics test

To measure the thermal characteristics of bare soil and SBC, a calculated amount of oven-dried soil and biochar were weighed, considering the volume of mold and target density. Thereafter, the weighed soil mass and biochar were homogenously mixed with a calculated amount of distilled water equal to the target moisture content of the composite on

a glass plate using the spatulas. Further, the moist soil or soil-biochar mix was kept in closed plastic bags for 24 h in a desiccator to allow uniform distribution of moisture throughout the soil mass. Thereafter, it was poured into the acrylic mold and then was compacted in three-layer to desired density by a static loading machine with the help of a plunger. To investigate the influence of biochar type on the thermal characteristics, the tests were conducted on soils and SBC samples at three different compaction conditions along the individual compaction curve. These compaction conditions correspond to three different moisture contents (OMC, OMC − 4, OMC + 4) and at MDD. The (OMC – 4) corresponds to a compaction water content, which is 4 % less than the OMC, while (OMC + 4) corresponds to a compaction water content which is 4 % more than the OMC. The rationale for choosing moisture variation in this chapter was to investigate the effect of variable compaction conditions expected in the field (Gupt et al., 2021b). The increment in 4% moisture content (OMC − 4, OMC, OMC + 4) was selected as per the expected variation in the degree of saturation (70% to nearly 100%) in the field due to different weather conditions. In the case of biochar particle size fraction study, the samples were prepared at OMC and MDD conditions.

5.2.2 Unconfined compressive strength test

The unconfined compressive strength (UCS) for bare soils and SBC were conducted according to the ASTM standard (ASTM D2166-16, 2016). The soil-biochar mix preparation procedure was the same as for thermal properties measurement, and the sample was prepared at OMC and MDD conditions. A cylindrical sample (38 mm in diameter and 76 mm in height) was prepared in a cylindrical sampler, facilitating static compaction, and a sample extruder was used to extract the sample. Further, the sample was subjected to compressive stress at a constant strain rate of 1.25 mm min^{-1}. Three replicate samples were tested for each test condition to check repeatability in UCS results, and their average value of peak stress was reported as UCS value. The improvement in strength and ductility of SBC can be determined from the strength improvement factor (SIF) and mobilized peak strain factor (MPSF). The SIF is defined as the ratio of UCS value of SBC to bare soil, while the MPSF is defined as the ratio of the peak strain of SBC to that of the peak strain of bare soil for the same compaction state (Gupt et al., 2021b). Any value higher than unity indicates an enhancement in strength and ductility of SBC with respect to bare soil.

5.3 Results and discussion

5.3.1 Biochar thermal characteristics

The measured thermal conductivity and volumetric heat capacity of MH soil at the dry density of 1.2 Mg m^{-3} were noted to be 0.21 Wm^{-1} K^{-1} and 1.145 MJ m^{-3} K^{-1}. The thermal characteristics of different biochar types and biochar particle size fractions are presented in Tables 5.1 and 5.2. It is clear from the table that the biochar has a lower value of *K* and *C* in comparison with the bare soil. A reason for the lower *K* and *C* values of biochar is the presence of air in the intrapores of biochar skeleton. This result is also supported by the FESEM analysis of biochar, as presented in Fig. 3.2, which shows the intra-pores in biochar. The details of lower *K* and *C* values of biochar are explained in the earlier section 4.5.2. Therefore, the biochar amendment decreases the *K* and *C* of soil.

Table 5.1 Thermal characteristics and dry density of different biochar types

Biochar Type	Thermal conductivity, (Wm^{-1} K^{-1})	Volumetric heat capacity, (MJ m^{-3} K^{-1})	Dry density, (Mg m^{-3})
HWBC	0.130±0.002	0.713±0.016	0.420±0.06
WHBC	0.112±0.004	0.483±0.006	0.182±0.07
SBBC	0.100±0.001	0.444±0.005	0.121±0.08

Table 5.2 Thermal characteristics and dry density of different biochar particle size fractions

Biochar Particle size, (mm)	Thermal conductivity, (Wm^{-1} K^{-1})	Volumetric Heat capacity, (MJ m^{-3} K^{-1})	Dry density, (Mg m^{-3})
Fine (0.425-0.075)	0.127	0.729	0.457
Medium (2-0.425)	0.124	0.684	0.386
Coarse (4.75-2)	0.121	0.723	0.363

5.3.2 Effect of biochar types and fraction on compaction characteristics of SBC

The variation of OMC and MDD of soils with the different biochar types and different biochar particle size fractions is presented in Table 5.3 and Table 5.4. The MDD of both MH and SC soils was observed to reduce by 4%, 7%, and 10%, with the respective amendment of 2.5%, 5%, and 7.5% of HWBC. However, the OMC of the MH soil was found to be increased by 9%, 16%, and 20%, while the SC soil was observed to be enhanced by 7%, 13%, and 19% with the amendment of 2.5%, 5%, and 7.5% of HWBC. Similarly, the increase in OMC and decrease in MDD were also noted when the soils were amended with

WHBC and SBBC. The MDD of the MH soil was observed to reduce by 7%, 11%, and 16%, while SC soil decreased by 9%, 15%, and 21% with the amendment of 5%, 10%, and 15% of finer-fraction biochar. However, the OMC of the MH soil was found to be increased by 17%, 26%, and 40%, while the SC soil was observed to be enhanced by 21%, 37%, and 50% with the amendment of 5%, 10%, and 15% of finer fractions of biochar. A similar trend in OMC and MDD was noted when the soils were amended with medium and coarser biochar fractions.

The decrease in MDD of the soil is caused by the substitution of high-density soil particles with lower-density biochar particles. The increase in the OMC of bare soil could be due to the higher surface area and macro-porosity of biochar particles that lead to an increase in the water absorptive capacity of SBC (Blanco-Canqui, 2017). The soils amended with the finer fractions of biochar exhibited a higher value of OMC and MDD. It can be attributed due to an arrangement of the biochar particles in the soil matrix. The smaller biochar particles can occupy the pores in the soil resulting in more effective packing, reducing the total porosity, and an increase in the dry soil density, which may not be possible if the biochar particle size is bigger. Further, smaller biochar particles have a higher specific surface area, which increases the water retention capacity of SBC, contributing to an increase in the soil moisture content, which is reflected in the higher value of OMC (Blanco-Canqui, 2017).

Table 5.3 Compaction characteristics of soils amended with different biochar types

Soil-biochar composite							
Content by dry weight: %		Biochar					
		HWBC		WHBC		SCBC	
MH	BC	OMC, %	MDD, Mg m^{-3}	OMC, %	MDD, Mg m^{-3}	OMC, %	MDD, Mg m^{-3}
100	0	22.72	1.579	22.72	1.579	22.72	1.579
97.5	2.5	24.77	1.515	25.25	1.482	26.55	1.441
95.0	5.0	26.25	1.461	27.50	1.396	29.55	1.313
92.5	7.5	27.28	1.422	29.52	1.318	32.50	1.235
SC	BC	OMC, %	MDD, Mg m^{-3}	OMC, %	MDD, Mg m^{-3}	OMC, %	MDD, Mg m^{-3}
100	0	17.72	1.738	17.72	1.738	17.72	1.738
97.5	2.5	18.91	1.675	20.75	1.609	21.52	1.578
95.0	5.0	19.95	1.615	24.32	1.465	24.76	1.442
92.5	7.5	21.00	1.565	28.12	1.351	28.92	1.305

Table 5.4 Compaction characteristics of soils amended with different biochar fractions

Soil-biochar composite							
Content by dry weight: %		Hardwood Biochar (HWBC)					
		Fine		Medium		Coarse	
MH	BC	OMC, %	MDD, Mg m^{-3}	OMC, %	MDD, Mg m^{-3}	OMC, %	MDD, Mg m^{-3}
100	0	22.72	1.579	22.72	1.579	22.72	1.579
95	5	26.68	1.472	26.42	1.418	26.12	1.391
90	10	28.72	1.412	28.55	1.341	28.21	1.304
85	15	31.71	1.332	31.35	1.282	31.01	1.234
SC	BC	OMC, %	MDD, g cm^{-3}	OMC, %	MDD, g cm^{-3}	OMC, %	MDD, g cm^{-3}
100	0	17.72	1.738	17.72	1.738	17.72	1.738
95	5	21.52	1.575	21.31	1.555	21.08	1.524
90	10	24.18	1.478	23.54	1.438	23.15	1.391
85	15	26.62	1.379	25.52	1.343	25.12	1.305

5.3.3 Influence of biochar type on thermal characteristics of SBC

Fig. 5.2 presents the thermal characteristics variation of bare soil (BS) amended with the different biochar content and biochar types at three different compaction conditions. The *K* value was observed to be 1.595 and 1.712 $Wm^{-1}K^{-1}$ for MH and SC soil, respectively, compacted at OMC and MDD conditions. However, the *C* value was noticed to be higher for MH soil (3.301 $MJm^{-3}K^{-1}$) compared to SC soil (3.104 $MJm^{-3}K^{-1}$) soil. Previous studies also reported similar results (Abu-Hamdeh, 2003; Abu-Hamdeh and Reeder, 2000). The thermal characteristics of bare soils were found to be reduced with biochar amendment. Previous researchers also documented a similar result with the amendment of biochar into the soil (Zhao et al., 2016; Liu et al., 2018). The *K* value of the MH soil was found to be decreased by 11%, 17%, and 22% with the respective amendment of 2.5%, 5%, and 7.5% of HWBC, compacted at OMC and MDD state. Similarly, the reduction in *C* value was observed to be 9%, 13%, and 16% with the addition of 2.5%, 5%, and 7.5% of HWBC, respectively (Fig. 5.2). The observed trend was in the same line when the MH soil was amended with WHBC and SBBC. A similar trend was also observed in the SC soil with the addition of HWBC, WHBC, and SBBC (see Fig. 5.3). Furthermore, similar observations were also found at (OMC-4) and (OMC+4) compaction conditions. This is attributed to the reduction in the density of the soils with the amendment of biochar, which is reflected in the compaction characteristics presented in Table 5.3 and Table 5.3. Since the decrease in dry density leads to an increase in the porosity and the number of air-filled pores in the soil-

biochar composite. This resulted in the separation of the contacts among soil solid particles and water and subsequent reduction in the thermal properties of SBC. Further, this might be due to the presence of biochar particles in between the soil particles in the soil-biochar composite, which reduces the heat transfer because of its low thermal characteristics.

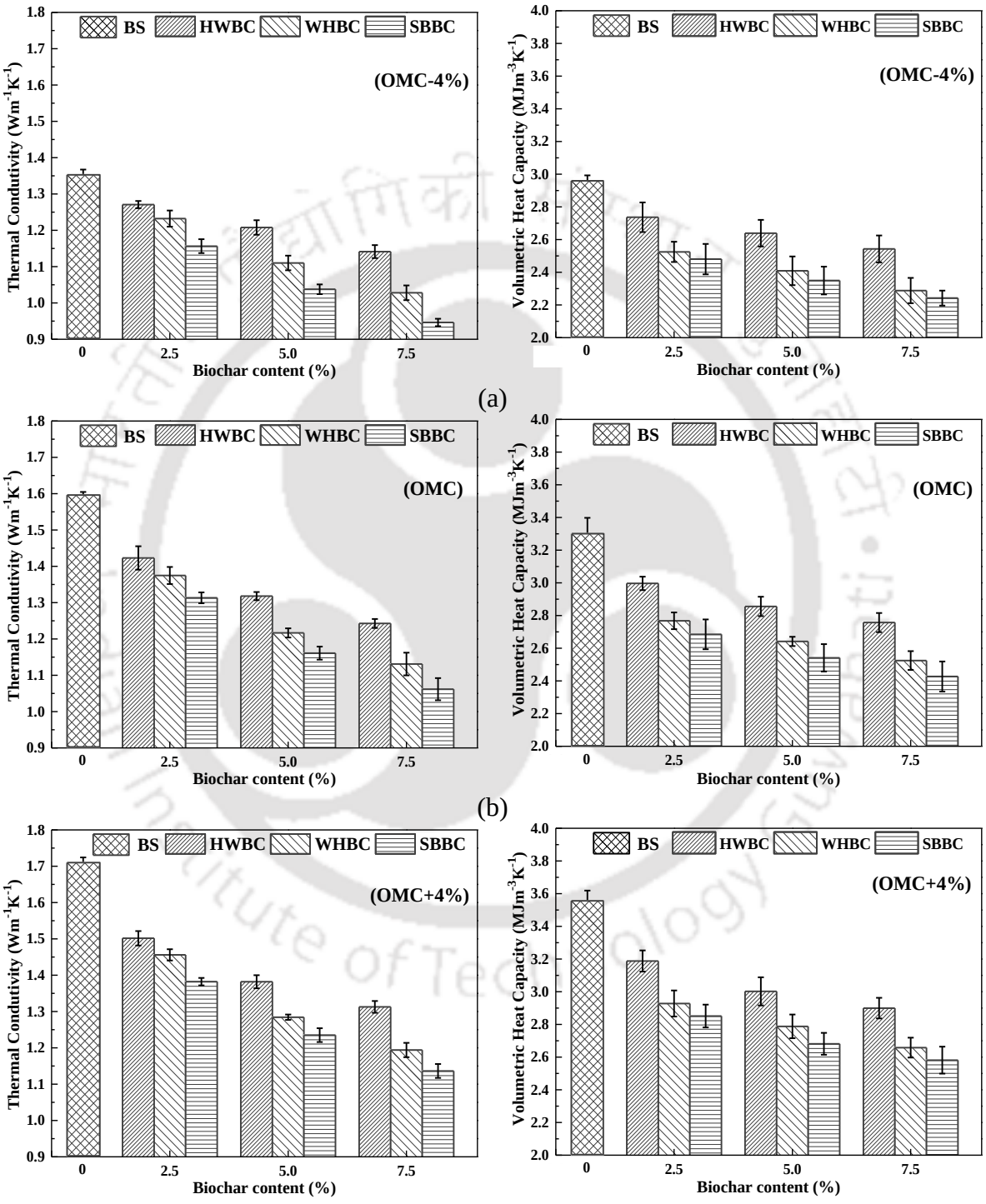

Figure 5.2 Variation of *K* and *C* of MH soil amended with different biochar types and percentages at (a) OMC-4; (b) OMC; (c) OMC+4 compaction conditions

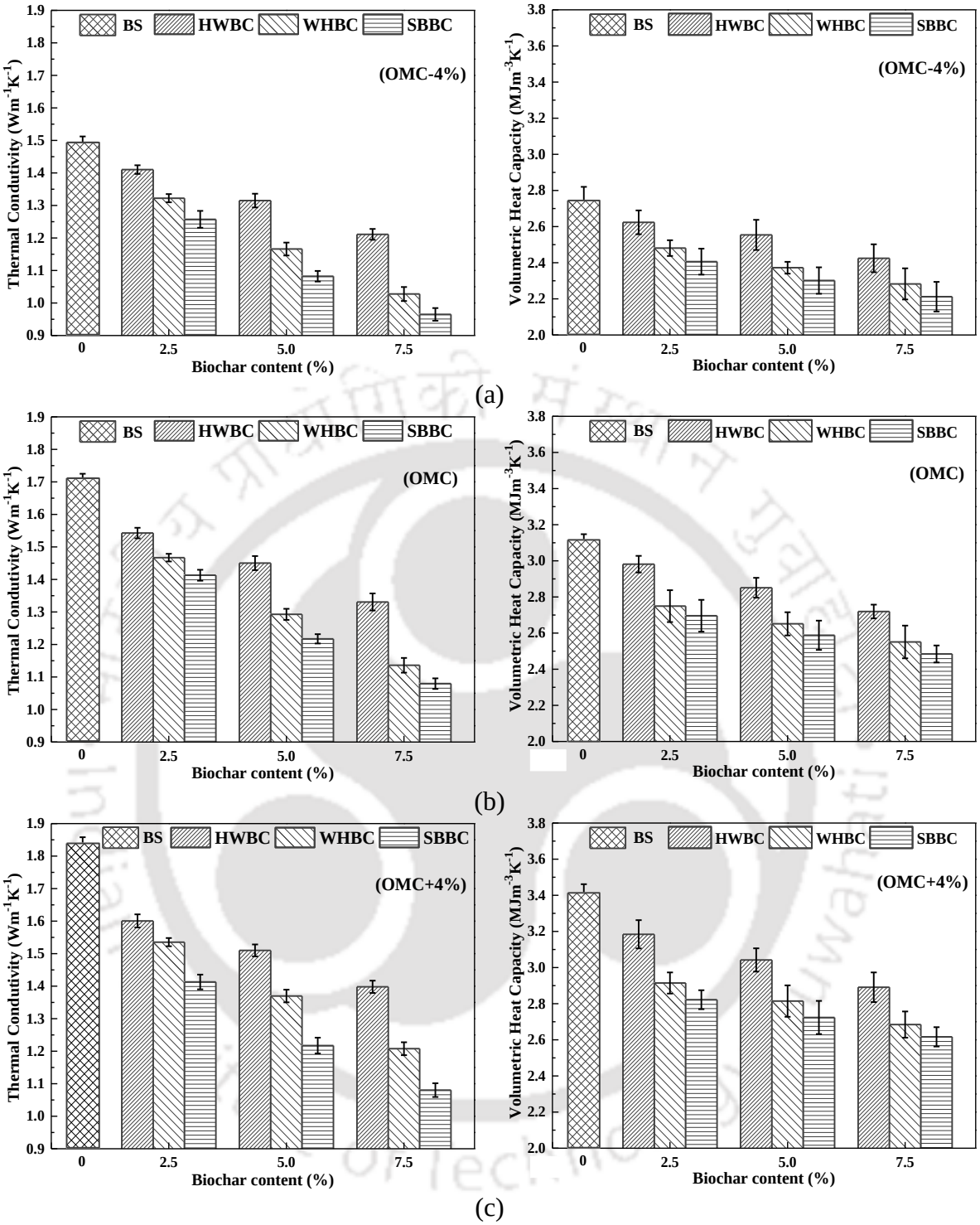

Figure 5.3 Variation of thermal characteristics of SC soil amended with different biochar types and percentages at (a) OMC-4; (b) OMC; (c) OMC+4 compaction conditions

Since the *K* of air (0.025 $Wm^{-1}K^{-1}$) is 24 times lower than water (0.594 $Wm^{-1}K^{-1}$, at 20 °C) and nearly one hundred times lower than other soil constituents, that can reduce heat conduction through soil solid and liquid phrase (Liu et al., 2018). Additionally, the increase in organic matter content with biochar amendment also contributes to reducing the thermal conductivity of soil (Zhao et al., 2016). Moreover, biochar itself has a lower *K* value that

reduces the *K* value of SBC (Zhao et al., 2016; Liu et al., 2018). The *C* value of air is 0.00125 $MJm^{-3}K^{-1}$, which is much smaller than the soil mineral (1.898 $MJm^{-3}K^{-1}$) constituent, organic matter, and water (4.182 $MJm^{-3}K^{-1}$) value. Moreover, biochar itself has a lower *C* value that reduces the C value of SBC (Zhao et al., 2016; Liu et al., 2018). Moreover, it is remarkable to point out that from Fig. 5.2 that the soils amended with the HWBC exhibited higher *K* and *C* values for the same percentage of biochar content compared to WHBC and SBBC. This is attributed to the higher MDD value of HWBC, which increases the *K* and *C* values of BAS. Since the *K* and *C* value increases with an increase in density. Therefore, well-compacted soil exhibited a high value of *K* and *C* by reducing the total void volume and improving contact between the solid grains (Abu-Hamdeh and Reeder, 2000; Abu-Hamdeh, 2003; Tong et al., 2020). Moreover, the HWBC has higher quartz content as compared to WHBC and SBBC, which can be seen from the XRD spectra, as presented in Fig.3.3. Since the *K* of quartz (7.7 $Wm^{-1}K^{-1}$) is higher than any other material, this also explains the higher *K* value of HWBC amended soil.

Fig. 5.4 presents the percentage reduction in thermal characteristics of bare soils with the amendment of different types of biochar with different biochar content at three different compaction conditions. The reduction in *K* and *C* values was observed to be more in the SBBC than WHBC and HWBC amended highly plastic silt (MH) soil at all different compaction conditions. This is mainly credited to the higher decrement in the MDD value of SBBC than WHBC and HWBC amended MH soil (refer to Table 5.3). The trend was found in the same line with the amendment of different biochar types with clayey sand (SC) soil (see Fig. 5.5). Further, it was also observed that there is a significant difference in the percentage reduction in *C* value between the HWBC and WHBC and SBBC amended soils. This is mainly due to the higher difference in OMC and MDD values of HWBC and WHBC, and SBBC amended soils. Moreover, the marginal difference between the percentage reduction in *C* value was also found between the WHBC and SBBC amended soils. A probable reason for this could be due to the nearly similar value of OMC with the amendment of WHBC and SBBC amended soils.

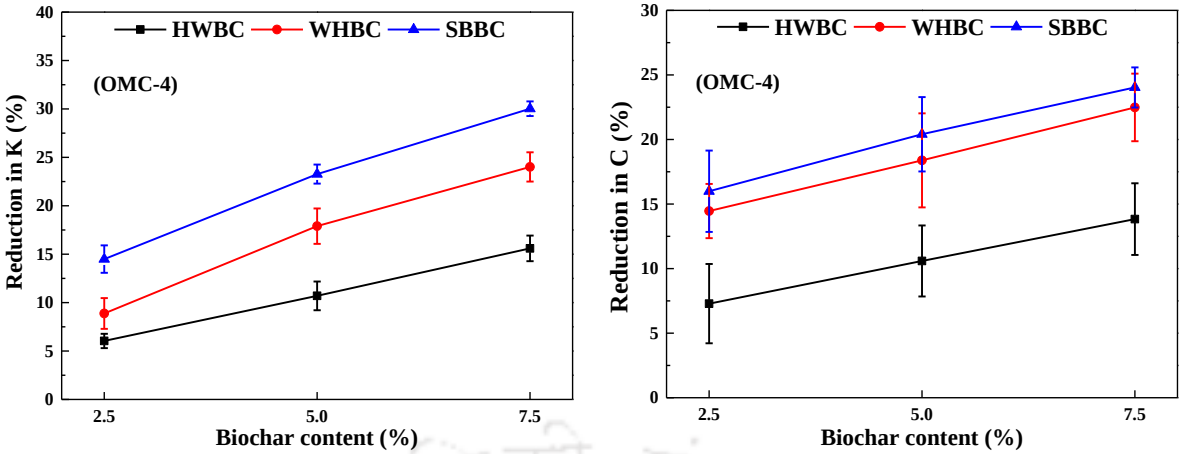

(a)

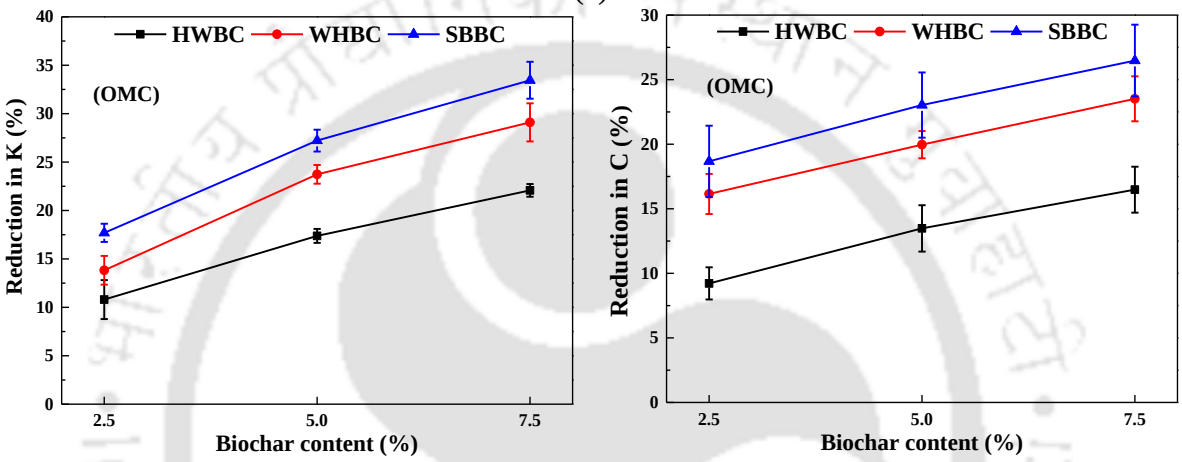

(b)

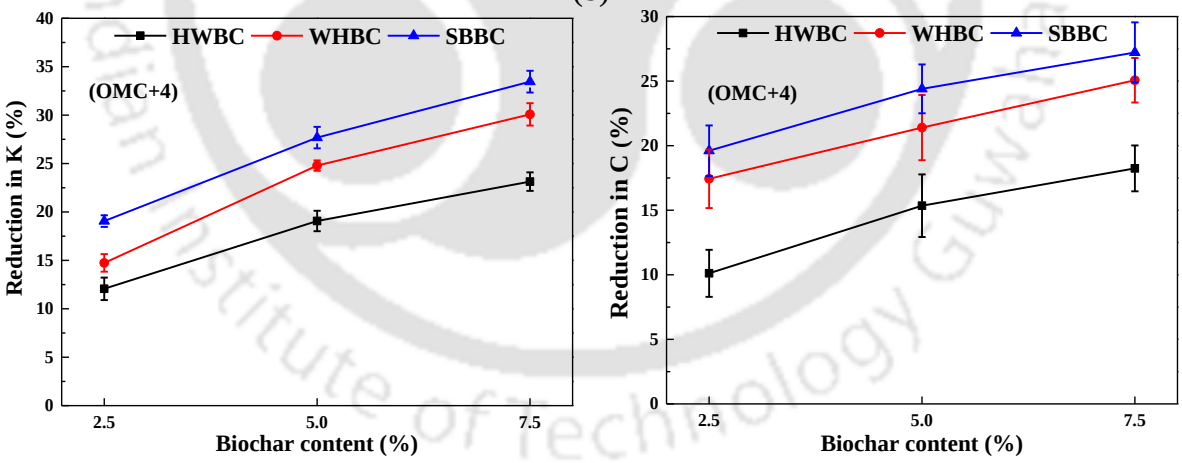

(c)

Figure 5.4 Reduction in thermal characteristics of MH soil amended with different biochar types and percentages at (a) OMC-4; (b) OMC; (c) OMC+4 compaction conditions

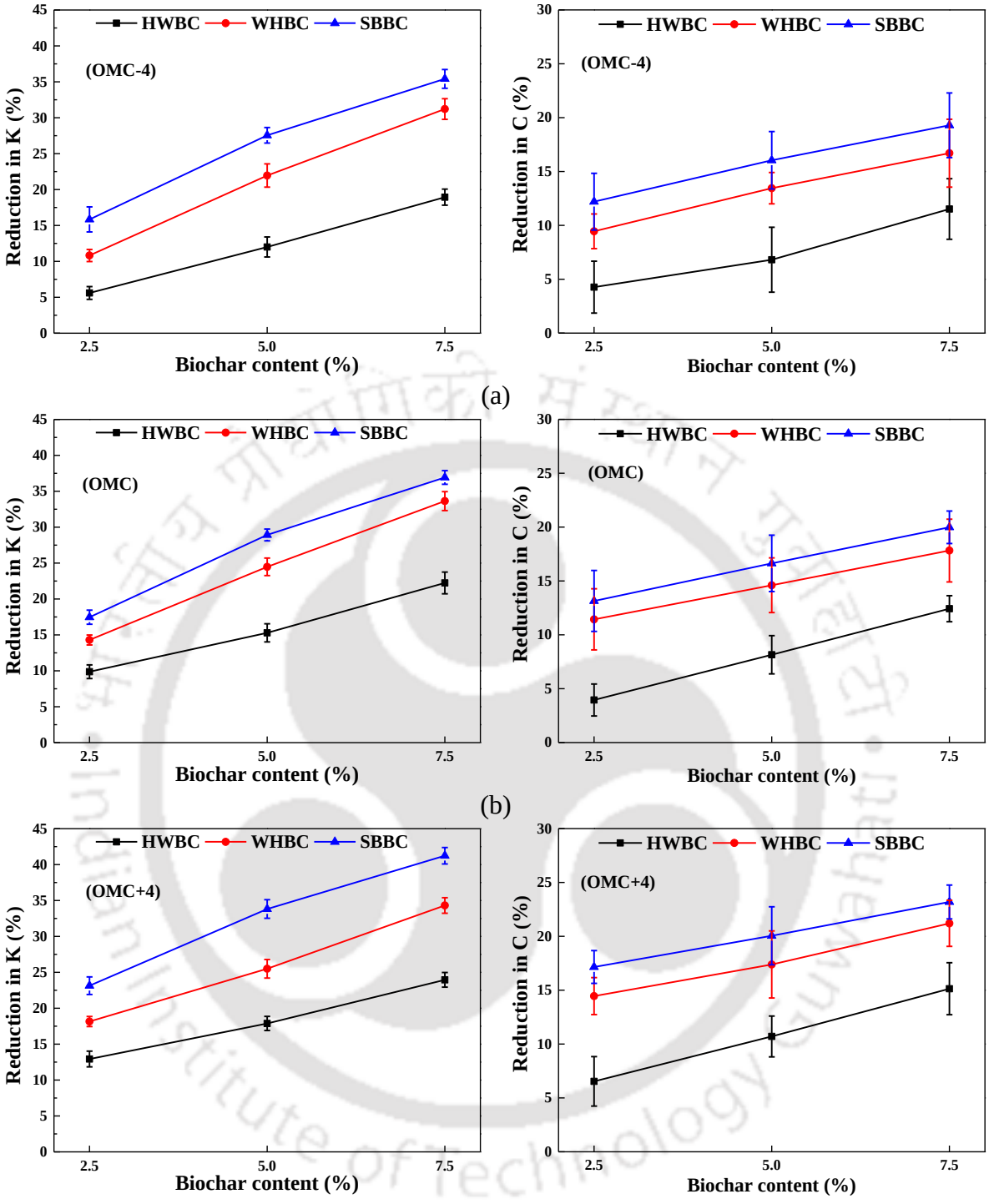

Figure 5.5 Reduction in thermal characteristics of SC soil amended with different biochar types and percentages at (a) OMC-4; (b) OMC; (c) OMC+4 compaction conditions

5.3.3.1 Effect of compaction conditions on thermal characteristics of bare soil and BAS

Fig. 5.6 presents the effect of compaction conditions on the thermal characteristics of soils amended with different biochar types and percentages. As the compaction conditions change from (OMC-4) to (OMC+4), the thermal characteristics gradually increase. This is due to the higher thermal conductivity and volumetric heat capacity of water as compared to air. Further, a percentage decrease and increase in thermal characteristics of bare soils and SBC at (OMC-4) and (OMC+4) conditions were evaluated with respect to the OMC and MDD conditions. At (OMC-4) conditions, the thermal conductivity value was observed to be decreased by 15% in bare soil (MH), while it was found to be decreased by 11%, 10%, and 12% with the amendment of 2.5% of HWBC, WHBC, and SBBC, respectively (refer to Fig. 5.6). Similarly, the C value was noted to be reduced by 11% in bare soil (MH), while it was found to be decreased by 9%, 9%, and 8% with the respective addition of 2.5% of HWBC, WHBC, and SBBC. Comparatively, at (OMC+4) conditions, the *K* value was observed to be increased by 7% in bare soil (MH), while it was found to be increased by 6%, 6%, and 5% with the amendment of 2.5% of HWBC, WHBC, and SBBC, respectively (refer to Fig. 5.6). Likewise, the *C* value was noted to be enhanced by 7% in bare soil (MH), while it was found to be rise by 6%, 6%, and 6% with the respective addition of 2.5% of HWBC, WHBC, and SBBC. The trend was found to be in the same line when the clayey sand (SC) soil was amended with different biochar types and amendment rates (refer to Fig. 5.7).

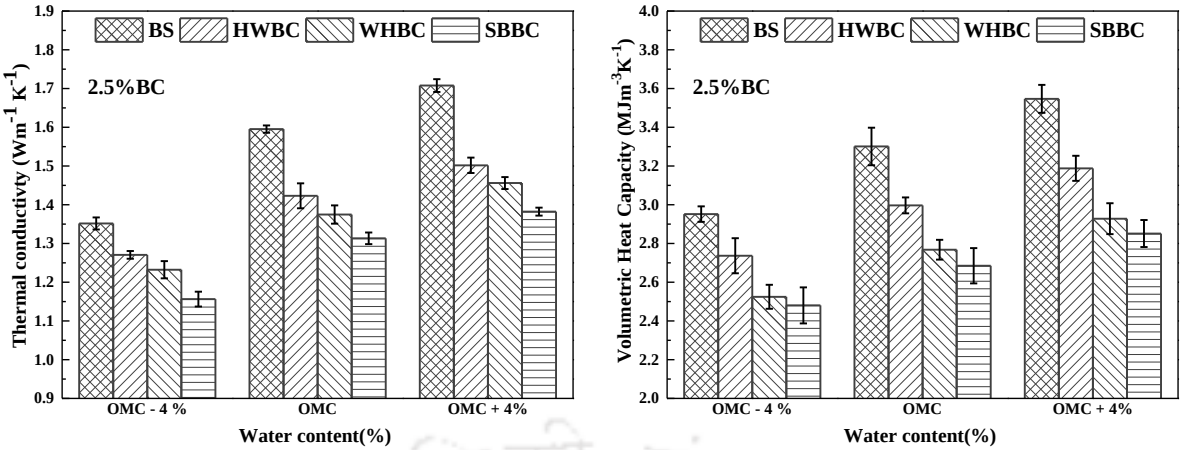

(a)

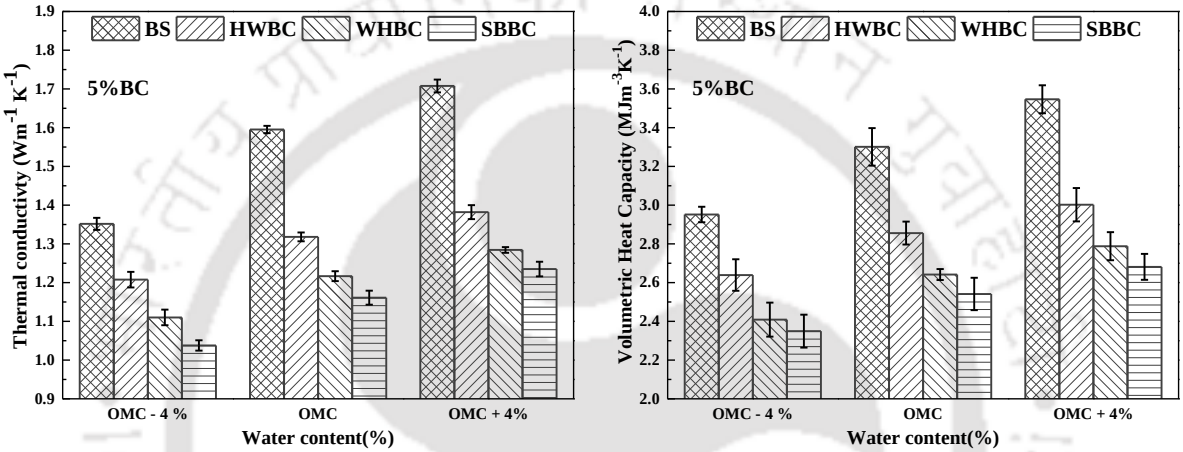

(b)

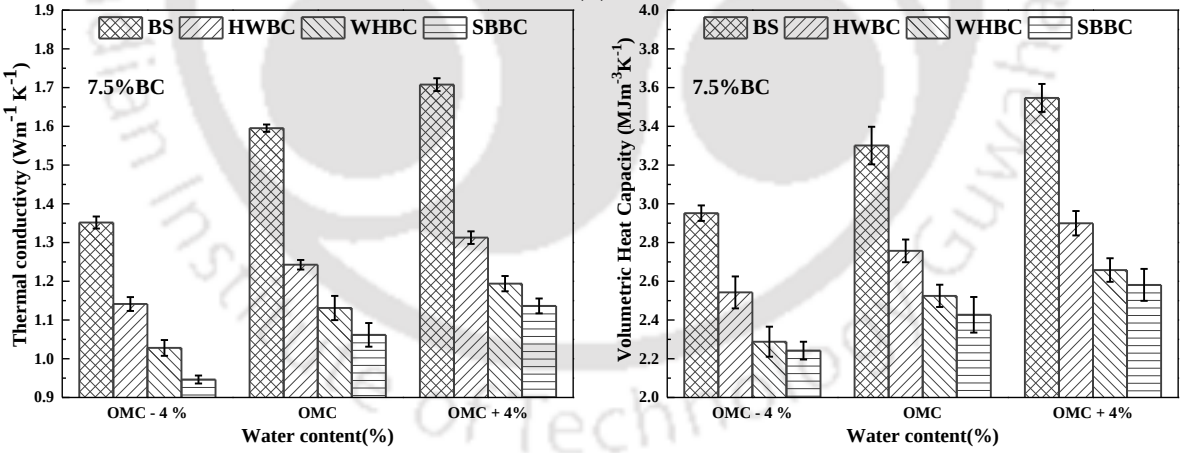

(c)

Figure 5.6 Effect of compaction conditions on the thermal characteristics of MH soil amended with different biochar types and percentages (a) 2.5%; (b) 5%; (c) 7.5%

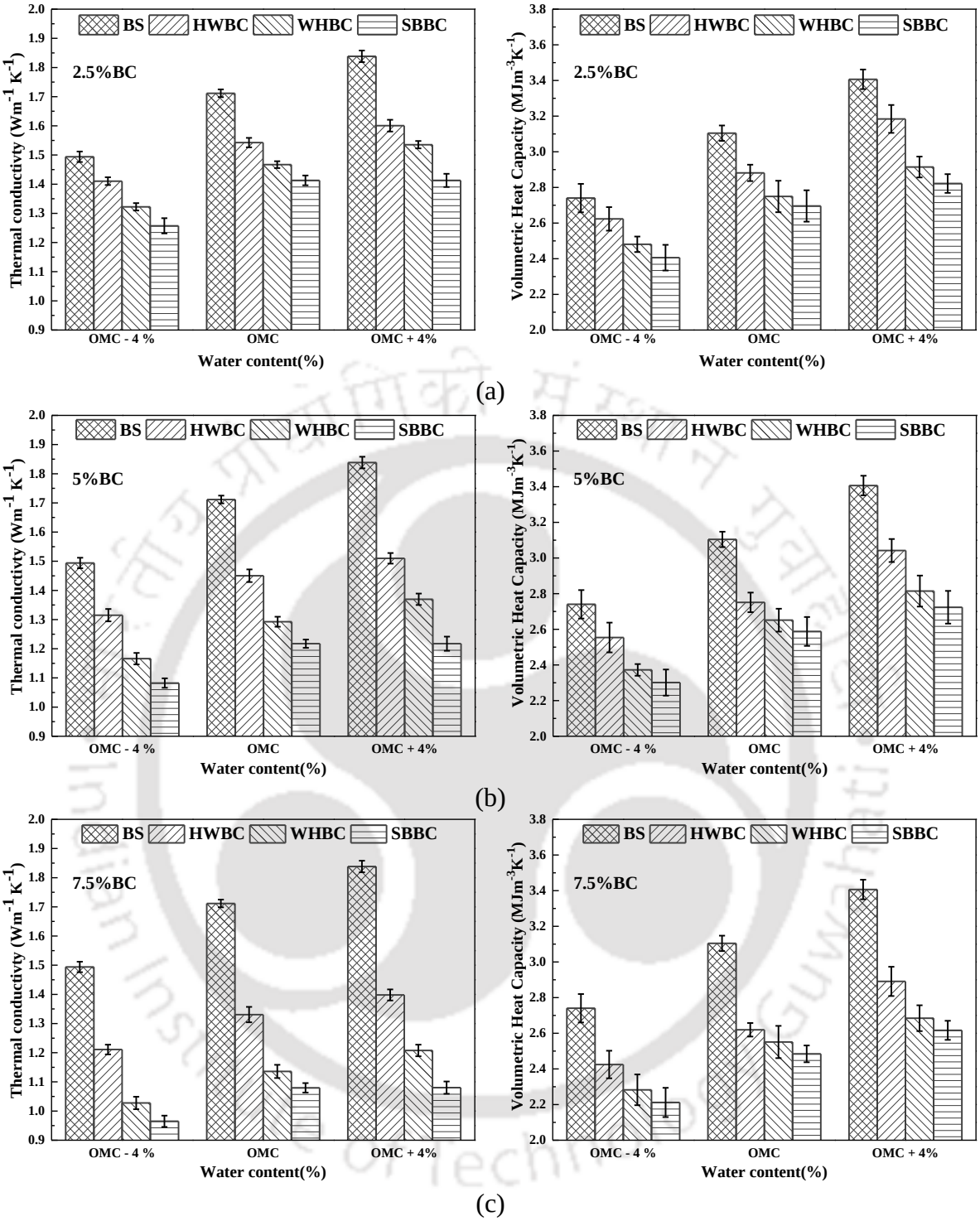

Figure 5.7 Effect of compaction conditions on the thermal characteristics of SC soil amended with different biochar types and percentages (a) 2.5%; (b) 5%; (c) 7.5%

Moreover, it is remarkable to point out that from Fig. 5.6 and Fig. 5.7 that the percentage decrement in thermal properties was higher in dry compaction conditions (OMC-4) than the increment in wet compaction conditions (OMC+4) for both bare and BAS. Since it is well established that the soil *K* and *C* values are more strongly correlated with porosity (air-content) as compared to the volume fraction of water (Tong et al., 2020; Xie et al., 2020).

Thus, with a decrease in water content (i.e., dry compaction condition), the amount of air content will increase, reducing the *K* and *C* values to a higher amount than the wet compaction conditions. Furthermore, this can also be attributed to the change in orientation of soil particles, i.e., flocculated (in dry compaction state) to dispersed structure (in wet compaction condition) (refer to Fig. 5.8). It is well documented that the soil particles are oriented in the flocculated structure at the dry side of OMC, and it becomes a dispersed structure at the wet side of OMC. Since the contact area is lesser in flocculated structure (edge-to-face contact), which forms larger voids than the dispersed structure (face-to-face contact) that exhibits lower voids volume. Therefore, the percentage decrement in *K* and *C* values were higher in the dry compaction conditions.

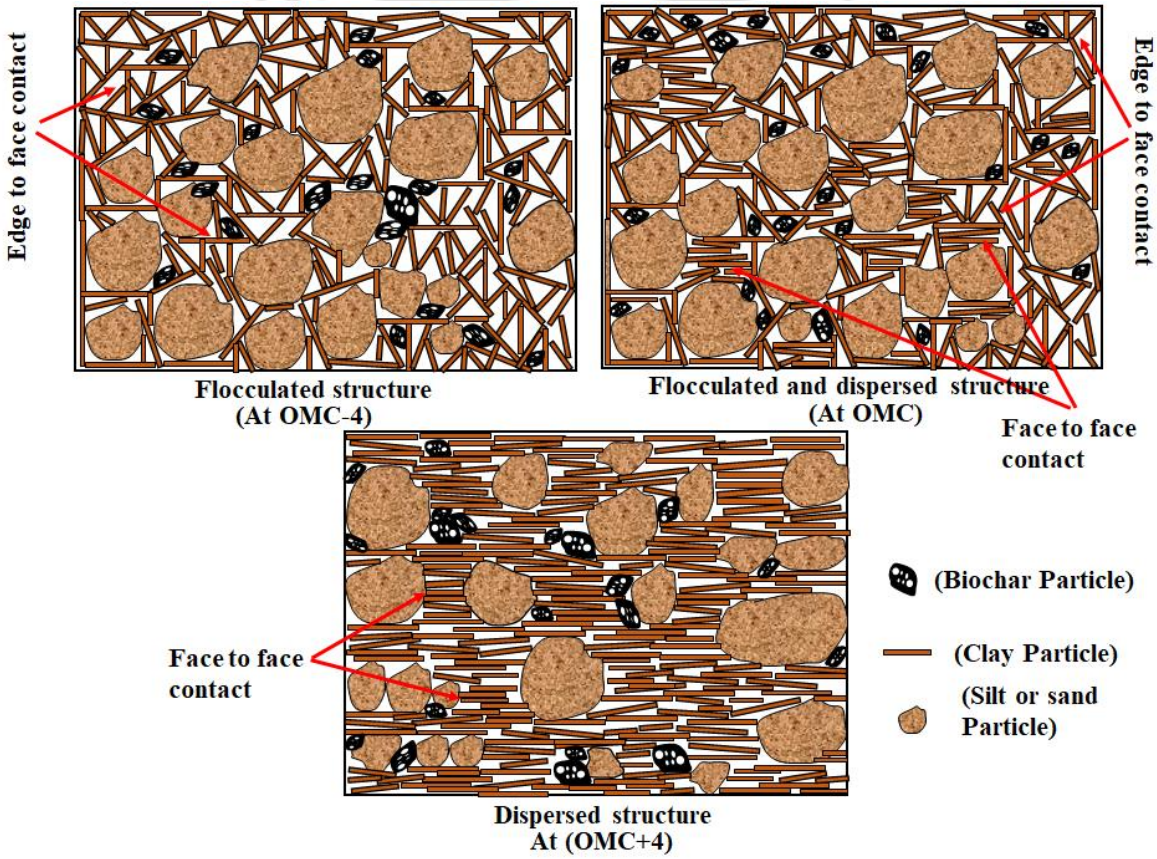

Figure 5.8 Conceptual diagram showing the change in soil particle orientation with water content

5.3.4 Influence of biochar particles size fractions on thermal characteristics of SBC

The variation of thermal characteristics of bare soils (BS) amended with the different biochar content, and different biochar particle size fractions are presented in Fig. 5.9. The *K* value of the MH soil was observed to be reduced by 15, 26, and 35 % with the amendment of 5, 10, and 15 % of finer fraction of biochar. Similarly, the reduction in *C* values was found

to be 6, 15, and 21 % with the addition of 5, 10, and 15 % of finer fractions of biochar. A similar trend in *K* and *C* values was found when the MH soil was amended with medium and coarser biochar fractions. The observed trends were found to be the same when different biochar particle fractions were added to SC soil. This is attributed to the reduction in the density of the soils with the amendment of biochar, which is already explained in section 5.3.3.

Moreover, it is remarkable to point out that from Fig. 5.9 that the soils amended with the finer fractions of biochar exhibited higher *K* and *C* values for the same percentage of biochar content compared to medium and coarser fractions of biochar. This is mainly due to the higher OMC and MDD value of finer SBC, which increases the *K* and *C* values of SBC. Since the *K* and *C* values increases with an increase in density and water content. Therefore, a well-compacted soil exhibited a high *K* and *C* value by reducing the total void volume and improving contact between the solid grains.

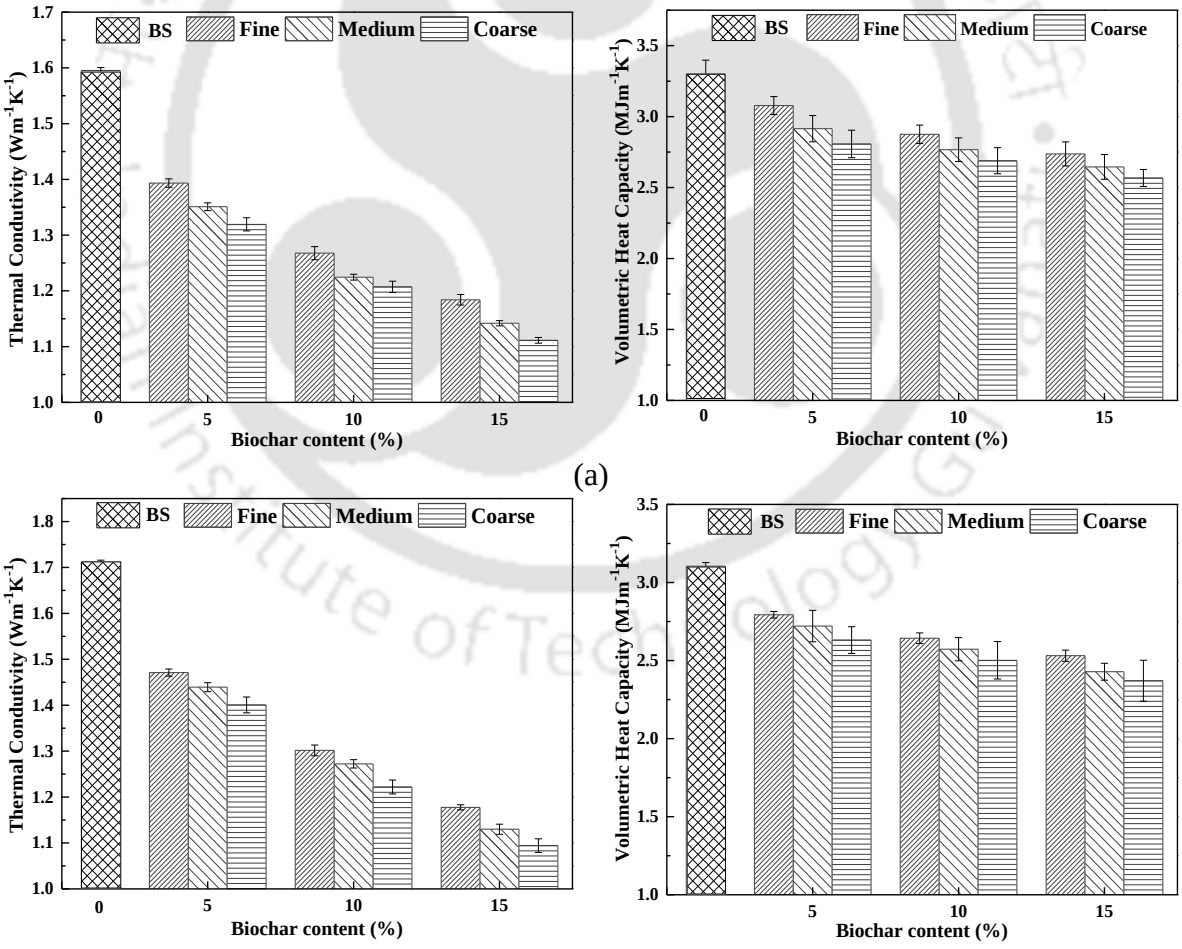

Figure 5.9 Variation of thermal characteristics of BS: (a) MH; and (b) SC with different biochar content and particle size fractions.

Moreover, the finer biochar fraction has higher quartz content than other size fractions, which can be seen from the XRD spectra, as presented in Fig. 5.10. Since the *K* of quartz (7.7 $Wm^{-1}K^{-1}$) is higher than any other material, this also supports the higher *K* of finer SBC. The decrement trends in *K* and *C* values were not observed to be linear for different biochar particle size fractions at different biochar amendment rates.

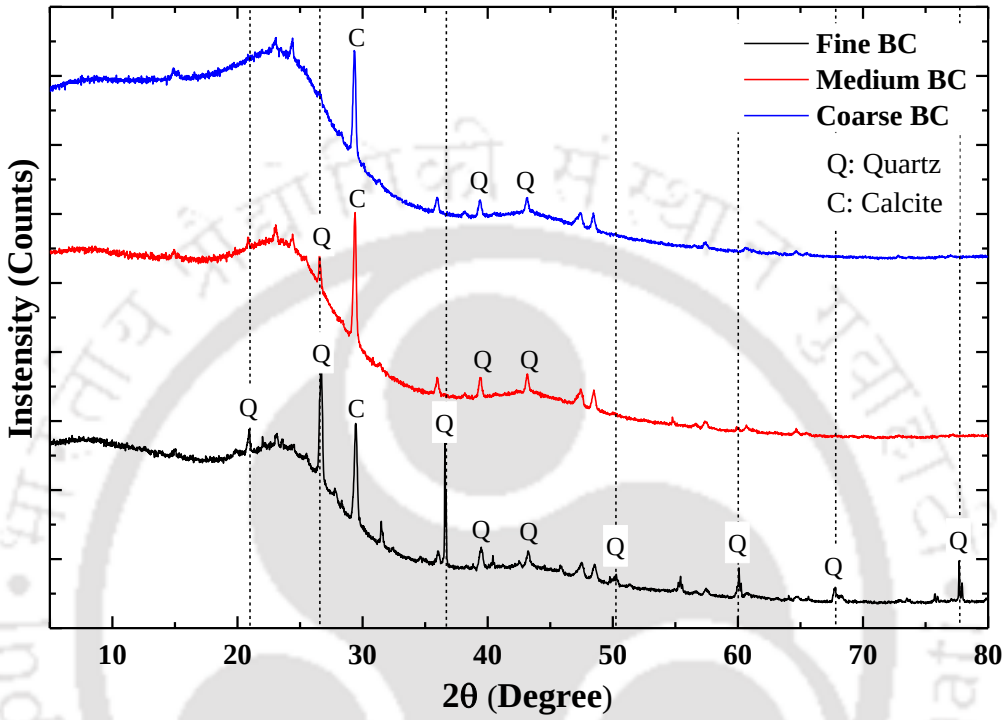

Figure 5.10 X-ray diffraction spectra of different biochar fractions

Fig. 5.11 presents the percentage reduction in thermal properties of bare soils with different biochar content and different biochar particle size fractions. The reduction value was observed to be more in the coarser fraction of biochar. Further, it was also observed that the reduction in thermal properties was higher in SC soil than in MH soil. This is mainly credited to the higher decrement in the MDD value of SC soil than MH soil (refer to Table 5.4). Moreover, the presence of a higher amount of clay content in MH soil leads to more chances that a greater amount of clay particles would fill up the biochar intra-pores than in SC soil. The ingression of clay particles in biochar intra-pores was also reported by previous researchers (Wong et al., 2016; Williams et al., 2020). The ingression of clay particles in biochar intra-pores can be seen from the micrographic analysis of soil biochar composite (refer to Fig. 5.12). It is clearly displayed from the SEM micrograph that the majority of the biochar intra-pores were unfilled, while some of the biochar intra-pores were partially sealed with the ingression of clay particles.

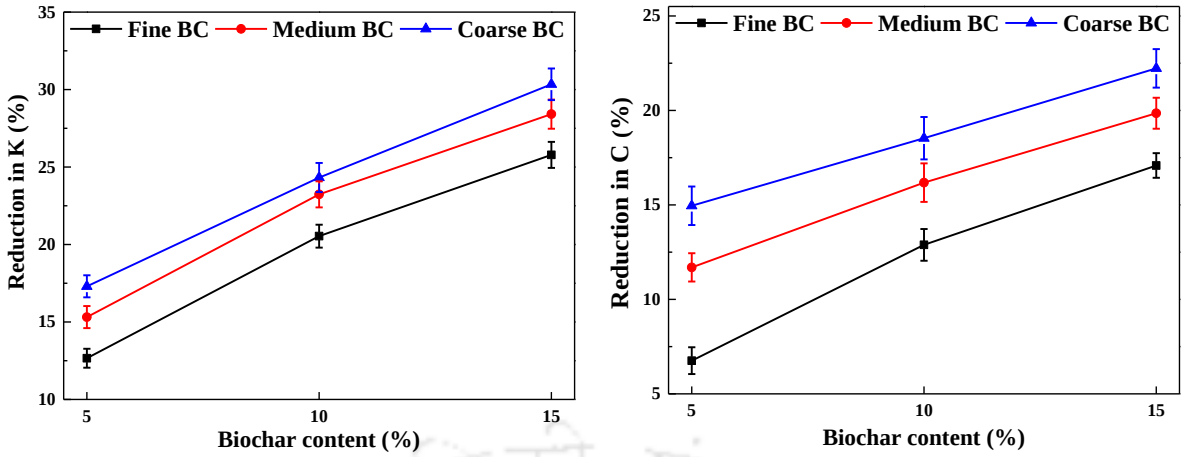

(a)

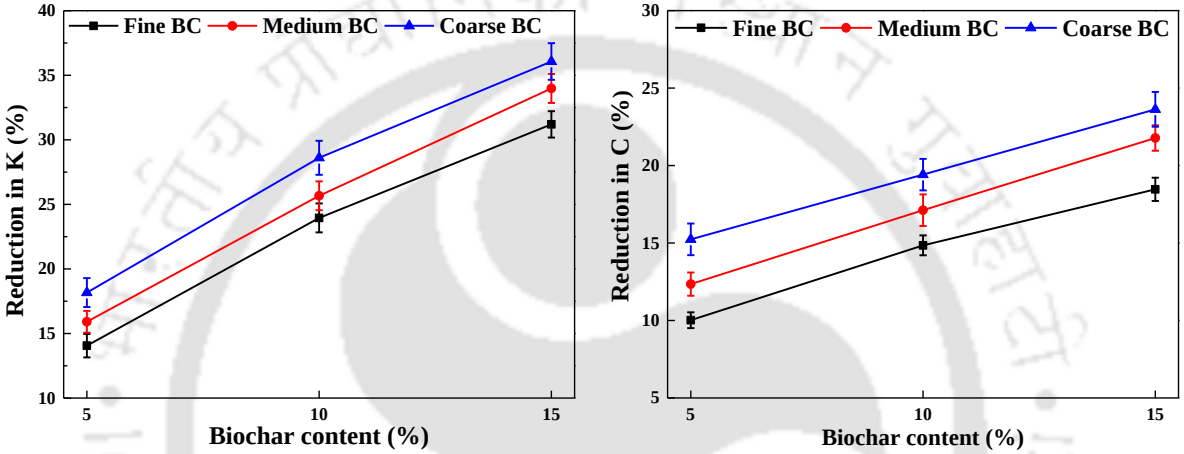

(b)

Figure 5.11 Reduction in thermal characteristics: (a) MH; and (b) SC with different biochar content and particle size fractions.

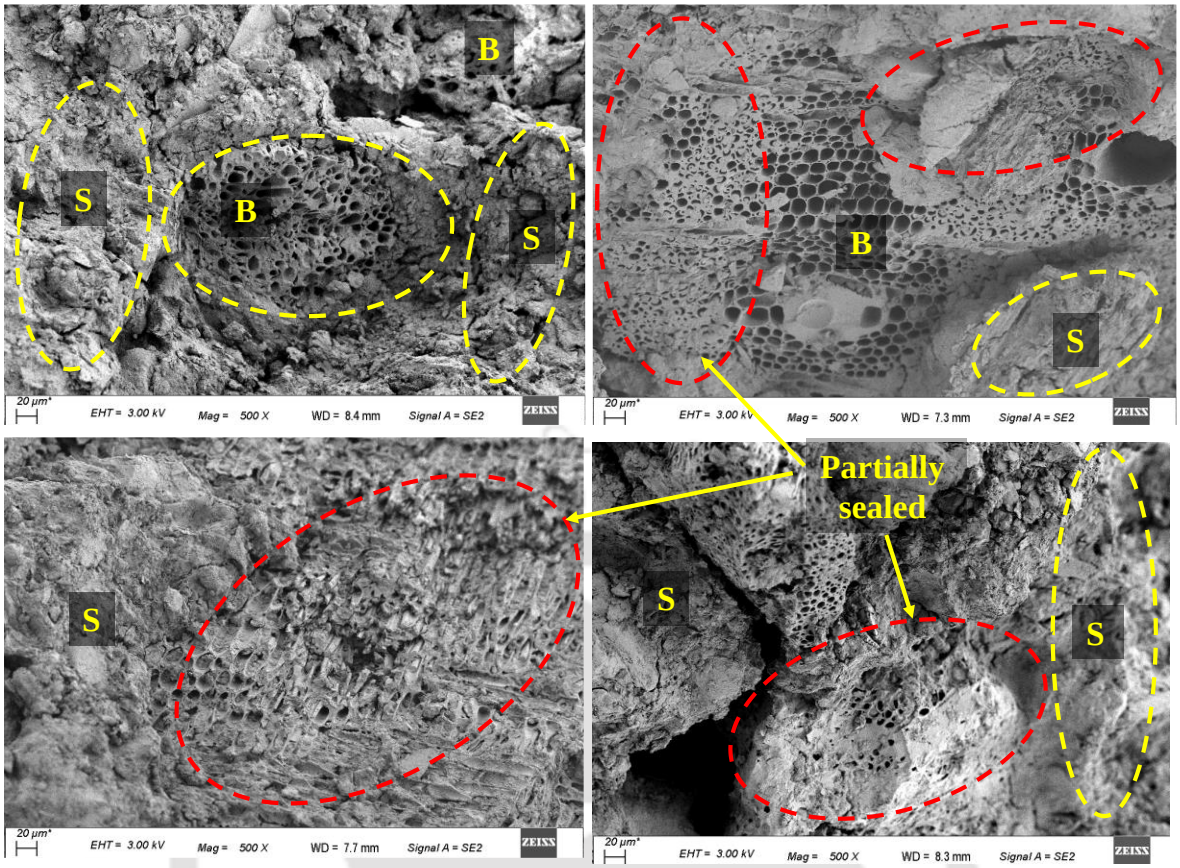

Figure 5.12 SEM micrograph showing the ingression of clay particles in biochar intra-pores (S: Soil, B: Biochar)

5.3.5 Impact of biochar fraction on UCS of SBC

Fig. 5.13 presents the UCS variation of bare soils amended with the different biochar content and particle size fractions compacted at OMC and MDD states for the UCS test. The cohesion and frictional interlocking among the soil particles and biochar govern the soil sample's failure mechanism. The UCS of the MH soil was observed to be reduced by 46%, 54%, and 62%, while for SC soil, it was found to be decreased by 44%, 39%, and 37% with the amendment of 5%, 10%, and 15% of finer fractions of biochar. The observed trends in UCS value were found to be the same when the soil was amended with medium and coarser biochar fractions. All the SBC exhibit lower UCS values than that of bare soil. A similar result was also reported by previous researchers (Bora et al., 2021). The prime reason for the strength reduction with an increase in biochar content in the SBC samples is the decrease in the overall density. Furthermore, biochar is non-cementitious, unlike cement or biopolymers. Therefore, a decrease in density is explicitly disadvantageous for the strength of the SBC. The reduction in UCS of SBC is also aided by the diminution in the cohesive force and frictional interlocking between the soil particles with the addition of biochar (Kumar et al. 2019, Bora et al. 2021). Additionally, the presence of hydrophilic and hydrophobic

functional groups in biochar interacts with water and forms a complex network between the biochar particle and water, increasing the distance among the soil particles. Due to this, the electrostatic force of attraction between soil particles is reduced, which lowers the cohesiveness of the soil-biochar matrix (Pardo et al., 2019). All these factors collectively contribute to the decay in the strength of soil upon biochar increment.

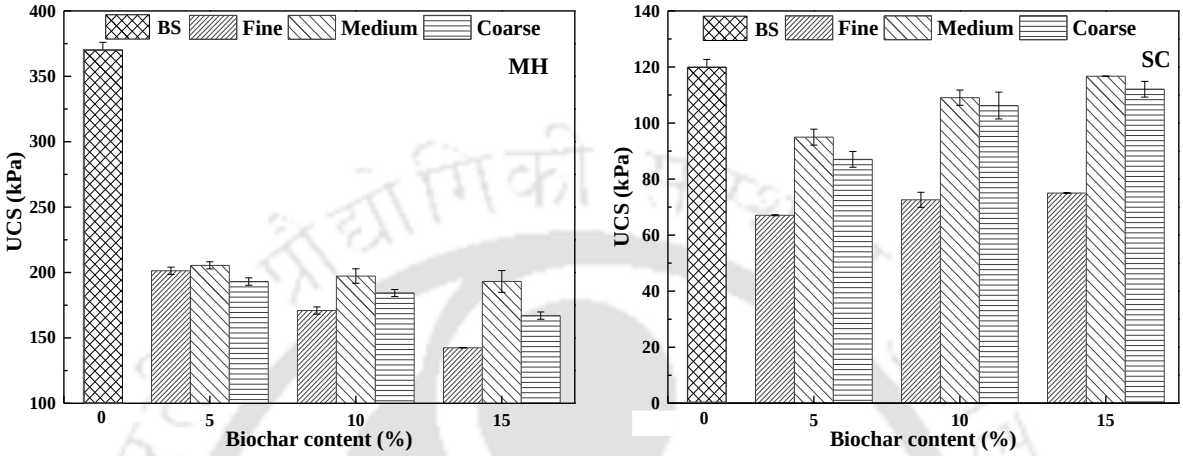

Figure 5.13 UCS of bare soil (BS) and SBC

Moreover, it is noteworthy to point out that from Fig. 5.13 that the soils amended with the finer fractions of biochar exhibited lower UCS value (201.30 kPa) for the same percentage (5%) of biochar content compared to medium (205.44 kPa) and coarser (193.09 kPa) biochar fractions. A similar trend in UCS value was also observed when the soils were amended with 10% and 15% biochar content. This is mainly due to the higher specific surface area (SSA) of finer biochar particles that leads to more contact between soil particles, biochar, and water that hindered the ability of the soil particles to draw closer according to the intergranular theory, which leads to the more reduction in frictional interlocking and cohesion. In addition, the engulfment of fine biochar dust on soil particles is expected to further decrease the cohesive forces of the soil (Kumar et al., 2019). Moreover, the UCS of biochar-amended MH soil was found to decrease with an increase in biochar percentage, while it was observed to be increased with an increase in biochar percentage in the case of SC soil. However, in both soils, the UCS value of SBC was observed to be less than the bare soil. The increment in UCS value in the case of SC soil may be due to the increase in friction of SBC with a higher proportion of biochar addition (Zong et al., 2014).

Fig. 5.14 presents the strength improvement factor (SIF) and mean peak strain factor (MPSF) of all soil-biochar mixes compacted at OMC and MDD. It was observed that all soil-biochar mixes exhibited reduced strength with respect to bare soil (SIF < 1). This can

be attributed to the decrease in cohesion between the soil particles with the biochar (cohesionless material) amendment. Comparatively, the finer and medium fractions SBC shows enhancement in ductility (MPSF > 1) with respect to bare soil, while it was found to diminish with the addition of coarser fraction SBC (MPSF ranged from 0.78 to 0.93). The increase in ductility of soils with fine and medium biochar fractions amendment can be attributed to the lower density (higher porosity) and higher compacting water content of soil-biochar composites. The presence of lower density and higher water content assists the soil-biochar composites to undergo a more particle rearrangement or deformation without failure leading to the increase of elasticity or strain at failure. The decrement in ductility in soil with the amendment of coarser biochar fraction may be due to the higher separation between soil particles, leading to earlier failure of SBC compared to bare soil. Moreover, the enhancement in ductility with the addition of medium and finer biochar fractions was observed to be more in MH soil than in SC soil. This may be due to the more contact between soil and biochar particles in MH soil, which has a high SSA than SC soil.

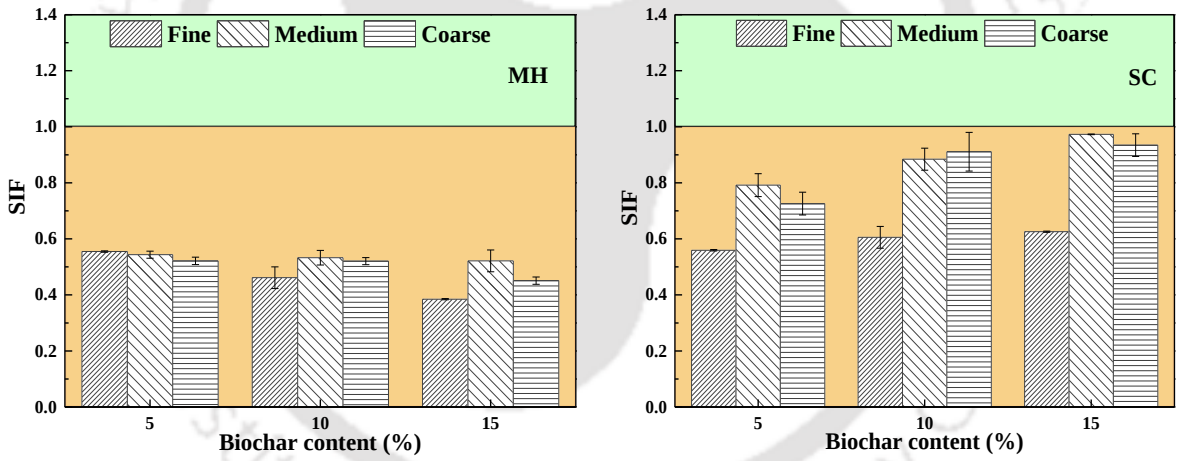

Figure 5.14 (a) SIF and (b) MPSF of SBC with respect to bare soil.

Currently, there is no report or literature documented for the threshold value of thermal characteristics and geotechnical properties of thermal backfill material for heat insulation. The current study has investigated the thermal and strength characteristics performance of biochar-based thermal backfill and compared it to conventionally used material (i.e., bare soil). The finding of this study indicates that the biochar-based thermal backfill is a better backfill material compared to bare soil.

5.3.6 Correlation between Thermal and UCS Value of SBC

Fig. 5.15 presents the correlation between percentage reduction in *K* and *C* values with the percentage reduction in UCS value for soils amended with different biochar content and particle size fractions. The main objective of this correlation is to identify the better fraction of biochar to be used for thermal backfill. The biochar amendment in soil decreases the compaction density of soil and hence increases the porosity of the soil-biochar mixes. It is well established that the compaction density is directly related to the thermal properties and UCS of soil (Abu-Hamdeh, 2003; Tong et al., 2020). Moreover, the thermal properties and UCS of soil are also governed by the organic content (biochar amendment). It was reported that the inclusion of organic matter reduces the thermal conductivity and UCS of soil (Abu-Hamdeh and Reeder, 2000; Dec et al., 2009; Zhao et al., 2016; Varghese et al., 2021). However, it is not highlighted in terms of biochar particle size fractions, which is focused on in this chapter.

It can be noted from the figures that for the same percentage of biochar amendment, the thermal properties were observed to be relatively less reduced in comparison to the reduction in UCS value for all biochar particle size fractions. It is mainly because the thermal properties are governed by porosity, while UCS is governed by the initial state of the soil (Farouki, 1981; Holtz et al., 1981). Moreover, it can also be observed from the figures that the soils amended with medium fraction biochar show less decrement in UCS value compared to the soils amended with finer and coarser biochar fractions for the same amendment rate. Based on the above observations, it is indicative that the soils amended with medium fraction biochar are more suitable as thermal backfill for underground crude oil pipelines and crude oil storage tanks with respect to thermal and strength aspects.

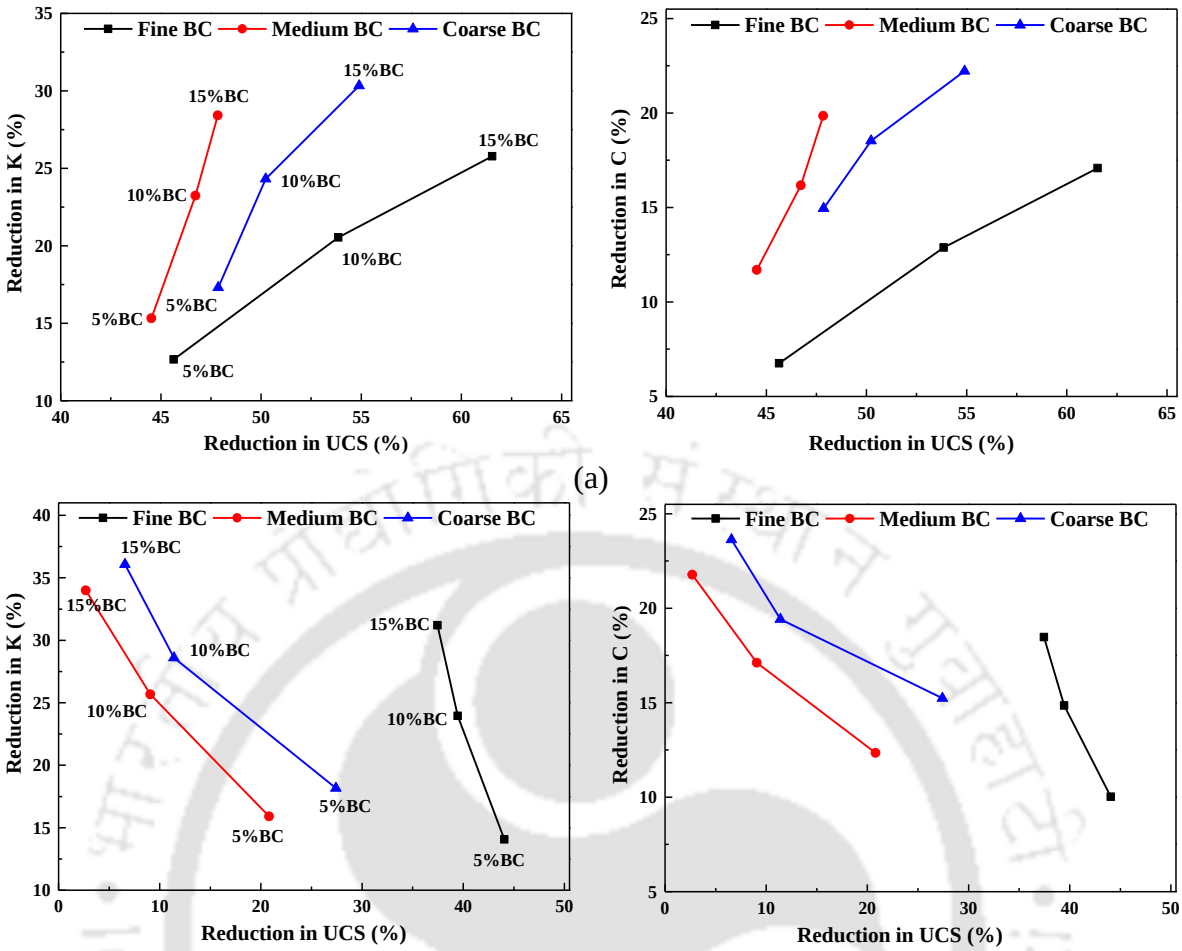

Figure 5.15 Relationship between reduction in thermal and UCS value of SBC: (a) MH; and (b) SC.

5.4 Summary

The current chapter explores the potential of a natural soil-biochar composite (SBC) as a thermal backfill. The SBC were studied under different compaction conditions using biochar types and biochar particle size fractions for thermal characteristics. Further, the UCS of SBC was also investigated using different biochar particle size fractions. The findings of the thermal and strength reduction and is also revealed by micrographic analysis of SBC. The major findings from the current chapter are as follows:

- Thermal characteristics of both the soils and SBC are affected by the compaction parameters (OMC and MDD). The biochar amendment decreases the MDD and increases the OMC of soils, which depends upon the type of biomass of the biochar.
- The reduction in *K* and *C* values of soils depends upon the soil types, biochar types, and biochar particle size fractions amended to the soil. The reduction in thermal characteristics is higher for sugarcane bagasse biochar (SBBC), followed by water

hyacinth biochar (WHBC), and least noted for hardwood biochar (HWBC). This is mainly credited to the higher decrement in MDD value of soils with the amendment of SBBC. For a 7.5% amendment rate, the reduction in *K* is 34, 29, and 22% (for MH soil) and 37, 34, and 23% (for SC soil) for SBBC, WHBC, and HWBC. Similarly, the reduction in *C* is 27, 24, and 17% (for MH soil) and 21, 18, and 13% (for SC soil) for SBBC, WHBC, and HWBC.

- The decrement in thermal characteristics was found to be higher in dry compaction state (OMC − 4) as compared to increment in wet compaction state (OMC + 4) for both the BS and SBC. This could be attributed to the change in soil particle orientation from flocculated in dry compaction state to dispersed in wet compaction state.
- The reduction in *K* and *C* values is higher for coarser biochar fractions, followed by medium and least noted for finer fractions. For the 15% amendment rate, the reduction in *K* is 31, 29, and 26% (for MH soil) and 36, 34, and 32% (for SC soil) for coarser, medium, and finer fraction biochar. Similarly, the reduction in *C* is 23, 20, and 17% (for MH soil) and 24, 22, and 19% (for SC soil) for coarser, medium, and finer fraction biochar.
- The UCS of soil reduces with biochar amendment, which depends upon soil type and biochar particle size fractions. For the 15% amendment rate, the reduction in UCS value is 48, 55, and 62% for the medium, coarser, and finer fraction biochar for MH soil. Similarly, the UCS value is reduced by 3, 7, and 38% for the medium, coarser, and finer fraction biochar for SC soil.

CHAPTER 6
THERMAL AND STRENGTH CHARACTERISTICS OF SOIL-BIOCHAR-BIOPOLYMER COMPOSITE

6.1 Introduction

The obtained results from the previous chapter clearly indicate that SBC has lower thermal characteristics than bare soil at OMC and MDD state. However, a notable decrease in soil strength was observed upon biochar amendment despite a beneficial decrement in thermal characteristics, which restricts its application to a certain extent for field applications. Every so often, TAS is installed in the vicinity of residential and transportation infrastructures. Thus, the backfills are expected to have high strength to support the TAS in such conditions. Therefore, there is a need for a sustainable binder that can increase the strength of the SBC while maintaining thermal conductivity.

Most of the soil strength improvement techniques, such as cementation, geo-polymerization, and bio-mineralization, result in an increase in thermal conductivity (Balaji et al., 2017; Cheng et al., 2021; Ocłoń, 2021; Xiao et al., 2021). Although these techniques can be useful for improving heat dissipation, they are not favorable for applications requiring thermal insulation. Moreover, the use of cement is also responsible for 10% of the global carbon emission (Habert et al., 2010). Previous studies examined the applicability of biopolymers such as xanthan gum, guar gum, and gellan gum in the stabilization of coarse and fine-graded soil (Chang et al., 2015, 2016; Latifi et al., 2016; Ayeldeen et al., 2017; Lee et al., 2017; Muguda et al., 2017; Qureshi et al., 2017; Vydehi and Moghal, 2022). The biopolymer-based soil stabilization (BpS) requires a considerably low quantity of biopolymer for soil strength improvement (Chang et al., 2020; Muguda et al., 2020; Devrani et al., 2021; Fatehi et al., 2021; Mahamaya et al., 2021; Ramachandran et al., 2021; Dubey et al., 2022) contrary to other binders, such as cement and biocement. Therefore, we hypothesized that incorporating biopolymer in the SBC can help in developing a high-strength sustainable composite capable of providing efficient thermal insulation.

Some previous researchers reported that polymeric fluids have slightly lower thermal conductivity compared to water (Lee et al., 1981; Broniarz-Press and Pralat, 2009; Abed, 2021). In this way, initially, the investigation of thermal conductivity of the biopolymer (xanthan gum) solutions at different concentrations was measured. The obtained results show

a marginally lower thermal conductivity compared to water, as reported by the previous researcher.

Within the context of the above-discussed literature and hypothesis, we have attempted to create a soil-biochar-biopolymer composite (SBPC) that can be tailored for its strength and thermal characteristics for the backfill of TAS requiring extreme insulation. The present chapter aims to advance the knowledge of such composites by-

- Examining the thermal conductivity (*K*) and unconfined compressive strength (UCS) of a local soil blended with biochar proportions varying up to 7.5%.
- Investigating *K* of the biopolymer solutions in the concentrations recommended for soil strength improvement. Later, examining the *K* and UCS of the soil stabilized with biopolymer proportions varying up to 1.5%.
- Exploring the potential of SBPC at various blends for thermal backfill applications by evaluating their *K* and UCS.
- Investigating the microstructure and mineralogy of the developed composites.

Moreover, while the backfill is expected to be prepared at the optimal moisture content (OMC) for maximum density, moisture loss is inevitable while insulating TAS. Therefore, all the specimens were examined at OMC and MDD state and after drying to investigate the influence of moisture loss on the strength and thermal conductivity of the proposed thermal backfill.

6.2 Sample preparation and test setup

The highly plastic silt (MH) soil is used in this chapter due to its clay-rich content, which is determined to be around 38%. From the previous chapter, it was reported that the soil amended with medium fraction biochar (2 mm-0.425 mm) is more suitable for thermal insulation and strength purposes. Analytical grade powder of the bacterial biopolymer Xanthan Gum (XG) was procured from Himedia Laboratories Pvt. Ltd., India, for the current study. XG is produced via fermentation of glucose or sucrose by the bacterium *Xanthomonas campestris*. Xanthan Gum is selected due to its high solubility in water and superior strength efficiency in soils (Chang et al., 2020).

Table 6.1 describes the different blends of soil-biochar composites (SBC), biopolymer-stabilized soil (BpS), and soil-biochar-biopolymer composites (SBPC) composites tested in the current chapter. An outline of the experiments conducted in the current chapter is presented in Fig. 6.1. The prepared specimens were investigated

extensively for their thermal conductivity, unconfined compressive strength (UCS), and microstructure. Howard (1996) suggested that the thermal backfill must be compacted at a minimum of 0.95 MDD and OMC state for optimal performance. Therefore, the samples were tested at OMC and MDD state.

Table 6.1 Blends of soil samples used in current chapter

Group	S.N.	Name	Soil (%)	Biochar (%)	Biopolymer (%)	Moisture content (%)	Dry density (Mg/m^3)
Control (Bare Soil)	1	SB0P0	100	0	0	22.70	1.58
Soil-Biochar-Composites (SBC)	2	SB2.5P0	97.5	2.5	0	24.51	1.50
	3	SB5P0	95	5	0	26.42	1.42
	4	SB7.5P0	92.5	7.5	0	27.54	1.37
Biopolymer stabilized soil (BpS)	5	SB0P0.5	100	0	0.5		
	6	SB0P1	100	0	1	22.7	1.58
	7	SB0P1.5	100	0	1.5		
Soil-Biochar-Biopolymer Composites (SBPC)	8	SB2.5P0.5	97.5	2.5	0.5		
	9	SB2.5P1	97.5	2.5	1	24.51	1.50
	10	SB2.5P1.5	97.5	2.5	1.5		
	11	SB5P0.5	95	5	0.5		
	12	SB5P1	95	5	1	26.42	1.42
	13	SB5P1.5	95	5	1.5		
	14	SB7.5P0.5	92.5	7.5	0.5		
	15	SB7.5P1	92.5	7.5	1	27.54	1.37
	16	SB7.5P1.5	92.5	7.5	1.5		
Number of Samples prepared for testing				UCS at OMC and MDD state			16×3
				UCS after drying			16×3
				Thermal conductivity test (at OMC & MDD state; after drying)			16×3
				Total number of samples prepared			144

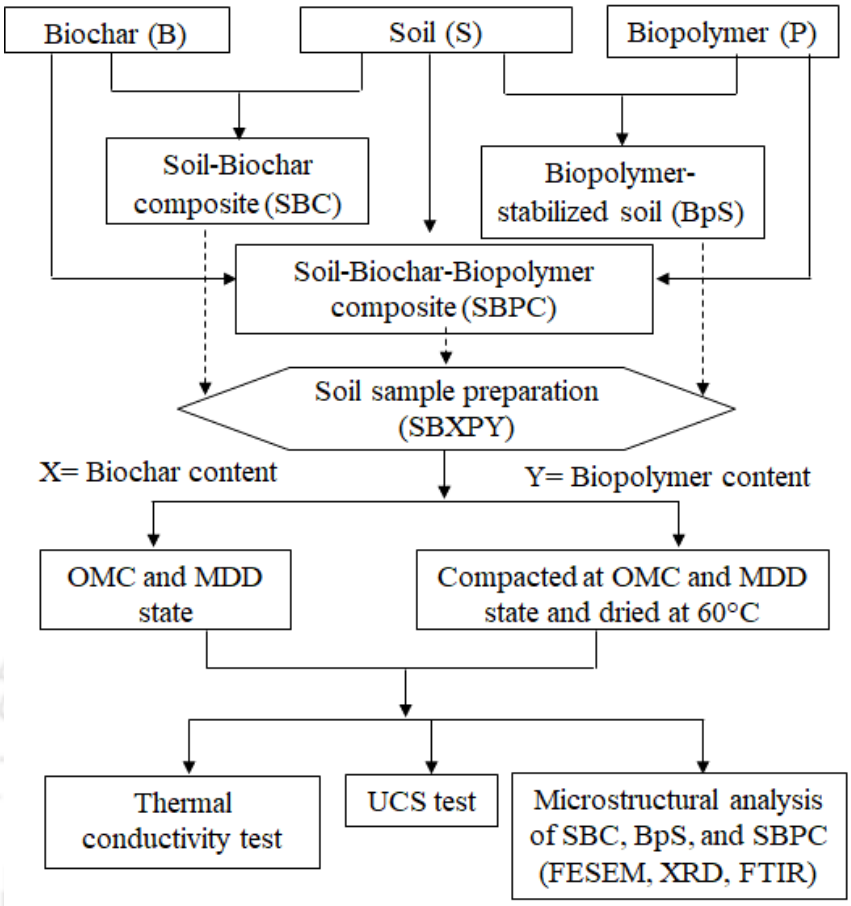

Figure 6.1 Summary of the experimental program

The TAS that requires storing heat, i.e., crude oil transportation pipelines and geo-energy storage units, the temperature of the interface between TAS and backfill is expected to have a much higher temperature (40 °C to 80 °C). Moisture loss is unavoidable in such conditions. Therefore, investigation of the thermal conductivity and unconfined compressive strength (UCS) of the proposed backfill after moisture loss is also critical. Hence, a duplicate set of samples were prepared for testing the specimens in the OMC state and after drying for the evaluation of thermal conductivity, UCS, and microstructural properties of the specimens. In this study, all the samples were dried at 60 °C for seven days in a fan-equipped oven, except for the microstructural analysis. For the microstructural analysis, the samples were dried at 105 °C for 24 hours. It is to be noted that biopolymer-stabilized soils gain strength while drying homogenously, and their controlled drying is conventionally termed "curing" (Ramachandran et al., 2021). Previous studies have also recommended accelerated drying at 60 °C for non-detrimental drying of biopolymer-stabilized soils (Fatehi et al., 2018; Chang et al., 2020; Ramachandran et al., 2021).

The sample preparation methodology was alike for the thermal conductivity and UCS tests for the SBC, BpS, and SBPC specimens, although with a difference in their dimensions. For thermal conductivity determination, the specimens were poured into the acrylic cylindrical of 80 mm internal diameter and 60 mm height, as explained in section 4.3.1. In contrast, cylindrical samples (38 mm diameter and 76 mm height) were prepared for the UCS tests. All the samples were filled in three layers and statically compacted to the desired density by static compaction.

For the preparation of SBC samples, the dry soil was homogenously mixed with the selected percentage of biochar on a glass plate using a spatula first. Later, the water equivalent to the optimum moisture content was mixed. In the current chapter, biochar content was investigated in a range varying from 2.5% to 7.5%. For the preparation of BpS specimens, the xanthan gum (XG) solution was added to the soil and hand-mixed on a glass plate with a clean pair of spatulas. The biopolymer solutions were prepared by adding the required amount of required XG powder in deionized water equivalent to OMC of soil. The solution was prepared on a hot plate at 60 °C with continuous stirring to avoid agglomeration. Later, the biopolymer solution was sealed air-tight and kept for 24 hours so that their helical coils unravel upon hydration. The biopolymer content was investigated in a range of 0.5% to 1.5% in the current chapter.

For the preparation of SBPC specimens, all the combinations of prepared biopolymer solutions (0.5% to 1.5%) and SBC (2.5% to 7.5%) were prepared. The dry SBC mixture was mixed with the biopolymer solution on a glass plate with a clean pair of spatulas. The details of SBPC blends are stated in Table 6.1. Since the overall density of the mixture, the biopolymer quantity and water content for the sample influence the thermal and strength properties (Chang et al., 2015). Therefore, the SBPC has been prepared based on the MDD of SBC specimens solely with the purpose of investigating the influence of certain biopolymer quantities on the UCS and thermal conductivity at a fixed density, as discussed in Table 6.1.

6.2.1 Thermal conductivity test

The thermal conductivity of specimens was measured through a dual needle SH-1 thermal probe, as explained in section 4.3.1. The needle probe was installed at the center of specimens at the OMC state. The samples were allowed to rest for 15 minutes before taking the measurements to attain an equilibrium temperature between the thermal probe and the

sample. Later, the samples were dried, and their thermal conductivity was measured again. The thermal properties of samples are recorded for triplicates in this study, and the average values, along with deviations, are plotted. In addition to the SBC, BpS, and SBPC specimens, the thermal conductivity of biopolymer solutions at various concertation has also been measured to determine if the increase in the viscosity of the biopolymer solution affects the thermal conductivity. The thermal conductivity of biopolymer solutions was measured by a single-needle KS1 thermal probe. The upper limit of biopolymer content in the current study is 1.5% (by soil weight), implying 66.67 g/l as the maximum concentration of XG powder in water. Therefore, the thermal conductivity of the biopolymer solutions having a concentration from 5 g/l to 70 g/L is investigated.

6.2.2 UCS test

The unconfined compressive strength (UCS) of samples was carried out in accordance with the ASTM D2166-16 (2016). The UCS test was conducted at a constant strain rate of 1.25 mm/min. For each sample, the stress-strain response was plotted. Thereafter, the UCS and secant modulus of elasticity (E_{50}) were calculated from the stress-strain response. E_{50} is defined as the secant modulus at 50% of the peak stress. The moisture content of the samples was also evaluated before and after the test to confirm if all the samples were dried equally. All the samples were tested in triplicates. The average values of UCS and E_{50} have been reported along with the standard deviations to ensure repeatability.

6.3 Results and Discussion

6.3.1 Influence of biochar content on thermal and strength characteristics

6.3.1.1 Thermal conductivity of SBC

Fig. 6.2 illustrates the thermal conductivity (*K*) of the bare soil amended with different biochar percentages at the OMC condition and after drying. The *K* values reduced notably with the increase in biochar percentage in both states. At the OMC state, the *K* value of the bare soil falls from 1.61 $Wm^{-1}K^{-1}$ to 1.26 $Wm^{-1}K^{-1}$ upon 7.5% biochar amendment. In comparison, the *K* value reduced from 0.48 $Wm^{-1}K^{-1}$ to 0.35 $Wm^{-1}K^{-1}$ in the dry state upon the same amendment. The *K* value of soil is majorly dependent on water content, porosity, and grain size distribution (Côté and Konrad, 2005b). Therefore, the *K* of the soil in the dry condition is significantly lower. Overall, the *K* values of soil were recorded to decrease by 9%, 17%, and 21% in the OMC condition upon biochar amendment by 2.5%, 5%, and 7.5%,

respectively. At the same time, a fall of 12%, 21%, and 28% in the *K* values are noted upon biochar amendment of 2.5%, 5%, and 7.5%, respectively, after drying.

Biochar is a low thermally conductive material. The *K* of the selected biochar fraction is only 0.124 $Wm^{-1}K^{-1}$. Moreover, adding biochar to the soil reduces the MDD of SBC, and the resulting drop in density raises both the overall porosity and the proportion of air components in the SBC. This results in the contact separation between soil particles and water, reducing the soil's thermal conductivity. Further, the entrapped biochar particle between soil particles also reduces the heat transfer in the soil-biochar matrix resulting in lower thermal conductivity. These factors are primarily responsible for the diminution of the thermal conductivity of the SBC. This result is also supported by micrographical analysis, which is explained in the microstructural analysis section 6.3.5.

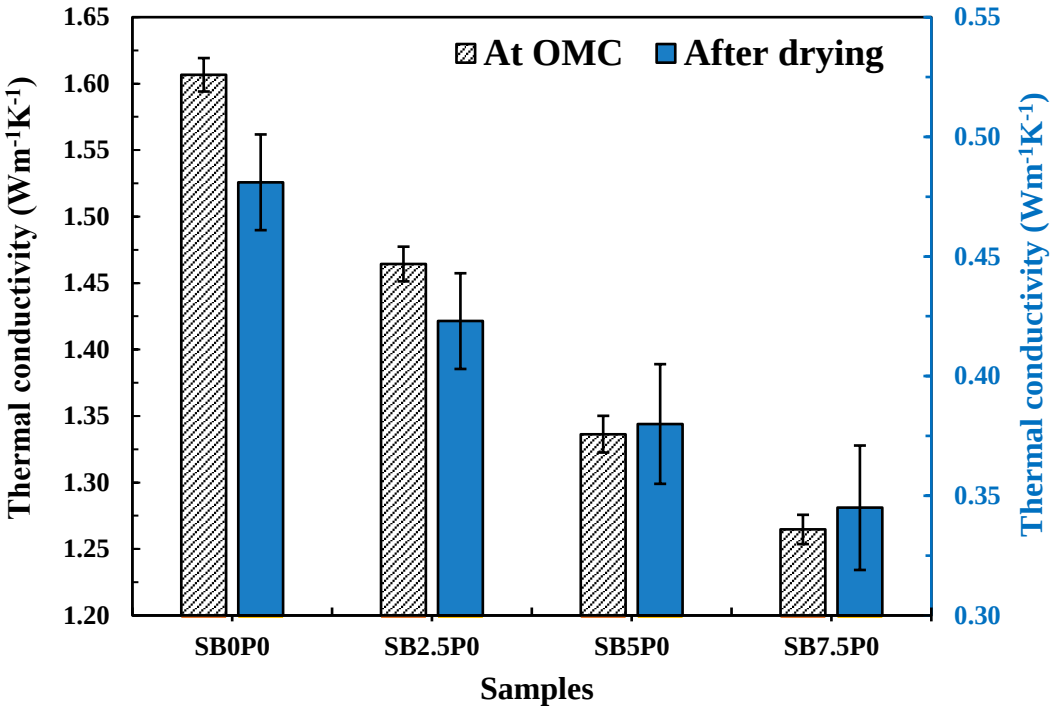

Figure 6.2 Influence of biochar amendment on *K* of soil at OMC and after drying

6.3.1.2 UCS of SBC

Fig. 6.3(a) and Fig. 6.3(b) demonstrate the stress-strain response of the SBC in comparison to bare soil at OMC state and after drying. In Fig. 6.3(c), the moisture content of the specimens at the preparation stage (OMC) and after drying is compared. The moisture content measurements revealed the moisture content to be less than 2% for all the oven-dried samples, ensuring uniform drying for all the specimens. Figs. 6.4(a) and 6.4(b) present the

estimated UCS and E_{50} of the different SBC blend at the OMC state and dry state in comparison to the bare soil. It is evident from Fig. 6.3(a-b) and Fig. 6.4(a-b) that the soil loses its strength upon incremental amendment with the biochar in both the states, i.e., OMC state and dry state. A strain-softening behavior with elastoplastic deformation is evident in Fig. 6.3(a-b). At the OMC state, the UCS decreases from 366 kPa to 186 kPa, whereas after drying, the UCS falls from 1.29 MPa to 0.95 MPa upon 7.5% biochar amendment. It was noted that the strength of the soil and SBC increases drastically upon drying. Around three-fold to five-fold increase in the strength of the soil and SBC was observed upon drying. Upon drying, the frictional interlocking between particles and soil particle conglomeration improves, which is possibly the reason for higher strength.

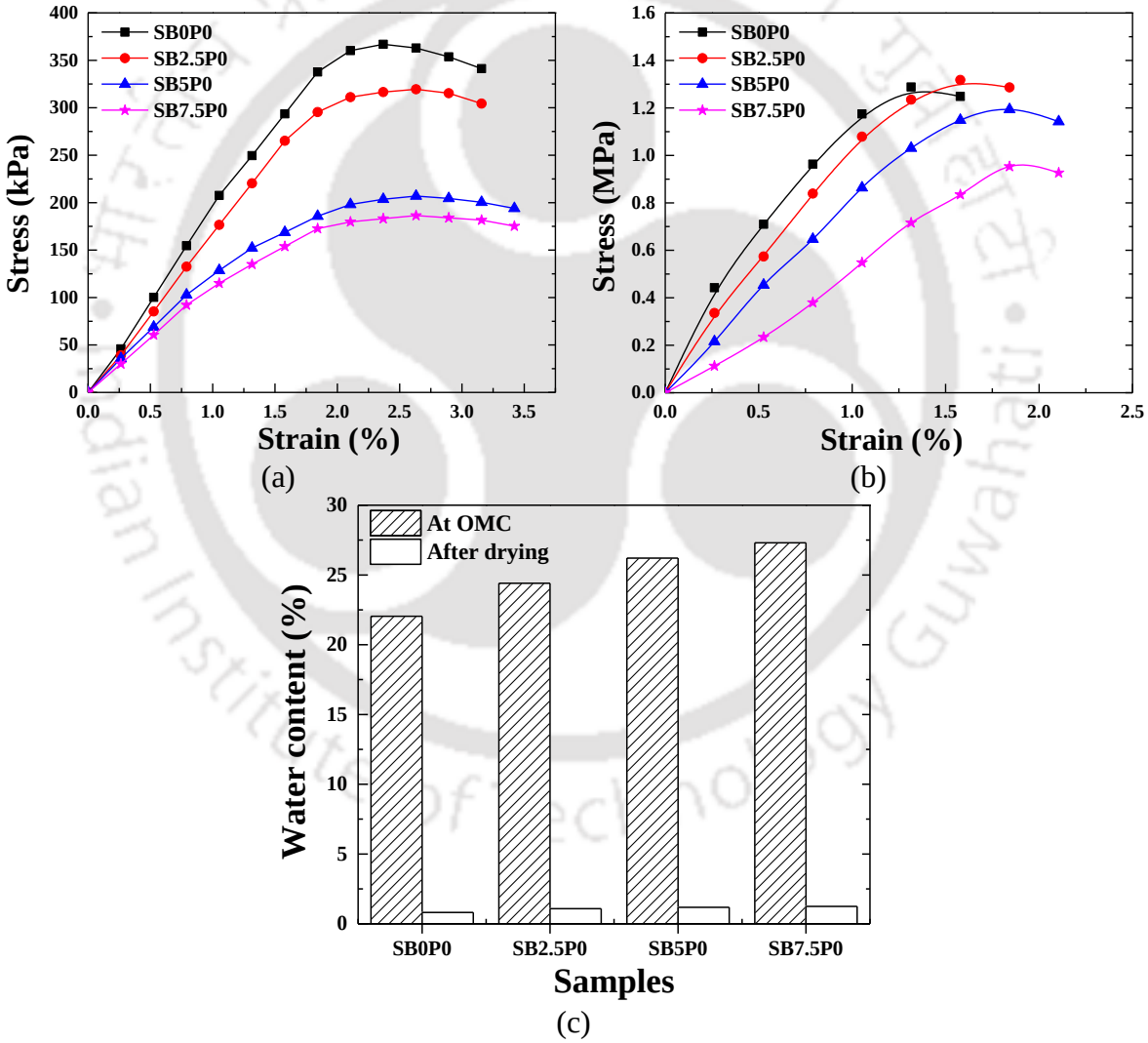

Figure 6.3 Stress-strain behavior of SBC (a). At OMC and (b). After drying; (c) Water content at OMC and after drying

Overall, the UCS of the SBC was observed to be reduced by 13%, 43%, and 49% upon biochar amendment of 2.5%, 5%, and 7.5%, respectively, at the OMC state. The

reduction in UCS value with biochar amendment at OMC state was also documented by Bora et al. (2021). The corresponding decrease in the E_{50} was noted to be 15%, 34%, and 42%. After drying, the UCS of the SB2.5P0 specimen demonstrated equivalent strength to plain soil. This might be due to the small quantity of biochar and the absence of water. However, a 7% and 26% decrease in the UCS value was observed with 5% and 7.5% biochar amendment in the dry state. The E_{50} of the soil was also observed to be reduced by 25%, 41%, and 64%, with the addition of 2.5%, 5%, and 7.5% of biochar in the dry state.

An increase in failure strain along with plastic deformation was also noted with biochar amendment indicating an increase in the ductility of SBC at the OMC state, which is due to particle rearrangement and deformation caused by the presence of highly porous and more compressible biochar particles (Sadasivam and Reddy, 2015). Upon drying, the failure strain is reduced due to high friction between the soil-soil and soil-biochar interface in the absence of water. Moreover, the plastic deformation ceased in the SBC upon drying, resulting in loss of ductility.

The prime reason for the strength reduction with an increase in biochar content in the SBC samples is the decrease in the overall density. Furthermore, biochar is non-cementitious, unlike cement or biopolymers. Therefore, a decrease in density is explicitly disadvantageous for the strength of the SBC. The reduction in UCS of SBC is also aided by the diminution in the cohesive force and frictional interlocking between the soil particles with the addition of biochar (Bora et al., 2021). Additionally, the presence of hydrophilic and hydrophobic functional groups in biochar interacts with water and forms a complex network between the biochar particle and water, increasing distance among the soil particles. Due to this, the electrostatic force of attraction between soil particles is reduced, which lowers the cohesiveness of the soil-biochar matrix (Pardo et al., 2019). All these factors collectively contribute to the decay in the strength of soil upon biochar increment.

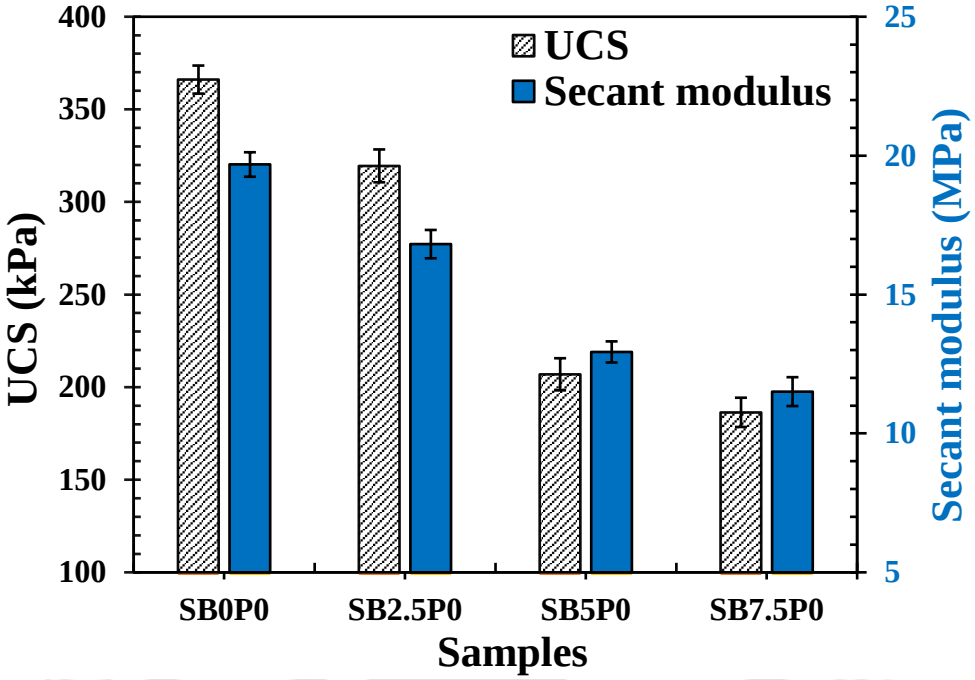

(a)

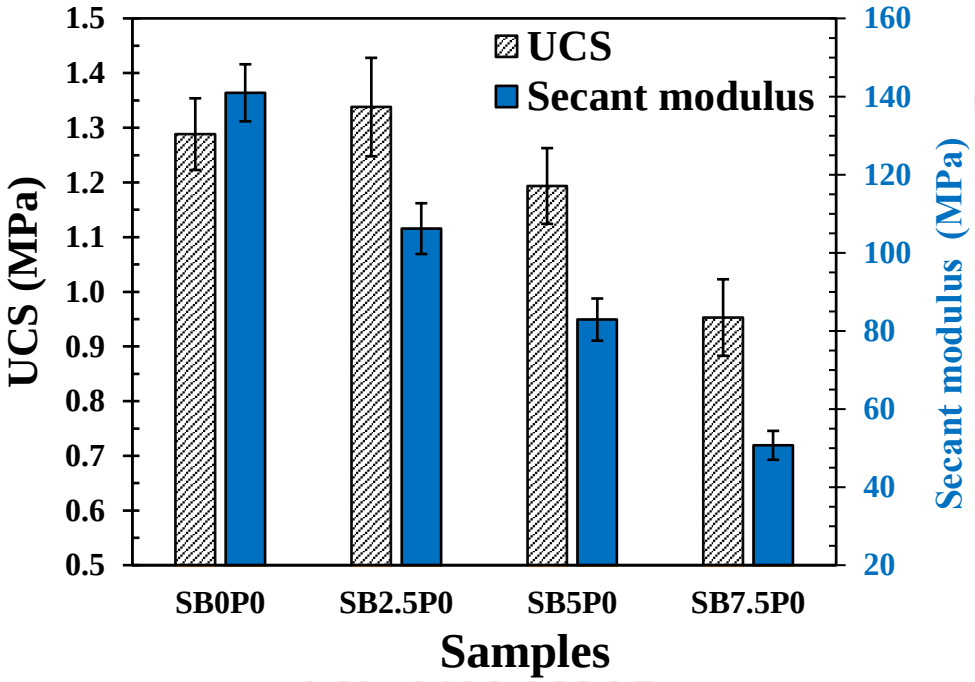

(b)

Figure 6.4 UCS and secant modulus (E_{50}) of SBC (a). At OMC and (b). After drying

6.3.2 Thermal conductivity of biopolymer

Fig. 6.5 presents the *K* of biopolymer solution at different concentrations. Interestingly, no significant change in thermal conductivity was observed with an increase in the XG concentrations. The *K* values of biopolymer solutions for XG concentration varying from 0.5 g/l to 70 g/l varies in a range of 0.581±0.018 $Wm^{-1}K^{-1}$. Similar results were also reported by previous researchers with other polymeric fluids (Lee et al., 1981; Broniarz-

Press and Pralat, 2009; Abed, 2021). This is attributed to the differences in size between the molecules of the solvent and the solute, which restrict the convective intercellular heat transfer between these polymeric molecules (Abed, 2021). The results implied that the biopolymer solutions might have the potential to improve the strength while maintaining control over thermal conductivity. However, drying of the biopolymer solution results in an improvement of particle contacts which is liable for an increase in interparticle friction (Chang et al., 2020), therefore it is imperative to study the effect of the biopolymer content and drying on the thermal conductivity of the biopolymer stabilized soil.

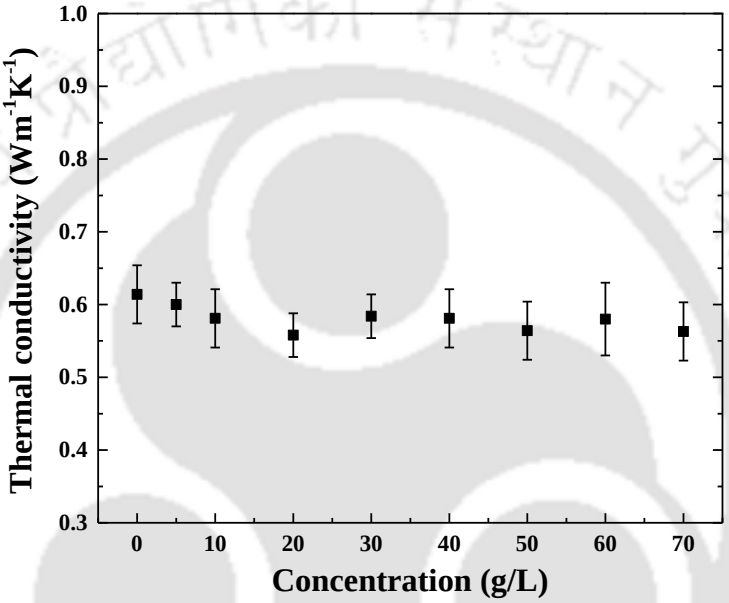

Figure 6.5 Thermal conductivity variation of xanthan gum with different concentrations

6.3.3 Influence of biopolymer content on thermal and strength characteristics

6.3.3.1 Thermal conductivity of BpS

Fig. 6.6 presents *K* values of the biopolymer-stabilized soils (BpS) in comparison to the bare soil at OMC state and after drying. Trivial variations were observed in the thermal conductivity of the BpS in OMC conditions and after drying, individually. The *K* values of BpS were noted to be marginally reduced at the OMC state and contrariwise marginally improved after drying with the increase in biopolymer content. At OMC, the *K* values for all the BpS samples varied in a range of 1.55±0.04 $Wm^{-1}K^{-1}$, whereas after drying, the *K* values were noted to be in a range of 0.50±0.02 $Wm^{-1}K^{-1}$. After drying, the thermal conductivity decreased due to the dehydration of biopolymer solution in the soil pores. The results revealed that the *K* of bare soil is comparable with the BpS up to 1.5% biopolymer content in the individual cases of OMC state and after drying.

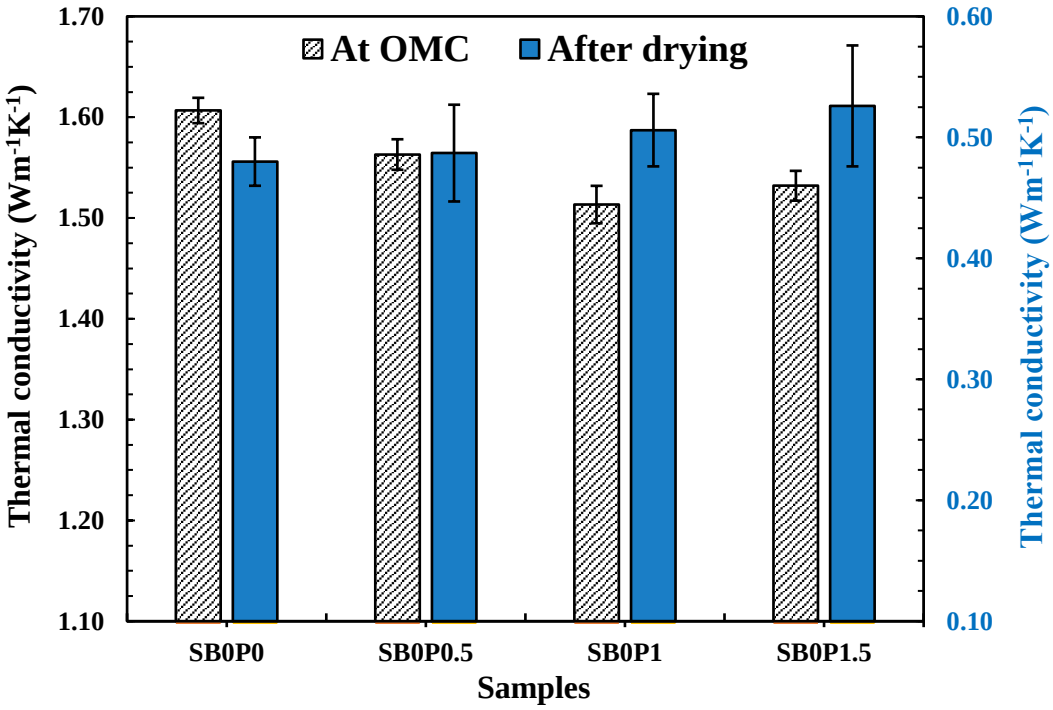

Figure 6.6 Influence of biopolymer stabilization on thermal conductivity of soil at OMC and after drying

6.3.3.2 UCS of BpS

Fig. 6.7(a) and Fig. 6.7(b) present the stress-strain response of the BpS in comparison to bare soil at OMC state and after drying. Fig. 6.7(c) shows that the moisture content for all the BpS specimens after drying was less than 2%, confirming the loss of moisture for all the specimens. Figs. 6.8(a) and 6.8(b) present the estimated UCS and E_{50} of the different BpS blends at OMC state and dry state.

It is clear from Figs. 6.7(a-b) and Fig. 6.8(a-b) that upon biopolymer stabilization, the soil gains strength in both states, i.e., OMC state and dry state. A strain-softening behavior with elastoplastic deformation was observed at the OMC state. Contrarily, a brittle mode of failure was observed, along with a reduction in plastic strain upon drying. A sharp fall in stress values was observed against the deformation after attaining the peak stress, as illustrated in Fig. 6.7(b).

At the OMC state, the UCS steadily increased from 366 kPa to 505, 558, and 681 kPa upon 0.5, 1, and 1.5% biopolymer amendment, respectively. The corresponding increase in the E_{50} was noted to be 3%, 6%, and 14% in comparison to the plain soil. The increase in strength of the biopolymer stabilized sample is credited to the formation of bridges between

the soil grains, hydrogen bonds, and the development of cohesive forces between xanthan gum and electrically charged clay particles (Fatehi et al., 2021; Ramachandran et al., 2021).

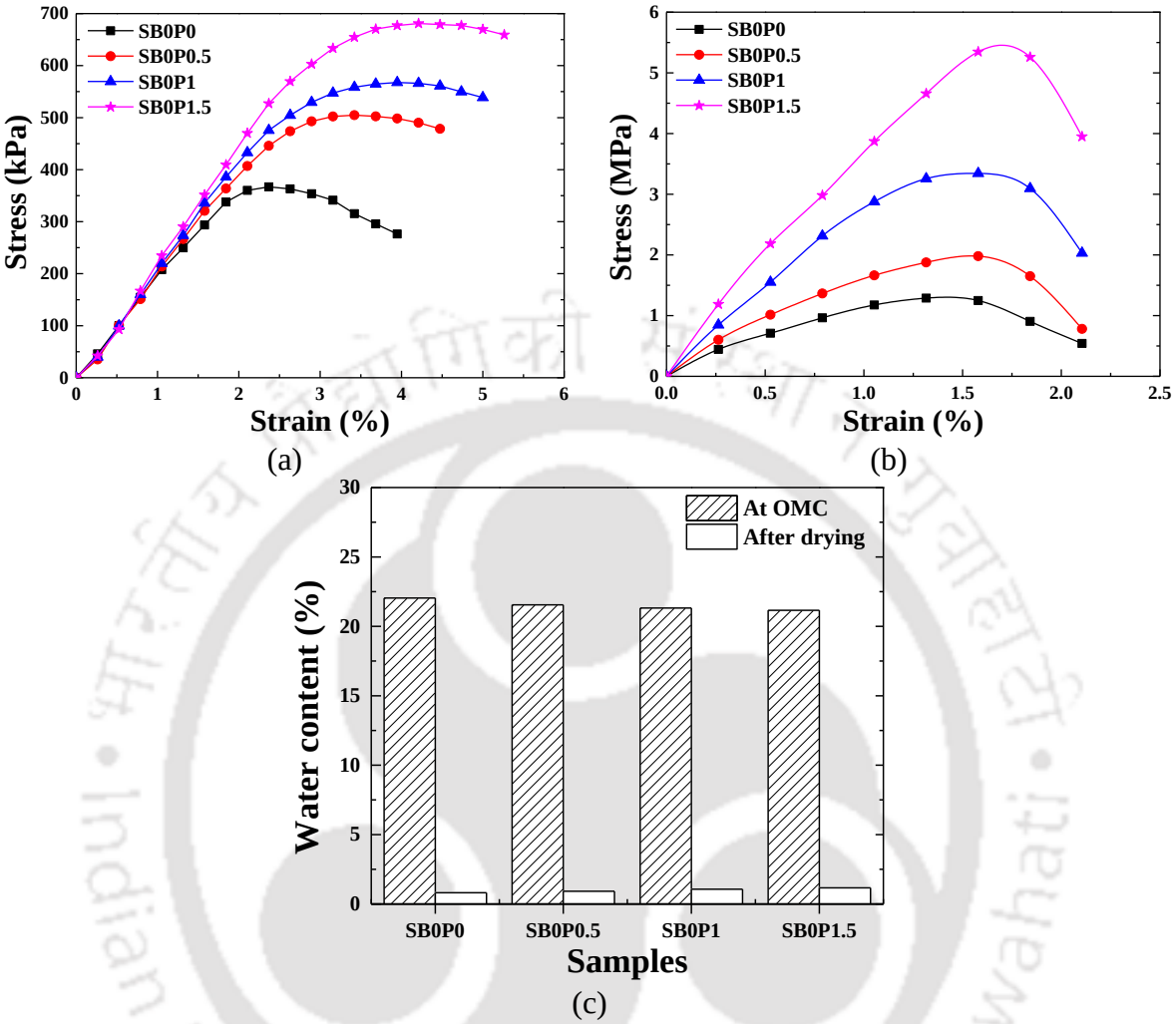

Figure 6.7 Stress-strain behavior of biopolymer-stabilized soil (BpS) (a). At OMC, (b). After drying; and (c) Water content at OMC and after drying

Whereas after drying, the UCS remarkably rise from 1.29 MPa to 1.98, 3.34, and 5.35 MPa upon the same biopolymer amendment of 0.5, 1, and 1.5%. After drying, the UCS of the BpS was observed to be increased by 315% upon biopolymer stabilization by 1.5%. Similarly, the E_{50} was noted to be increased by 33%, 108%, and 171% upon the same biopolymer amendment. It is to be noted that around a three-fold to eight-fold increase in the strength of the soil and BpS specimens are recorded upon drying. The strength of a sample stabilized with the addition of biopolymer greatly depends upon its moisture content (Chang et al., 2016, 2020; Ramachandran et al., 2021). Upon drying, the condensation of biopolymer hydrogel occurs, followed by dehydration, which improves the particle conglomeration (Chang et al., 2020). Therefore, the dried sample has a higher UCS value than the OMC state (refer to Fig. 6.7c).

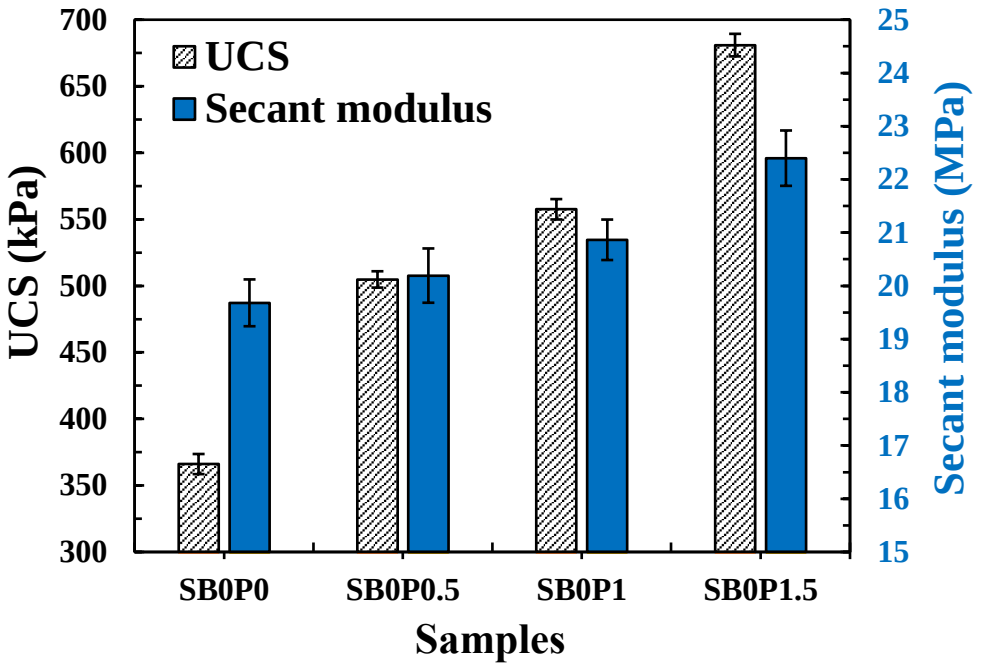

(a)

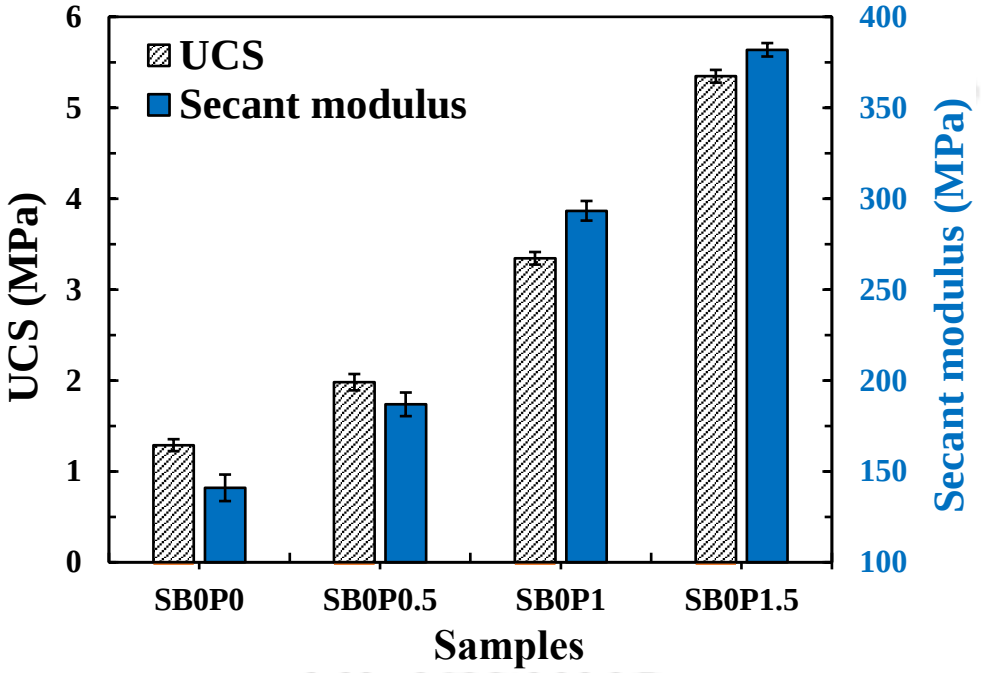

(b)

Figure 6.8 UCS and secant modulus (E_{50}) of BpS (a). At OMC and (b). After drying

The failure strain also increased upon the biopolymer addition along with plastic deformation at OMC, similar to biochar amendment. Upon 1.5% biopolymer treatment at the OMC state, the failure strain of the bare soil gradually increased to 4.21% from 2.37%. At OMC, the increase in ductility upon biopolymer treatment is due to the flexible biopolymer bridging around the soil particles (Lee et al., 2017). Whereas after drying, the failure strain rose slightly from 1.32% to 1.58% upon the same biopolymer treatment, mostly due to dehydration of the flexible biopolymer hydrogel coating and bridging around the soil

particles. This finding is further supported by micrographical analysis, which is explained in the microstructural analysis section 6.3.5.

6.3.4 Synergistic effect of biochar and biopolymer amendment on thermal and strength characteristics

6.3.4.1 Thermal conductivity of SBPC

The thermal conductivity variation of the soil-biochar-biopolymer composite (SBPC) in OMC state and after drying is displayed in Fig. 6.9(a) and Fig. 6.9(b). The *K* values of the bare soil were found to be 1.60 $Wm^{-1}K^{-1}$ at OMC state and 0.48 $Wm^{-1}K^{-1}$ after drying. The *K* values were observed to be reduced with biochar amendment. Regardless of biochar and biopolymer content, distinctively lower values of the thermal conductivity of all the SBP composites were observed at the OMC state, as illustrated in Fig. 6.9(a). However, in the dry state, the *K* value of SBPC at a particular biochar content was observed to increase with the addition of biopolymer. This is mainly due to the formation of bonding among soil-biochar-biopolymer matrix. However, in all the cases, the thermal conductivity of the SBPC was less than the bare soil except for sample SB2.5P1.5. Sample SB2.5P1.5 exhibited an average *K* value equivalent to bare soil in dry conditions, which is possibly the cumulative influence of a low biochar content and a high biopolymer content, both liable for a higher *K* value in comparison to other composites. Hence, it is certain from the findings that the SBPC has notably lower thermal conductivity in comparison to bare soil and their strength characteristics are of utmost importance to decide if the proposed composite is applicable for thermal backfill applications.

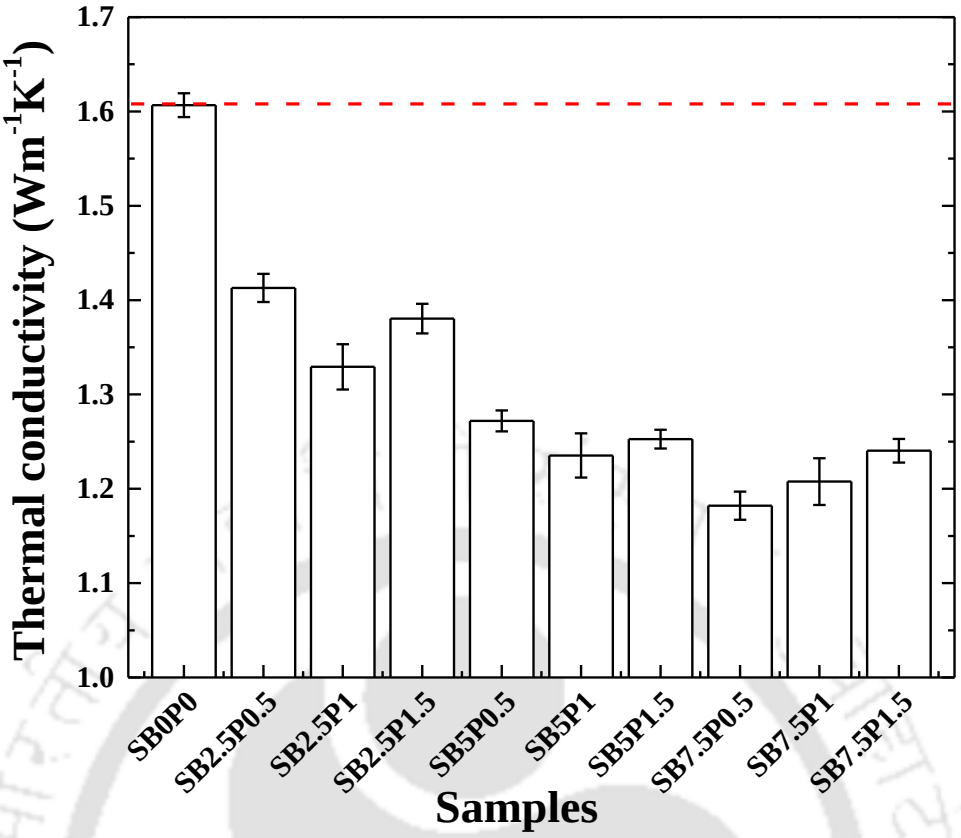

(a)

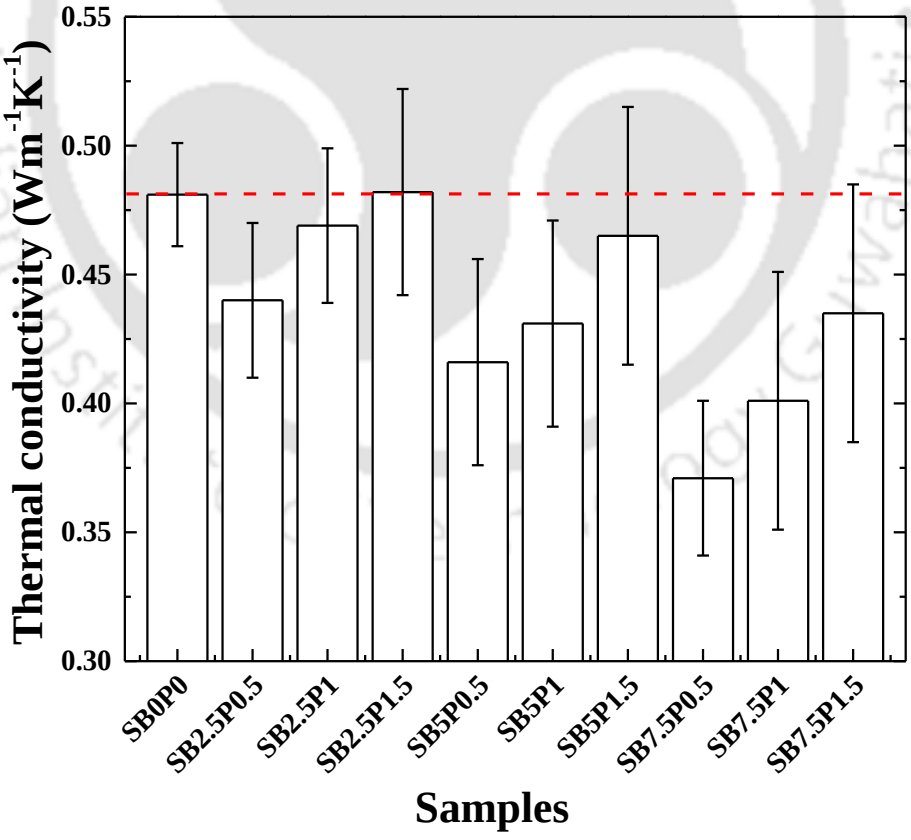

(b)

Figure 6.9 Thermal conductivity of SBPC (a). At OMC and (b). After drying

6.3.4.2 UCS of SBPC

The stress-strain response of the SBPC is illustrated in Figs. 6.10. In the set, Fig. 6.10 (a) and Fig. 6.10 (d) represent SBPC with biochar content of 2.5% at OMC state and after drying, respectively. Similarly, Figs. 6.10 (b,e) represents SBPC with a biochar content of 5% and Figs. 6.10 (c,f) represent SBPC with a biochar content of 7.5%. The moisture content of the specimens at the preparation stage (OMC) and after drying is compared in Fig. 6.10 (g-i). The moisture content is observed to be less than 2% for all the samples. Figs. 6.11 (a-b) and Fig. 6.11 (c-d) present the computed UCS and E_{50} of the different SBP blends at the OMC state and after drying.

The SBPC exhibited a strain-softening behavior with elastoplastic deformation and ductile failure at the OMC state regardless of the biochar content, as illustrated in Fig. 6.10(a-c). The stress-strain responses of SBC specimens (SB2.5P0, SB5P0, and SB7.50) are also added in Fig. 6.10(a-f) for comparison with the strength characteristic of SBPC. Regardless of the biochar content, the brittle failure mode was observed for all the SBPC after drying, with a notable reduction in the plastic strain.

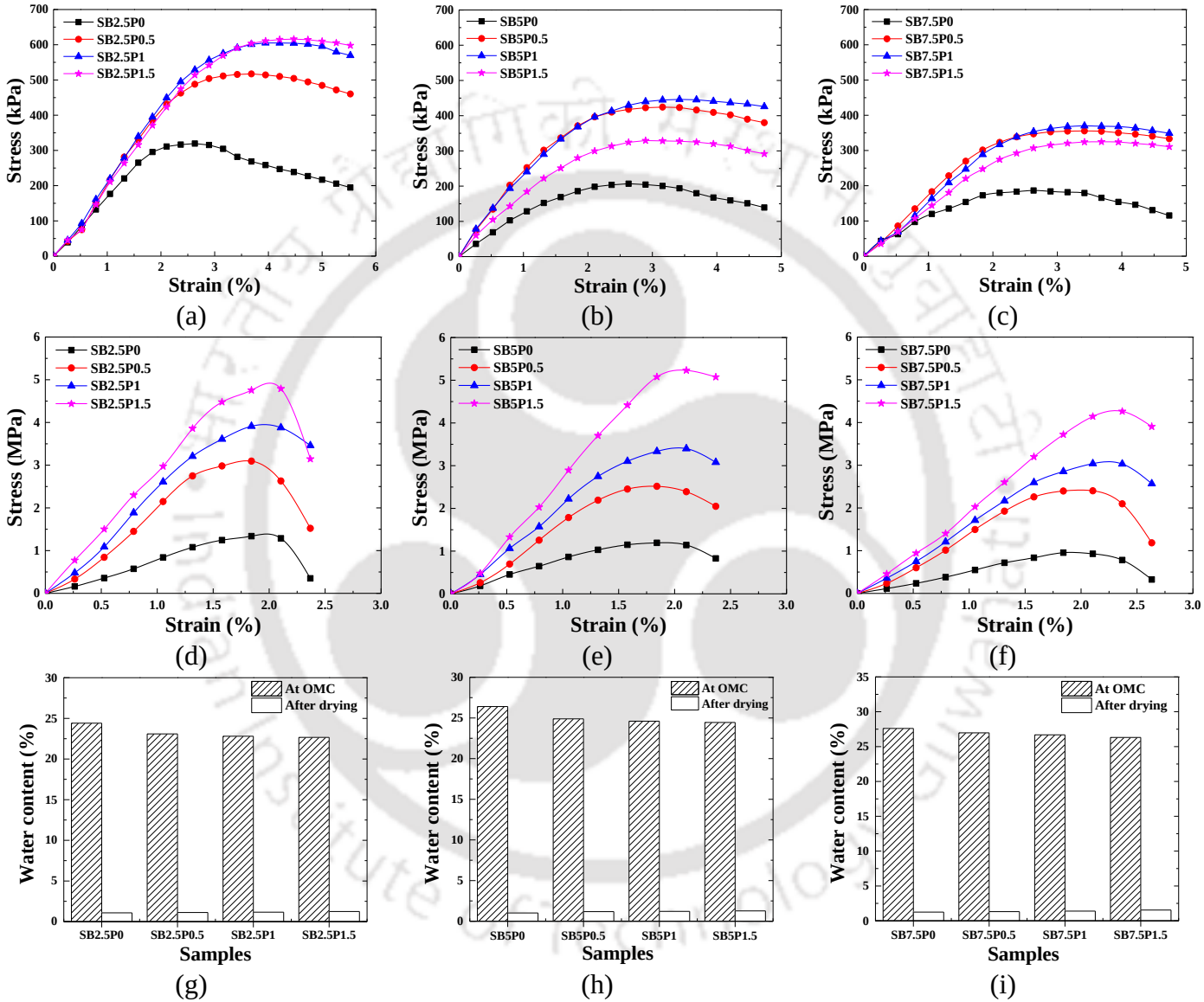

Figure 6.10 Stress-strain behavior of SBPC (a-c). At OMC and (d-f). After drying; and (g-i). Water content at OMC and after drying

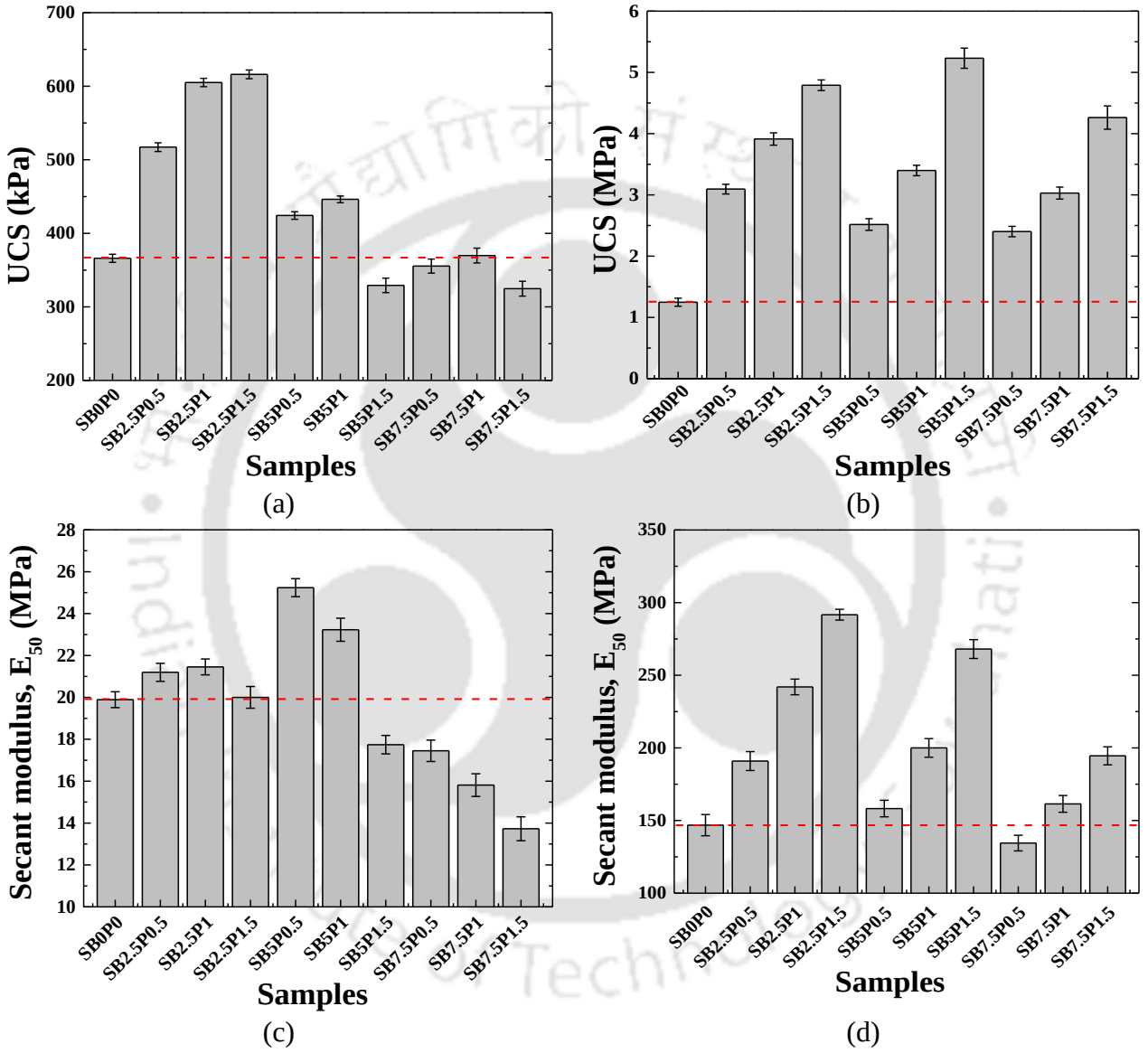

Figure 6.11 UCS and Secant modulus of SBPC; (a, c). At OMC and (b, d). After drying

It is to be recalled from Fig. 6.4 that the UCS value of 320, 207, and 186 kPa was measured for 2.5, 5, and 7.5% BAS at the OMC state. In Fig. 6.11(a), upon biopolymer addition at the OMC state, the UCS improved from 320 kPa to 517 kPa, 207 kPa to 424 kPa, and 186 kPa to 355 kPa with a mere addition of 0.5% biopolymer for 2.5, 5, and 7.5% biochar content in the SBP composites, respectively. At OMC state, most of the SBP composites exhibited enhanced strength, except for SB5P1.5, SB7.5P0.5, SB7.5P1, and SB7.5P1.5. The strength is lower at 7.5% biochar content in the OMC condition due to the hydrated biopolymer. The inclusion of the hydrated polymer in the soil-biochar matrix can cause a loss in frictional resistance due to the lubrication effect between biochar-biochar and soil-biochar particles at higher biopolymer content, as shown in Fig. 6.12.

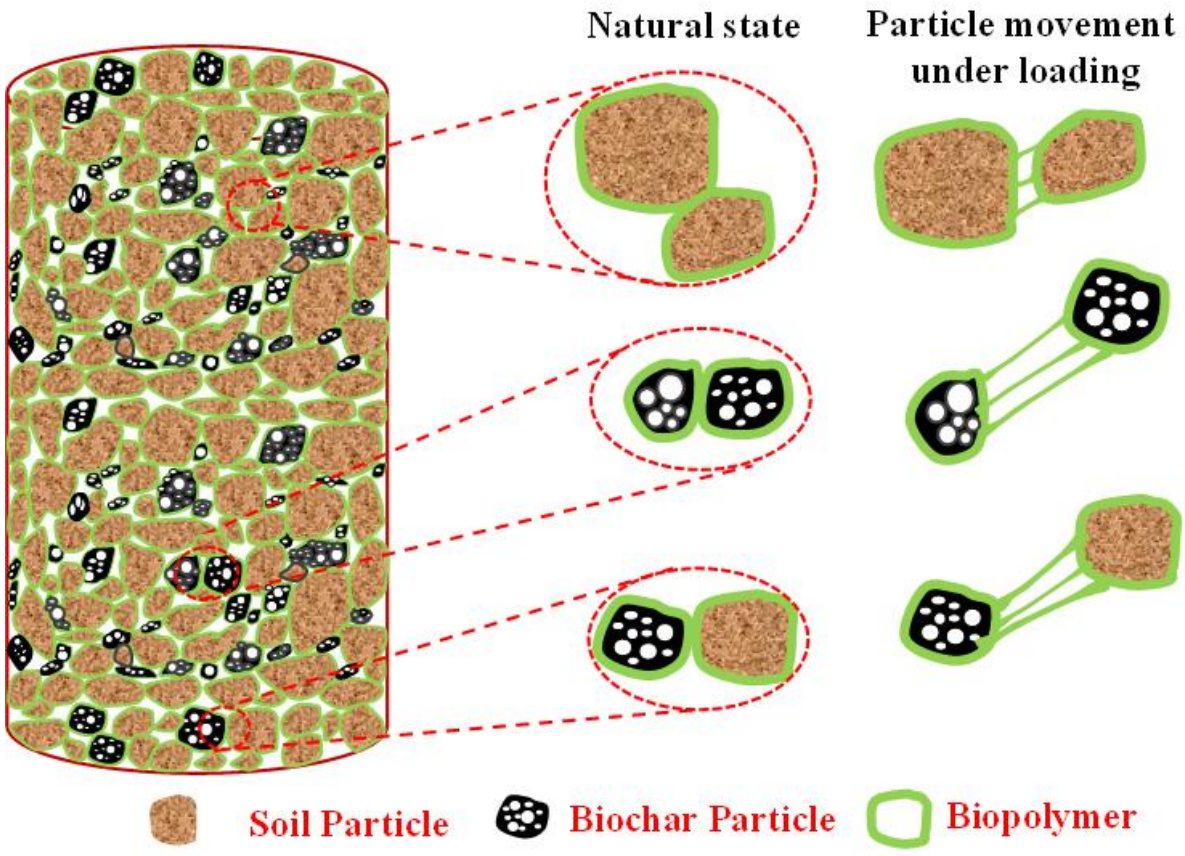

Figure 6.12 Interaction of soil-biochar-biopolymer composite at OMC

The bare soil exhibits a UCS of 1.34 MPa after drying. Whereas upon drying, the SBP composite with 2.5% biochar exhibited high UCS values of 3.09, 3.91, and 4.78 MPa with the addition of 0.5%, 1.0%, and 1.5% biopolymer, respectively. The trend was found to be consistent for SBP composites containing 5% and 7.5% biochar. All the SBPC samples have remarkably higher UCS values than the bare soil after drying. The higher UCS of the SBPC samples after drying is a result of the grain conglomeration and aggregation cumulatively induced by the biopolymer coating on soil and biochar particles, interparticle bridging of soil-biochar interfaces, and electrostatic adhesion of clay particles to biopolymer (Chang et al., 2020; Fatehi et al., 2021; Ramachandran et al., 2021). This finding is also reinforced by micrographical analysis, which is explained in the microstructural analysis section.

Further, the performance of SBPC at the OMC state and after drying has been comparatively analyzed in terms of the strength improvement factor (SIF) and thermal conductivity reduction factor (TCRF) in Fig. 6.13. SIF is defined as the ratio of UCS value of SBPC to the UCS of plain soil for the same compaction state (Gupt et al., 2021b), while TCRF is defined as the ratio of the *K* value of SBPC to the *K* value of plain soil for the same compaction state. Therefore, a SIF value greater than unity and a TCRF value less than unity is desired for the SBPC for the enhanced performance of the thermal backfill at the OMC state as well as after drying. Fig. 6.13(a-b) presents the SIF and TCRF of all SBPC at the OMC state. It is obvious that the SBPC with 7.5% biochar content had SIF ≤ 1 in OMC states, which indicates their unsuitability for thermal backfill applications even though they exhibit lower thermal conductivity. Even SB5P1.5 has SIF lower than 1 in the OMC condition. But it must be noted that these composites cannot be completely discarded for other applications as they have much higher strength and a fairly lower thermal conductivity after drying. All other composites, as illustrated in Fig. 6.13 (c-d), have higher strength and lower thermal conductivity than the plain soil in both conditions, i.e., at OMC state and after drying. The SBPC can be tailored as per the thermal insulation and strength enhancement characteristics as per the site requirement.

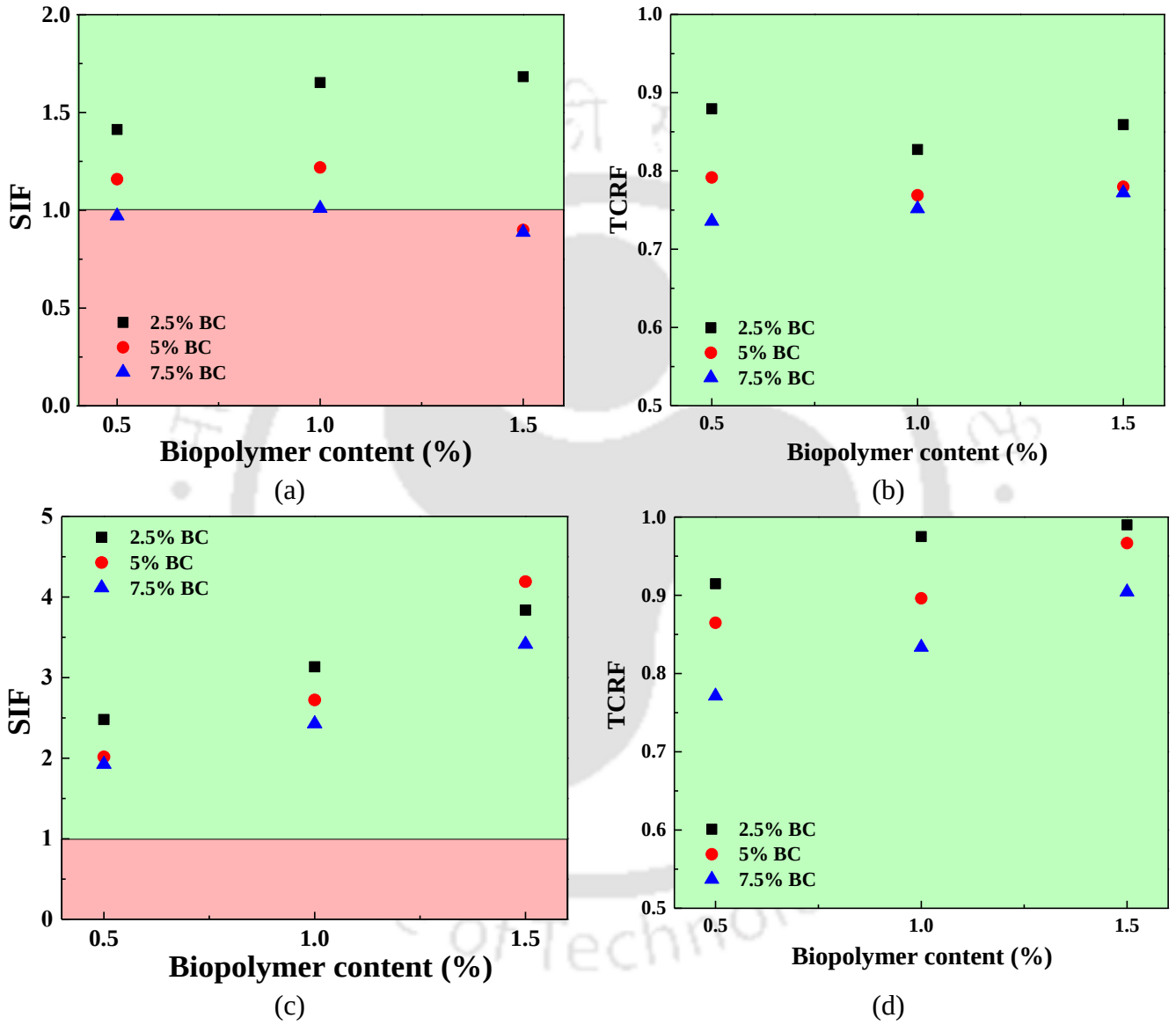

Figure 6.13 SIF and TCRF of SBPC (a-b). At OMC; (c-d). After drying

6.3.5 Microstructural analysis

A systematic investigation of the microstructure of SBC, BpS, and SBPC was carried out through FESEM analysis to comprehend the mechanics behind the enhanced strength and thermal insulation characteristics of the SBPC. Their microstructure is demonstrated through micrographs illustrated in Fig. 6.14 to Fig. 6.16.

6.3.5.1 FESEM analysis

In Fig. 6.14, the interaction between biochar and soil has been demonstrated. Biochar is an intra-porous with high chemical stability in soil. At a particular density, the BAS samples are more porous than the plain soil resulting in lower thermal conductivity due to a higher fraction of pore air in SBC. In Fig. 6.15, the fundamental microscale interaction of biopolymer and clay particles of BpS specimen SB0P1.5 is shown. The overall biopolymer reinforcement typically includes pore filling, particle coating, and soil-particle bridging (Chang et al., 2020), as evident by the conglomeration and aggregation of the soil grains in Fig. 6.15(a). Moreover, a new cementitious binder has also been reported with a clay-biopolymer matrix lately (Latifi et al., 2017). The new cementitious binder is possibly formed due to cation and hydrogen bonding of carboxylic group of biopolymer on the clay particles, specifically in the case of abundance of Kaolinite (Chang et al., 2020; Ramachandran et al., 2021). The soil utilized in the current study is also rich in Kaolinite minerals. Fig. 6.15(b) demonstrates the coating of the soil particles by the dehydrated hydrogel biopolymer. At the time of loading, the biopolymer sheets between soil particles get stretched, thereby offering apparent cohesion between the soil particles, as observed in Fig. 6.15(c-d). Because of this, the BpS specimens can withstand higher stress compared to the plain soil or BAS. Fig. 6.16 presents the FESEM micrographs of the SBP composite SB7.5P1.5 sample illustrating heat transfer and bonding mechanism. A soil-biochar-biopolymer matrix is observed in Fig. 6.16(a-b). The interaction among the soil and biopolymer in the SBPC is magnified in Fig. 6.16(c-d). As postulated earlier, it is obvious from the micrographs that biochar amendment in soil enhances heat insulation, while the biopolymer contributes to increases in the strength of the SBPC.

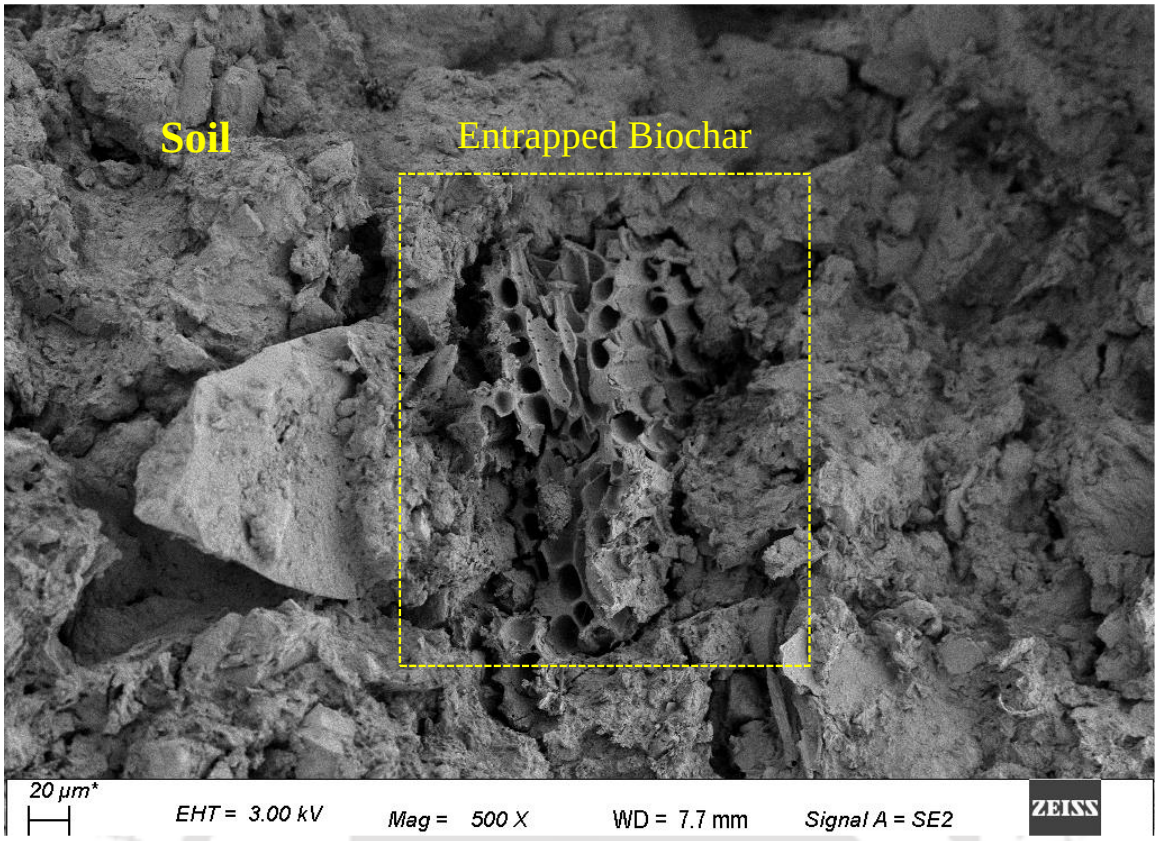

Figure 6.14 FESEM micrographs of SBC sample (SB7.5P0) highlighting the intra-porous biochar-soil matrix

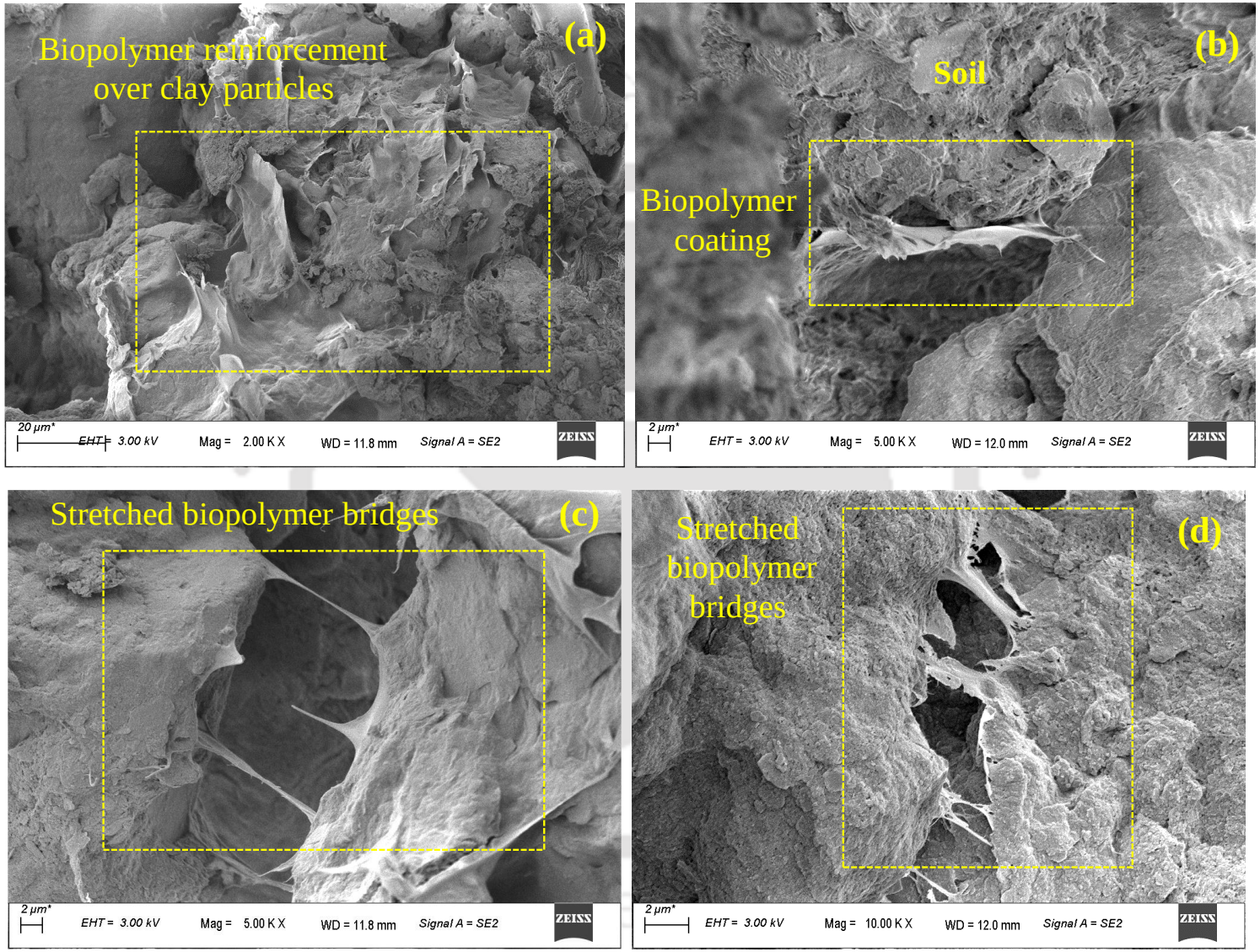

Figure 6.15 FESEM micrographs of BpS sample (SB0P1.5) highlighting- (a). Biopolymer reinforcement, (b). Biopolymer coating over soil particles, and (c-d). Stretched biopolymer bridges resisting deformation.

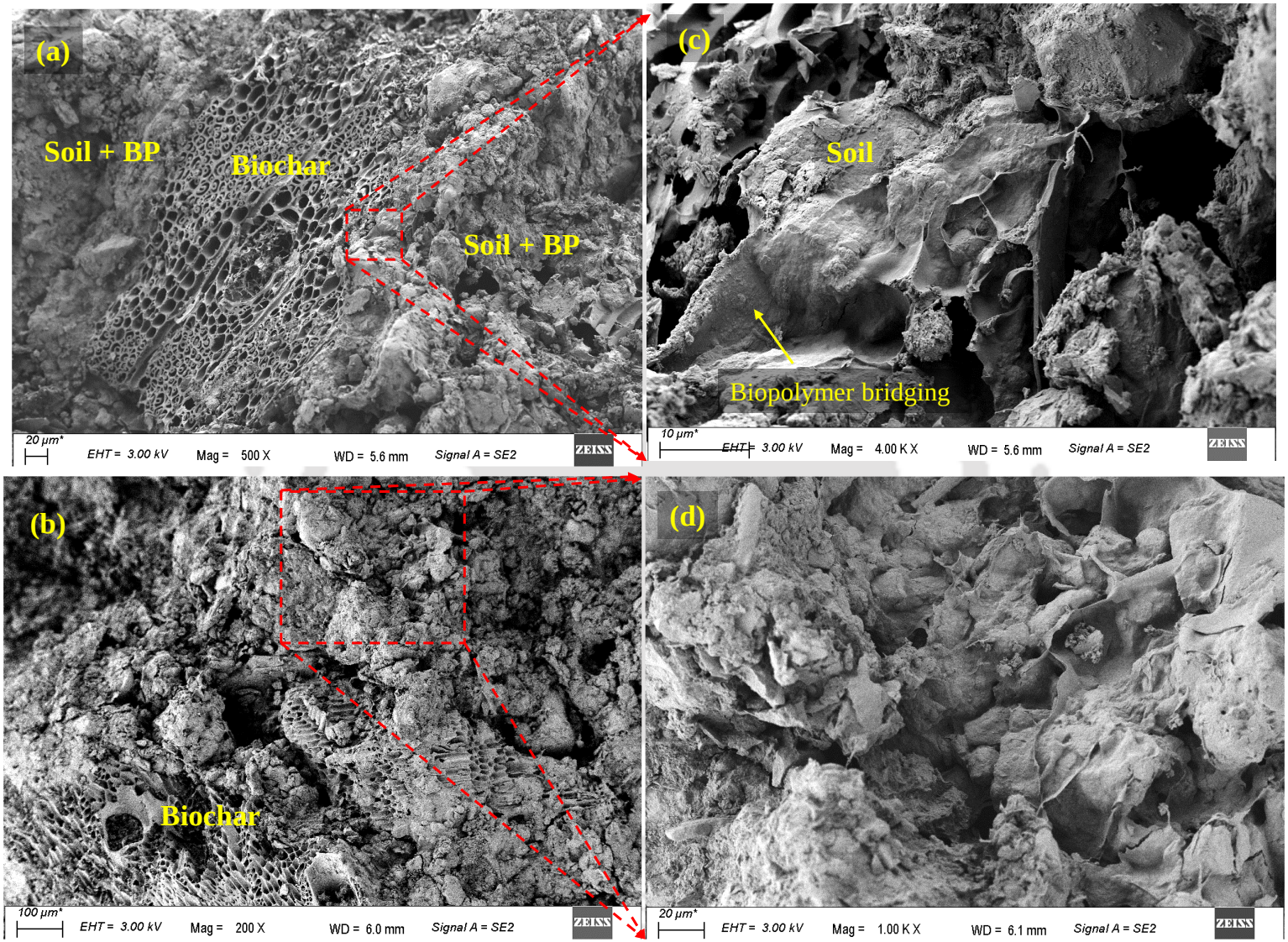

Figure 6.16 FESEM micrographs of SBPC sample (SB7.5P1.5) illustrating- (a-b). Soil-biopolymer-biochar matrix, and (c-d). Magnified biopolymer reinforcement.

6.3.5.2 XRD and FTIR analysis

The XRD and FTIR spectra of the bare soil, SBC, BpS, and SBPC have been displayed in Fig. 6.17(a-b). The XRD spectra of soil before and after stabilization with xanthan gum biopolymer were carried out to examine the change in mineralogical structure. Whereas change in the functional group was investigated using FTIR spectral response. Fig. 6.17(a) makes it abundantly evident that no new peaks were observed during the stabilization of soil using biopolymer. On the other hand, a reduction in peak intensity is also noted with addition of biochar and xanthan gum to the soil in SBC, BpS, and SBPC. This is credited to the organic nature and low quantity of xanthan gum in BpS and SBPC. Similar results were also reported in a previous study (Ghasemzadeh et al., 2022). Similar to XRD spectra, Fig. 6.17(b) suggests that the change in spectral characteristics is negligible during the stabilization of soil. Only a marginal shift in peak spectra was noted in SBPC compared to bare soil. The transmittance band in the range of 3550-3200 cm^{-1} in the soil is due to the stretching of the intermolecular hydroxyl (-OH) group involved in extensive hydrogen bonding (Gupt et al., 2021a). The peak around 1636 cm^{-1} corresponds to C=C stretching of alkenes groups. The peak at 1034 cm^{-1} is attributed to Si-O, while the spectral peak around 913 cm^{-1} is related to Al-OH-Al. The peak of quartz spotted nearby at 797 cm^{-1} is ascribed to Si-O stretching, and peaks near 695 cm^{-1} and 539 cm^{-1} designate the Al-Si-O bond (Rezende et al., 2018). A peak shift in wavenumber from 3435 cm^{-1}, 1636 cm^{-1}, 1034 cm^{-1}, 539 cm^{-1} to 3392 cm^{-1}, 1634 cm^{-1}, 1033 cm^{-1}, 538 cm^{-1} in FTIR spectroscopy in the case of soil amended with 1.5% biopolymer. This shift in spectral peak indicates the formation of bonds in biopolymer-stabilized soil. Furthermore, a reduction in spectral peak intensity indicates the biopolymer interaction with the soil.

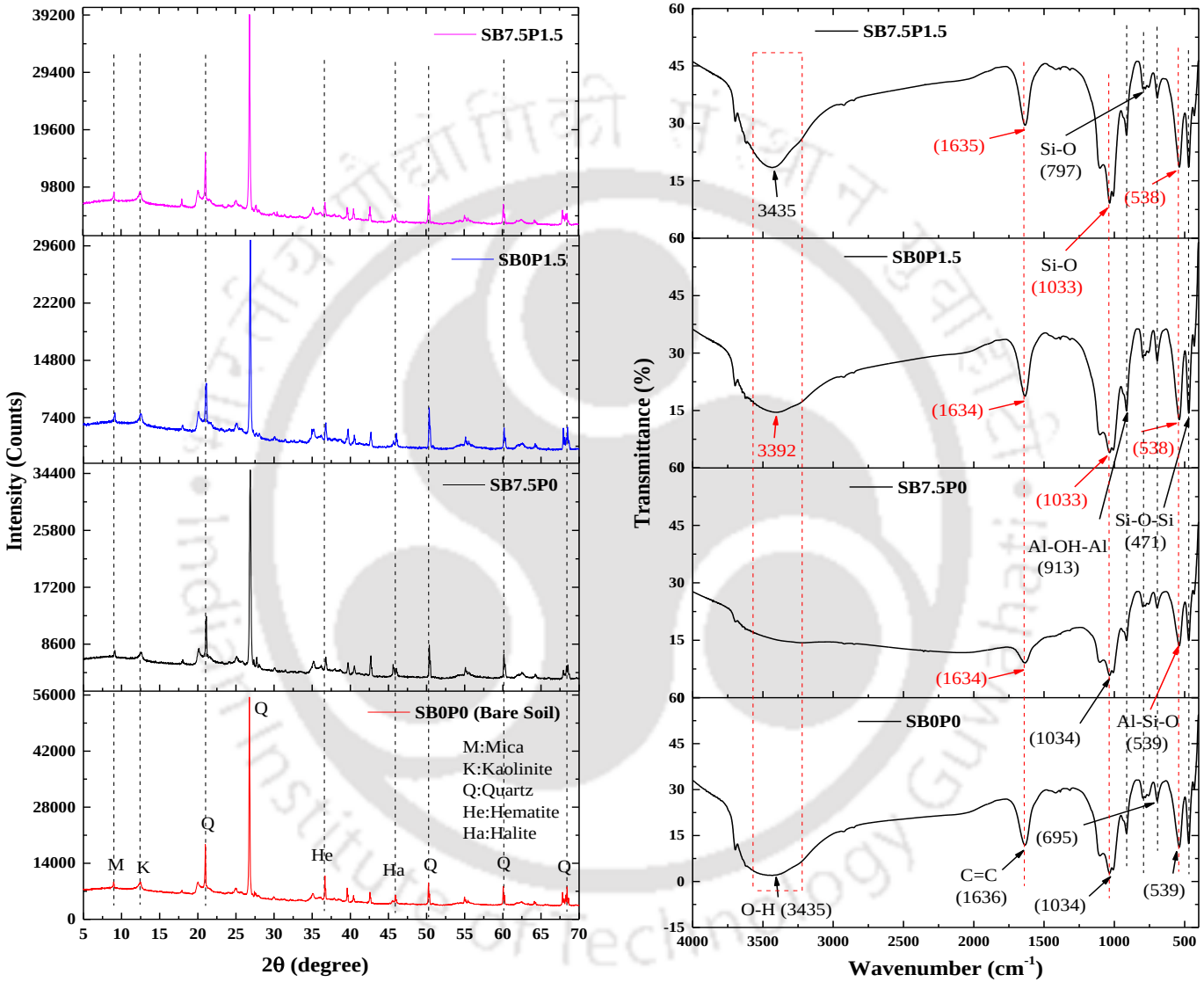

(a) (b)

Figure 6.17 (a). XRD and (b). FTIR spectra of SBPC

Fig. 6.18 summarizes the heat transfer and stabilization mechanism of soil, SBC, BpS, and SBPC. Fig. 6.18(a) illustrates the bare soil particles bonded through the electrostatic force of attraction between the clay particles. The clay-rich soil is one of the most conventional options for thermal backfill applications for heat-resisting TAS due to its natural abundance and lower thermal conductivity. However, their thermal conductivity can be controlled further with biochar amendment. Upon biochar amendment in soil, the heat transfer in the soil decreases due to inclusion of the lower thermal conductivity of highly intra-porous biochar. However, the strength is also reduced due to a decrease in the cohesive and electrostatic force of attraction between the clay particles present in the soil-biochar matrix with the presence of an inert-soil-biochar interface, as explained in Fig. 6.18(b). In case of strength is not a concern, SBC can be a very convenient option for the thermal backfill. However, in case the strength of the soil is to be improved, biopolymer incorporation can be useful. The BpS specimens have amazingly higher strength in comparison to the bare soil or SBC, with an equivalent thermal conductivity to the bare soil. With the addition of biopolymer (xanthan gum) to the soil, the strength of soil increases due to the formation of bridges between the soil grains and hydrogen-cation bonds between xanthan gum and electrically charged clay particles, as shown in Fig. 6.18(c). A cumulative influence of biochar and biopolymer was observed in the SBPC, as illustrated in Fig. 6.18(d). The SBPC showed dual advantages in terms of thermal insulation and strength.

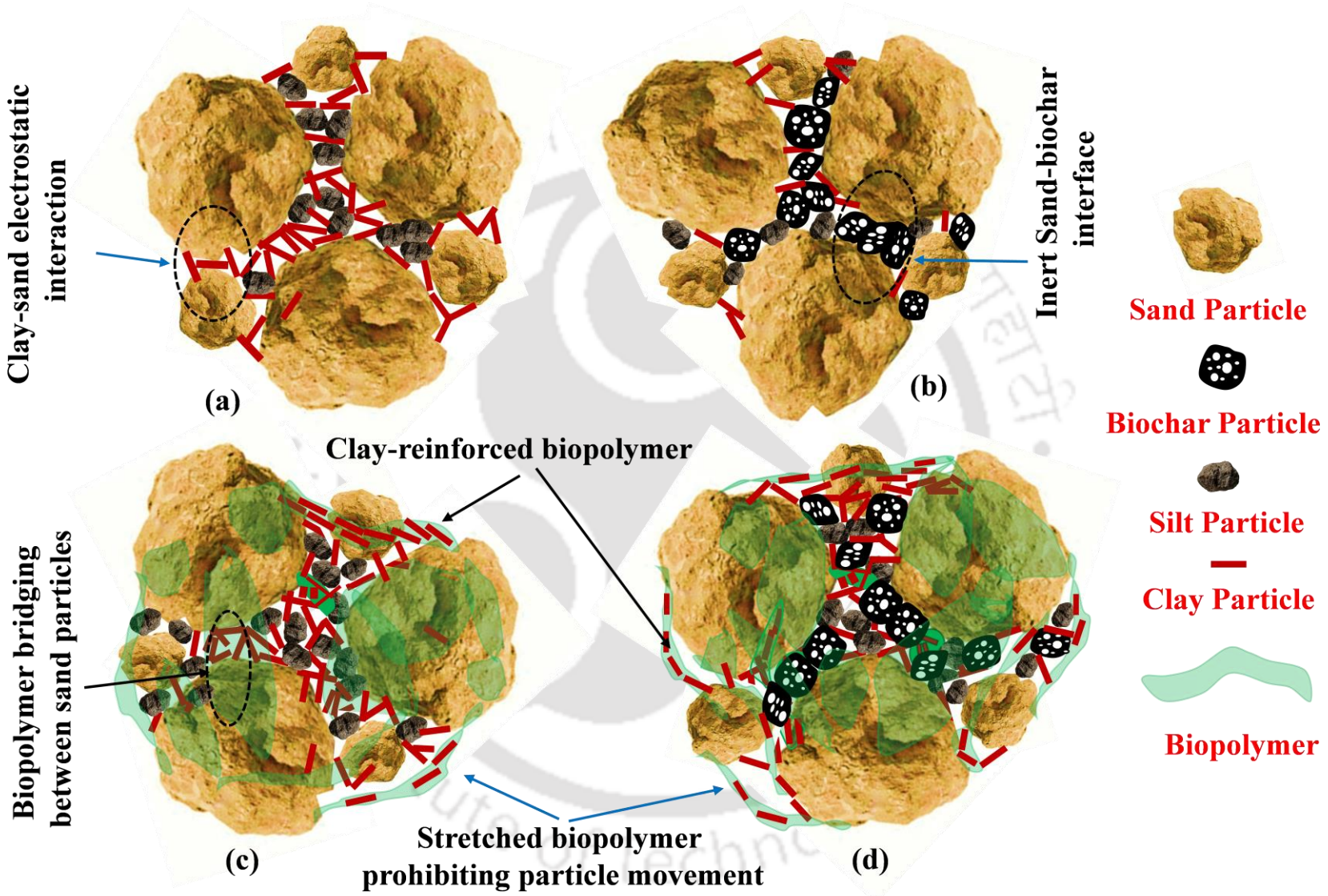

Figure 6.18 Schematic representation of the micro-level interaction between particles of- (a). Bare soil, (b). SBC, (c). BpS, and (d). SBPC

6.4 Summary

The current chapter reports a natural soil-biochar-biopolymer composite (SBPC) that can fulfill the strength and thermal insulation requirements of advanced thermal backfills. For developing the SBPC, the thermal conductivity (*K*) and unconfined compressive strength (UCS) of the soil-biochar composite (SBC) and biopolymer-stabilized soil (BpS) were studied. The findings unraveled the underlying synergistic mechanism in the SBPC induced by the thermal insulation characteristics of biochar and the strength enhancement characteristics of biopolymer. The major finding from the current study are as follows:

- A consistent favorable decrease in *K* values of plain soil from 1.61 $Wm^{-1}K^{-1}$ to 1.26 $Wm^{-1}K^{-1}$ in the OMC state was recorded upon 7.5% biochar amendment. Upon the same amendment, the *K* values decreased from 0.48 to 0.35 $Wm^{-1}K^{-1}$ in the dry state. The UCS and secant modulus of elasticity (E_{50}) of soil are adversely impacted by biochar amendment. The UCS of the soil falls from 366 kPa to 186 kPa at the OMC state and 1.29 MPa to 0.95 MPa in the dry state upon 7.5% biochar amendment.
- The thermal conductivity of the Xanthan Gum (XG) biopolymer solutions was unaffected by its concentration. The *K* values of the biopolymer solution are determined to be in the range of 0.581±0.018 $Wm^{-1}K^{-1}$ for a concentration of XG varying from 0.5 g/l to 70 g/l in water.
- No practical difference in thermal conductivity was noted with biopolymer addition at OMC state and after drying. The *K* values were found to vary 1.55±0.04 $Wm^{-1}K^{-1}$ at the OMC state, whereas after drying, *K* was determined to be in a range of 0.50±0.02 $Wm^{-1}K^{-1}$ upon biopolymer treatment varying from 0.5% to 1.5%. A tremendous increase in the UCS and E_{50} at OMC state and after drying was noted. The UCS was found to increase from 366 kPa to 681 kPa at OMC state and 1.29 MPa to 5.35 MPa after drying for 1.5% biopolymer (w/w) treatment.
- The SBP composites were developed incorporating SBC and BpS treatment. It was observed that although the *K* values gradually fall upon incremental biochar amendment, the strength component of four of the SBPC (SB5P1.5, SB7.5P0.5, SB7.5P1, SB7.5P1.5) exhibited slightly lower UCS than the bare soil at the OMC state. The loss of strength at the OMC state is attributed to biopolymer lubrication to the inert biochar particles. However, these composites have much higher strength and lower *K* values than the bare soil upon drying and, therefore, can be used accordingly.

All the other SBPC exhibited equivalent, if not lower thermal conductivity than the plain soil, along with an enhanced strength in OMC state and after drying.

- SEM micrographic analysis confirmed the heat transfer and stabilization mechanism. The higher thermal insulation and strength characteristics of the composite were due to increased porosity (attributed to biochar addition) and improved binding of soil particles (attributed to biopolymer treatment).

Although the findings from this chapter have provided insights into the development of a natural thermal backfill, future studies are essential to ensure its field-scale applicability. In the current chapter, the focus was restricted to assessing the mechanism of the composite behavior and its development. Field evaluation of thermal backfill needs to be performed to assess the long-term performance, durability, and cost viability of the proposed composite thermal backfill.

CHAPTER 7
EXPERIMENTAL INVESTIGATION OF THERMAL MIGRATION IN SBC AND SBPC

7.1 Introduction

Heat transfer in the soil mainly depends upon the initial degree of saturation, thermal characteristics of the soil, porosity, and pore geometry of the soil matrix (Moradi et al., 2015, 2016). The results from the previous chapters confirm that the soil-biochar composite (SBC) and soil-biochar biopolymer composite (SBPC) can be used as potential thermal backfill material for TAS to reduce thermal migration. However, there is limited study on the investigation of heat transfer in biochar-amended soil (Zhang et al., 2015). Therefore, to investigate the thermal insulation efficiency in terms of heat transfer through SBC, a bench-scale study is necessary to move toward field-scale applications. Within the context of the above-discussed literature, this study investigates the temporal distribution of heat transfer in SBC and SBPC. For this purpose, a soil column was fabricated utilizing the locally available highly plastic silty soil, biochar prepared from the hardwood of mesquite and sugarcane bagasse, and xanthan gum biopolymer. The radial distribution of heat transfer in the prepared soil column was investigated using a heater rod and temperature sensors installed in the radial direction in the soil column. Further, the micrographical analysis was also carried out via Field-Emission Scanning Electron Microscopy (FESEM) to investigate the mechanism of heat transfer in SBC and SBPC.

7.2 Sample preparation and experimental setup

The soil heating system used in this study, as shown in Fig. 7.1, contains the heater rod, temperature sensor, and temperature controller. A nichrome wire wrapped around a ceramic core having a length of 190 mm and diameter of 15 mm with 1000 W power as a heater rod was used in this study. A temperature thermistor was used to measure the temperature (ACETEQ, Model No. DTM-X7). The diameter and measurement range of this thermistor probe is 2.5 mm and -50°C to 300 °C. The accuracy of this sensor is ±1°C for the temperature range of -10°C to +110°C. A digital thermostat temperature controller switch was also used to control the temperature of the heater rod. The measurement and control range of this temperature controller is -50°C to 110°C. The control precision and measuring accuracy of this controller is ±0.1 °C and ±0.2 °C. The controlling temperature in the temperature controller was set to 100±1 °C.

Figure 7.1 Soil heating system (a) Electric heating rod; (b) Temperature measurement thermistor; (c) Temperature controller

Fig. 7.2 shows the schematics diagram and photographic view of the experimental setup used in this study for the measurement of heat transfer in bare soil, SBC, and SBPC. A cylindrical acrylic mold with an internal diameter of 300 mm and a height of 250 mm with a base plate was fabricated for preparing the soil column. Howard (1996) recommended that the thermal backfill should be compacted at a minimum of 95% maximum dry density and ± 2% of optimum moisture content. Thus, the bare soil and SBC samples were prepared at OMC and 0.95MDD according to the compaction characteristics of soil and SBC. Liu et al. (2018) reported that the amendment of biochar up to 2.5% did not significantly affect the thermal characteristics of the soil. Therefore, the biochar contents in the SBC and SBPC were selected as 5% and 15% by the total dry weight of the composite.

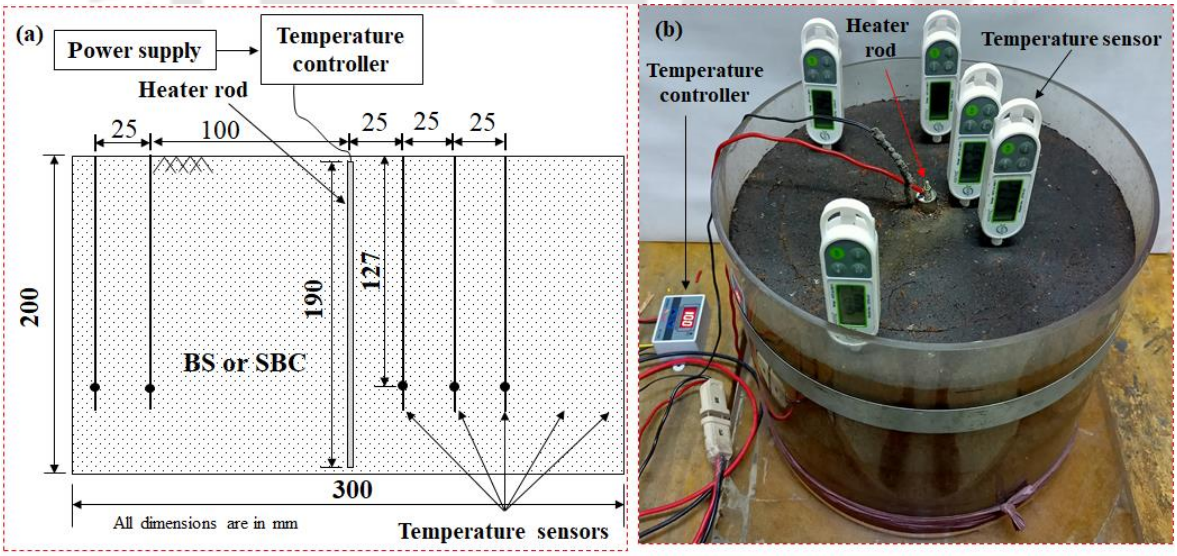

Figure 7.2 Experimental setup (a) sectional view (b) Photographic view

The sample preparation procedure for the SBC and SBPC was the same as explained in section 6.2. Thereafter, the prepared SBC and SBPC samples were compacted at a target dry density of 0.95 MDD in a four-layer up to a height of 200 mm by maintaining a fixed mass of the prepared samples and volume in each layer. A dummy steel rod diameter slightly

less than the heater rod was used during the compaction of the soil-biochar mixture. A heater rod was installed in the center of the soil column. Further, the temperature probe was installed into the sample from the top surface at a radial distance of 25 mm, 50 mm, 75 mm, 100 mm, and 125 mm from the heater rod, as shown in Fig. 7.2 (a and b). Thereafter, the heater rod was on using an electric power supply, and the temperature in the heater rod was controlled using a temperature controller. In this way, the soil column heating was carried out. Subsequently, the temperatures were measured at different radial distances from the heater rod until they attained a constant value, termed the heating cycle in the current study. Afterward, the heater rod was off, and the soil column temperature was measured again at different radial distances, termed ambient cooling in the current chapter. Similarly, the temperature of the soil column was measured in the second cycle of heating and ambient cooling.

7.3 Results and discussion

7.3.1 Effect of biochar amendment rate on thermal migration in SBC

The temporal variation of soil column temperature at a radial distance of 25 mm, 50 mm, 75 mm, 100 mm, and 125 mm from the heat source for bare soil and SBC in the first and second cycles of heating and ambient cooling is presented in Fig. 7.3 and Fig. 7.4. It was observed from Fig. 7.3 that evaluation of the soil temperature indicates that the steady-state conditions were established within 200 hours at all radial distances during heating in the first cycle of heating. In contrast, the steady-state conditions were achieved within 30 hours in the second cycle of heating (refer to Fig. 7.4). Moreover, in both cycles of ambient cooling, the steady-state conditions were achieved within 30 hours. Since thermal diffusivity describes the rate of heat conduction through the soil. The longer period for the first heating cycle is primarily due to the smaller thermal diffusivity of wet soil compared to dry soil, which is attributed to the lesser thermal diffusivity of water (0.147 $mm^2 s^{-1}$) as compared to air (23.5 $mm^2 s^{-1}$). Further, a peak in soil temperature was noted at around 10 hours for both bare and SBC at all radial distances in the first heating cycle, while no peak value was observed in the second heating cycle (refer to Fig. 7.4).

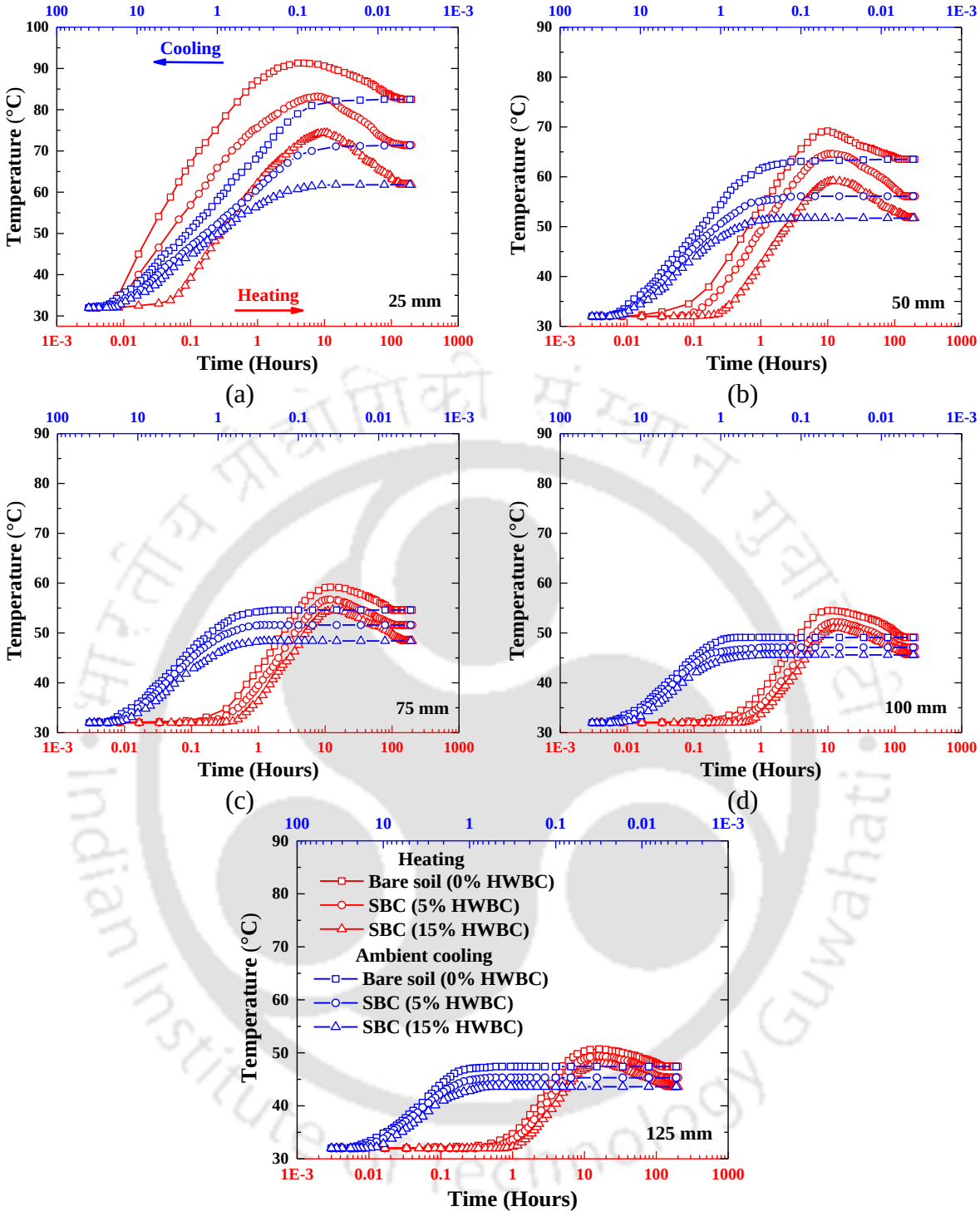

Figure 7.3 Soil temperature distribution at (a) 25; (b) 50; (c) 75; (d)100; and (e) 125 mm radial distances in 1st heating cycle and ambient cooling at different biochar content

The peak value in the first heating cycle is attributed to the heat transfer due to the continuous generation of water vapor in wet soil. The water vapor has higher thermal diffusivity compared to water, which increases the heat transfer in the initial phase. Afterward, it decreases consistently and reaches a steady state around 200 hours. In addition, an increase in temperature lag was also noted with an increase in radial distance from the

heat source. This might be attributed to the higher thermal resistance at a greater distance from the heat source. Moreover, an increase in temperature lag was also found in SBC compared to bare soil, primarily due to the lower thermal conductivity and thermal diffusivity of biochar.

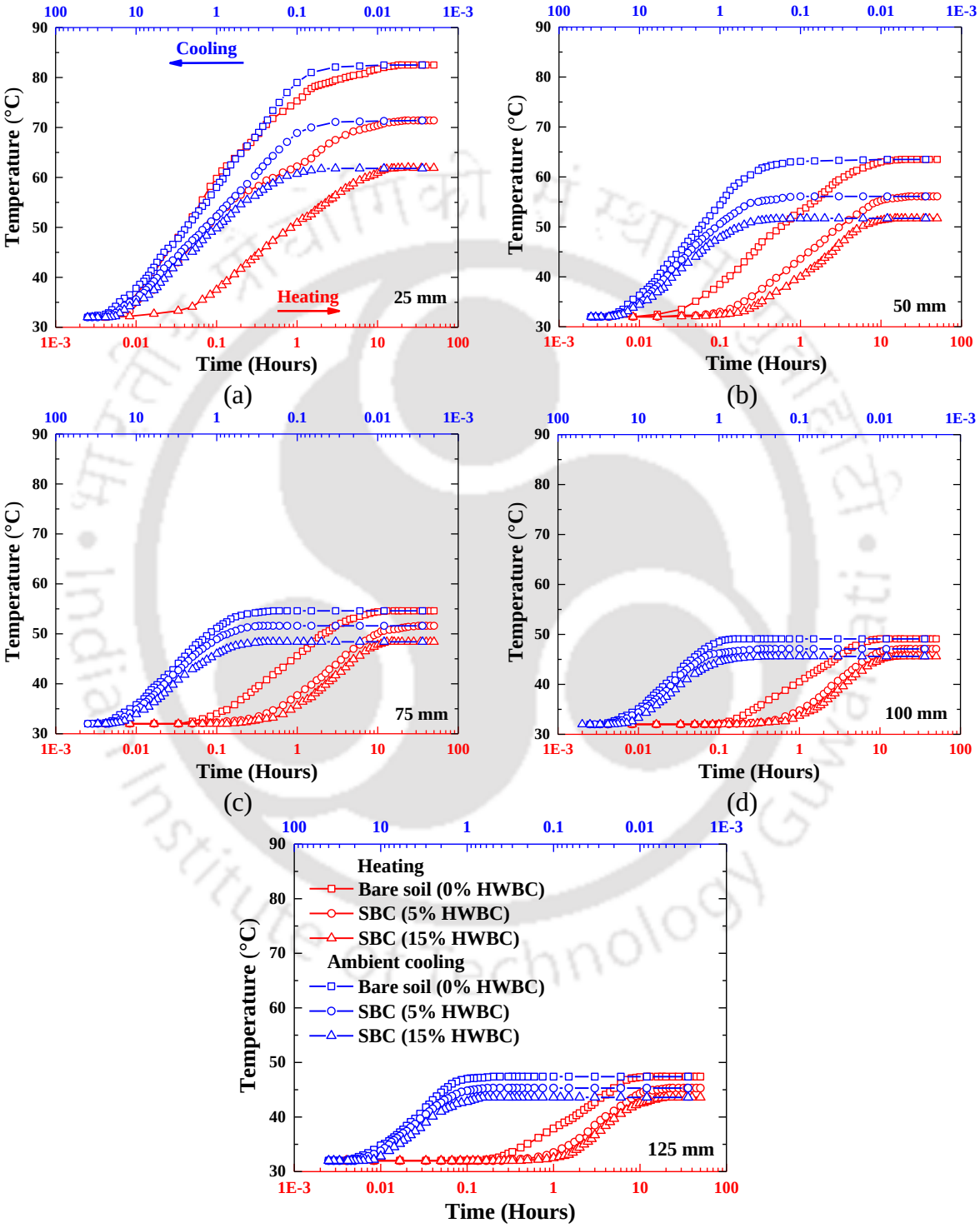

Figure 7.4 Soil temperature distribution at a) 25; (b) 50; (c) 75; (d)100; and (e) 125 mm radial distances in 2nd heating cycle and ambient cooling at different biochar content

At the elapsed time of 200 hours and 15% BC amendment rate, the temperature difference between bare soil and SBC varies from 4°C (at 125 mm) to 20°C (at 25 mm), depending upon the distance from the heater rod. This is mainly ascribed to the lower thermal conductivity and thermal diffusivity of SBC as compared to bare soil. The micrographical analysis of SBC makes it abundantly evident that the biochar particles are trapped between the soil grains, posing a barrier to heat transfer and increasing the thermal insulation efficiency of SBC (refer to Fig. 7.5).

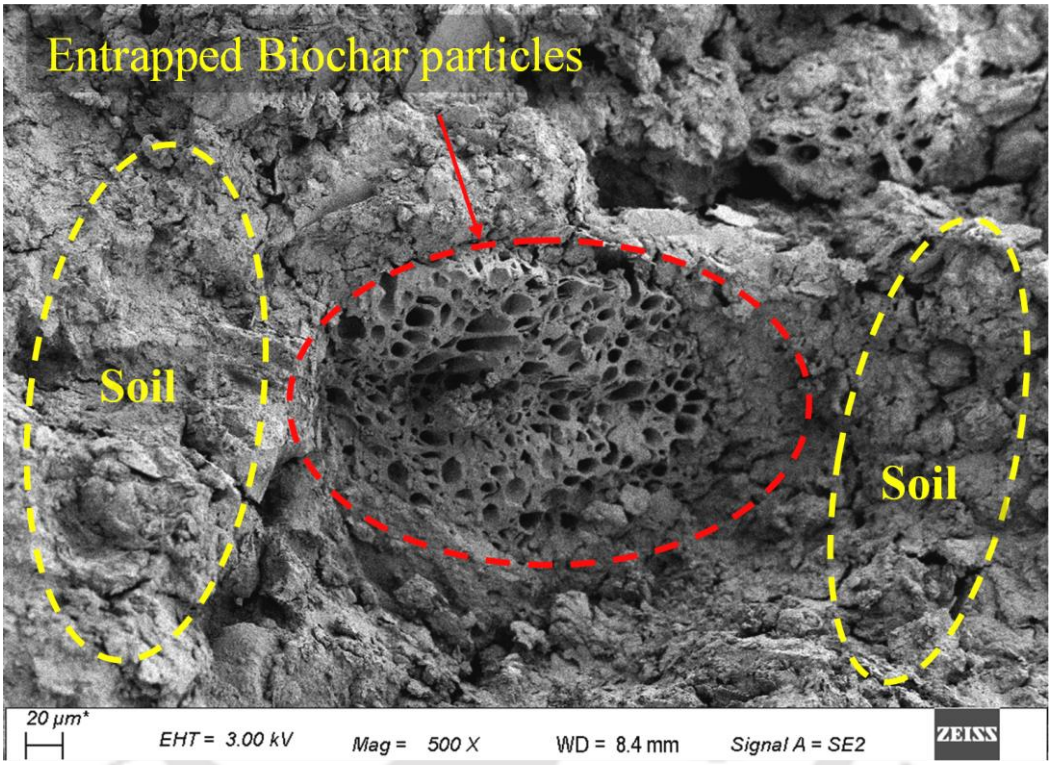

Figure 7.5 FESEM micrographs of BAS sample highlighting the intra-porous biochar-soil matrix

7.3.2 Effect of biochar type on thermal migration in SBC

Fig. 7.6 and Fig. 7.7 show the variation of soil column temperature with elapsed time at a radial distance of 25 mm, 50 mm, 75 mm, 100 mm, and 125 mm from the heat source for bare soil and SBC (soil amended with hardwood biochar, HWBC and sugarcane bagasse biochar, SBBC) in the first and second cycles of heating and ambient cooling. The amendment rate for both biochar types was selected as 5% of the total dry weight of SBC. The temperature reduction value in the SBC column amended with SBBC is more as compared to HWBC-amended soil at all times and radial distances. At the elapsed time of 200 hours and for the same amendment rate (5% BC), the temperature difference between HWBC and SBBC amended soil column varies from 1.6°C (at 125 mm) to 8°C (at 25 mm)

depending upon the distance from the heater rod. This is mainly credited to the lower maximum dry density value of SBC with SBBC amendment. Further, SBBC has lower thermal diffusivity and thermal conductivity as compared to HWBC.

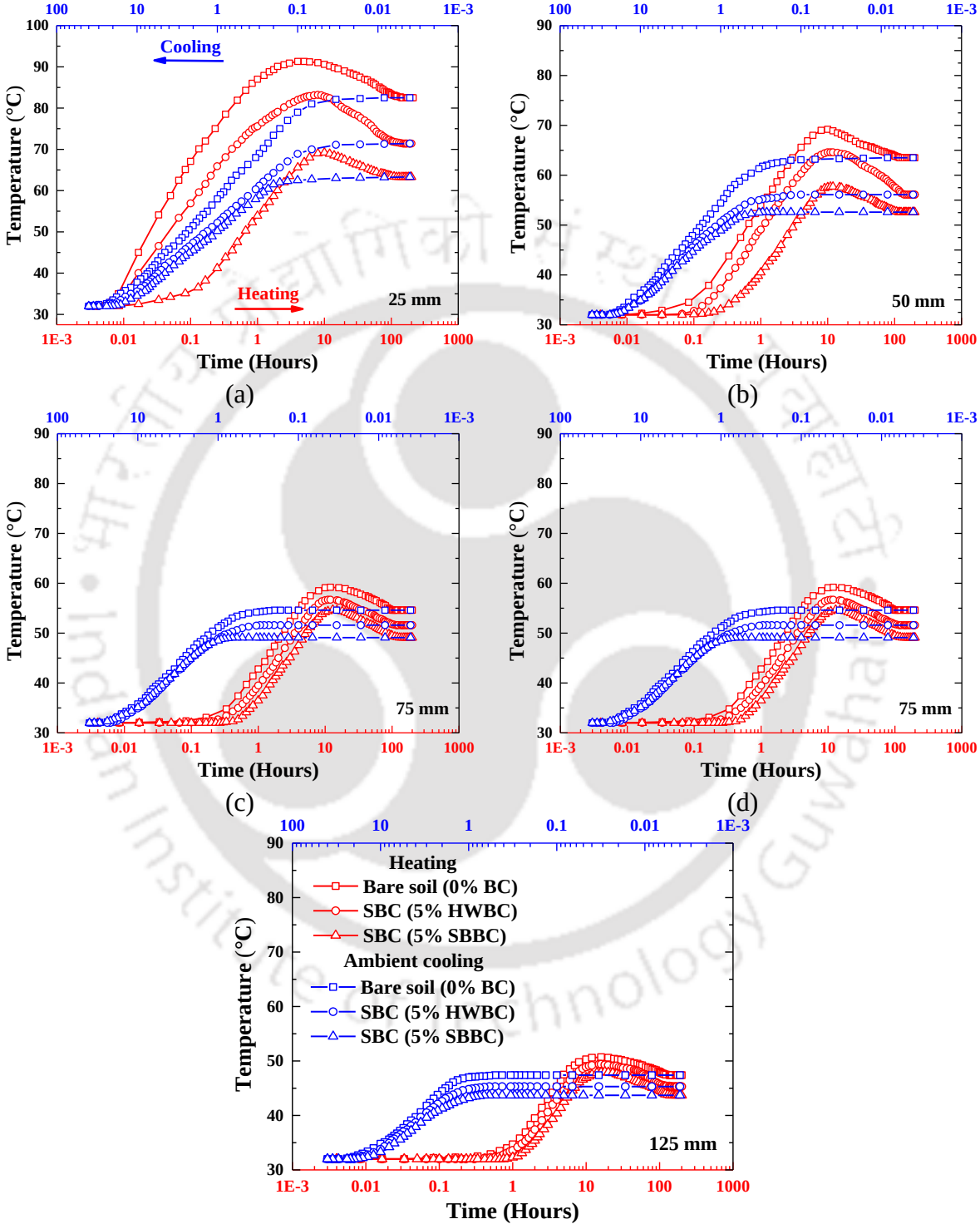

Figure 7.6 Soil temperature distribution at (a) 25; (b) 50; (c) 75; (d)100; and (e) 125 mm radial distances in 1st heating cycle and ambient cooling for different biochar type

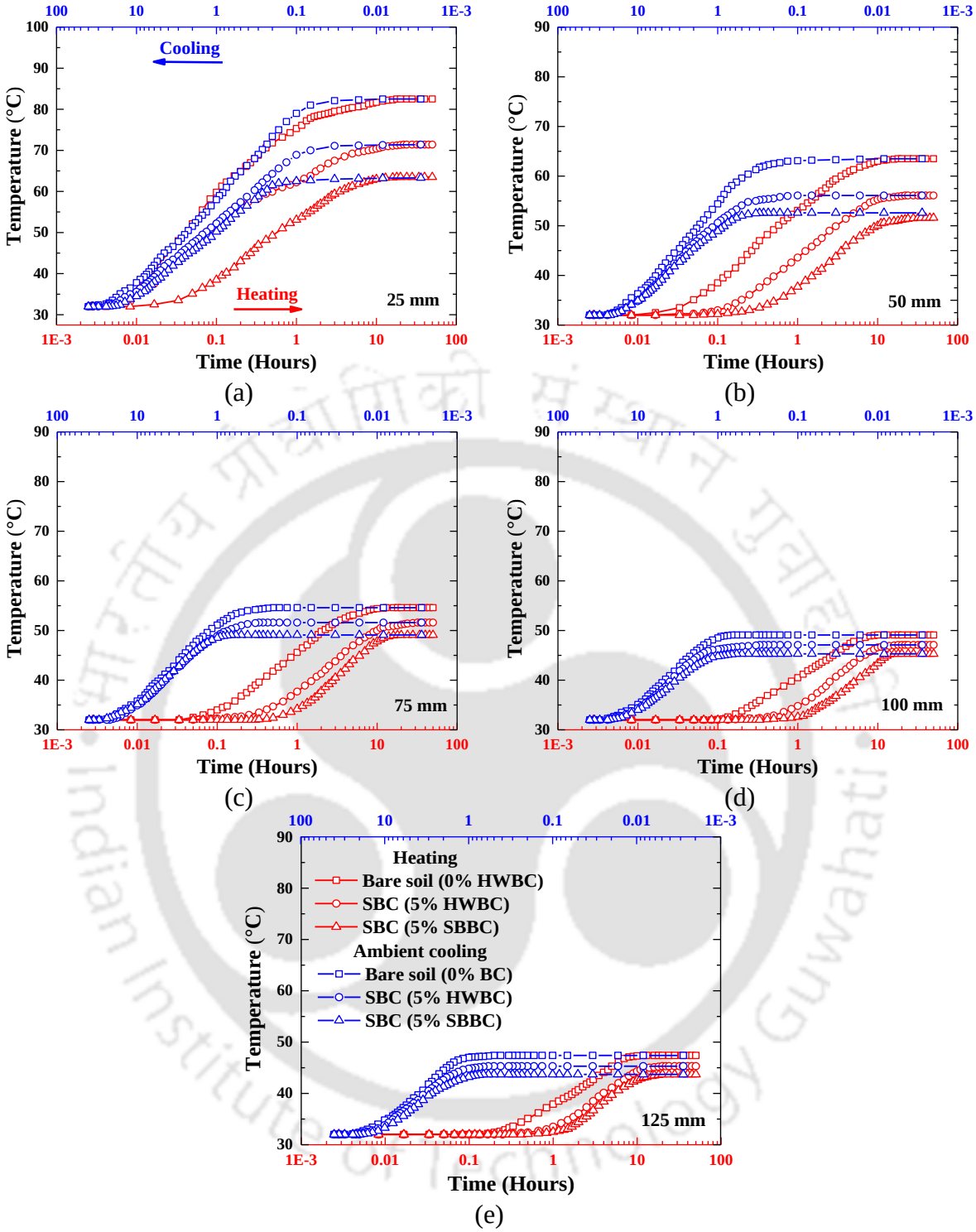

Figure 7.7 Soil temperature distribution at (a) 25; (b) 50; (c) 75; (d)100; and (e) 125 mm radial distances in 2nd heating cycle and ambient cooling for different biochar type

7.3.3 Synergistic effect of biochar and biopolymer amendment on thermal migration

Fig. 7.8 and Fig. 7.9 show the variation of soil column temperature with elapsed time at a radial distance of 25 mm, 50 mm, 75 mm, 100 mm, and 125 mm from the heat source for bare soil, SBC (soil amended with 5% hardwood biochar) and SBPC (soil amended with

5% hardwood biochar and 0.5% xanthan gum) in the first and second cycles of heating and ambient cooling.

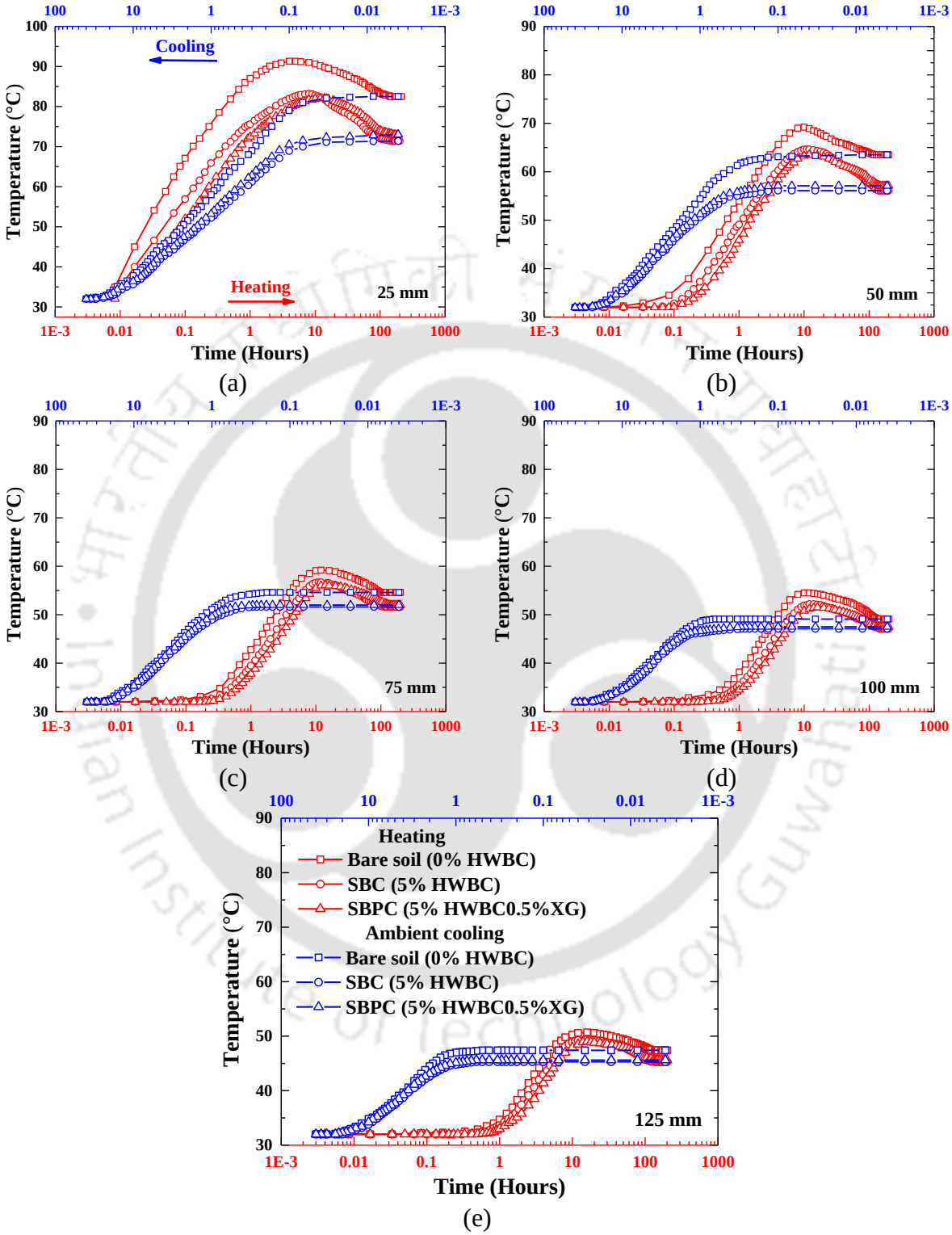

Figure 7.8 Soil temperature distribution at (a) 25; (b) 50; (c) 75; (d)100; and (e) 125 mm radial distances in 1st heating cycle and ambient cooling for SBC and SBPC

The SBC mixed with 0.5% XG displays a lower temperature in the wet state and a slightly higher temperature in the dry state than SBC at all radial distances. At the elapsed time of

200 hours, a marginal temperature difference between SBC and SBPC soil column varies from 0.3°C (at 125 mm) to 1.6°C (at 25 mm) depending upon the distance from the heater rod. This is mainly credited to the marginal difference in the thermal conductivity value of SBC and SBPC, as reported in the previous chapter in section 6.3.4.

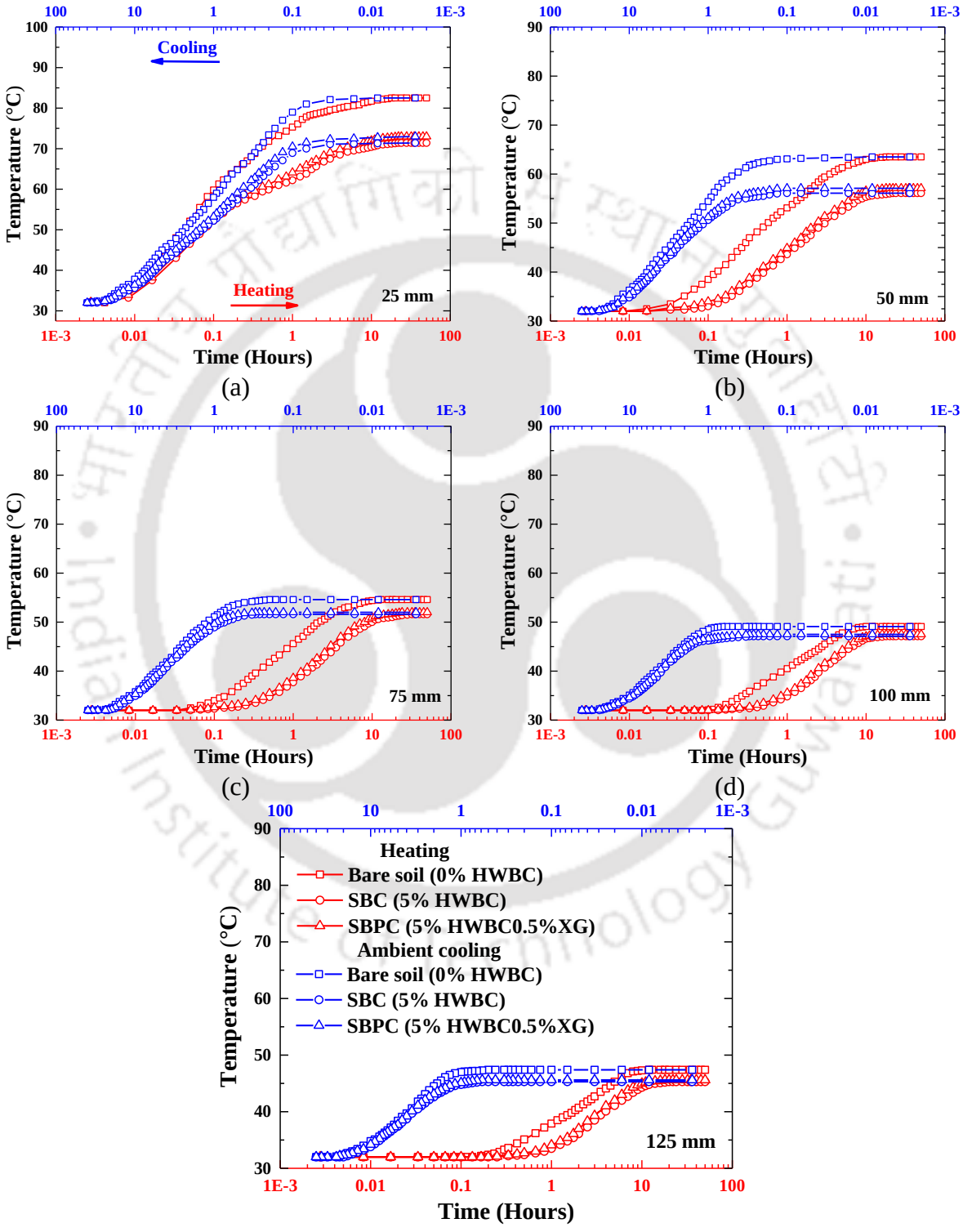

Figure 7.9 Soil temperature distribution at (a) 25; (b) 50; (c) 75; (d)100; and (e) 125 mm radial distances in 2nd heating cycle and ambient cooling for SBC and SBPC

Moreover, it is noteworthy to point out from Fig. 7.3 to Fig. 7.9 that the margin of decrease in temperature value of SBC and SBPC with respect to bare soil was noted to be reduced with an increase in radial distance from the heat source for all elapsed time. A minimal difference in temperature reduction value was observed between the 100 mm and 125 mm radial distances for bare soil and SBC or SBPC. A probable reason for this can be credited to the critical influence zone of the heat source. Therefore, it is suggested to provide the insulation of the SBC layer up to a certain thickness only, as there is not much difference in the temperature reduction of SBC compared to bare soil after a certain radial distance from the heater source.

Fig. 7.10 presents the temperature variation with radial distance in bare soil and soil amended with different biochar content at the elapsed time of 0.5, 1, 10, and 100 hours in the first cycle of heating. It can be seen from the figure that the temperature decreases with an increase in radial distance from the heat source in both bare and SBC.

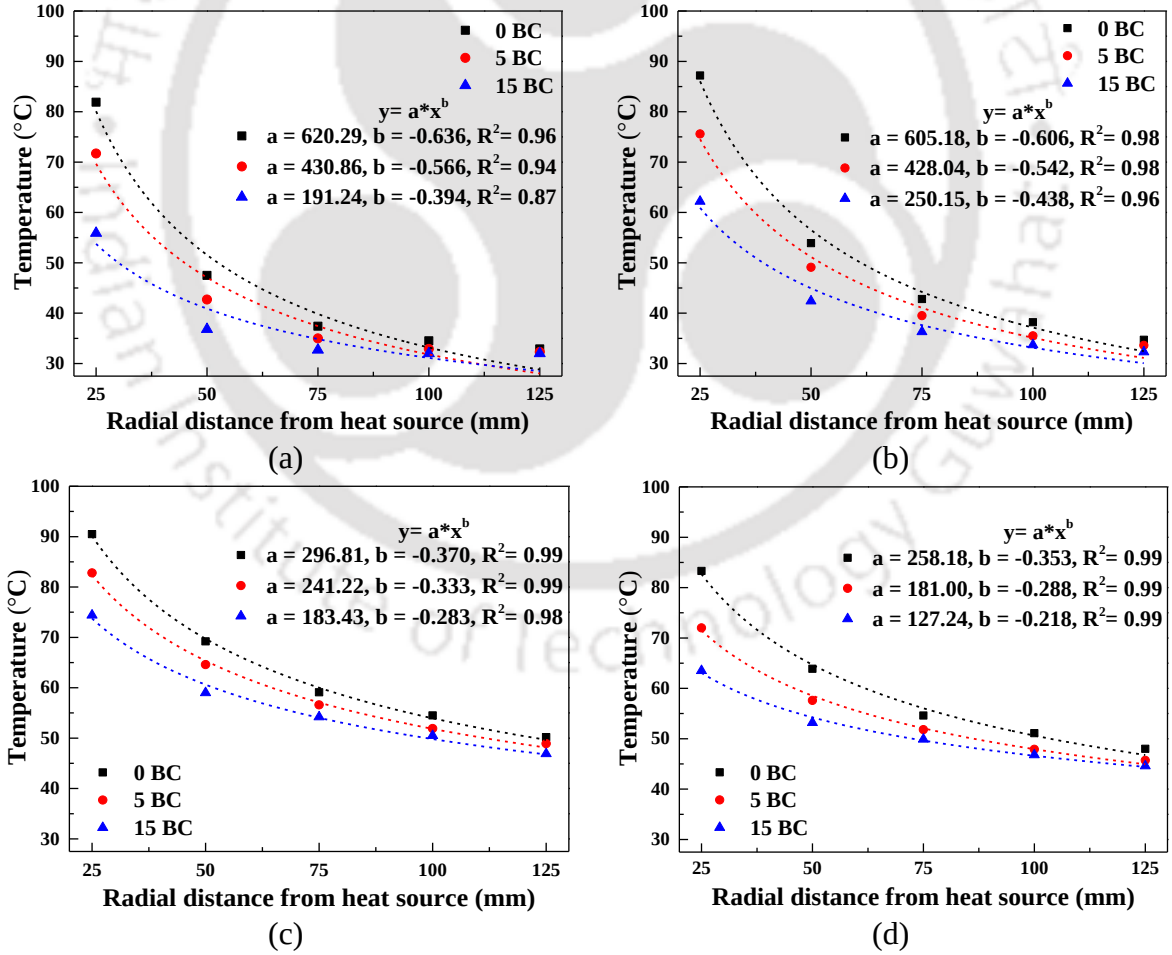

Figure 7.10 Temperature variation according to radial distance from heater rod (a) 0.5 hours; (b) 1 hour; (c) 10 hours; and (d) 100 hours

The test results were best fitted, and a non-linear inverse power function correlation (R2 > 0.95) between temperature and radial distance was observed for bare soil and SBC. Moreover, it is remarkable to point out from Fig. 7.10 that the margin of decrease in temperature value of SBC with respect to bare soil was noted to be reduced with an increase in radial distance from the heat source for all elapsed time. A probable reason for this can be credited to the critical influence zone of the heat source.

7.4 Summary

The present chapter investigated the experimental investigation of heat migration in SBC and SBPC. A soil column was fabricated by mixing the highly plastic silty soil with commercially available hardwood biochar (HWBC), sugarcane bagasse biochar (SBBC), and xanthan gum biopolymer. Thereafter, the prepared sample was compacted at the dry density of 95% of maximum dry density and optimum moisture content condition in an acrylic mold. Subsequently, the heater rod and temperature sensors were installed in the mold to measure temperature distribution during heating and ambient cooling. The following results can be drawn based on the investigation:

- The SBC and SBPC exhibit lower temperatures as compared to bare soil at all radial distances and times for both the heating and cooling cycle. This is mainly ascribed to the entrapped biochar particles between the soil particles that have an intra-porous structure with lower thermal conductivity and thermal diffusivity than bare soil.
- An increase in temperature lag was found in SBC and SBPC than in bare soil, primarily due to the lower thermal conductivity and thermal diffusivity of biochar.
- The margin of decrease in temperature value of SBC and SBPC with respect to bare soil was noted to be reduced with an increase in radial distance from the heat source. Thus, it is suggested to provide the insulation of the BAS layer up to a certain thickness only.
- A non-linear inverse power function correlation ($R^2 > 0.95$) between temperature and radial distance was observed for both bare soil and SBC.

The finding of the present chapter unravels the potential of SBC and SBPC to restrict heat transfer from TAS. Therefore, the proposed SBC and SBPC can be utilized effectively as thermal backfill material for underground crude oil pipelines, crude oil storage tanks, subsurface cold storage, and geothermal energy storage systems to improve their performance.

CHAPTER 8
DEVELOPMENT OF ENERGY-EFFICIENT BIOCHAR FOR THERMAL BACKFILL APPLICATION

8.1 Introduction

This study aims to make biochar production energy-efficient by optimizing the pyrolysis temperatures, specifically for thermal backfill applications. The thermal characteristics of any material rely hugely on its mineralogical composition, surface structural characteristics, and physicochemical properties, which might be controlled with the pyrolysis temperature (Klett et al., 2004; Hassan et al., 2020; Pariyar et al., 2020; Zhang et al., 2020; Nzediegwu et al., 2021). The thermal backfill is intended for large-scale crude oil industries. Therefore, the manufacturing process of biochar should meet the minimum energy consumption requirements maintaining the desired thermal characteristics for minimizing the material cost. Previous literature on optimizing the pyrolysis temperatures for biochar production in terms of yield (Manyà, 2012; Zhang et al., 2020). However, there are limited numbers of studies that have attempted to quantify the energy required for producing biochar (Xu et al., 2011; Yu et al., 2019). Therefore, an investigation of the energy efficiency of the pyrolysis process at various temperatures in the context of the specific thermal, microstructural, and physicochemical properties of the produced biochar is of paramount importance.

In this study, the collection and pre-treatment of waste biomass (feedstocks) were done, and then biochar was prepared by the slow pyrolysis method. A total of ten forms of biochar are formed from the water hyacinth (WH) and sugarcane bagasse (SB) feedstocks by varying the pyrolysis temperatures ranging from 300 °C to 700 °C. First, the chosen feedstocks and pyrolysis processes are compared based on their energy efficiency and biochar yield. In the second stage, the produced biochars are characterized through their physicochemical characteristics, microstructure, mineralogy, surface functional groups, and thermal stability following standard protocols. Then, the thermal properties of the produced biochar and biochar-amended soils are assessed. The carbon stability of the biochars in the soil is evaluated with the help of the Van-Krevelen method based on the proximate and ultimate analysis. A brief summary of the experimental program is summarised in Fig. 8.1.

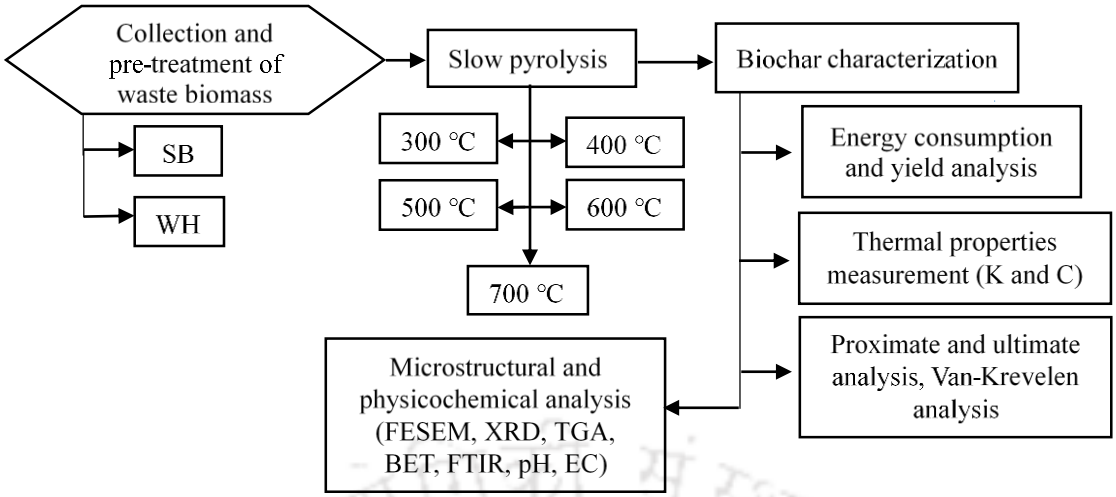

Figure 8.1 Schematics of the experimental program

8.2 Biochar production, energy consumption, and yield

The biomass from the WH stem and SB was used to make biochar. SB and WH biomass were collected in Amingaon, Assam, India (26.1847°N, 91.6672°E) from a local market and a lake, respectively. WH biomass was collected on the same day from the lake to eliminate the genetic variance. Both the feedstocks were first rinsed with running water to remove dirt and eliminate contaminants. It was then sun-dried for seven days at room temperature before being cut to a size of around 30 mm to ensure complete pyrolysis of the biomass. It was then oven-dried for 72 h at 60 °C and stored in an airtight box.

In a fixed batch reactor containing an argon atmosphere, the sun-dried WH and SB feedstocks were pyrolyzed at temperatures of 300 °C, 400 °C, 500 °C, 600 °C, and 700 °C with a heating rate of 10 °C per minute and a holding time of 45 minutes (Muigai et al., 2021). The procedure was repeated three times to test repeatability. The biochar was crushed and sieved to a fineness of 1 mm. The biochar was then sieved into three fractions: 1 mm-0.425 mm, 0.425 mm-0.075 mm, and less than 0.075 mm. Later, the three fractions were combined in proportions of 70:20:10 and stored in an airtight box for further testing. The biochar produced from WH at pyrolysis temperatures of 300, 400, 500, 600, and 700 degrees Celsius is named WH300, WH400, WH500, WH600, and WH700. Similarly, the biochar prepared from SB was abbreviated as SB300, SB400, SB500, SB600, and SB700.

The energy consumption per kg of biochar production was calculated based on the electricity consumption by the 4kW furnace provided with the reactor. All the calculations were made considering (pyrolysis temperature + 20 °C) for all the samples. The extra 20 °C was given as input to the PID (proportional–integral–derivative) temperature programmer

controller (FUJI, PXF9) to correct the mismatch between input and output temperature of the furnace. The total time for pyrolysis was assumed to consist of the heating time (depending on pyrolysis temperature and rate of heating) and holding time (45 minutes) for each sample. The time for cooling the instrument was not considered in energy calculation as the reactor was kept for natural cooling. The biochar yield is stated as a percentage and is defined as the mass of produced biochar divided by the initial mass of biomass.

8.3 Thermal characteristics of biochar and SBC

Two acrylic molds with the same inner diameter of 80 mm and differing heights of 70 mm and 60 mm were utilized to investigate the thermal characteristics of biochar and SBC. To measure thermal characteristics (*K* and *C*) of biochar, the fixed mass of oven-dry biochar (70 gm for WH and 40 gm for SB biochar) was taken and compacted in three layers by applying a static load of 0.1 kN with the help of a loading frame, proving ring, and plunger. To determine thermal characteristics of control (bare) soil, 400 gm of soil and 100 ml of distilled water were homogenously mixed in an aluminum pan. Similarly, for SBC, a soil-biochar composite with 380 gm of soil, 20 gm of dry biochar, and 100 ml of water were homogenously mixed in an aluminum pan. Following that, the homogeneous SBC was placed in an airtight plastic bag and placed in a desiccator for 24 hours to allow uniform moisture circulation throughout the sample. 450 grams of bare soil and SBC samples were collected from the created composite and compacted in three layers using a static load of 1kN. After then, the probe was placed vertically into the biochar and SBC sample's core. Prior to the tests, a 15-minute window was set aside to achieve an equilibrium temperature around the thermal probe and the biochar. The mean value of three duplicate samples was used to calculate the thermal characteristics of biochar in this investigation.

8.4 Results and discussion

8.4.1 Energy consumption and yield capacity of biomass

The energy required to produce one kg of biochar from WH and SB biomass is compared in Fig. 8.2. It is evident that the pyrolysis rate at lower temperatures requires significantly lesser energy than pyrolysis at higher temperatures. For producing an equivalent amount of biochar from WH feedstock, pyrolysis at 300 °C required 130% lesser energy when compared to the maximum temperature of 700 °C. Similarly, SB feedstock required 169% lesser energy at 300 °C pyrolysis temperature. The yield is also presented in Fig. 8.2. The biochar yield was noted to be decreased remarkably as the pyrolysis

temperature was raised. The WH feedstock yielded 49% higher at 300 °C temperature compared to the pyrolysis at maximum temperature. At the same minimum pyrolysis temperature, SB yielded 77% higher when compared to the maximum temperature. Both parameters, including energy consumption and yield, suggest that pyrolysis at the minimum temperature (300 °C) is best suited in terms of energy efficiency and yield capacity.

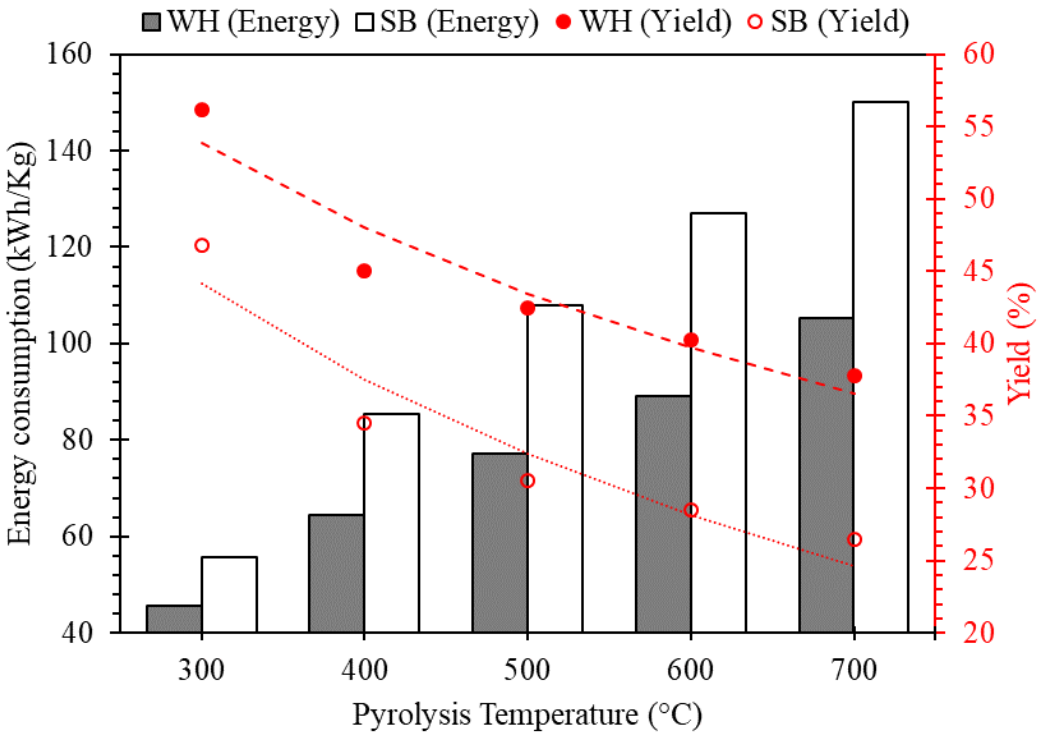

Figure 8.2 Energy consumption and yield during pyrolysis of WH and SB biochar

Another interesting finding was that the yield of WH biochar was notably higher when compared to SB biochar. At 300 °C pyrolysis, WH yielded 20% higher than SB. At 700 °C pyrolysis, WH yielded 42% higher. This might be attributed to the high ash content and low volatile matter of WH biomass. The low biochar yield from SB might be because of the maximum degradation of cellulose and hemicellulose material. The production of biochar steadily reduced as the temperature approached 400 °C. As found in one of the previous studies, this phenomenon could be attributed to the release of more volatile matter below 400 °C and the sluggish rate of lignin degradation above 400 °C (Shen et al., 2019). The yield of biochar and pyrolysis temperature have a logarithmic decreasing relationship. The trends in the same line were reported by Zhang et al. (2020), as shown in equations (8.1) and (8.2).

$$Y_{WH}(\%) = -20.47\ Ln\ (T) + 170.62 \quad (8.1)$$

$$Y_{SB}(\%) = -23.03\ Ln\ (T) + 175.47 \quad (8.2)$$

Where Y is the yield (%), and T is the pyrolysis temperature**.** As per the equation, the biochar yield showed a steadier decrement with an increased pyrolysis temperature.

8.4.2 Physicochemical and Microstructural properties of biochars

8.4.2.1 EDX and XRD analysis

Carbon (C) was found to be the most abundant element in all of the biochar generated, followed by oxygen (O) (Table 8.1). Alkali was another important element found in biochar, and alkaline earth metals such as calcium (Ca) and potassium (K) were evaluated using energy dispersive x-ray (EDX). As the temperature rises, the O concentration of biochar decreases, lowering the intensity of the O-H hydrophilic group. As a result, biochar made at higher temperatures has a higher hydrophobicity. The XRD diffractograms of the produced biochar are presented in Fig. 8.3. The XRD diffractogram of WH biochar show well defined sharp peak, which reveals its crystalline nature. Sylvite (KCl) and calcite ($CaCO_3$) are the major mineral presents in the WH biochar, while carbon (C), quartz (SiO_2), and sylvite are the major mineral in the SB biochar. When the temperature was raised to 400 °C, the peaks of sylvite (2θ = 15.1° and 24.5°) in the XRD diffractogram disappeared. At the 700 °C pyrolytic temperature, additional calcite ($CaCO_3$) peak was discovered. Wang et al. (2017) also discovered an additional calcite peak at 500 °C. In comparison, the XRD pattern of SB biochar revealed amorphous carbon (C) (002) due to large humps and a temperature range of 15° to 25°. A hump was also seen at a 43° diffraction angle with increased pyrolysis temperature, indicating the synthesis of aromatic carbon (graphite) in biochar generated at higher temperatures (Ahmed et al., 2021). Since the thermal conductivity of any material is related to the type of mineral present in it (Li et al., 2021; Ye et al., 2022). Therefore, the thermal conductivity of biochar produced at different pyrolysis temperatures is likely to vary due to changes in mineral compositions, which can be captured by XRD analysis. As discussed above, the changes in the mineral compositions of biochar are not significant. Therefore, the influence of the mineralogy of biochars produced at the different pyrolysis temperatures is expected to be minimal on its thermal conductivity.

Table 8.1 Elemental composition of the produced biochar using EDX analysis

Element	WH300	WH400	WH500	WH600	WH700	SB300	SB400	SB500	SB600	SB700
C	62.6±3.2	63.1±2.1	70.1±1.7	69±1.9	66.7±2	76.2±2	80.9±1.8	88.8±1.7	88.9±4	85.7±3.9
O	23.3±2.0	21.7±1.8	15.6±1.5	14.2±1.5	15±1.6	22.2±1.9	16.4±1.7	8.7±1.6	7.1±1.5	6±1.3
K	5.9±0.6	6.4±0.5	6.1±0.5	7.6±0.6	8.3±0.7	0.7±0.2	1.7±0.3	1.2±0.3	1.9±0.3	1.3±0.3
Cl	4±0.4	5.4±0.5	5.3±0.4	6.4±0.5	6.6±0.5	0.3±0.3	0.3±0.2	0.2±0.2	0.1±0.2	0.4±0.2
Ca	2±0.4	3.4±0.4	2.6±0.3	2.7±0.4	3±0.4	0.2±0.2	0.2±0.2	0.3±0.2	0±0.2	0.3±0.2
Si	0.1±0.2	0±0	0.3±0.1	0.1±0.1	0.4±0.2	0.5±0.2	0.5±0.2	0.8±0.2	0.7±0.2	0.3±0.1
N	2.1±3.8	0±0	0±0	0±0	0±0	0±0	0±0	0±0	1.1±4.1	5.9±4.1

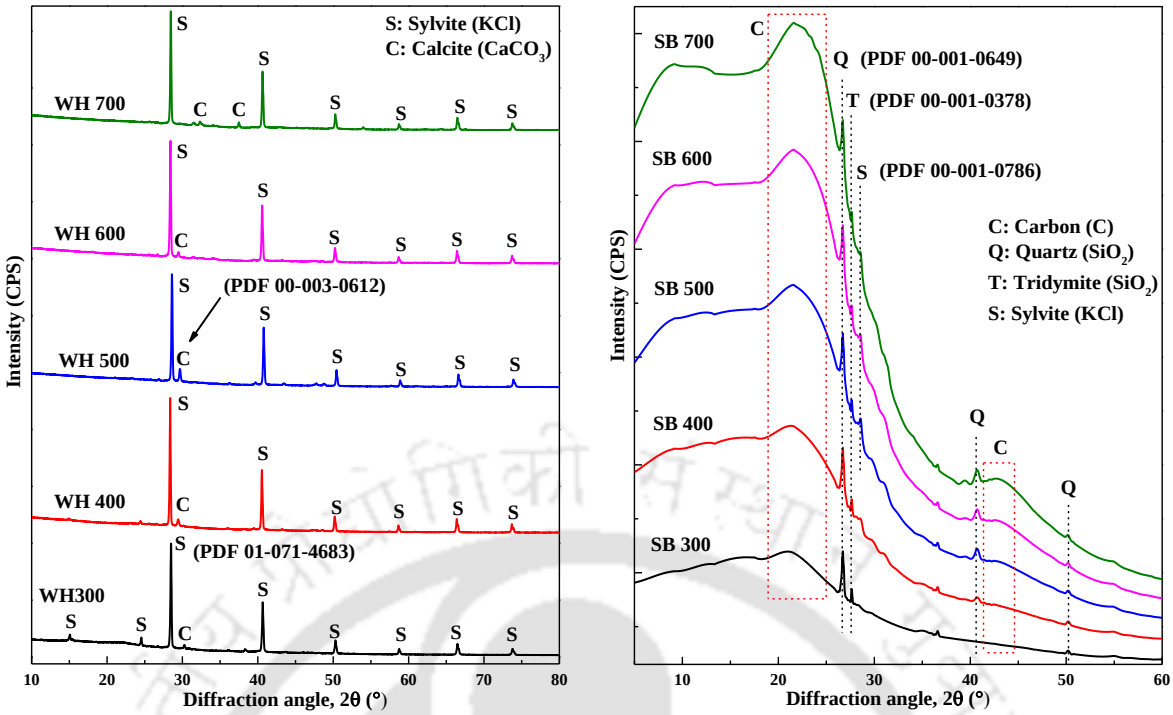

Figure 8.3 XRD spectra of WH and SB biochar at different pyrolysis temperatures

8.4.2.2 FTIR analysis

Fig 8.4. depicts the FTIR spectrum of raw biomass and biochar prepared at various temperatures. The structural development of several functional groups initially presented in biomass following pyrolysis is shown by comparing the FTIR spectrum of biochar and biomass. Table 8.2 shows the FTIR band assignments for biomass and biochar. The stretching of the -OH hydroxyl group around 3340 cm^{-1} is due to the amount of adsorbed water in biochar reducing dramatically above 400 °C. This is linked to lignin degradation in biochar, which caused the phenolic groups to break down at high pyrolysis temperatures (Wang et al., 2009). Due to greater CH_4 evolution at higher temperatures, the peak found at 2926 cm^{-1}, 2917 cm^{-1}, and 2850 cm^{-1} rapidly declined with temperature (Wang et al., 2009). The polar groups -OH and C=O- were greatly reduced at 500 °C due to the production of carbon monoxides (Rahman, 2018). The presence of aromatic hydrogen in biochar was suggested by the peak range of 600 cm^{-1} to 900 cm^{-1} (Morali and Şensöz, 2015). With a considerable amount of hydrogen released, the peak spectrum of these bands was shown to drop with rising temperatures (Rahman, 2018). Moreover, the wavenumber shift was also observed at peaks of 1619 cm^{-1}, 1601 cm^{-1}, 1418 cm^{-1}, and 893 cm^{-1} with the increased temperature, where the shift is highlighted in bold (Table 8.2). The shift for C=O and C=C aromatic groups to lower wavenumber with higher temperatures may be due to the increase

in mass of aromatic compounds. The shifting of the Si-O-Si bond for SB samples at higher temperatures may result from the weakening of the hydrogen bond, which causes a change in vibrational frequency. Another possible reason for the shifts might be attributed to the change in bond length. FTIR provides insight into the formation or debonding of a functional group at different temperatures, indicating different mineralogical states. Also, changes in functional groups of material influence its thermal conductivity (Zabihi and Araghi, 2016; Sun et al., 2017; Yuan et al., 2019). However, the findings from the current study suggested that there are no considerable changes in the functional group of the biochar, which might result in similar thermal conductivity even at different pyrolysis temperatures.

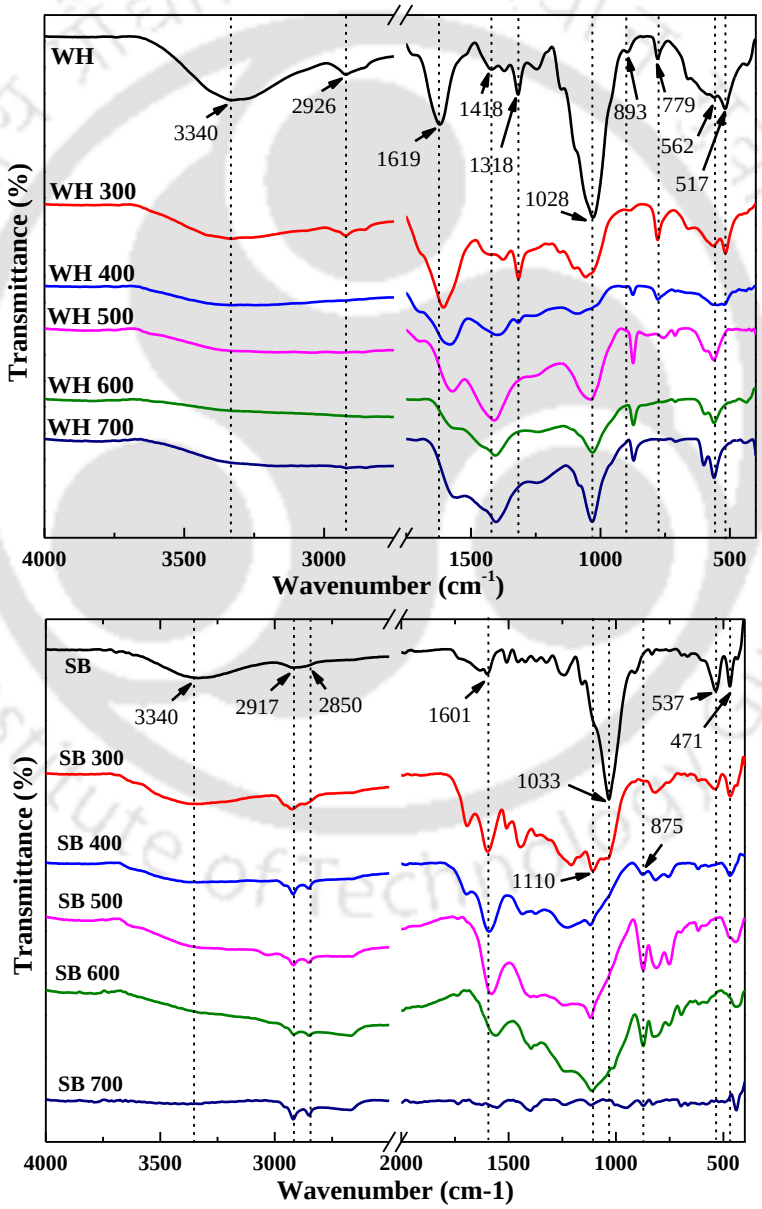

Figure 8.4 FTIR spectra of WH and SB biochar at different pyrolysis temperatures

Table 8.2 FTIR band assignment of biomass and biochar

	Peak position (cm^{-1})											
Assignment	WH	WH300	WH400	WH500	WH600	WH700	SB	SB300	SB400	SB500	SB600	SB700
−OH, Hydroxyl	3340	3340	----	----	----	----	3340	3340	----	----	----	----
−CH, Aliphatic	2926	2926	----	----	----	----	2917	----	----	----	----	----
−CH, Aliphatic	----	----	----	----	----	----	2850	----	----	----	----	----
C=O, C=C, Aromatic	1619	**1604**	**1579**	**1569**	**1567**	**1563**	1601	**1595**	**1590**	**1579**	**1157**	**1555**
C=C, Aliphatic	1418	----	**1408**	**1408**	**1408**	**1403**	----	----	----	----	----	----
−COOH Aromatic	1318	1318	1318	----	----	----	----	----	----	----	----	----
C-O-C stretching	1028	**1058**	**1078**	**1033**	1028	1028	----	1110	1115	1120	1119	1115
C-H, Aromatic	893	888	**873**	**873**	**873**	**873**	----	----	875	875	875	875
C-H, Aromatic	779	779	**778**	----	----	----	----	----	----	----	----	----
Si-O-Si stretching	562	562	----	562	562	562	537	537	----	----	----	----
Si-O-Si stretching	517	517	----	----	----	----	471	**470**	**469**	**442**	**439**	**438**

8.4.2.3 Surface morphology and BET analysis

The presence of cellulose, hemicellulose, and lignin in biochar is responsible for its honeycomb structure. During pyrolysis, cellulose and hemicellulose degrade first, followed by lignin. Thermal decomposition of biomass produced volatile materials in the form of CH_4, CO_2, CO, and H_2, creating pores on the facade. Further, volatile materials trapped inside biomass swelled the interior surface due to cellulose and hemicellulose expansion and heat breakdown, making the biochar porous (Muigai et al., 2021). The FESEM image of WH and SB at different pyrolysis temperatures, which gives a visualization of the surface morphology of biochar, is presented in Fig. 8.5. The pore structure of water hyacinth biochar appeared to show a well-arranged structure similar to a honeycomb, while some pores of sugarcane biochar were observed to close at 300 °C temperature. The honeycomb pores of biochar started to distort as the temperature climbed, pore size reduced, and the number of pores increased, which might be owed to the disruptions of internal pore structure or desiccation of cell structure at the higher temperature. The thermal conductivity of the porous material is influenced by its pore structure, such as the continuity and discontinuity of the pore network (Deng et al., 2017). The observation discussed above suggests that the WH biochar might have different thermal conductivity than SB biochar due to different pore structure networks.

The results of the BET analysis of biochar synthesized at various pyrolysis temperatures are shown in Table 8.3. The BET surface area, the number of pores, and the pore volume of biochar particles increased as the pyrolysis temperature was raised. This was ascribed to the release of volatile matter through dehydration, softening, melting, and carbonization resulting in high SSA and pore volume of biochar. The SSA increases marginally when the temperature rises from 300 to 500 °C. At 600 °C, however, the BET surface area of both biochars increases dramatically. This could be because partial carbonization of reactants occurs at lower temperatures, whereas total carbonization occurs at higher temperatures. Furthermore, a greater number of pores were detected at higher temperatures, owing to the degradation of lignin content.

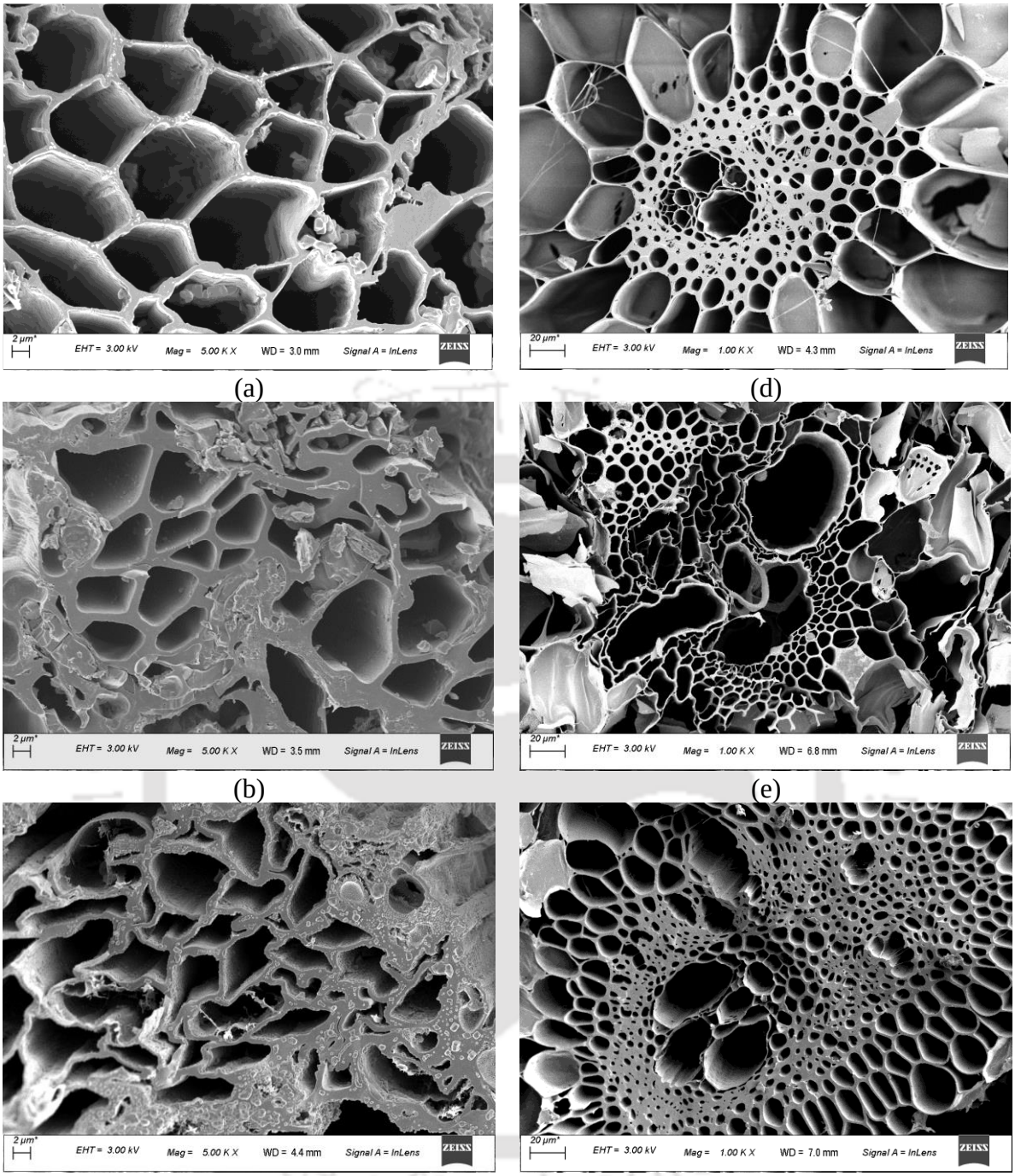

Figure 8.5 Surface morphology of WH and SB biochar (a)WH300 (b) WH500 (c) WH700 (d) SB300 (e) SB500 (f) SB700

Table 8.3 Physicochemical and surface characteristics of the produced biochar

Properties	WH300	WH400	WH500	WH600	WH700	SB300	SB400	SB500	SB600	SB700
Yield (%)	56.2±0.96	45.0±0.75	42.5±0.61	40.25±0.56	37.75±0.51	46.80±0.66	34.50±0.57	30.50±0.47	28.50±0.48	26.50±0.45
Proximate analysis (%)										
Moisture content	2.03±0.08	2.47±0.07	2.78±0.05	3.02±0.09	3.53±0.10	2.44±0.05	2.93±0.06	3.53±0.08	3.76±0.08	3.97±0.10
Volatile matter	40.80±0.37	30.34±0.32	19.77±0.18	17.78±0.24	16.15±0.17	43.87±0.51	27.89±0.37	19.45±0.27	16.87±0.21	14.30±0.24
Ash content	12.21±0.18	13.64±0.12	17.07±0.11	18.82±0.13	19.62±0.09	4.01±0.05	4.63±0.06	5.00±0.07	5.93±0.08	6.55±0.10
Fixed carbon[a]	44.96±0.24	53.54±0.32	60.38±0.37	60.37±0.48	60.70±0.62	49.67±0.42	64.56±0.34	72.02±0.58	73.44±0.28	75.18±0.17
Ultimate Analysis (%)										
Carbon (C)	44.75	47.36	50.66	51.64	52.97	62.38	73.83	81.48	84.54	84.23
Hydrogen (H)	3.42	2.48	1.40	1.21	1.01	4.51	3.28	2.22	1.57	0.87
Nitrogen (N)	2.23	1.71	1.37	1.51	1.22	0.51	0.34	1.51	1.03	1.29
Oxygen (O)	37.38	34.81	29.51	26.81	25.18	28.59	17.93	9.80	6.94	7.06
Atomic ratios										
H:C	0.92	0.63	0.33	0.28	0.23	0.87	0.53	0.33	0.22	0.12
O:C	0.63	0.55	0.44	0.39	0.36	0.34	0.18	0.09	0.06	0.06
C:N	23.37	32.24	43.14	39.85	50.62	143.84	252.58	63.16	96.13	76.12
(O+C):N	0.67	0.58	0.46	0.41	0.38	0.35	0.19	0.11	0.07	0.08
Specific gravity	1.416±0.07	1.461±0.05	1.501±0.06	1.531±0.04	1.626±0.03	0.759±0.06	1.103±0.07	1.165±0.05	1.217±0.06	1.270±0.04
pH	7.90±0.01	9.62±0.01	10.32±0.02	10.78±0.02	11.30±0.01	7.77±0.02	9.33±0.02	10.13±0.01	10.33±0.01	10.51±0.01
EC (mS cm^{-1})	18.41±0.14	19.80±0.26	20.80±0.10	21.60±0.20	23.10±0.20	0.54±0.01	0.84±0.01	1.27±0.01	1.63±0.02	1.91±0.02
Water holding capacity (%)	691±4.5	657.5±3.5	624±2.5	597±5.1	517±1.5	1101±7.5	1017±6.5	897±4.0	852±8.6	771±18.5
Specific surface area ($m^2 g^{-1}$)	4.791	5.835	8.960	98.581	146.887	5.713	7.874	10.094	18.355	19.418
Average pore diameter (nm)	17.410	13.105	12.146	3.250	2.943	13.163	12.979	10.778	6.894	6.313
Total pore volume ($cm^3 g^{-1}$)	0.0209	0.0191	0.0272	0.0802	0.1081	0.0188	0.0256	0.0272	0.0316	0.0307
Maximum pore diameter (nm)	108.3733	145.5568	148.5567	107.174	180.1281	226.3858	279.3338	223.433	545.8262	2158.5685

[a]By difference

8.4.2.4 Specific gravity and WHC of biochar

Table 8.3 presents the specific gravity and WHC of biochars synthesized at various pyrolysis temperatures. The typical specific gravity value of WH biochar was distributed over the range of 1.41 to 1.62, while for SB biochar, it was noted between 0.76 to 1.27. The specific gravity of biochar increased remarkably with the increase in temperature. This is primarily credited to transforming disordered carbon owing to low-density to turbostratic carbon owing to high-density with increased pyrolysis temperature (Kercher and Nagle, 2002). Furthermore, an increase in temperature separates or partially volatilizes an organic component of biomass and raises mineral content, potentially increasing specific gravity. With an increase in temperature, the WHC was shown to decrease considerably. This is due to the release of oxygen and hydroxyl (–OH) functional groups at higher temperatures, which aids in the polarization of water molecules. Thus, the biochar prepared at higher pyrolysis temperatures has less water-holding capacity. It is established from the previous results that the thermal characteristics of SBC are influenced by density (refer to section 4.5.3). Since biochar possesses a lower value of specific gravity than the soil, its amendment in soil results in an increase in the volume of composite and consequently decreases the density of composite.

8.4.2.5 pH and EC of biochar

The pH and EC of biochar were found to steadily increase as the pyrolysis temperature was raised. The pH of biochar increased dramatically as the pyrolysis temperature was increased to 400 °C, but the increase was only minimal as the pyrolysis temperature was increased further. The higher pH value at higher temperatures was mostly attributable to the biochar's increased ash concentration at those temperatures. Moreover, the increment in calcite and other alkali earth metals also contributed to the increment in pH value. These results are supported by the EDX analysis, which shows the higher amount of alkali metals in biochar with the increase in temperature. Additionally, FTIR results also confirm there is a drop-in concentration of the acidic functional group with the increase in temperature, which will increase the pH of biochar. The results also noted that the WH biochar has a high pH value compared to SB biochar. This is ascribed to the presence of higher ash content and alkali earth metal in WH biochar. The EC of biochar also depended on the biomass and was significantly correlated with biochar ash content. Higher ash content contributes to the higher ion content in the solution, which increases the EC. The WH biochar

had a high value of EC which is mainly because of the high value of ash content in WH biochar. Increasing temperature remarkably increased the EC of biochar which is primarily credited to the increase in ash content.

8.4.3 Thermal characteristics of biochar and SBC

Fig. 8.6 shows the thermal characteristics properties of WH and SB biochar prepared at various pyrolysis temperatures. The values of thermal conductivity (*K*) were found to be distributed over the range of 0.123 to 0.132 $Wm^{-1}K^{-1}$ and 0.102 to 0.117 $Wm^{-1}K^{-1}$ for WH and SB biochar, respectively. Further, the volumetric heat capacity (*C*) was noted in the range between 0.539-0.689 $MJm^{-3}K^{-1}$ and 0.483-0.592 $MJm^{-3}K^{-1}$ for WH and SB biochar, respectively.

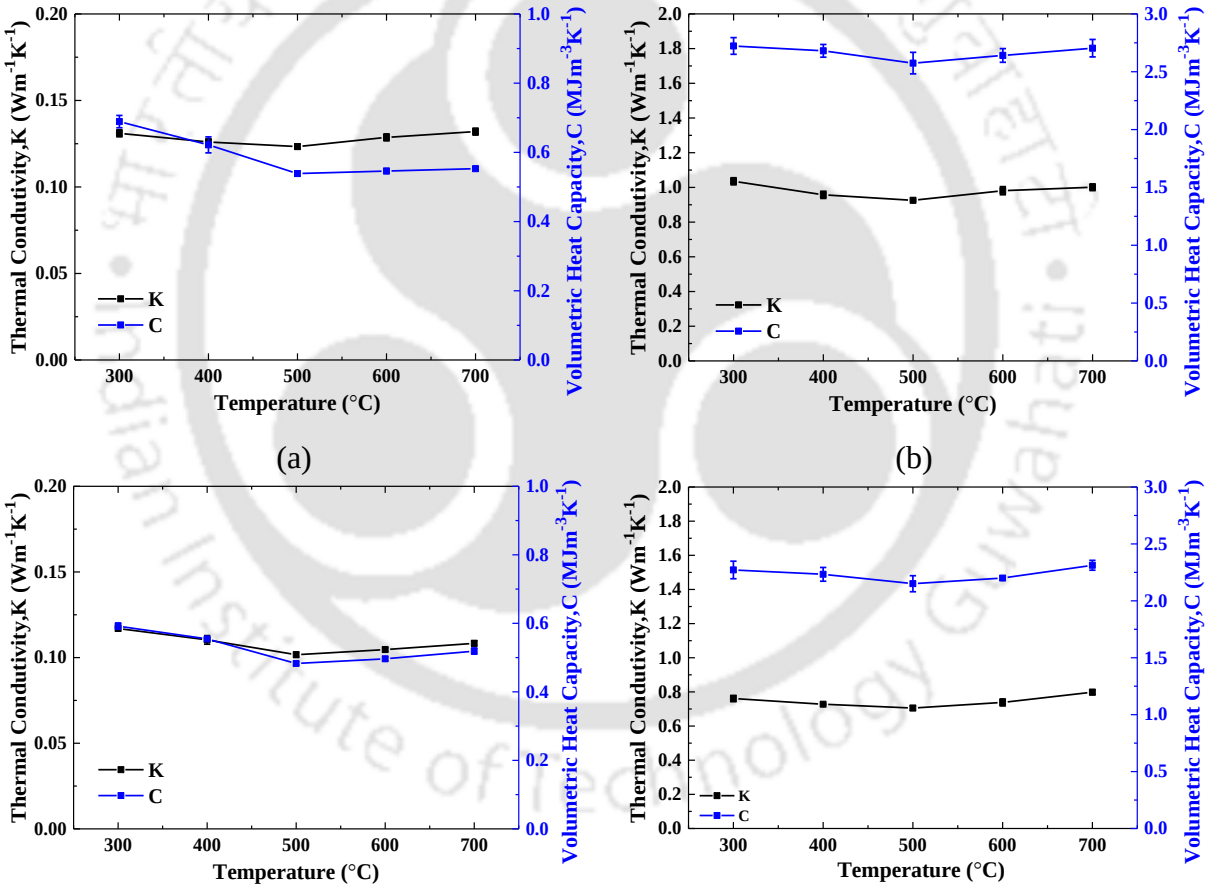

Figure 8.6 Variation in thermal characteristics properties at various pyrolysis temperatures for (a) WH biochar, (b) WH SBC, (c) SB biochar, and (d) SB SBC.

It was noted from Fig. 8.6(a) that the thermal characteristics of WH biochar first decreased till 500 °C and followed the uptrend on further increase in pyrolysis temperature. These results were also supported by XRD results, as illustrated in Fig. 8.3(a). At 400 °C, the peak of sylvite (2θ = 15.1° and 24.5°) in the XRD pattern disappeared, which was

observed for WH300, which might have decreased *K* and *C* values. Further, at 500 °C, a slight decrease in peak intensity of sylvite (2θ =28.55°) was observed. Therefore, the thermal properties values were noted to be lower at 500°C temperature. Again, at 600 °C pyrolysis temperature, there was a slight increase in peak intensity of sylvite (2θ =28.55°), which might have increased the *K* and *C* values. Extra calcite ($CaCO_3$) peak was detected at the 700 °C pyrolytic temperature, which might increase the *K* and *C* values. In conclusion, negligible variation in *K* and *C* values of WH biochars prepared at various temperatures were observed. The trends were found to be in the same line for SB biochars pyrolyzed at various temperatures. Moreover, the WH biochar has a higher thermal conductivity value as compared to SB biochar which might be due to the more chemical functional group in WH biochar (Table 8.2).

Fig. 8.6 shows the variation in thermal characteristics of bare soil treated with biochar generated at various pyrolysis temperatures (b and d). The typical *K* and *C* values for control soil were 1.271 $Wm^{-1}K^{-1}$ and 2.824 $MJm^{-3}K^{-1}$, respectively. The reason for the reduction in thermal characteristics is due to low thermal characteristics of biochar itself. The typical *K* existed between 0.925 to 1.035 $Wm^{-1}K^{-1}$ and 0.705 to 0.798 $Wm^{-1}K^{-1}$ for soil amended with WH and SB biochar, respectively. Comparatively, the *C* values were noted to exist in the range of 2.574 to 2.723 $MJm^{-3}K^{-1}$ and 2.151 to 2.312 $MJm^{-3}K^{-1}$ for soil amended with WH and SB biochar, respectively. The amendment with WH biochar resulted in a 19% to 28% reduction of the thermal conductivity of the soil, whereas a 37% to 44% reduction of thermal conductivity was observed in SB-amended soil. However, the above test results clearly indicate that no significant difference in *K* and *C* at different temperatures was observed. Therefore, the biochar prepared at lower pyrolysis temperature may be suitable for thermal backfill application as it can save energy in the process of biochar production, as shown in Fig. 8.2.

The *K* and *C* values of conventional thermal insulator materials such as aerogel, polyurethane, cork, cellulose, rice husk, flax, hemp, and natural fibers (bamboo, coir, wood) are found over the range of 0.025-0.123 $Wm^{-1}K^{-1}$ and 0.008-1.054 $MJm^{-3}K^{-1}$ (Kumar et al., 2020). Comparatively, the *K* and *C* values of biochar were also observed in the competitive range 0.123 to 0.132 $Wm^{-1}K^{-1}$ and 0.483 to 0.689 $MJm^{-3}K^{-1}$. The findings from the current study indicate that the produced biochars can be used as insulator material for amending the locally available soil around the underground crude oil backfill material. It should be noted that although the above-mentioned materials, including rice husk and natural fibers, have

been tested for their thermal conductivity, however, their application in soil has been largely unaddressed. Comparative investigations on their performances in soil with the biochar amended soil are recommended for future studies for determining the nature-inspired thermal backfill material.

This study attempted to investigate the influence of different pyrolysis temperatures on the thermal characteristics of the biochars, which are chiefly controlled by their mineralogy, microstructural and thermal properties. A marginal change in mineralogy, functional group, and pore structure of biochar is observed at different pyrolysis temperatures (refer to sections 8.2.21, 8.2.2.2, 8.2.2.3, and 8.2.2.4). The observed changes in the physicochemical properties and microstructure were not enough to practically change the thermal properties of biochar. This is a critical finding as the biochars can be produced at the lowest pyrolysis temperature (300 °C) does not only provide maximum yield but also consumes the minimum energy (refer to section 8.2.1). Moreover, SB biochar is a lighter material than WH biochar due to its lower specific gravity (refer to section 8.2.2.4). Thus, the amendment of SB biochar reduces the thermal characteristics of soil higher as compared to WH biochar-amended soil.

8.4.4 Proximate and ultimate analysis

The findings of the proximate and final analyses of biochar at various pyrolysis temperatures are presented in Table 8.3. The moisture content, ash content, and fixed carbon content of the biochar increased as the temperature climbed, whereas the volatile matter content declined. The degradation of mineral materials, which were turned into ash during carbonization, was blamed for the rise in ash concentration (Muigai et al., 2021). Because of the high mineral concentration, the WH biochar has a high ash content, which was confirmed by EDX and XRD data (see Table 8.1 and Fig. 8.3). The high amount of volatile matter in biochar presented at low pyrolysis temperature was ascribed to the incomplete carbonization that is verified by the presence of high-intensity peak of C-H and C=O functional group in biochar identified by FTIR results (refer Fig. 8.4). The decrease in volatile matter content with increased temperature might be due to breakdown into the liquids and gases of low molecular weight instead of biochar.

The carbon (C) content of WH biochar increased till 500 °C, then fell somewhat at 600 °C and 700 °C. SB biochar also showed an increase in C content until 600 °C, then a minor drop at 700 °C. The rise in C content was mainly due to thermal decomposition,

dehydration, decarboxylation, and aromatization at higher pyrolysis temperatures (Muigai et al., 2021). The obtained results were further supported by the remarkable reduction of volatile matter in biochar as pyrolysis temperature rose. The slight decrease in C content at higher pyrolysis temperatures might be because of the conversion of carbon into ash content. The hydrogen (H) and oxygen (O) contents were noted to reduce consistently with increased temperature. This was attributed to the breakage of oxygenated bonds and the generation of lower molecular weight bi-products containing H and O (syngas and bio-oil). However, no consistent change in nitrogen (N) content was noted with an increase in pyrolysis temperature.

8.4.4.1 Van-Krevelen analysis

For greater carbon stability in soil, the minimum H/C ratio of biochar should not be more than 0.7, according to IBI standards from 2015 (IBI Standard 2.1, 2015). The O/C ratio was also utilized to demonstrate biochar's stability in soil (Elmquist et al., 2006; Spokas, 2010; Aller, 2016; Pariyar et al., 2020). The H/C ratio shows aromaticity, but the O/C and (O+N)/C ratios indicate biochar polarity, which was seen to decrease as temperature increased. The dehydration and decarboxylation reactions, which could be well delineated by the Van-Krevelen plot shown in Fig. 8.7, were primarily responsible for the consistent decline in H/C and O/C atomic ratio with rising pyrolysis temperature. A lower H/C ratio reveals the highly aromatic structure does more stability in soil. Further, the biochar with a lower O/C ratio also indicates a highly aromatic structure which confirms the presence of stable crystal (graphite), which is presented in Fig. 8.8. As the temperature increased, removal of oxygen and O-H functional groups occurred, as confirmed by EDX and FTIR analysis, which led the biochar to become more hydrophobic. Therefore, the biochar produced at higher pyrolysis temperatures is stable to a greater extent and less hydrophobic. The O/C atomic ratio of stable biochar should be lower. The half-life is expected to be less than 100 years if the O/C atomic ratio is more than 0.6. Furthermore, the O/C ratio of 0.2 to 0.6 has a half-life of 100-1000 years, while a ratio of less than 0.2 has a half-life of more than 1000 years (Elmquist et al., 2006; Spokas, 2010; Pariyar et al., 2020). Therefore, 400 °C can be recommended as a suitable pyrolysis temperature. However, it must be noted that just one type of soil was used in this study, and the impact of clay mineralogy on biochar carbon stability has not been investigated. Jing et al. (2022) have reported that kaolinite and montmorillonite influence the carbon stability of biochar in a different manners.

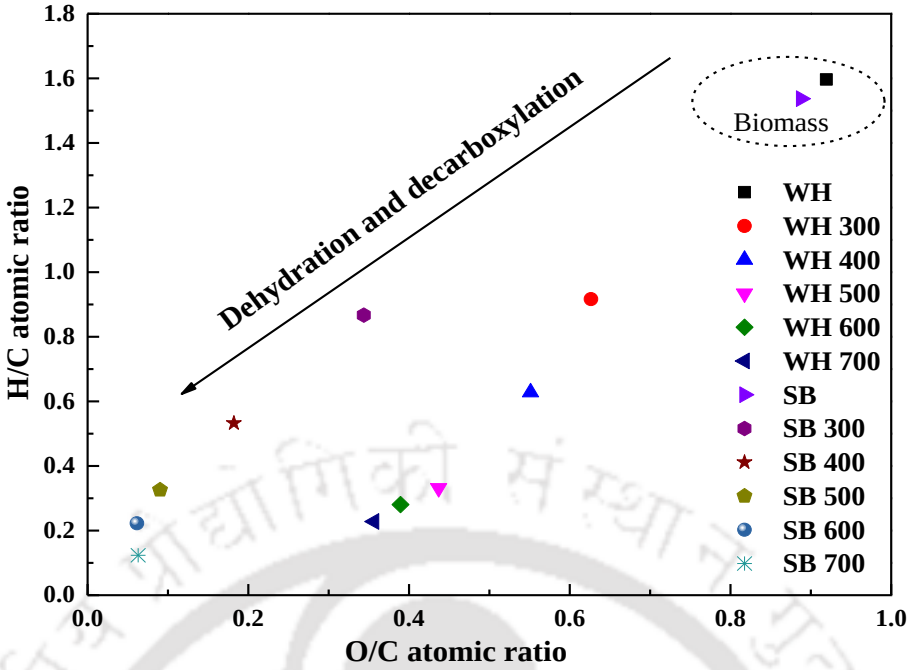

Figure 8.7 Van-Krevelen plot of biomass and biochar

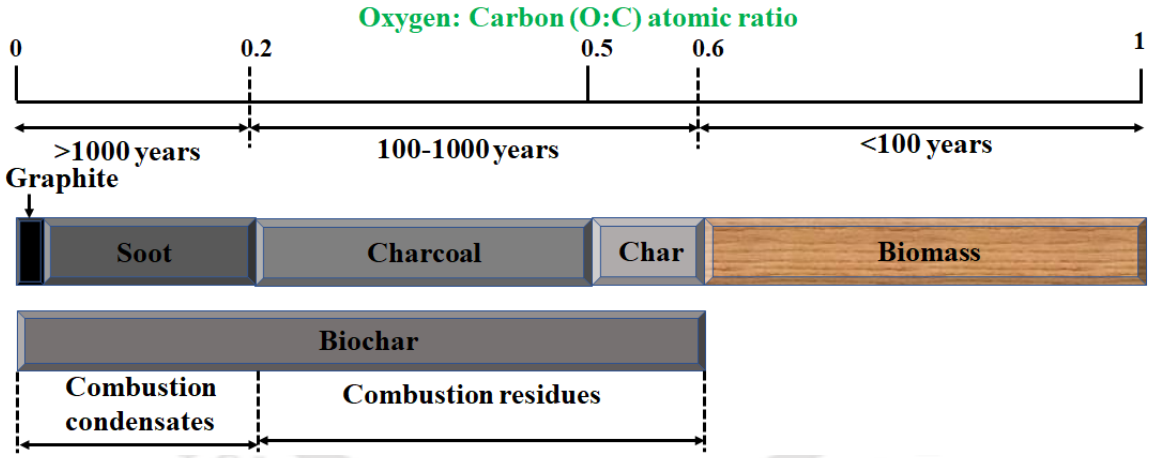

Figure 8.8 The half-life period of combustion product continuum spectrum of biomass.

8.4.5 Comparison of the different feedstocks for thermal backfills

It is to be recalled that the H/C ratio of the WH and SB biochar at 300 °C is higher than 0.7, making it unsuitable for long-term soil application as per the guidelines of IBI, 2015. It was observed that the energy expenditure increases consistently with an increase in the pyrolysis temperature for both feedstocks. WH biochar produced at 400 °C expends 63.5% lower energy when compared to the energy required for the production of an equivalent quantity of biochar at 700 °C. Similarly, SB biochar produced at 400 °C utilizes 75.8% lesser energy when compared to the energy required for producing an equivalent quantity of biochar at 700 °C. This finding broadly implies that pyrolysis at the

recommended temperature of 400 °C results in biochar that fulfills the desired properties required for a thermal backfill, saving at least 60% of energy irrespective of the feedstock type. Moreover, WH and SB biochar yields are significantly higher at the recommended pyrolysis temperature (400 °C) than the yield at maximum pyrolysis temperature (700 °C), as illustrated in Fig. 8.2.

In Fig. 8.9, a comparison between the energy consumption, yield, and thermal conductivity of the amended soil for both the biochar at various temperatures is presented, highlighting the biochar type's importance. WH outperforms SB in terms of energy-saving and yields superiority at all pyrolysis temperatures. It can be inferred from Fig. 8.9 that for making an equivalent quantity of biochar, WH feedstock will result in energy savings varying from 18% to 30% in comparison to SB feedstock at different pyrolysis temperatures. The corresponding yield of WH feedstock is superior to SB feedstock in a range of 20% to 42% at different pyrolysis temperatures. However, it must also be noted that the thermal conductivity (*K*) of SB biochar was around 20% lower than WH biochar at all the pyrolysis temperatures, making it a competitive candidate for thermal backfills despite being considerably energy-intensive and low-yielding.

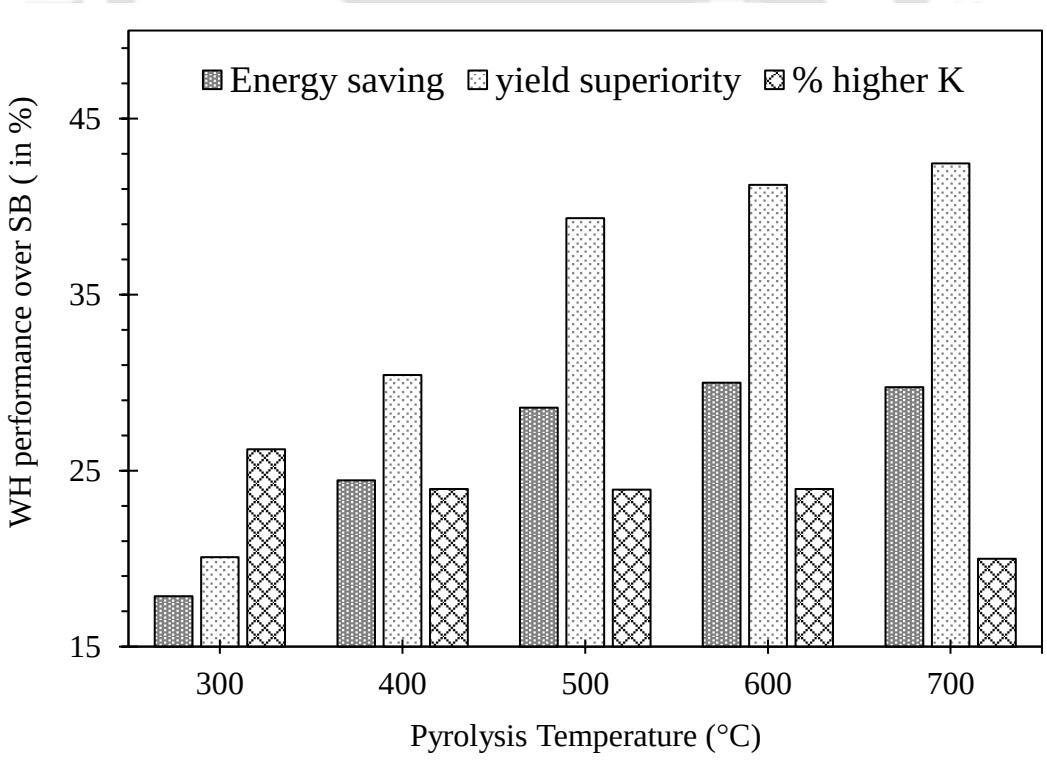

Figure 8.9 Performance of WH biochar in comparison to SB biochar in terms of energy, yield, and thermal conductivity (in %)

8.5 Summary

The present investigation is conducted with the aim of tailoring the pyrolysis process to produce biochar that can satisfy the requirement of thermal backfill materials. The optimum pyrolysis temperature is crucial for making the pyrolysis process energy-efficient and cost-effective. Within this context, the current chapter investigates the impact of different pyrolysis temperatures on the biochar characteristics produced from two different waste biomass, i.e., WH and SB. Their yield, physicochemical, microstructural, mineralogical, organic, and thermal characteristics were investigated. The major findings of the current chapter can be encapsulated as follow-

- The energy efficiency and yield were found to be inversely related to the pyrolysis temperature. For producing an equivalent amount of biochar from both the feedstocks, pyrolysis at 300 °C expends at least 130% lesser energy and yields 49% higher when compared to the maximum temperature of 700 °C.
- Biochar produced from both the feedstocks led to stable biochar (H/C< 0.7 and O/C < 0.6) when pyrolysis temperature was set on or above 400 ºC. In summary, it was observed that eight out of the ten biochar fulfill the required stability criteria for a design period of 25 to 50 years.
- The thermal conductivity of produced biochars was found to be in a narrow range of 0.102 to 0.132 $Wm^{-1}K^{-1}$ for all the produced biochars, which is linked with the marginal variations in the microstructural, mineralogical, and physicochemical characteristics with the different pyrolysis temperatures.
- Around 25% and 43% reduction in the soil thermal conductivity was recorded when the soil was mixed with WH and SB biochar, respectively.
- A pyrolysis temperature of 400 ºC is determined to be the most suitable temperature regardless of the feedstock type because of the least energy consumption, considerable yield, required thermal properties, and carbon stability for the design period. At the recommended pyrolysis temperature, the WH feedstock required 64.4 kWh of electrical energy to produce one kg of biochar at 400 ºC, which is 63% more energy-efficient than 700 ºC pyrolysis. Similar trends were recorded for SB biochar too.
- SB biochar amended soil was observed to be possessing 20% to 25% lower thermal conductivity than the WH biochar at all the pyrolysis temperatures, raising its potential applicability as per site requirement despite being energy-intensive.

Biochar is an advantageous material for thermal backfill applications because it contributes to sustainable development by means of waste biomass valorization. The current chapter also provided evidence that biochar production at 400 °C is the most economical in terms of energy consumption and yield, along with the desired thermal properties. Further investigations are necessary to confirm if the biochar produced from other feedstocks also possesses similar characteristics. Moreover, the current chapter does not compare biochar with conventional material on economic aspects, which must be considered for future studies for field-scale application. Another restriction of the current chapter is the unavailability of a threshold of thermal conductivity and geotechnical properties for such novel applications of biochar. This chapter encourages the crude-oil industries and future researchers to participate in the real-field application of biochar as thermal backfills that can be extended to formulate standard design criteria.

CHAPTER 9

CONCLUSIONS AND FUTURE SCOPE

9.1 Overall technology roadmap for research

The overall technology roadmap for research is presented in Fig. 9.1, which represents that the biochar-based thermal backfill material has potential to mitigate the heat transfter from thermal energy storage system.

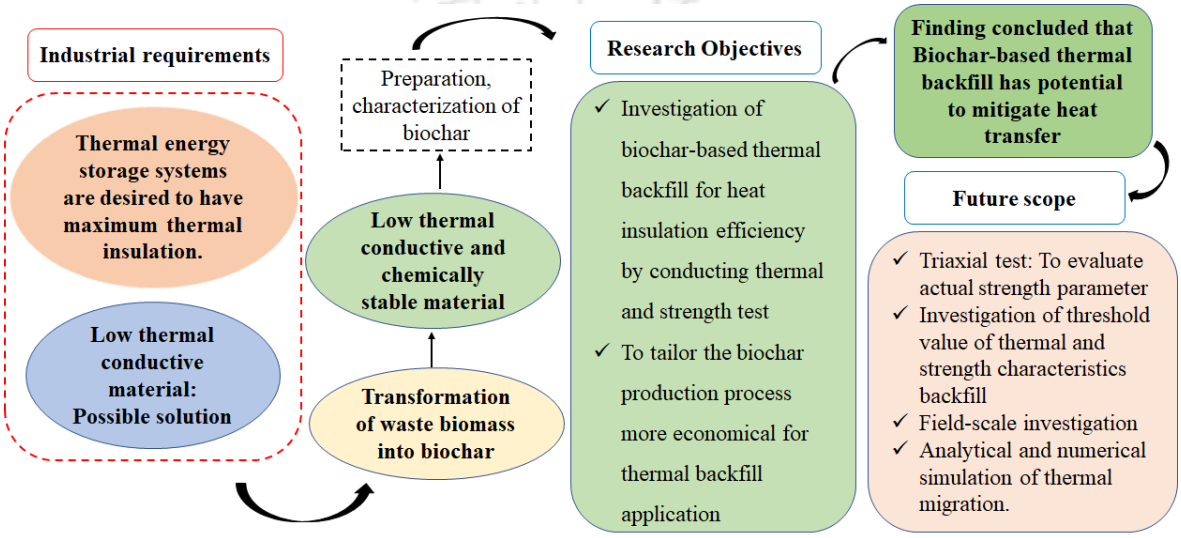

Figure 9.1 Technology roadmap for biochar-based thermal backfill material

9.2 Conclusions

Biochar is a highly porous, highly chemically stable, and eco-friendly material that has low thermal characteristics. In the current study, the ability of soil-biochar-composites (SBC) and soil-biochar-biopolymer composites (SBPC) were explored as thermal backfill for underground crude oil pipelines and crude oil storage tanks. The major findings from the current study can be encapsulated as follows-

- The thermal conductivity (K) and volumetric heat capacity (C) of the SBC are found to be consistently decreasing with incremental biochar amendment, which is greatly influenced by the molding water content and dry density (ρ_d). This is due to the entrapped biochar particles between the soil particles that have an intra-porous structure. Upon moisture migration, the thermal characteristics of the SBC improved significantly. The sensitivity index results indicate that the ρ_d significantly influences K and C values, followed by water content (w) and biochar content (BC) for all SBC.

- Thermal characteristics of both the soils and SBC are affected by the compaction parameters (OMC and MDD). The reduction in *K* and *C* values of soils depends upon the soil type, biochar types, biochar particle size fraction, and amendment rate. For a 7.5% amendment rate, the reduction in *K* is 34, 29, and 22% (for MH soil) and 37, 34, and 23% (for SC soil) for sugarcane bagasse biochar (SBBC), water hyacinth biochar (WHBC), and hardwood biochar (HWBC). Similarly, the reduction in *C* is 27, 24, and 17% (for MH soil) and 21, 18, and 13% (for SC soil) for SBBC, WHBC, and HWBC.
- The reduction in *K* and *C* values is higher for coarser biochar fractions, followed by medium and least noted for finer fractions. For the 15% amendment rate, the reduction in *K* is 31, 29, and 26% (for MH soil) and 36, 34, and 32% (for SC soil) for coarser, medium, and finer fraction biochar. Similarly, the reduction in *C* is 23, 20, and 17% (for MH soil) and 24, 22, and 19% (for SC soil) for coarser, medium, and finer fraction biochar.
- The unconfined compressive strength (UCS) of soil reduces with biochar amendment, which depends upon soil type and biochar particle size fractions. For the 15% amendment rate, the reduction in UCS value is 48, 55, and 62% for the medium, coarser, and finer fraction biochar for MH soil. Similarly, the UCS value is reduced by 3, 7, and 38% for the medium, coarser, and finer fraction biochar for SC soil. Therefore, medium fractions of biochar are more suitable as thermal backfill for underground crude oil pipelines with respect to thermal and strength aspects.
- The addition of Xanthan Gum (XG) biopolymer to SBC increases its UCS value by at least two times without compromising the thermal characteristics after drying. Out of nine SBPC devised in the current study, five composites exhibited superior strength and lowered thermal conductivity than the bare soil in both conditions, i.e., optimum moisture state and upon drying.
- The SBC and SBPC exhibit lower temperatures at all radial distances and times for both the heating and cooling cycle. At the elapsed time of 200 hours (i.e., nearly dry condition), the temperature difference between bare soil and SBC varies from 4 to 20 °C depending upon the distance from the heater rod. This is mainly ascribed to the lower thermal conductivity and thermal diffusivity of SBC and SBPC as compared to bare soil. The SBC mixed with 0.5% XG displays a lower temperature in the wet state and a slightly higher temperature in the dry state than SBC.

- Biochar produced at 400 °C is economical in terms of energy consumption and yield, along with the desired thermal characteristics for thermal backfill applications. The recommended pyrolysis temperature was found to be at least 60% energy efficient in comparison to pyrolysis at 700 °C for both the SBBC and WHBC.

9.3 Major contributions from the study

- ❖ Developed a new SBPC as thermal backfill material by utilizing the biochar produced from waste biomass.
- ❖ Explored the thermal and strength characteristics of SBC considering two different soil types and three biochar types.
- ❖ Evaluated the thermal and strength characteristics of SBPC under wet and dry conditions to consider field conditions.
- ❖ Established that the SBC and SBPC have higher thermal insulation efficiency compared to bare soil through a bench-scale study.
- ❖ Developed energy-efficient biochar for thermal backfill applications.

9.4 Limitations and future scope

While the present study has several valuable conclusions, future research is necessary for several areas. The major areas which are recommended for future studies are as follows-

- ❖ The current study recommends a pyrolysis temperature of 400 °C for thermal backfill applications based on only two types of feedstock. Further investigations are necessary to confirm if the biochar produced from other feedstocks also possesses similar characteristics.
- ❖ The current study performed only UCS test to assess the strength of SBC and SBPC. However, a triaxial test should be performed to evaluate actual strength parameters for design purposes for field application.
- ❖ This study mainly focuses on the mechanism and development of SBC and SBPC for thermal backfill. However, a study on the threshold value of thermal and strength characteristics of biochar-based thermal backfill material should formulate for standard design criteria.
- ❖ A field-scale investigation of the proposed SBC and SBPC needs to be performed to assess the long-term performance, durability, and cost viability of the proposed composite.

- Analytical and numerical simulation of thermal migration in SBC and SBPC needs to be investigated before field application.
- Durability of SBC and SBPC thermal backfill needs to be examined during wetting-drying cycle.
- Effect of initial temperature on thermal and strength characteristics of SBC and SBPC needs to be investigated by varying temperatures from freezing conditions (-10 °C) to high-temperature conditions (up to 70 °C).
- Effect of cyclic temperature variation on the thermal and strength characteristics of SBC and SBPC needs to be explored considering long-term field application.
- Evaluation of the techno-economic analysis of the biochar prepared at different pyrolysis temperatures.

References

Abed, W.M., 2021. Experimental Measurements of Thermal Conductivity for Non-Newtonian Polymeric Fluids Using a Concentric Cylindrical Cell Under Static Conditions. *Int. J. Thermophys. 42*, 1–17. https://doi.org/10.1007/s10765-021-02834-9

Abu-Hamdeh, N.H., 2003. Thermal properties of soils as affected by density and water content. *Biosyst. Eng. 86*, 97–102. https://doi.org/10.1016/S1537-5110(03)00112-0

Abu-Hamdeh, N.H., Reeder, R.C., 2000. Soil Thermal Conductivity Effects of Density, Moisture, Salt Concentration, and Organic Matter. *Soil Sci. Soc. Am. J. 64*, 1285–1290. https://doi.org/10.2136/sssaj2000.6441285x

Ahmed, A., Gariepy, Y., Raghavan, V., 2017. Influence of wood-derived biochar on the compactibility and strength of silt loam soil. *Int. Agrophysics 31*, 149–155. https://doi.org/10.1515/intag-2016-0044

Ahmed, K., Hasan, M., Haider, J., 2021. Electrical and mechanical properties of sugarcane bagasse pyrolyzed biochar reinforced polyvinyl alcohol biocomposite films. *J. Compos. Sci. 5*, 1–14. https://doi.org/10.3390/jcs5090249

Ajayi, A.E., Horn, R., 2017. Biochar-Induced Changes in Soil Resilience: Effects of Soil Texture and Biochar Dosage. *Pedosphere 27*, 236–247. https://doi.org/10.1016/S1002-0160(17)60313-8

Aller, M.F., 2016. Biochar properties: Transport, fate, and impact. *Crit. Rev. Environ. Sci. Technol. 46*, 1183–1296. https://doi.org/10.1080/10643389.2016.1212368

ASTM D2166-16 (2016). Standard Test Method for Unconfined Compressive Strength of Cohesive Soil 1. ASTM Int. 1–7. https://doi.org/10.1520/D2166

ASTM D422-63 (2007) Standard Test Method for Particle-Size Analysis of Soils. ASTM Int. West Conshohocken, PA United States D422-63, 1–8. https://doi.org/10.1520/D0422-63R07E02.2

ASTM D4318-10 (2010). Standard Test Methods for Liquid Limit, Plastic Limit, and Plasticity Index of Soils. ASTM Int. West Conshohocken, PA United States 04, 1–14. https://doi.org/10.1520/D4318-17E01.

ASTM D698-12 (2012). Standard Test Methods for Laboratory Compaction Characteristics of Soil Using Standard Effort (12 , 400 ft-lbf / ft 3 (600 kN-m / m 3)) 1. ASTM Int. West Conshohocken, PA United States 3, 1–11. https://doi.org/10.1520/D0698-12E01.1

ASTM D854-14 (2014). Standard Test Methods for Specific Gravity of Soil Solids by Water Pycnometer 2458000, 1–7. https://doi.org/10.1520/D0854-14.

ASTM D3173/D3173M-17a, 2017. Standard Test Method for Moisture in the Analysis Sample of Coal and Coke. ASTM International, West Conshohocken, PA https://doi.org/10.1520/D3173_D3173M-17A.

ASTM D3174-12(2018)e1, 2018. Standard Test Method for Ash in the Analysis Sample of Coal and Coke from Coal. ASTM International, West Conshohocken, PA https://doi.org/10.1520/D3174-12R18E01

ASTM D3175-20, 2020. Standard Test Method for Volatile Matter in the Analysis Sample of Coal and Coke. ASTM International, West Conshohocken, PA https://doi.org/10.1520/D3175-20.

ASTM D3174-12(2018)e1, 2018. Standard Test Method for Ash in the Analysis Sample of Coal and Coke from Coal. ASTM International, West Conshohocken, PA https://doi.org/10.1520/D3174-12R18E01.

ASTM E870-82(2019), 2019. Standard Test Methods for Analysis of Wood Fuels. ASTM International, West Conshohocken, PA https://doi.org/10.1520/E0870-82R19

Ayeldeen, M., Negm, A., El-Sawwaf, M., Kitazume, M., 2017. Enhancing mechanical behaviors of collapsible soil using two biopolymers. *J. Rock Mech. Geotech. Eng. 9*, 329–339. https://doi.org/10.1016/j.jrmge.2016.11.007

Azargohar, R., Nanda, S., Kozinski, J.A., Dalai, A.K., Sutarto, R., 2014. Effects of temperature on the physicochemical characteristics of fast pyrolysis bio-chars derived from Canadian waste biomass. *Fuel 125*, 90–100. https://doi.org/10.1016/j.fuel.2014.01.083

Balaji, N.C., Mani, M., Venkatarama Reddy, B.V., 2017. Thermal conductivity studies on cement-stabilised soil blocks. *Proc. Inst. Civ. Eng. - Constr. Mater. 170*, 40–54. https://doi.org/10.1680/jcoma.15.00032

Barry-Macaulay, D., Bouazza, A., Singh, R.M., Wang, B., Ranjith, P.G., 2013. Thermal conductivity of soils and rocks from the Melbourne (Australia) region. *Eng. Geol. 164*, 131–138. https://doi.org/10.1016/j.enggeo.2013.06.014

Başer, T., Dong, Y., Moradi, A.M., Lu, N., Smits, K., Ge, S., Tartakovsky, D., McCartney, J.S., 2018. Role of Nonequilibrium Water Vapor Diffusion in Thermal Energy Storage Systems in the Vadose Zone. *J. Geotech. Geoenvironmental Eng. 144*, 1–13. https://doi.org/10.1061/(asce)gt.1943-5606.0001910

Bejan, A., Kraus, A.D., 2003. Heat Transfer Handbook, Volume 1.

Blanco-Canqui, H., 2017. Biochar and Soil Physical Properties. *Soil Sci. Soc. Am. J. 81*, 687–711. https://doi.org/10.2136/sssaj2017.01.0017

Brandon, T.L., Mitchell, J.K., 1989. Factors Influencing Thermal Resistivity of Sands. *J. Geotech. Eng. 115*, 1683–1698. https://doi.org/10.1061/(ASCE)0733-9410(1989)115:12(1683)

Broniarz-Press, L., Pralat, K., 2009. Thermal conductivity of Newtonian and non-Newtonian liquids. *Int. J. Heat Mass Transf. 52*, 4701–4710. https://doi.org/10.1016/j.ijheatmasstransfer.2009.06.019

Burrell, L.D., Zehetner, F., Rampazzo, N., Wimmer, B., Soja, G., 2016. Long-term effects of biochar on soil physical properties. *Geoderma 282*, 96–102. https://doi.org/10.1016/j.geoderma.2016.07.019

Busscher, W.J., Novak, J.M., Evans, D.E., Watts, D.W., Niandou, M.A.S., Ahmedna, M., 2010. Influence of Pecan Biochar on Physical Properties of a Norfolk Loamy Sand. *Soil Sci. 175*, 10–14. https://doi.org/10.1097/SS.0b013e3181cb7f46

Cabalar, A.F., Canakci, H., 2011. Direct shear tests on sand treated with xanthan gum. *Proc. Inst. Civ. Eng. Gr. Improv. 164*, 57–64. https://doi.org/10.1680/grim.800041

Cai, G., Zhang, T., Puppala, A.J., Liu, S., 2015. Thermal characterization and prediction model of typical soils in Nanjing area of China. *Eng. Geol. 191*, 23–30. https://doi.org/10.1016/j.enggeo.2015.03.005

Campbell, G.S., Calissendorff, C., Williams, J.H., 1991. Probe for Measuring Soil Specific Heat Using A Heat-Pulse Method. *Soil Sci. Soc. Am. J. 55*, 291–293. https://doi.org/10.2136/sssaj1991.03615995005500010052x

Chang, I., Im, J., Cho, G.C., 2016. Geotechnical engineering behaviors of gellan gum biopolymer treated sand. *Can. Geotech. J. 53*, 1658–1670. https://doi.org/10.1139/cgj-2015-0475

Chang, I., Im, J., Prasidhi, A.K., Cho, G.C., 2015. Effects of Xanthan gum biopolymer on soil strengthening. *Constr. Build. Mater. 74*, 65–72. https://doi.org/10.1016/j.conbuildmat.2014.10.026

Chang, I., Lee, M., Tran, A.T.P., Lee, S., Kwon, Y.M., Im, J., Cho, G.C., 2020. Review on biopolymer-based soil treatment (BPST) technology in geotechnical engineering practices. *Transp. Geotech. 24*, 100385. https://doi.org/10.1016/j.trgeo.2020.100385

Chatterjee, R., Sajjadi, B., Chen, W.Y., Mattern, D.L., Hammer, N., Raman, V., Dorris, A., 2020. Effect of Pyrolysis Temperature on PhysicoChemical Properties and Acoustic-Based Amination of Biochar for Efficient CO2 Adsorption. Front. *Energy Res. 8*, 1–18. https://doi.org/10.3389/fenrg.2020.00085

Chen, R., Zhang, L., Budhu, M., 2013. Biopolymer Stabilization of Mine Tailings. *J. Geotech. Geoenvironmental Eng. 139*, 1802–1807. https://doi.org/10.1061/(asce)gt.1943-5606.0000902

Chen, W.H., Wang, C.W., Ong, H.C., Show, P.L., Hsieh, T.H., 2019. Torrefaction, pyrolysis and two-stage thermodegradation of hemicellulose, cellulose and lignin. *Fuel 258*, 116168. https://doi.org/10.1016/j.fuel.2019.116168

Cheng, L., Afur, N., Shahin, M.A., 2021. Bio-cementation for improving soil thermal conductivity. *Sustain. 13*. https://doi.org/10.3390/su131810238

Chintala, R., Mollinedo, J., Schumacher, T.E., Malo, D.D., Julson, J.L., 2014. Effect of biochar on chemical properties of acidic soil. *Arch. Agron. Soil Sci. 60*, 393–404. https://doi.org/10.1080/03650340.2013.789870

Côté, J., Konrad, J.M., 2005a. A generalized thermal conductivity model for soils and construction materials. *Can. Geotech. J. 42*, 443–458. https://doi.org/10.1139/t04-106

Côté, J., Konrad, J.M., 2005b. Thermal conductivity of base-course materials. *Can. Geotech. J. 42*, 61–78. https://doi.org/10.1139/t04-081

Danielewicz, J., Śniechowska, B., Sayegh, M.A., Fidorów, N., Jouhara, H., 2016. Three-dimensional numerical model of heat losses from district heating network pre-insulated

pipes buried in the ground. *Energy 108*, 172–184. https://doi.org/10.1016/j.energy.2015.07.012

De Vries, D., 1963. Thermal properties of soils. In Physics of Plant Environment. North-holl. Publ. Co., Amsterdam, Netherlands. 1963.

Dec, D., Dörner, J., Horn, R., 2009. Effect of soil management on their thermal properties. *J. Soil Sci. Plant Nutr. 9*, 26–39. https://doi.org/10.4067/S0718-27912009000100003

Deng, Z., Liu, X., Huang, Y., Zhang, C., Chen, Y., 2017. Heat conduction in porous media characterized by fractal geometry. *Energies 10*. https://doi.org/10.3390/en10081230

Devrani, R., Dubey, A.A., Ravi, K., Sahoo, L., 2021. Applications of bio-cementation and bio-polymerization for aeolian erosion control. *J. Arid Environ. 187*, 104433. https://doi.org/10.1016/j.jaridenv.2020.104433

Domingues, R.R., Trugilho, P.F., Silva, C.A., De Melo, I.C.N.A., Melo, L.C.A., Magriotis, Z.M., Sánchez-Monedero, M.A., 2017. Properties of biochar derived from wood and high-nutrient biomasses with the aim of agronomic and environmental benefits. *PLoS One 12*, 1–19. https://doi.org/10.1371/journal.pone.0176884

Dubey, A.A., Hooper-Lewis, J., Ravi, K., Dhami, N.K., Mukherjee, A., 2022. Biopolymer-biocement composite treatment for stabilisation of soil against both current and wave erosion. *Acta Geotech. 2*. https://doi.org/10.1007/s11440-022-01536-2

Elmquist, M., Cornelissen, G., Kukulska, Z., Gustafsson, Ö., 2006. Distinct oxidative stabilities of char versus soot black carbon: Implications for quantification and environmental recalcitrance. *Global Biogeochem. Cycles 20*, 1–11. https://doi.org/10.1029/2005GB002629

Farouki, O.T., 1981. The thermal properties of soils in cold regions. *Cold Reg. Sci. Technol. 5*, 67–75. https://doi.org/10.1016/0165-232X(81)90041-0

Fatehi, H., Abtahi, S.M., Hashemolhosseini, H., Hejazi, S.M., 2018. A novel study on using protein based biopolymers in soil strengthening. *Constr. Build. Mater. 167*, 813–821. https://doi.org/10.1016/j.conbuildmat.2018.02.028

Fatehi, H., Ong, D.E.L., Yu, J., Chang, I., 2021. Biopolymers as green binders for soil improvement in geotechnical applications: *A review. Geosci. 11*, 1–39. https://doi.org/10.3390/geosciences11070291

Fazeli Sangani, M., Abrishamkesh, S., Owens, G., 2020. Physicochemical characteristics of biochars can be beneficially manipulated using post-pyrolyzed particle size modification. *Bioresour. Technol. 306*, 123157. https://doi.org/10.1016/j.biortech.2020.123157

Folaranmi, J., 2009. Effect of Additives on the Thermal Conductivity of Clay. Leonardo J. Sci. 74–77.

Gangadhara Rao, M.V.B.B., Singh, D.N., 1999. A generalized relationship to estimate thermal resistivity of soils. *Can. Geotech. J. 36*, 767–773. https://doi.org/10.1139/t99-037

Garg, A., Bordoloi, S., Ni, J., Cai, W., Maddibiona, P.G., Mei, G., Poulsen, T.G., Lin, P., 2019. Influence of biochar addition on gas permeability in unsaturated soil. *Geotech. Lett. 9*, 66–71. https://doi.org/10.1680/jgele.18.00190

Ghasemzadeh, H., Modiri, F., Darvishan, E., 2022. A novel clean biopolymer-based additive to improve mechanical and microstructural properties of clayey soil. *Clean Technol. Environ. Policy 24*, 969–981. https://doi.org/10.1007/s10098-021-02234-5

Ghosh, B., Pekkat, S., 2019. Effect of Initial Compaction State on Near-Saturated Hydraulic Conductivity. *J. Irrig. Drain. Eng. 145*, 1–10. https://doi.org/10.1061/(asce)ir.1943-4774.0001428

Głąb, T., Palmowska, J., Zaleski, T., Gondek, K., 2016. Effect of biochar application on soil hydrological properties and physical quality of sandy soil. *Geoderma 281*, 11–20. https://doi.org/10.1016/j.geoderma.2016.06.028

Gupt, C.B., Bordoloi, S., Bhatlu, M.N., Sekharan, S., 2021a. Hydraulic conductivity variation in compacted bentonite–fly ash mixes under constant-volume and free-swelling flow conditions. *Can. Geotech. J. 1113*, 1–18. https://doi.org/10.1139/cgj-2021-0239

Gupt, C.B., Bordoloi, S., Sahoo, R.K., Sekharan, S., 2021b. Mechanical performance and micro-structure of bentonite-fly ash and bentonite-sand mixes for landfill liner application. *J. Clean. Prod. 292*, 126033. https://doi.org/10.1016/j.jclepro.2021.126033

Gupta, S., Kua, H.W., 2017. Factors Determining the Potential of Biochar As a Carbon Capturing and Sequestering Construction Material: Critical Review. *J. Mater. Civ. Eng. 29*. https://doi.org/10.1061/(asce)mt.1943-5533.0001924

Habert, G., Billard, C., Rossi, P., Chen, C., Roussel, N., 2010. Cement production technology improvement compared to factor 4 objectives. *Cem. Concr. Res. 40*, 820–826. https://doi.org/10.1016/j.cemconres.2009.09.031

Hall, M., Allinson, D., 2009. Assessing the effects of soil grading on the moisture content-dependent thermal conductivity of stabilised rammed earth materials. *Appl. Therm. Eng. 29*, 740–747. https://doi.org/10.1016/j.applthermaleng.2008.03.051

Hanson, J.L., Edil, T.B., Yesiller, N., 2000. Thermal Properties of High Water Content Materials. *ASTM SPEC TECH PUBL 1374*, 137–151.

Haque, A., Tang, C.K., Islam, S., Ranjith, P.G., Bui, H.H., 2014. Biochar Sequestration in Lime-Slag Treated Synthetic Soils: A Green Approach to Ground Improvement. *J. Mater. Civ. Eng. 26*, 1–5. https://doi.org/10.1061/(asce)mt.1943-5533.0001113

Hart, A., 2014. A review of technologies for transporting heavy crude oil and bitumen via pipelines. *J. Pet. Explor. Prod. Technol. 4*, 327–336. https://doi.org/10.1007/s13202-013-0086-6

Hasan, S.W., Ghannam, M.T., Esmail, N., 2010. Heavy crude oil viscosity reduction and rheology for pipeline transportation. *Fuel 89*, 1095–1100. https://doi.org/10.1016/j.fuel.2009.12.021

Hassan, M., Liu, Y., Naidu, R., Parikh, S.J., Du, J., Qi, F., Willett, I.R., 2020. Influences of feedstock sources and pyrolysis temperature on the properties of biochar and functionality as adsorbents: A meta-analysis. *Sci. Total Environ. 744*, 140714. https://doi.org/10.1016/j.scitotenv.2020.140714

Hillel, D., 2013. Introduction to soil physics. New York, USA.

Holtz, R.D., Kovacs, W.D., Sheahan, T.C., 1981. An introduction to geotechnical engineering, Eaglewoods, Cliff, New Jersey, USA. Prentice-Hall, Inc, Eaglewoods, Cliff, New Jersey, USA.

Howard, A.K., 1996. Pipe Bedding and Backfill Geotechnical Training Manual No. 7 Second Edition [WWW Document]. United States Dep. Inter. Bur. Reclam. URL https://www.usbr.gov/tsc/techreferences/mands/mands-pdfs/pipebed.pdf

Huang, H., Reddy, N.G., Huang, X., Chen, P., Wang, P., Zhang, Y., Huang, Y., Lin, P., Garg, A., 2021. Effects of pyrolysis temperature, feedstock type and compaction on water retention of biochar amended soil. *Sci. Rep. 11*, 1–20. https://doi.org/10.1038/s41598-021-86701-5

IBI Standard 2.1, 2015. International Biochar Initiative (IBI) Standardized Product Definition and Testing Guidelines for Biochar that Is Used in Soil [WWW Document]. IBI 2015. URL https://biochar-international.org/characterizationstandard/

Jing, F., Sun, Y., Liu, Y., Wan, Z., Chen, J., Tsang, D.C.W., 2022. Interactions between biochar and clay minerals in changing biochar carbon stability. *Sci. Total Environ. 809*, 151124. https://doi.org/10.1016/j.scitotenv.2021.151124

Jyoti Bora, M., Bordoloi, S., Kumar, H., Gogoi, N., Zhu, H.H., Sarmah, A.K., Sreeja, P., Sreedeep, S., Mei, G., 2021. Influence of biochar from animal and plant origin on the compressive strength characteristics of degraded landfill surface soils. *Int. J. Damage Mech. 30*, 484–501. https://doi.org/10.1177/1056789520925524

Kameyama, K., Iwata, Y., Miyamoto, T., 2017. Biochar amendment of soils according to their physicochemical properties. *Japan Agric. Res. Q. 51*, 117–127. https://doi.org/10.6090/jarq.51.117

KD2 Pro, 2016. KD2 Pro Thermal Properties Analyzer Operator's Manual Version 4. Decagon Devices, Pullman, WA. KD2 Pro Therm. Prop. Anal. Oper. Man. version 4.

KELLY, C.N., BENJAMIN, J., CALDERÓN, F.C., MIKHA, M.M., RUTHERFORD, D.W., ROSTAD, C.E., 2017. Incorporation of Biochar Carbon into Stable Soil Aggregates: The Role of Clay Mineralogy and Other Soil Characteristics. *Pedosphere 27*, 694–704. https://doi.org/10.1016/S1002-0160(17)60399-0

Kercher, A.K., Nagle, D.C., 2002. Evaluation of carbonized medium-density fiberboard for electrical applications. *Carbon N. Y. 40*, 1321–1330. https://doi.org/10.1016/S0008-6223(01)00299-8

Klett, J.W., McMillan, A.D., Gallego, N.C., Walls, C.A., 2004. The role of structure on the thermal properties of graphitic foams. *J. Mater. Sci. 39*, 3659–3676. https://doi.org/10.1023/B:JMSC.0000030719.80262.f8

Kumar, D., Alam, M., Zou, P.X.W., Sanjayan, J.G., Memon, R.A., 2020. Comparative analysis of building insulation material properties and performance. *Renew. Sustain. Energy Rev. 131*, 110038. https://doi.org/10.1016/j.rser.2020.110038

Kumar, H., Ganesan, S.P., Bordoloi, S., Sreedeep, S., Lin, P., Mei, G., Garg, A., Sarmah, A.K., 2019. Erodibility assessment of compacted biochar amended soil for geo-environmental applications. *Sci. Total Environ. 672*, 698–707. https://doi.org/10.1016/j.scitotenv.2019.03.417

Latifi, N., Horpibulsuk, S., Meehan, C.L., Abd Majid, M.Z., Tahir, M.M., Mohamad, E.T., 2017. Improvement of Problematic Soils with Biopolymer—An Environmentally Friendly Soil Stabilizer. *J. Mater. Civ. Eng. 29*, 1–11. https://doi.org/10.1061/(asce)mt.1943-5533.0001706

Latifi, N., Horpibulsuk, S., Meehan, C.L., Majid, M.Z.A., Rashid, A.S.A., 2016. Xanthan gum biopolymer: an eco-friendly additive for stabilization of tropical organic peat. *Environ. Earth Sci. 75*, 1–10. https://doi.org/10.1007/s12665-016-5643-0

Lee, S., Chang, I., Chung, M.K., Kim, Y., Kee, J., 2017. Geotechnical shear behavior of xanthan gum biopolymer treated sand from direct shear testing. *Geomech. Eng. 12*, 831–847. https://doi.org/10.12989/gae.2017.12.5.831

Lee, W.Y., Cho, Y.I., Hartnett, J.P., 1981. Thermal conductivity measurements of non-Newtonian fluids. *Lett. Heat Mass Transf. 8*, 255–259. https://doi.org/10.1016/0094-4548(81)90039-4

Lehmann, J., Joseph, S., 2015. Biochar for Environmental Management: Science, Technology and Implementation. Routledge, New York, USA.

Li, F., Shen, K., Long, X., Wen, J., Xie, X., Zeng, X., Liang, Y., Wei, Y., Lin, Z., Huang, W., Zhong, R., 2016. Preparation and characterization of biochars from eichornia crassipes for cadmium removal in aqueous solutions. *PLoS One 11*, 7–9. https://doi.org/10.1371/journal.pone.0148132

Li, K.Q., Li, D.Q., Chen, D.H., Gu, S.X., Liu, Y., 2021. A generalized model for effective thermal conductivity of soils considering porosity and mineral composition. *Acta Geotech. 16*, 3455–3466. https://doi.org/10.1007/s11440-021-01282-x

Liu, Z., Xu, J., Li, X., Wang, J., 2018. Mechanisms of biochar effects on thermal properties of red soil in south China. *Geoderma 323*, 41–51. https://doi.org/10.1016/j.geoderma.2018.02.045

Lu, S., Ren, T., Gong, Y., Horton, R., 2007. An Improved Model for Predicting Soil Thermal Conductivity from Water Content at Room Temperature. *Soil Sci. Soc. Am. J. 71*, 8–14. https://doi.org/10.2136/sssaj2006.0041

Lu, S.G., Sun, F.F., Zong, Y.T., 2014. Effect of rice husk biochar and coal fly ash on some physical properties of expansive clayey soil (Vertisol). *Catena 114*, 37–44. https://doi.org/10.1016/j.catena.2013.10.014

Mahamaya, M., Das, S.K., Reddy, K.R., Jain, S., 2021. Interaction of biopolymer with dispersive geomaterial and its characterization: An eco-friendly approach for erosion control. *J. Clean. Prod. 312*, 127778. https://doi.org/10.1016/j.jclepro.2021.127778

Manyà, J.J., 2012. Pyrolysis for biochar purposes: A review to establish current knowledge gaps and research needs. *Environ. Sci. Technol. 46*, 7939–7954. https://doi.org/10.1021/es301029g

Melo, L.C.A., Coscione, A.R., Abreu, C.A., Puga, A.P., Camargo, O.A., 2013. Influence of pyrolysis temperature on cadmium and zinc sorption capacity of sugar cane straw-derived biochar. *BioResources 8*, 4992–5004. https://doi.org/10.15376/biores.8.4.4992-5004

Moradi-Choghamarani, F., Moosavi, A.A., Sepaskhah, A.R., Baghernejad, M., 2019. Physico-hydraulic properties of sugarcane bagasse-derived biochar: the role of pyrolysis temperature. *Cellulose 26*, 7125–7143. https://doi.org/10.1007/s10570-019-02607-6

Moradi, A., Smits, K.M., Lu, N., McCartney, J.S., 2016. Heat Transfer in Unsaturated Soil with Application to Borehole Thermal Energy Storage. *Vadose Zo. J. 15*, 1–17. https://doi.org/10.2136/vzj2016.03.0027

Moradi, A., Smits, K.M., Massey, J., Cihan, A., McCartney, J., 2015. Impact of coupled heat transfer and water flow on soil borehole thermal energy storage (SBTES) systems: Experimental and modeling investigation. *Geothermics 57*, 56–72. https://doi.org/10.1016/j.geothermics.2015.05.007

Morali, U., Şensöz, S., 2015. Pyrolysis of hornbeam shell (Carpinus betulus L.) in a fixed bed reactor: Characterization of bio-oil and bio-char. *Fuel 150*, 672–678. https://doi.org/10.1016/j.fuel.2015.02.095

Muguda, S., Booth, S.J., Hughes, P.N., Augarde, C.E., Perlot, C., Bruno, A.W., Gallipoli, D., 2017. Mechanical properties of biopolymer-stabilised soil-based construction materials. *Geotech. Lett. 7*, 309–314. https://doi.org/10.1680/jgele.17.00081

Muguda, S., Lucas, G., Hughes, P.N., Augarde, C.E., Perlot, C., Bruno, A.W., Gallipoli, D., 2020. Durability and hygroscopic behaviour of biopolymer stabilised earthen construction materials. *Constr. Build. Mater. 259*, 119725. https://doi.org/10.1016/j.conbuildmat.2020.119725

Muigai, H.H., Bordoloi, U., Hussain, R., Ravi, K., Moholkar, V.S., Kalita, P., 2021. A comparative study on synthesis and characterization of biochars derived from lignocellulosic biomass for their candidacy in agronomy and energy applications. *Int. J. Energy Res. 45*, 4765–4781. https://doi.org/10.1002/er.6092

Ng, C.W.W., Cai, W., So, P.S., Liao, J., Lau, S.Y., 2022. Effects of biochar on shear strength of completely decomposed granite. *Environ. Sci. Pollut. Res.* https://doi.org/10.1007/s11356-022-20707-y

Ni, J.J., Chen, X.W., Ng, C.W.W., Guo, H.W., 2018. Effects of biochar on water retention and matric suction of vegetated soil. *Géotechnique Lett. 8*, 124–129. https://doi.org/10.1680/jgele.17.00180

Nzediegwu, C., Arshad, M., Ulah, A., Naeth, M.A., Chang, S.X., 2021. Fuel, thermal and surface properties of microwave-pyrolyzed biochars depend on feedstock type and pyrolysis temperature. *Bioresour. Technol. 320*, 124282. https://doi.org/10.1016/j.biortech.2020.124282

Ocłoń, P., 2021. The effect of soil thermal conductivity and cable ampacity on the thermal performance and material costs of underground transmission line. *Energy 231*, 1–13. https://doi.org/10.1016/j.energy.2021.120803

Olajire, A.A., 2021. Review of wax deposition in subsea oil pipeline systems and mitigation technologies in the petroleum industry. *Chem. Eng. J. Adv. 6*, 100104. https://doi.org/10.1016/j.ceja.2021.100104

Omondi, M.O., Xia, X., Nahayo, A., Liu, X., Korai, P.K., Pan, G., 2016. Quantification of biochar effects on soil hydrological properties using meta-analysis of literature data. *Geoderma 274*, 28–34. https://doi.org/10.1016/j.geoderma.2016.03.029

Otomi, O.K., Onochie, U.P., Obanor, A.I., 2020. Steady state analysis of heat transfer in a fully buried crude oil pipeline. *Int. J. Heat Mass Transf. 146*, 118893. https://doi.org/10.1016/j.ijheatmasstransfer.2019.118893

Pardo, G.S., Sarmah, A.K., Orense, R.P., 2019. Mechanism of improvement of biochar on shear strength and liquefaction resistance of sand. *Geotechnique 69*, 471–480. https://doi.org/10.1680/jgeot.17.P.040

Pariyar, P., Kumari, K., Jain, M.K., Jadhao, P.S., 2020. Evaluation of change in biochar properties derived from different feedstock and pyrolysis temperature for environmental and agricultural application. *Sci. Total Environ. 713*, 136433. https://doi.org/10.1016/j.scitotenv.2019.136433

Park, D., Seo, Y., 2018. A Study on Heat Loss from Offshore Pipelines Depending on the Thermal Conductivity of Backfills and Burial Depth 4, 1–6. https://doi.org/10.5574/JAROE.2018.4.1.001

Priyadharshini, P., Ramamurthy, K., Robinson, R.G., 2019. Influence of Temperature and Duration of Thermal Treatment on Properties of Excavated Soil as Fine Aggregate in Cement Mortar. *J. Mater. Civ. Eng. 31*. https://doi.org/10.1061/(asce)mt.1943-5533.0002759

Puspanathan, T.K., Jayawardane, V.S., Paul, S.C., Ying, K.S., Shukla, S.K., Anggraini, V., 2022. Effect of biochar on desiccation of marine soils under constant and cyclic temperatures. *Acta Geotech. 17*, 5441–5464. https://doi.org/10.1007/s11440-022-01613-6

Qureshi, M.U., Chang, I., Al-Sadarani, K., 2017. Strength and durability characteristics of biopolymer-treated desert sand. *Geomech. Eng. 12*, 785–801. https://doi.org/10.12989/gae.2017.12.5.785

Rahman, M.A., 2018. Pyrolysis of water hyacinth in a fixed bed reactor: Parametric effects on product distribution, characterization and syngas evolutionary behavior. *Waste Manag. 80*, 310–318. https://doi.org/10.1016/j.wasman.2018.09.028

Ramachandran, A.L., Dubey, A.A., Dhami, N.K., Mukherjee, A., 2021. Multiscale Study of Soil Stabilization Using Bacterial Biopolymers. *J. Geotech. Geoenvironmental Eng. 147*, 1–16. https://doi.org/10.1061/(asce)gt.1943-5606.0002575

Reddy, K.R., Yaghoubi, P., Yukselen-Aksoy, Y., 2015. Effects of biochar amendment on geotechnical properties of landfill cover soil. *Waste Manag. Res. 33*, 524–532. https://doi.org/10.1177/0734242X15580192

Rezende, J.C.T., Ramos, V.H.S., Oliveira, H.A., Oliveira, R.M.P.B., Jesus, E., 2018. Removal of Cr(VI) from aqueous solutions using clay from calumbi geological formation, N. Sra. Socorro, SE State, Brazil. *Mater. Sci. Forum 912 MSF*, 1–6. https://doi.org/10.4028/www.scientific.net/MSF.912.1

Sadasivam, B.Y., Reddy, K.R., 2015. Engineering properties of waste wood-derived biochars and biochar-amended soils. *Int. J. Geotech. Eng. 9*, 521–535. https://doi.org/10.1179/1939787915Y.0000000004

Sah, P.K., Sreedeep, S., 2014. Evaluation of bentonite-based thermal backfill materials. *Environ. Geotech. 1*, 179–188. https://doi.org/10.1680/envgeo.13.00037

Saraiva, J.P., Lima, B.S., Gomes, V.M., Flores, P.H.R., Gomes, F.A., Assis, A.O., Reis, M.R.C., Araujo, W.R.H., Abrenhosa, C., Calixto, W.P., 2017. Calculation of sensitivity index using one-at-a-time measures based on graphical analysis. *Proc. 2017 18th Int. Sci. Conf. Electr. Power Eng. EPE 2017*. https://doi.org/10.1109/EPE.2017.7967329

Shen, Z., Hou, D., Jin, F., Shi, J., Fan, X., Tsang, D.C.W., Alessi, D.S., 2019. Effect of production temperature on lead removal mechanisms by rice straw biochars. *Sci. Total Environ. 655*, 751–758. https://doi.org/10.1016/j.scitotenv.2018.11.282

Singh, D.N., Devid, K., 2000. Generalized relationships for estimating soil thermal resistivity. *Exp. Therm. Fluid Sci. 22*, 133–143. https://doi.org/10.1016/S0894-1777(00)00020-0

Spokas, K.A., 2010. Review of the stability of biochar in soils: Predictability of O:C molar ratios. *Carbon Manag. 1*, 289–303. https://doi.org/10.4155/cmt.10.32

Sudhakar, A., Remya, N., Varghese, G.K., 2017. Estimation of effect of sugarcane bagasse biochar amendment in landfill soil cover on geotechnical properties and landfill gas emission. *Environ. Qual. Manag. 27*, 33–39. https://doi.org/10.1002/tqem.21528

Sun, L., Chen, D., Wan, S., Yu, Z., 2018. Adsorption Studies of Dimetridazole and Metronidazole onto Biochar Derived from Sugarcane Bagasse: Kinetic, Equilibrium, and Mechanisms. *J. Polym. Environ. 26*, 765–777. https://doi.org/10.1007/s10924-017-0986-5

Sun, Y., He, Y., Tang, B., Tao, C., Ban, J., Jiang, L., 2017. Influence from the types of surface functional groups of RGO on the performances of thermal interface materials. *RSC Adv. 7*, 55790–55795. https://doi.org/10.1039/c7ra12034f

Tang, A.-M., Cui, Y.-J., Le, T.-T., 2008. A study on the thermal conductivity of compacted bentonites. *Appl. Clay Sci. 41*, 181–189. https://doi.org/10.1016/j.clay.2007.11.001

Tang, C.S., Cheng, Q., Gong, X., Shi, B., Inyang, H.I., 2022. Investigation on microstructure evolution of clayey soils: A review focusing on wetting/drying process. *J. Rock Mech. Geotech. Eng.* https://doi.org/10.1016/j.jrmge.2022.02.004

Tarnawski, V.R., Leong, W.H., Gori, F., Buchan, G.D., Sundberg, J., 2002. Inter-particle contact heat transfer in soil systems at moderate temperatures. *Int. J. Energy Res. 26*, 1345–1358. https://doi.org/10.1002/er.853

Tarnawski, V.R., Momose, T., McCombie, M.L., Leong, W.H., 2015. Canadian Field Soils III. Thermal-Conductivity Data and Modeling. *Int. J. Thermophys. 36*, 119–156. https://doi.org/10.1007/s10765-014-1793-z

Tomczyk, A., Sokołowska, Z., Boguta, P., 2020. Biochar physicochemical properties: pyrolysis temperature and feedstock kind effects. *Rev. Environ. Sci. Biotechnol. 19*, 191–215. https://doi.org/10.1007/s11157-020-09523-3

Tong, B., Kool, D., Heitman, J.L., Sauer, T.J., Gao, Z., Horton, R., 2020. Thermal property values of a central Iowa soil as functions of soil water content and bulk density or of soil air content. *Eur. J. Soil Sci. 71*, 169–178. https://doi.org/10.1111/ejss.12856

Usowicz, B., Lipiec, J., Łukowski, M., Marczewski, W., Usowicz, J., 2016. The effect of biochar application on thermal properties and albedo of loess soil under grassland and fallow. *Soil Tillage Res. 164*, 45–51. https://doi.org/10.1016/j.still.2016.03.009

Usowicz, B., Lipiec, J., Usowicz, J.B., Marczewski, W., 2013. Effects of aggregate size on soil thermal conductivity: Comparison of measured and model-predicted data. *Int. J. Heat Mass Transf. 57*, 536–541. https://doi.org/10.1016/j.ijheatmasstransfer.2012.10.067

Varghese, R., Chandrakaran, S., Rangaswamy, K., 2021. Influence of type of organic substances on the strength and consolidation behaviour of inorganic clay soil. *Int. J. Geotech. Eng. 15*, 1165–1176. https://doi.org/10.1080/19386362.2019.1591739

Vydehi, K.V., Moghal, A.A.B., 2022. Effect of Biopolymeric Stabilization on the Strength and Compressibility Characteristics of Cohesive Soil. *J. Mater. Civ. Eng. 34*. https://doi.org/10.1061/(asce)mt.1943-5533.0004068

Wang, H., Xia, W., Lu, P., 2017. Study on adsorption characteristics of biochar on heavy metals in soil. *Korean J. Chem. Eng. 34*, 1867–1873. https://doi.org/10.1007/s11814-017-0048-7

Wang, Z., Cao, J., Wang, J., 2009. Pyrolytic characteristics of pine wood in a slowly heating and gas sweeping fixed-bed reactor. *J. Anal. Appl. Pyrolysis 84*, 179–184. https://doi.org/10.1016/j.jaap.2009.02.001

Wang, Z., Wang, F., Ma, Z., Wang, X., Wu, X., 2016. Research of heat and moisture transfer influence on the characteristics of the ground heat pump exchangers in unsaturated soil. *Energy Build. 130*, 140–149. https://doi.org/10.1016/j.enbuild.2016.08.043

Williams, J.M., Vahedifard, F., Latifi, N., 2020. Mechanical, Chemical, Hydraulic, and Microstructural Properties of Buckshot Clay Amended with Gasification Biochar. *J. Environ. Eng. 146*. https://doi.org/10.1061/(asce)ee.1943-7870.0001809

Wong, J.T.F., Chen, Z., Ng, C.W.W., Wong, M.H., 2016. Gas permeability of biochar-amended clay: potential alternative landfill final cover material. *Environ. Sci. Pollut. Res. 23*, 7126–7131. https://doi.org/10.1007/s11356-015-4871-2

Xiao, Y., Nan, B., McCartney, J.S., 2019. Thermal Conductivity of Sand–Tire Shred Mixtures. *J. Geotech. Geoenvironmental Eng. 145*, 1–8. https://doi.org/10.1061/(asce)gt.1943-5606.0002155

Xiao, Y., Tang, Y., Ma, G., McCartney, J.S., Chu, J., 2021. Thermal Conductivity of Biocemented Graded Sands. *J. Geotech. Geoenvironmental Eng. 147*, 1–15. https://doi.org/10.1061/(asce)gt.1943-5606.0002621

Xie, X., Lu, Y., Ren, T., Horton, R., 2020. Thermal conductivity of mineral soils relates linearly to air-filled porosity. *Soil Sci. Soc. Am. J. 84*, 53–56. https://doi.org/10.1002/saj2.20016

Xu, R., Ferrante, L., Hall, K., Briens, C., Berruti, F., 2011. Thermal self-sustainability of biochar production by pyrolysis. *J. Anal. Appl. Pyrolysis 91*, 55–66. https://doi.org/10.1016/j.jaap.2011.01.001

Ye, X., Yu, Z., Zhang, Y., Kang, J., Wu, S., Yang, T., Gao, P., 2022. Mineral Composition Impact on the Thermal Conductivity of Granites Based on Geothermal Field Experiments in the Songliao and Gonghe Basins, China. *Minerals 12*. https://doi.org/10.3390/min12020247

Yu, S., Park, Jinje, Kim, M., Ryu, C., Park, Jungkeuk, 2019. Characterization of biochar and byproducts from slow pyrolysis of hinoki cypress. *Bioresour. Technol. Reports 6*, 217–222. https://doi.org/10.1016/j.biteb.2019.03.009

Yuan, H., Lu, T., Huang, H., Zhao, D., Kobayashi, N., Chen, Y., 2015. Influence of pyrolysis temperature on physical and chemical properties of biochar made from sewage sludge. *J. Anal. Appl. Pyrolysis 112*, 284–289. https://doi.org/10.1016/j.jaap.2015.01.010

Yuan, P., Zhang, P., Liang, T., Zhai, S., Yang, D., 2019. Effects of functionalization on energy storage properties and thermal conductivity of graphene/n-octadecane composite phase change materials. *J. Mater. Sci. 54*, 1488–1501. https://doi.org/10.1007/s10853-018-2883-2

Yun, T.S., Santamarina, J.C., 2008. Fundamental study of thermal conduction in dry soils. *Granul. Matter 10*, 197–207. https://doi.org/10.1007/s10035-007-0051-5

Zabihi, Z., Araghi, H., 2016. Effect of functional groups on thermal conductivity of graphene/paraffin nanocomposite. *Phys. Lett. Sect. A Gen. At. Solid State Phys. 380*, 3828–3831. https://doi.org/10.1016/j.physleta.2016.09.028

Zhang, H., Chen, C., Gray, E.M., Boyd, S.E., 2017. Effect of feedstock and pyrolysis temperature on properties of biochar governing end use efficacy. *Biomass and Bioenergy 105*, 136–146. https://doi.org/10.1016/j.biombioe.2017.06.024

Zhang, J., Chen, Q., You, C., 2015. Numerical simulation of mass and heat transfer between biochar and sandy soil. *Int. J. Heat Mass Transf. 91*, 119–126. https://doi.org/10.1016/j.ijheatmasstransfer.2015.07.104

Zhang, J., You, C., 2013. Water holding capacity and absorption properties of wood chars. *Energy and Fuels 27*, 2643–2648. https://doi.org/10.1021/ef4000769

Zhang, N., Yu, X., Pradhan, A., Puppala, A.J., 2017. A new generalized soil thermal conductivity model for sand–kaolin clay mixtures using thermo-time domain reflectometry probe test. *Acta Geotech. 12*, 739–752. https://doi.org/10.1007/s11440-016-0506-0

Zhang, Q., Wang, Y., Wu, Y., Wang, X., Du, Z., Liu, X., Song, J., 2013. Effects of Biochar Amendment on Soil Thermal Conductivity, Reflectance, and Temperature. *Soil Sci. Soc. Am. J. 77*, 1478–1487. https://doi.org/10.2136/sssaj2012.0180

Zhang, X., Zhang, P., Yuan, X., Li, Y., Han, L., 2020. Effect of pyrolysis temperature and correlation analysis on the yield and physicochemical properties of crop residue biochar. *Bioresour. Technol. 296*, 122318. https://doi.org/10.1016/j.biortech.2019.122318

Zhao, J., Ren, T., Zhang, Q., Du, Z., Wang, Y., 2016. Effects of Biochar Amendment on Soil Thermal Properties in the North China Plain. *Soil Sci. Soc. Am. J. 80*, 1157–1166. https://doi.org/10.2136/sssaj2016.01.0020

Zhao, L., Cao, X., Mašek, O., Zimmerman, A., 2013. Heterogeneity of biochar properties as a function of feedstock sources and production temperatures. *J. Hazard. Mater*. 256–257, 1–9. https://doi.org/10.1016/j.jhazmat.2013.04.015

Zong, Y., Chen, D., Lu, S., 2014. Impact of biochars on swell-shrinkage behavior, mechanical strength, and surface cracking of clayey soil. *J. Plant Nutr. Soil Sci. 177*, 920–926. https://doi.org/10.1002/jpln.201300596

Zong, Y., Xiao, Q., Lu, S., 2016. Acidity, water retention, and mechanical physical quality of a strongly acidic Ultisol amended with biochars derived from different feedstocks. *J. Soils Sediments 16*, 177–190. https://doi.org/10.1007/s11368-015-1187-2

List of publications

Journal

- **Patwa, D**., Chandra, A., Ravi, K., & Sreedeep, S. (2021). Influence of biochar particle size fractions on thermal and mechanical properties of biochar-amended soil. ***Journal of Materials in Civil Engineering,*** *33(9),* 04021236. **ASCE.** https://doi.org/10.1061/(ASCE)MT.1943-5533.0003915
- **Patwa, D**., Muigai, H. H., Ravi, K., Sreedeep, S., & Kalita, P. (2022). A novel application of biochar produced from invasive weeds and industrial waste in thermal backfill for crude oil industries. ***Waste and Biomass Valorization,*** *13(6),* 3025-3042. **Springer Nature.** https://doi.org/10.1007/s12649-022-01694-0
- **Patwa, D**., Bordoloi, U., Dubey, A. A., Ravi, K., Sekharan, S., & Kalita, P. (2022). Energy-efficient biochar production for thermal backfill applications. ***Science of The Total Environment,*** *833,* 155253. **Elsevier.** https://doi.org/10.1016/j.scitotenv.2022.155253
- **Patwa, D.,** Ravi, K., & Sreedeep, S. "Utilization of biochar-based soil composite for thermal backfills: Influence of initial molding parameters and natural moisture migration." ***Acta Geophysica,*** **Springer Nature.** https://doi.org/10.1007/s11600-022-00993-3
- **Patwa, D**., Dubey, AA., Ravi, K., & Sreedeep, S. "Investigation of thermal and strength characteristics of a natural backfill composite inspired by synergistic biochar-biopolymer amendment of clay loam." *Canadian Geotechnical Journal* (*Under revision*).
- Experimental study and numerical simulation of thermal migration in biochar and biochar-biopolymer based soil composite for heat loss mitigation. (To be communicated).

Conference proceeding/Book Chapters

- **Patwa, D**., Ravi, K., & Sreedeep, S. "Impact of Biochar Fraction on Thermal characteristics of Soil-Biochar Composite." ***Proceedings of Indian Geotechnical Conference,*** **2021, NIT Tiruchirappalli, India.** https://doi.org/10.1007/978-981-19-6774-0_29

- **Patwa, D**., Dubey, AA., Ravi, K., & Sreedeep, S. "Biopolymer stabilization of highly plastic silty soil for rammed earth construction materials." ***Proceedings of Indian Geotechnical Conference*, 2022. IGS Kochi chapter. (Accepted)**
- **Patwa, D**., Ravi, K., & Sreedeep, S. "Investigation of heat transfer in biochar-based thermal backfill for energy storage facilities." *International Congress on Environmental Geotechnics, ICEG-2023* **(Accepted).**